

Hydrogeochemistry – A Journey of Discovery

Warren W. Wood

Hydrogeochemistry *– A Journey of Discovery*

The Groundwater Project

Warren W. Wood

*Visiting Professor Hydrogeology
Department of Earth and Environmental Sciences,
Michigan State University
East Lansing, Michigan, USA*

***Hydrogeochemistry
– A Journey of Discovery***

*The Groundwater Project
Guelph, Ontario, Canada*

The Groundwater Project relies on private funding for book production and management of the Project.

Please consider donating to the Groundwater Project  so that books will continue to be freely available.

Thank you.

All rights reserved. This publication is protected by copyright. No part of this book may be reproduced in any form or by any means without permission in writing from the authors (to request permission, contact permissions@gw-project.org). Commercial distribution and reproduction are strictly prohibited.

Groundwater Project (The GW-Project) works are copyrighted and can be downloaded for free from gw-project.org. Anyone may use and share gw-project.org links to download GW-Project's work. It is not permissible to make GW-Project documents available on other websites nor to send copies of the documents directly to others. Kindly honor this source of free knowledge that benefits you and all those who want to learn about groundwater.

Copyright © 2025 Warren W. Wood (The Author).

Published by The Groundwater Project, Guelph, Ontario, Canada, 2025.

Wood, Warren W.

Hydrogeochemistry – A Journey of Discovery/ Warren W. Wood - Guelph, Ontario, Canada, 2025.

262 pages.

ISBN: 978-1-77470-118-8

DOI: <https://doi.org/10.62592/VKTX1330>.

Please consider signing up for the GW-Project mailing list to stay informed about new book releases, events, and ways to participate in the GW-Project. When you sign up for our email list, it helps us build a global groundwater community. [Sign up](#).

APA (7th ed.) Citation:

Wood, W. W. (2025). *Hydrogeochemistry – A journey of discovery*. The Groundwater Project. <https://doi.org/10.62592/VKTX1330>.



Domain Editors: Eileen Poeter and John Cherry.

Board: John Cherry, Shafick Adams, Gabriel Eckstein, Richard Jackson, Ineke Kalwij, Renée Martin-Nagle, Everton de Oliveira, Marco Petitta, and Eileen Poeter.

Cover Image: Ally Miscikoski

Dedication

This is dedicated to the late William Back of the United States Geological Survey, a colleague, mentor, and great friend who pioneered the concept of integrating flow and solute chemistry in the 1950s.

Table of Contents

DEDICATION	V
TABLE OF CONTENTS	VI
THE GROUNDWATER PROJECT FOREWORD	IX
FOREWORD	X
PROLOGUE	XII
ACKNOWLEDGMENTS	XVI
1 REVIEW OF HYDROGEOCHEMICAL FUNDAMENTALS	1
1.1 CHEMICAL PRINCIPALS	1
1.2 THE ORIGIN OF ELEMENTS AND THEIR ATOMIC STRUCTURE.....	5
1.3 GROUNDWATER COMPOSITION AND CONCENTRATION OF SOLUTES, GASSES, AND PARTICULATES.....	9
1.4 WATER ISOTOPES.....	21
1.5 COLLECTION OF GROUNDWATER SAMPLES.....	25
1.6 UNCERTAINTY.....	27
2 SOURCES AND MECHANISMS CONTROLLING SOLUTES	31
2.1 ADVECTIVE FLOW AND DIFFUSION AS TRANSPORT MECHANISMS	31
2.2 EXTERNAL SOLUTE SOURCE: PRECIPITATION, RIVER, LAKES, AND CONTIGUOUS AQUIFERS.....	33
2.3 INTERNAL SOLUTE SOURCES: FOSSIL, RELIC, LEGACY, OR CONNATE.....	36
2.4 INTERNAL SOLUTE SOURCE: RADIOACTIVE DECAY	37
2.5 INTERNAL SOURCE OF SOLUTES: WEATHERING.....	40
2.6 EQUILIBRIUM VARIABLES	41
2.6.1 <i>Mineral Solubility: A Fundamental Thermodynamic Property</i>	43
2.6.2 <i>Temperature: An Environmental Thermodynamic Property</i>	46
2.6.3 <i>pH: An Environmental Thermodynamic Property</i>	50
2.6.4 <i>Eh (Redox): An Environmental Thermodynamic Variable</i>	54
2.6.5 <i>Thermodynamic Activity: An Environmental Thermodynamic Property</i>	57
2.6.6 <i>Equilibrium Calculations</i>	61
2.7 KINETICS OF PRECIPITATION	62
2.7.1 <i>Cation Exchange and Adsorption</i>	63
2.7.2 <i>Adsorption — A Process of Removing Solutes</i>	64
2.8 HYDRODYNAMIC DISPERSION IN TRANSPORT	65
2.9 SOLUTE CONTROL IN OPEN AND CLOSED SYSTEMS.....	67
2.10 ULTRAFILTRATION (REVERSE OSMOSIS) AS A PHYSICAL CONTROL ON SOLUTES	71
2.11 SECTION WRAP-UP.....	72
3 GEOGENIC TRACE ELEMENTS RELATED TO HUMAN HEALTH	73
3.1 MANGANESE (MN)	78
3.2 ARSENIC (AS)	79
3.3 RADIONUCLIDES OF URANIUM (U), RADIUM (RA), RADON (RN), POLONIUM (PO), AND LEAD (PB).....	82
3.4 STRONTIUM (SR)	90
3.5 FLUORIDE (F)	92
3.6 MOLYBDENUM (MO)	95
3.7 LEAD (PB).....	97
3.8 ANTIMONY (SB).....	98
3.9 SELENIUM (SE)	99
3.10 ZINC (ZN)	100

3.11	LITHIUM (Li)	101
3.12	NUISANCE ELEMENTS.....	104
3.13	IRON (FE)	104
3.14	HYDROGEN SULFIDE (H ₂ S) AND METHANE (CH ₄)	104
3.15	SECTION WRAP-UP: SELECTED TRACE GEOGENIC ELEMENTS.....	105
4	GRAPHICAL DISPLAY OF HYDROGEOCHEMICAL DATA	107
4.1	PRINCIPALS OF GRAPH DESIGN	108
4.1.1	<i>Heat Map</i>	112
4.1.2	<i>Contour Map</i>	112
4.1.3	<i>Fence Diagram</i>	113
4.1.4	<i>Cumulative Frequency</i>	114
4.1.5	<i>Box-and-Whisker Plot</i>	114
4.1.6	<i>Histogram</i>	116
4.1.7	<i>Pie Diagram</i>	116
4.1.8	<i>X–Y Linear Graph</i>	117
4.1.9	<i>Bar Diagram</i>	118
4.1.10	<i>Stacked Diagram</i>	119
4.1.11	<i>Trilinear Diagram</i>	119
4.1.12	<i>Stick Diagram</i>	120
4.1.13	<i>Stiff Diagram</i>	121
4.1.14	<i>Scholler Diagram</i>	121
4.1.15	<i>Durov Diagram</i>	122
4.2	SECTION WRAP-UP.....	122
5	FIELD EXAMPLES OF DIFFERENT HYDROGEOCHEMICAL SOURCES AND PROCESSES	123
5.1	AQUIFER SOLUTES DOMINATED BY ATMOSPHERIC PRECIPITATION: THE SOUTHERN HIGH PLAINS AQUIFER OF TEXAS AND NEW MEXICO, USA.....	123
5.2	AQUIFER SOLUTE DOMINATED BY ROCK WEATHERING: UPPER GRAND RIVER BASIN, CENTRAL MICHIGAN, USA	127
5.3	AQUIFER SOLUTES DOMINATED BY ION EXCHANGE: ATLANTIC COASTAL PLAIN, US	129
5.4	AQUIFER SOLUTES DOMINATED BY ELEVATED PH: <i>BLUE POOLS</i> OF THE SULTANATE OF OMAN	132
5.5	AQUIFER SOLUTES DOMINATED BY LOW PH	136
5.6	AQUIFER SOLUTES IMPACTED BY ULTRAFILTRATION: SAGINAW FORMATION, MICHIGAN, USA	141
5.7	SOLUTES DOMINATED BY LOSS OF GAS TO THE ATMOSPHERE: NITROGEN AND BROMINE FROM THE COASTAL SABKHA OF ABU DHABI, UAE.....	143
5.8	RADON-222: SOLUTES DOMINATED BY DIFFUSION	147
5.9	SYSTEMS DOMINATED BY SOIL SALINIZATION.....	150
5.10	EVALUATING PRISTINE CONDITION	153
5.11	SECTION WRAP-UP.....	155
6	SOLUTE MASS BALANCE: SIMPLE MASS FLUX MODELING	156
6.1	REPRESENTATIVE CONTROL VOLUME (RCV) MASS FLUX MODEL	157
6.2	PORE VOLUMES.....	158
6.3	MASS FLUX MODELING IN THE SABKHA OF ABU DHABI, UAE	159
6.4	GLOBAL MASS FLUX MODELING OF CARBON, NITROGEN, AND TOTAL SOLUTES	164
6.4.1	<i>Carbon in Global Groundwater</i>	166
6.4.2	<i>Nitrogen in Global Groundwater</i>	169
6.4.3	<i>Groundwater Weathering of the Continents</i>	172
6.5	SECTION WRAP-UP.....	174
7	GEOCHEMICAL EVOLUTION OF GROUNDWATER SOLUTES	175
7.1	EVOLUTION OF SULFATE FROM DISSOLUTION OF GYPSUM.....	179

7.2	CATION EXCHANGE.....	181
7.3	PYRITE OXIDATION	182
7.4	MOLECULAR DIFFUSION IN SOLUTE EVOLUTION	183
7.5	GROUNDWATER AND EVOLUTION OF KARST TOPOGRAPHY.....	190
7.6	ON EVOLUTION OF GLOBAL GROUNDWATER SOLUTES	196
7.7	SECTION WRAP-UP.....	198
8	QUANTIFYING PHYSICAL HYDROLOGIC PROPERTIES USING GEOGENIC SOLUTES	200
8.1	MODEL OF THE REGIONAL RECHARGE FLUX: THE CHLORIDE MASS BALANCE (CMB)	201
8.2	ESTIMATES OF HYDRAULIC CONDUCTIVITY USING CHLORIDE MASS BALANCE (CMB).....	204
8.3	RUNOFF FLUX TO TOPOGRAPHIC FEATURES: CHLORIDE MASS BALANCE (CMB).....	207
8.4	RELATIVE GROUNDWATER RECHARGE AS A FUNCTION OF GEOMORPHOLOGY, SOILS, OR LAND USE/COVER	209
8.5	DEFINING MACROPORE OR DIFFUSE RECHARGE USING STABLE WATER ISOTOPES	210
8.6	WATER SOURCE OF PALEO RECHARGE USING STABLE WATER ISOTOPES.....	212
8.7	DATING GROUNDWATER WITH CARBON-14	214
8.8	ESTIMATE OF RECHARGE FLUX AND RAINFALL FROM A PALEO-GROUNDWATER SURFACE: LIWA, UAE.....	217
8.9	ESTIMATE OF ACTIVE GLOBAL GROUNDWATER VOLUME.....	219
9	WRAP-UP	221
10	EXERCISES.....	223
	EXERCISE 1 - INTRINSIC AND ENVIRONMENTAL CONTROLS	223
	EXERCISE 2 - CONCENTRATION OF TRACE ELEMENTS	223
	EXERCISE 3 - GRAPHICAL PRESENTATIONS.....	224
	EXERCISE 4 - IDENTIFYING HYDROGEOCHEMICAL PROCESSES IN THE FIELD.....	225
	EXERCISE 5 - SOURCES OF SOLUTES IN GROUNDWATER AND RCV	225
11	REFERENCES	226
12	BOXES.....	241
	BOX 1 – ATOMIC STRUCTURE	241
	BOX 2 – APPLYING ACTIVITY CALCULATIONS TO THE AVERAGE GROUNDWATER COMPOSITION	243
	BOX 3 – INSTRUCTIONS FOR RUNNING PHREEQC ON A MAC LAPTOP (INTEL AND APPLE M SILICON CHIP).....	246
	BOX 4 – AN UNEXPECTED JOURNEY IN HYDROGEOCHEMICAL THINKING.....	254
13	EXERCISE SOLUTIONS	256
	SOLUTION EXERCISE 1.....	256
	SOLUTION EXERCISE 2.....	257
	SOLUTION EXERCISE 3.....	258
	SOLUTION EXERCISE 4.....	259
	SOLUTION EXERCISE 5.....	259
14	NOTATIONS	260
15	ABOUT THE AUTHOR	261

The Groundwater Project Foreword

The United Nations (UN)-Water Summit on Groundwater, held from 7 to 8 December 2022, at the UNESCO headquarters in Paris, France, concluded with a call for governments and other stakeholders to scale up their efforts to better manage groundwater. The intent of the call to action was to inform relevant discussions at the UN 2023 Water Conference held from 22 to 24 March 2023 at the UN headquarters in New York City. One of the required actions is *strengthening human and institutional capacity*, for which groundwater education is fundamental.

The 2024 World Water Day theme is *Water for Peace*, which focuses on the critical role water plays in the stability and prosperity of the world. The [UN-Water website](#)[↗] states that *more than three billion people worldwide depend on water that crosses national borders*. There are 592 transboundary aquifers, yet most do not have an intergovernmental cooperation agreement in place for sharing and managing the aquifer. Moreover, while groundwater plays a key role in global stability and prosperity, it also makes up 99 percent of all liquid freshwater—accordingly, groundwater is at the heart of the freshwater crisis. *Groundwater is an invaluable resource*.

The Groundwater Project (GW-Project), a registered Canadian charity founded in 2018, is committed to advancement of groundwater education as a means to accelerate action related to our essential groundwater resources. We are committed to *making groundwater understandable* and, thus, *enable building the human capacity for us development and management of groundwater*. To that end, the GW-Project creates and publishes high-quality books about *all-things-groundwater*, for all who want to learn about groundwater. Our books are unique. They synthesize knowledge, are rigorously peer reviewed and translated into many languages and are free of charge. An important tenet of GW-Project books is a strong emphasis on visualization: Clear illustrations stimulate spatial and critical thinking. The GW-Project started publishing books in August 2020; by the end of 2023, we had published 44 original books and 58 translations. The books can be downloaded at [gw-project.org](#)[↗].

The GW-Project embodies a new type of global educational endeavor made possible by the contributions of a dedicated international group of volunteer professionals from a broad range of disciplines. Academics, practitioners, and retirees contribute by writing and/or reviewing books aimed at diverse levels of readers including children, teenagers, undergraduate and graduate students, professionals in groundwater fields, and the general public. More than 1,000 dedicated volunteers from 70 countries and six continents are involved—and participation is growing. Revised editions of the books are published from time to time. Readers are invited to propose revisions.

We thank our sponsors for their ongoing financial support. Please consider donating to the GW-Project so we can continue to publish books free of charge.

The GW-Project Board of Directors, January 2024

Foreword

This book, titled “*Hydrogeochemistry - a Journey of Discovery*,” is focused on the evolution of the chemical composition of groundwater as a function of the three fundamental sources of solutes and many natural chemical and physical processes. “A Journey of discovery” is a double entendre that refers to both an individual’s hydrogeochemistry learning process and the changing hydrochemical composition of natural dissolved constituents in groundwater as it moves along flow paths from recharge toward discharge. That is, the composition is a function of the memory of many chemical and physical processes over hundreds to thousands of years and contrasts with physical hydrogeology, which is largely about water level that has no memory. Groundwater is an abstract concept as it is not easily viewed, it is “the water beneath our feet”. Thus, much of our understanding has been by an abstract mathematical approach in both flow and solute chemistry, and the book cover, with its abstract view of the hydrologic cycle, is a testimony to this. As an alternative, the author has used simple figures and explanations to provide a largely conceptual approach to the processes of hydrogeochemistry.

When we look at the chemical composition of a groundwater sample taken from a well or spring and ponder why it is as it is, we are looking at a puzzle that invites us to consider the effects of all of the processes that have acted on the water from the time it started as precipitation; to its journey into and through the soil, the vadose zone, and the groundwater zone to the location where the sample is collected. This topic coverage is unconventional in that the chemical reactions between groundwater and the minerals (water-rock interaction) of subsurface materials are shown to be relevant, but its importance depends on the composition, depositional environment, climate, and age of the aquifer system as other processes may dominate the solute composition. In this multi-process look at the topic, the reader is invited to consider the processes important to groundwater chemical composition. These processes include molecular diffusion, osmosis, mineral dissolution and rate, ion filtering, cation exchange, the chemical openness of the system, and more that are dependent on environmental and aquifer deposition and evolution conditions. This book provides both insight into the hydrochemical evolution of aquifer systems and a background for societal questions, including contaminants in groundwater, aquifer storage and recovery, and other groundwater management procedures.

The first four sections of the book provide fundamental information about groundwater chemistry that makes the book accessible to those without a chemistry background. This is followed by many field examples of different hydrochemical sources and processes. The concepts of mass balance are discussed and used to shed light on the role of groundwater in both the weathering of the continents and the global cycle of carbon and nitrogen. It wraps up with examples of how hydrogeochemistry can be used to

determine the physical properties of the hydrologic flow system, providing readers with approaches that lead to the interdisciplinary application of groundwater chemistry and hydraulics—a valuable endeavor that is frequently omitted from groundwater projects because the team is stronger in either chemistry or hydraulics.

The author of this book, Dr. Warren Wood, Emeritus Scientist of the US Geological Survey, former Christensen Fellow at St. Catherin’s College, Oxford University, and John Hannah Professor at Michigan State University, is a distinguished hydrogeologist who has devoted his long career to the study of diverse groundwater questions in many different geologic and climatic regimes where insights from chemical analyses of water samples from wells and springs have proved essential for system understanding.

John Cherry, The Groundwater Project Leader
Guelph, Ontario, Canada, December 2024

Prologue

The purpose of this monograph is to clarify how solute chemistry evolves in groundwater systems, with a focus on developing an intuitive, big-picture understanding rather than delving into detailed technical explanations. It employs a conceptual, visually oriented approach that utilizes analogies and graphics to elucidate complex processes. This reduces reliance on complex mathematical, thermodynamic, and quantum mechanics calculations that can overwhelm readers without specialized backgrounds.

This monograph utilizes a narrative style and field examples to create a coherent story. Its focus is less on serving as a textbook and more on offering a contextually rich, accessible introduction to the journey of discovery of groundwater geochemistry. The intent is to offer a conceptual approach, targeting readers who may not have a technical background but who need to interpret and understand a broad view of groundwater geochemistry. It is particularly suited for policymakers, attorneys, undergraduates, and others who are new to the field and need a grasp of groundwater chemistry to make informed decisions or communicate effectively with specialists. It also provides a bridge for readers with technical expertise in other scientific areas who want an introduction to the origins and transformations of groundwater solutes. That is, to make hydrogeochemistry accessible by focusing on intuitive principles.

The generalized representation of a problem in science is known as a conceptual model. An assembly of conceptual models within a theme constitutes a *paradigm* or a set of ideas, assumptions, and/or practices that provide a broad theoretical framework (Kuhn, 1962). A guiding principle in the resolution of a problem is the concept of multiple working hypotheses, introduced by geologist T. C. Chamberlin in the 19th century. This method, foundational to scientific inquiry, advocates for considering a range of plausible hypotheses (paradigms) initially and then systematically testing each one. Through data collection and analysis, less likely explanations are eliminated, while those that remain viable are refined for further investigation. Importantly, as in all scientific endeavors, hypotheses can only be disproven, not proven to be correct.

A subset of sciences that are based on the history of prior events (e.g., hydrogeochemistry, geology, and astronomy) often look to the past to make sense of present conditions. That is, the solute chemistry of groundwater is typically the accumulation of chemical processes that have occurred over hundreds to thousands of years. This contrasts with physical groundwater levels that are a response to what happened very recently. This retrospective approach is intellectually parallel to predicting future changes, as it involves assembling and interpreting evidence to understand evolving processes.

Understanding the origin of geogenic solutes in groundwater—those naturally occurring dissolved elements unaffected by human activity—extends beyond the scope of

typical water resource investigations. These solutes have shaped the natural composition of water sources that humans, along with most terrestrial animals, have relied on over evolutionary periods. We have adapted to drinking water from springs, rivers, and seeps with specific, relatively stable solute compositions and concentrations. This natural balance of groundwater solutes is fundamental to ecological and human health. Maintaining this balance in the face of groundwater use and development requires a deep understanding of the natural processes that regulate solute concentration and composition. By uncovering the origins of these solutes and the geochemical mechanisms controlling them, we can better protect the integrity of groundwater resources and sustain the quality of water that supports both ecosystems and human life.

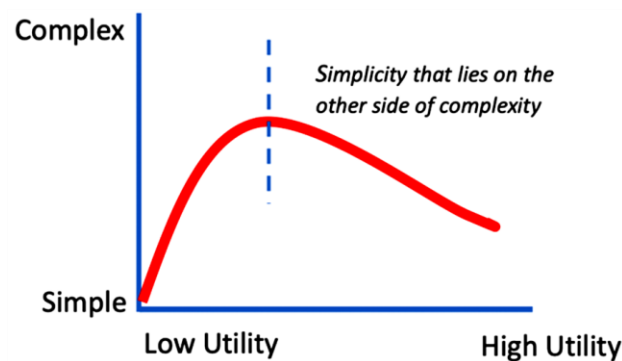
Hydrogeochemistry provides a broad, integrated framework for analyzing the composition and concentration of solutes in groundwater, considering a dynamic range of factors, including groundwater flow patterns, legacy solutes, rock-water interactions, and the transport of dissolved elements across different environments. This multifaceted approach contrasts with traditional groundwater geochemistry, which tends to concentrate on the direct relationships between solute concentrations and rock-water interactions in isolation.

Given the hidden nature of groundwater, “The water beneath our feet,” our understanding of its origins, distribution, and solute composition has often been fragmented and, at times, based on incomplete or even physically inconsistent explanations. This challenge extends to understanding the origins of the solutes within groundwater, which are present in minute amounts yet play significant roles in water quality and health.

In essence, hydrogeochemistry is the evaluation of all potential solute sources set in a conceptual framework of groundwater flow, including the following.

1. Solute remaining from the time of deposition, the so-called relic, fossil, legacy, or connate solutes.
2. Solute introduced from the surface (precipitation, rivers, lakes) and/or from adjacent, underlying, or overlying formations.
3. Solute generated from weathering and radioactive decay of the aquifer’s mineral/rock framework.

This monograph attempts to follow the goals of Oliver Wendell Holmes Jr., who reportedly stated, “*For the simplicity that lies this side of complexity, I would not give a fig, but for the simplicity that lies on the other side of complexity, I would give my life*” (graphically depicted in the following figure) or—as Leonardo Da Vinci is believed to have stated—“*Simplicity is the ultimate sophistication.*”



A graphical presentation of Holmes's concept of simplicity.

Reconstructing the history of groundwater composition is much like solving a puzzle, where the key lies in understanding the processes that add or remove solutes within a groundwater flow system. This process relies on the mass balance method—a straightforward yet powerful tool in hydrogeochemistry that accounts for the inputs and outputs of solutes over time to piece together past conditions.

Although the immense span of geologic time may feel distant from the immediate issues affecting groundwater quality, understanding these long-term processes often provides essential insights into the sources of solutes and the natural evolution of groundwater systems. This knowledge can be critical in addressing present-day water quality challenges, as it allows scientists and policymakers to distinguish between natural and anthropogenic influences on groundwater, guiding effective management practices.

Hydrogeochemistry is rarely the focus of a university course. Low-temperature geochemistry of groundwater is covered briefly in introductory courses on groundwater hydrogeology or as part of a course on environmental geochemistry, oceanography, or isotope geochemistry. The book [Groundwater](#) (Freeze & Cherry, 1979) allocates two out of 11 chapters (26 percent of total pages) to groundwater geochemistry, more than any other introductory groundwater textbook. *The Properties of Water* by Georg Matthes (1982), the second edition of *Groundwater Geochemistry and Isotopes* by Ian Clark (2015), and *Aqueous Environmental Geochemistry* by Donald Langmuir (1996) are excellent texts focused on classic groundwater geochemistry. The Matthes book emphasizes the chemical composition of groundwater in different terrains and consideration of equilibrium geochemistry, while the Clark and Langmuir books emphasize geochemical reaction processes, how to perform equilibrium calculations, and how to use isotopes to understand geochemical processes.

[The Geochemistry of Natural Waters: Surface and Groundwater Environments](#) (1997) by James Drever focuses more on environmental issues than the previous editions and provides insightful coverage of some aspects of groundwater geochemistry based on equilibrium geochemical concepts. The second edition of a book by Appelo and Postma—*Geochemistry, Groundwater, and Pollution* (2005)—comes close to the vision of incorporating flow into the geochemical process focused on groundwater contamination. Many of the US Geological Survey Regional Aquifer-System Analysis (RASA) studies of the 1990s also

integrate flow and solutes. In combination, these books provide excellent coverage of groundwater geochemistry represented by rock–water interaction but generally do not address the conceptualization of the origin and development of solute chemistry in aquifers. Publications by Alley and others (1999), Winter and others (1998), and Poeter and others (2020) are extremely clear and helpful in general understanding of aquifer systems but are not oriented toward solute chemistry.

The first four sections of this book are largely descriptive, whereas the last four sections contain some simple computational material. Section 1 provides a general overview of basic geochemical concepts related to atomic structure, concentration, composition, and other fundamental chemical information. Section 2 presents the processes and mechanisms controlling the source and removal of solutes in aquifer systems. Section 3 looks at the geochemical control and distribution of trace elements related to human health. Section 4 provides a rationale for numerous graphical methods of solute presentation. Section 5 delivers individual field studies related to several of the major processes controlling solute chemistry. Section 6 introduces the concept of mass balance and representative control volume. Section 7 provides some examples of the geochemical evolution of major solutes with time and flow. Section 8 illustrates how hydrogeochemistry—solute in a flow environment—can quantify some critical physical parameters in hydrogeology. No attempt is made to cover contamination or other anthropogenic impacts, which are described in numerous textbooks and for which a large body of journal material exists.

This book is written with a limited number of references (a characteristic noted by all reviewers) as it is intended as a broad general overview/introduction, a gateway to the literature on this topic, not a definitive review of the literature. A Google search on a topic of interest addressed in this book will provide many excellent references. Many of the references in this book are from my publications. This is not an ego response; rather, it reflects my limited knowledge and experience. This monograph is not intended to be a definitive scholarly work but a journey of learning and discovery.

Acknowledgments

I wish to thank John Cherry for the input, inspiration, motivation, and structure from many discussions that form the basis of this monograph, as it could not have been written without his major input of time and effort. I am deeply appreciative of the thoughtful review of this monograph by:

- ❖ Professor Ian Cartwright, Monash University, Melbourne, Victoria, Australia;
- ❖ Jeff Hanor, emeritus professor, Louisiana State University, Baton Rouge, Louisiana, USA; and
- ❖ Ward Sanford, US Geological Survey, Reston, Virginia, USA.

I have accepted most of their suggestions. Thanks also to Emily Saurette for suggestions on the clarity of an earlier draft of Chapter 2 and the creation of Box 2. Special thanks go to Eileen Poeter as Technical Editor who did much to improve the readability and enhance the information on the figures as well as saving me from many embarrassing technical errors. Thanks also go to Amanda Sills for her cheerful and efficient handling the manuscript many times over its 5-year gestation period and to Neto Breda for major improvement to my crude figures.

One learns a great deal from informal discussions with your colleagues, and over many years, I have much to thank from my interactions with Anthony Kendall and David Hyndman at Michigan State University, Bill Back, Mary Jo Baedeker, Bruce Hanshaw, Blair Jones, Lenny Konikow, Chris Neuzil, Allan Shapiro, Clif Voss, and—most importantly—Ward Sanford of the US Geological Survey. I have coauthored many papers with Ward and gained an incalculable amount of knowledge from his insight and quantitative approach.

Sources of figures and data presented in tables are acknowledged in the captions. Where a citation is absent in the caption, the figure or table is original to this book.

1 Review of Hydrogeochemical Fundamentals

1.1 Chemical Principals

The aphorism “It’s not what you don’t know that gets you in trouble; it’s what you know for certain that just isn’t true” aptly captures the challenges in hydrogeochemistry. Because groundwater is hidden beneath the earth’s surface, it has often been misunderstood, leading to entrenched but inaccurate assumptions about its origin, movement, and solute composition. This monograph addresses this by examining the processes that shape the chemistry of naturally occurring (geogenic) solutes, dispelling misconceptions, and clarifying our understanding of groundwater’s complex chemical evolution.

Hydrogeochemistry differs fundamentally from physical hydrogeology in its focus and the nature of its inquiries. Physical hydrogeology primarily examines the current state and near-future changes in water levels, dealing with parameters that reflect immediate conditions without retaining a record of past influences. In contrast, hydrogeochemistry is rooted in historical processes; the composition of solutes in groundwater carries a “memory” of past interactions, sources, and transformations that may span centuries to millennia. Physical hydrogeology’s main principles are relatively straightforward, often relying on foundational concepts like Darcy’s Law. In contrast, hydrogeochemistry involves a vast array of parameters, processes, and interactions, making it more akin to solving a complex puzzle where each piece—each solute or chemical signature—contributes to a long-standing history.

In this way, physical hydrogeology reads like a straightforward narrative, while hydrogeochemistry is more of a layered detective story, where piecing together the past helps to clarify the present chemical state of groundwater and resolve some of the longstanding mysteries in water quality and resource management.

Groundwater represents an immense and critical component of Earth’s freshwater resources, comprising 99% of all liquid freshwater globally and supporting 70-75% of human water consumption as well as essential ecological functions. This vast reservoir of water affects a range of natural systems, from the health of rivers, lakes, and wetlands to the weathering of rocks and minerals, the formation of brines, and even the origin of mineral deposits. Notably, groundwater may have played a role in the origin of life on Earth: some theories suggest that warm, mineral-rich groundwater interacting with feldspar minerals produced clays with crystal structures capable of organizing amino acids into patterns, potentially leading to the first self-replicating molecules and, ultimately, life itself (Kloprogge & Hartman, 2022).

The rock formations that can store and transmit significant amounts of water are known as aquifers. A classic example is a sand deposit where groundwater fills the spaces between sand grains, providing a readily accessible source of water. Active aquifers (those

with mostly younger water) are replenished by precipitation. This water infiltrates the surface and percolates downward through the unsaturated, or vadose, zone, where both water and air occupy the pore spaces. This zone is microbially active, which generates substantial carbon dioxide that contributes to the chemical weathering of the surrounding rock minerals, typically supplying over half of the dissolved solutes found in groundwater.

As water moves from the vadose zone to the saturated zone, where all pore spaces are filled with water, it reaches the water table and continues to flow, eventually discharging into rivers, wetlands, or lakes (Figure 1).

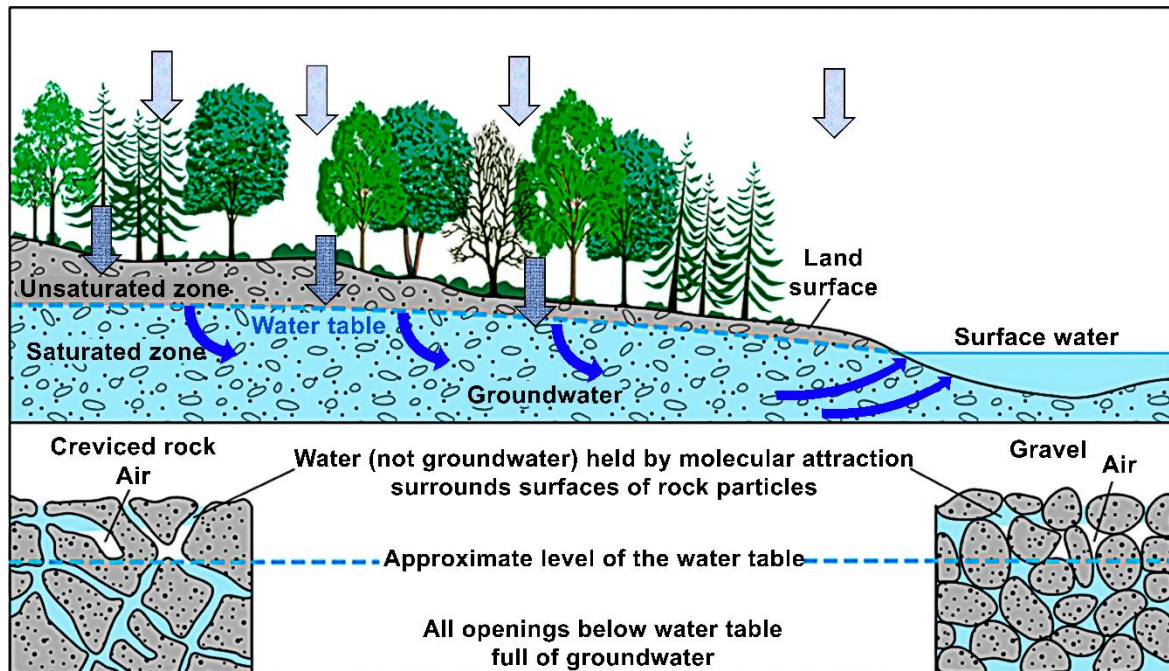


Figure 1 - Recharge from precipitation infiltrates into the porous earth materials, acquiring many of the solutes in the vadose zone (volume containing both air and water). Water and solutes then move to the water table where all pores are filled with water—the saturated zone—and ultimately discharge to a river, wetlands, or lake (modified from USGS, 2022). More complex aquifer systems are shown in Alley and others (1999), Winter and others (1998), and Poeter and others (2020).

The active freshwater aquifer system typically resides within the upper two kilometers of Earth's crust, where groundwater exhibits a blend of ages and flow paths. This groundwater mix includes small volumes of ancient water—thousands of years old—flowing through long or slow paths; moderate amounts of medium-aged water, hundreds of years old, traveling intermediate distances; and a larger proportion of young water, less than 100 years old, moving through shorter, faster flow paths. Each of these flow paths has unique age and solute characteristics shaped by the interactions and inputs encountered along its journey. The "age" of water in this context refers to the time elapsed since its last exposure to the atmosphere, marking the start of its underground journey (Figure 2).

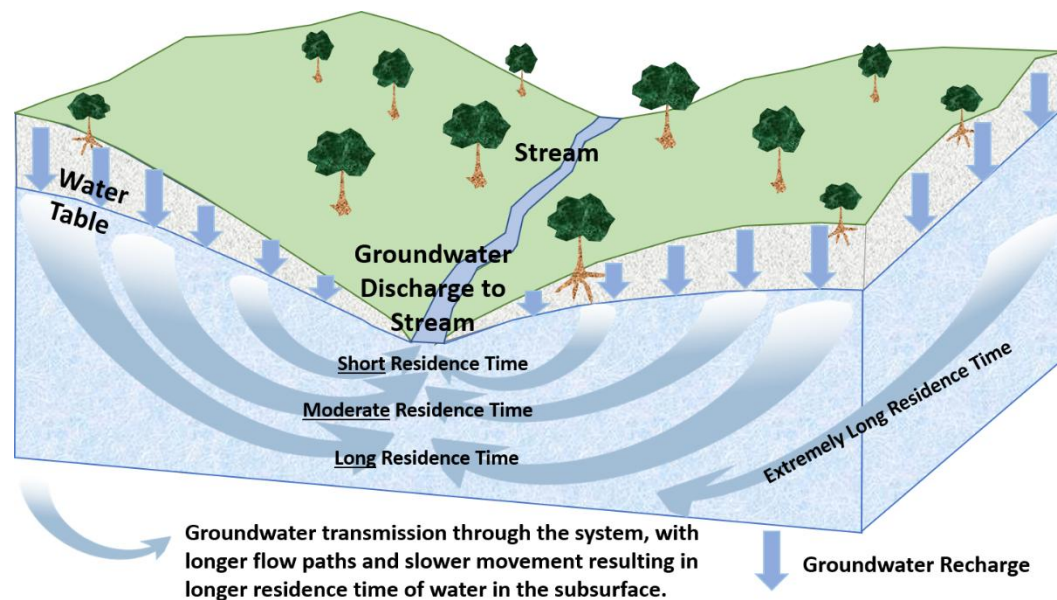


Figure 2 - Different lengths of groundwater flow lines result in water of different ages (time since recharge), experiencing different geochemical processes and environments, resulting in each flow path having a unique age, solute concentration, and composition (after Poeter et al, 2020).

Interestingly, fresh groundwater is occasionally found beneath the ocean, usually resulting from recent geological changes in sea level that trapped freshwater in these subsurface environments (Sanford, 2013). This phenomenon underscores the complexity of groundwater distribution and highlights the role of historical geological events in shaping current groundwater systems.

In this monograph, our focus is on understanding the origins and evolution of solutes within this dynamic, mixed-input environment of active aquifers. Meanwhile, a separate category of groundwater—consisting of ancient brines and fossil waters that do not receive present-day recharge—represents a vast but relatively inert reservoir, explored further in another volume of this series ([Wood, 2021](#)). This distinction between active and inactive groundwater bodies emphasizes the importance of recharge dynamics and flow paths in the study of hydrogeochemistry, as these factors fundamentally shape the solute composition and behavior of groundwater resources.

Groundwater in the active aquifers typically contains a low concentration of dissolved solutes in a ratio useful for most human and ecological needs. The fundamental criteria for the suitability of groundwater for use are based on the temperature, concentration—how much mass of an element is in a known volume of water—and composition—the relative mass of different solutes. The sources of these solutes are:

- solutes remaining from time of deposition—the so-called relic, fossil, legacy, or connate solutes;
- solutes introduced from the surface (precipitation, rivers, lakes), from adjacent, underlying, or overlying formations; and
- solutes generated from weathering and radioactive decay of the aquifer's mineral/rock framework (rock–water interaction) (Figure 3).

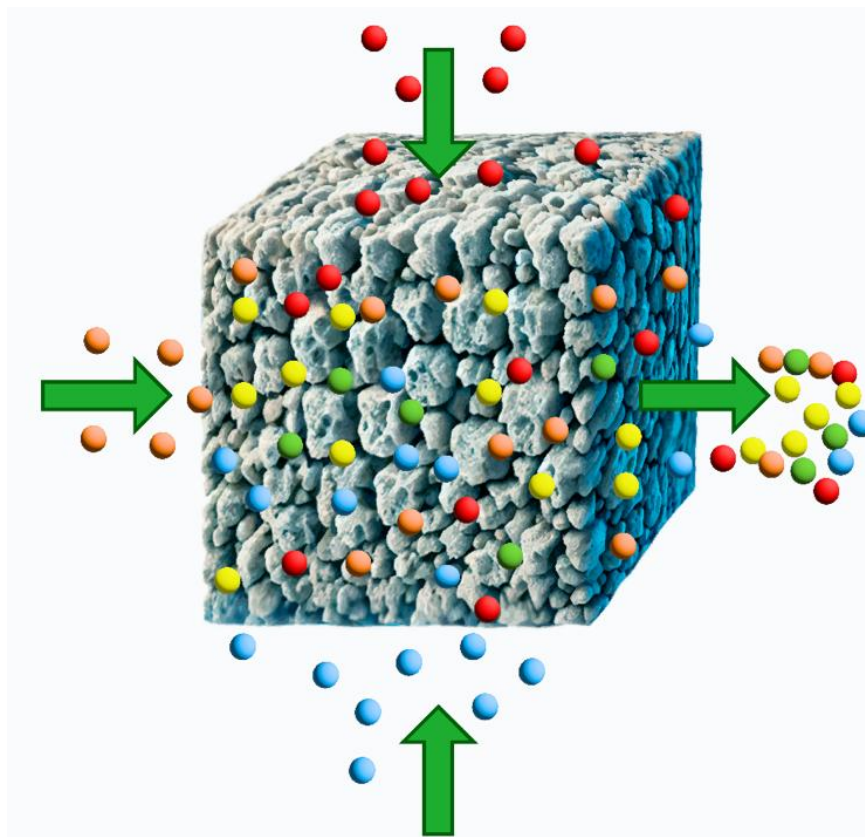


Figure 3 - Conceptual illustration of the three sources of solutes in an active aquifer. Some are derived from external sources, such as precipitation, recharging the aquifer (red); some from adjacent or underlying aquifers (orange and blue); some from “relic” or “fossil” solutes remaining from the time of deposition (green); and some from weathering “rock–water interaction” and radioactive decay (yellow). They combine to give the solute concentration and composition leaving the aquifer.

Groundwater as a global resource has become vital only relatively recently, following the development of high-capacity pumps in the late 1920s. Before this technological development, groundwater extraction was limited to low-yield wind-powered pumps and shallow-dug wells, with little attention paid to solute chemistry outside of brine production and public health concerns. The field of hydrogeochemistry in North America began to gain traction in the 1950s, spurred by the discovery that the regional distribution of secondary uranium minerals was influenced by groundwater movement. Although the focus has since shifted primarily to contaminant hydrogeology, understanding regional hydrogeochemistry remains crucial for educating hydrogeologists and for interpreting natural background processes that affect contaminant behavior.

To understand the origin and concentration of geogenic solutes in groundwater, both conceptual and quantitative models are essential. The qualitative, or conceptual, model identifies the critical factors and processes that shape groundwater chemistry, establishing a framework or hypothesis for how these elements combine to create observed solute patterns. This conceptual framework then serves as the basis for a mathematical model, allowing numerical simulations that test and refine the initial hypothesis.

This iterative process—refining the conceptual model based on simulation results and subsequently adjusting the computational model—continues until a solution emerges that aligns well with observed data. Such an approach not only enhances our understanding of current groundwater composition but also builds confidence in our ability to predict future changes and infer past conditions, advancing both groundwater management and resource conservation.

1.2 The Origin of Elements and Their Atomic Structure

Our exploration of groundwater geochemistry begins with a foundational look at the origin and structure of the elements that constitute the solutes in groundwater. The elements that make up matter on Earth have diverse cosmic origins. Hydrogen, as well as most of the helium and some of the lithium we observe, originated in the Big Bang approximately 13.7 billion years ago. The remaining elements were produced around 5.5 to 6 billion years ago when a massive supernova exploded near what would become our solar system. This supernova dispersed the elements, mineral grains, dust, and gases, which eventually coalesced to form our solar system.

In this early solar system, gravity condensed some of this material to form the Sun. Under immense gravitational pressure, hydrogen atoms in the Sun's core began to fuse into helium through nuclear fusion, releasing energy and producing a flux of gamma rays, alpha and beta particles. These particles, carried outward as solar winds, pushed lighter gases—including hydrogen, helium, methane, and ammonia—toward the outer regions of the solar system, where they eventually condensed into the gas giants: Jupiter, Saturn, Uranus, and Neptune. Heavier elements were left behind and condensed into the four inner, rocky planets—Mercury, Venus, Earth, and Mars—about 4.56 billion years ago.

Understanding the structure of these elements provides a basis for examining how they dissolve into groundwater and shape its chemical profile. The elements that originated in cosmic events billions of years ago have, through geological and chemical processes, become essential solutes in the groundwater that sustains ecosystems, human life, and countless geological processes.

Rocks are composed of minerals that are composed of elements that are composed of atoms. Atoms are composed of protons (positively charged particles), neutrons (neutral particles with no charge) in the center (the nucleus), and electrons (negatively charged particles) surrounding the nucleus (Figure 4). Within protons and neutrons, there are additional sub-particles, but they are not directly involved in the chemistry of the elements, and their discussion is beyond the scope of this monograph.

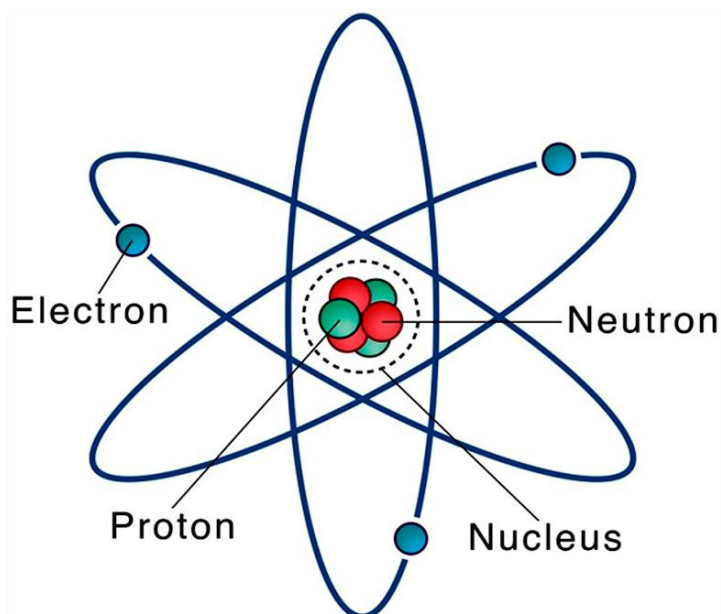


Figure 4 - Atoms are composed of protons (positively charged particles), and neutrons (particles with no charge) forming the nucleus. Electrons (negatively charged particles) move around the nucleus of this model of the lithium atom. The electron movement is more complex for elements heavier than lithium.

The elements of the universe are arranged in the Periodic Table that includes all 118 elements known in the universe (94 of which occur naturally on Earth) and organizes them in 18 columns (groups) and 7 rows (periods) depending on their chemical properties (Figure 5). The table is like a filing system where the position of each element in the table gives essential information about its structure, properties, and behavior in chemical reactions.

period	group	1	2	3	4	5	6	7	8	9	10	11	12	13	14	15	16	17	18
1		1 H																	2 He
2		3 Li	4 Be											5 B	6 C	7 N	8 O	9 F	10 Ne
3		11 Na	12 Mg											13 Al	14 Si	15 P	16 S	17 Cl	18 Ar
4		19 K	20 Ca	21 Sc	22 Ti	23 V	24 Cr	25 Mn	26 Fe	27 Co	28 Ni	29 Cu	30 Zn	31 Ga	32 Ge	33 As	34 Se	35 Br	36 Kr
5		37 Rb	38 Sr	39 Y	40 Zr	41 Nb	42 Mo	43 Tc	44 Ru	45 Rh	46 Pd	47 Ag	48 Cd	49 In	50 Sn	51 Sb	52 Te	53 I	54 Xe
6		55 Cs	56 Ba	71 Lu	72 Hf	73 Ta	74 W	75 Re	76 Os	77 Ir	78 Pt	79 Au	80 Hg	81 Tl	82 Pb	83 Bi	84 Po	85 At	86 Rn
7		87 Fr	88 Ra	103 Lr	104 Rf	105 Db	106 Sg	107 Bh	108 Hs	109 Mt	110 Ds	111 Rg	112 Cn	113 Nh	114 Fl	115 Mc	116 Lv	117 Ts	118 Og
lanthanoid series 6		57 La	58 Ce	59 Pr	60 Nd	61 Pm	62 Sm	63 Eu	64 Gd	65 Tb	66 Dy	67 Ho	68 Er	69 Tm	70 Yb				
actinoid series 7		89 Ac	90 Th	91 Pa	92 U	93 Np	94 Pu	95 Am	96 Cm	97 Bk	98 Cf	99 Es	100 Fm	101 Md	102 No				

Figure 5 - Periodic table with seven rows (periods) and 18 columns (groups) containing all known elements in the universe, 94 of which are found on Earth. The Lanthanides and Actinides series belong in the 6th and 7th periods, but to make the table fit on one page, they are commonly shown at the bottom of the table.

The periodic table organizes elements based on their atomic number—the number of protons in each atom's nucleus—beginning with hydrogen (H, with 1 proton) and ending with oganesson (Og, with 118 protons). This atomic number is fundamental, as it defines the element itself: gold, for example, always has 79 protons, silver has 47, and calcium has 20. The identity of an element is fixed by its proton count, whereas the number of neutrons can vary within atoms of the same element, forming isotopes. These isotopes differ in mass due to their varying neutron counts but retain the same chemical properties. For instance, uranium isotopes such as uranium-238, uranium-235, and uranium-234 differ in neutron number but are all chemically uranium.

An element's position in the periodic table provides insight into its electron configuration, which directly influences its chemical behavior. Only the outermost, or *valence*, electrons participate in chemical reactions, and their arrangement determines how an element interacts with others. This configuration is especially relevant to hydrogeochemistry because it dictates the element's *valence charge*, indicating whether it tends to form neutral, positive, or negative ions in solution. For example, the common ionized form of calcium, Ca^{2+} , shows a positive charge of +2, meaning it has two electrons less than its neutral state.

In geochemical contexts, our focus is largely on these valence electrons, as they determine the charge and reactivity of solutes in groundwater. Understanding the charges of solutes allows us to anticipate their interactions, behaviors, and potential reactions with other compounds in groundwater systems. This outer electron structure, therefore, plays a crucial role in shaping groundwater chemistry by influencing how elements dissolve, transport, and interact within aquifers.

The combinations of different elements form molecules—such as nitrate NO_3^- , which is composed of an atom of nitrogen N with a +5 charge, three atoms of oxygen each with a -2 charge, and thus an overall charge of -1. The bicarbonate molecule (HCO_3^-) has an atom of hydrogen with a +1 charge, one atom of carbon +4 charge, and three atoms of oxygen each with a -2 charge, and thus an overall charge of -1. Also present in groundwater are molecules with no charge such as water (H_2O) with two hydrogen atoms, each with one positive charge and one oxygen atom with a -2 charges. Commonly (but not always), uncharged solute molecules are indicated with a superscript of zero (i.e., ⁰). For example: H_4SiO_4^0 has 4 atoms of H, each with a +1 charge; one atom of Si with a +4 charge; and 4 atoms of oxygen, each with a -2-charge, resulting in a neutral molecule.

Electrons are commonly illustrated with paths resembling the configuration of planets revolving around the sun (Figure 4). This model is viable for two or three light elements of the periodic table, but the electron geometry of subshells for most elements is more nuanced. For example, the p subshell ([Box 1](#)) has several different orbital orientations that can be considered a cloud (Figure 6) of likely electron positions rather than

one specific orbit, like a planet around our sun. The quantum mechanics explanation of these electron probabilities is beyond the intended level of this monograph.

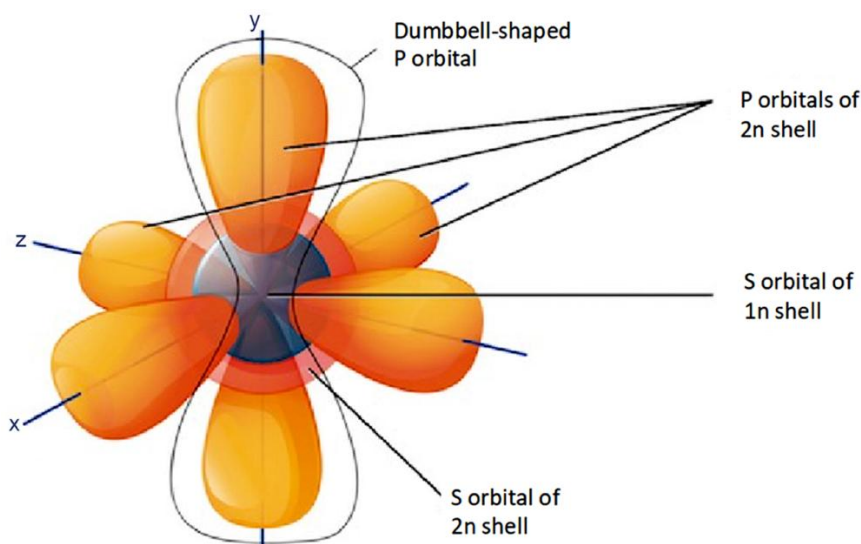


Figure 6 - Orbitals (electron paths) in the p subshell (reproduced from [the Khan Academy AP collage Chemistry](#)). Box 1 explains the shells.

A water molecule is comprised of two hydrogen (H^+) atoms (one proton each) and one oxygen (O^{2-}) atom (eight protons) that forms the stable H_2O molecule ($1s^2 2s^2 2p^6$ Box 1). One of the reasons solutes are present in water is the distribution of electrical charges on the water molecule that are asymmetrical, with the two positive hydrogen ions clustered near one end and the negative oxygen ion at the other, resulting in one end having a more positive charge and the other a more negative one (Figure 7). As the elements forming a mineral are either positively charged or negatively charged, the water molecule is attracted to the mineral face. As the water moves, it can pull the elements from the mineral. As the solution must remain electrically neutral, a corresponding oppositely charged ion from the mineral must also enter the solution.

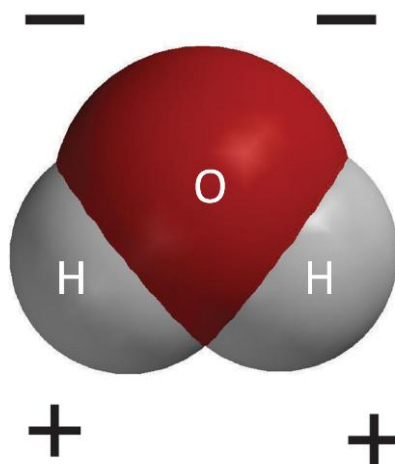


Figure 7 - Visualization of a water molecule illustrating its polar nature with one end being more positively charged and the other more negatively charged.

1.3 Groundwater Composition and Concentration of Solutes, Gasses, and Particulates

Solutes

Of the solutes present in groundwater typically, 95 percent of their mass is characterized by only seven elements or molecules (Figure 8):

- three cations (positively charged ions): calcium (Ca^{2+}), sodium (Na^{1+}), and magnesium (Mg^{2+});
- three anions (negatively charged ions): bicarbonate (HCO_3^{1-}), chloride (Cl^{1-}), and sulfate (SO_4^{2-}); and
- the uncharged silica molecule (H_4SiO_4^0).

The cations and anions charge must balance electrically as there is no net electrical charge in a water sample. The other 5 percent of their mass typically contains many additional elements in minor and trace amounts (Figure 9) that may have significant relevance to human health, ecology, agriculture, industry, and other uses.

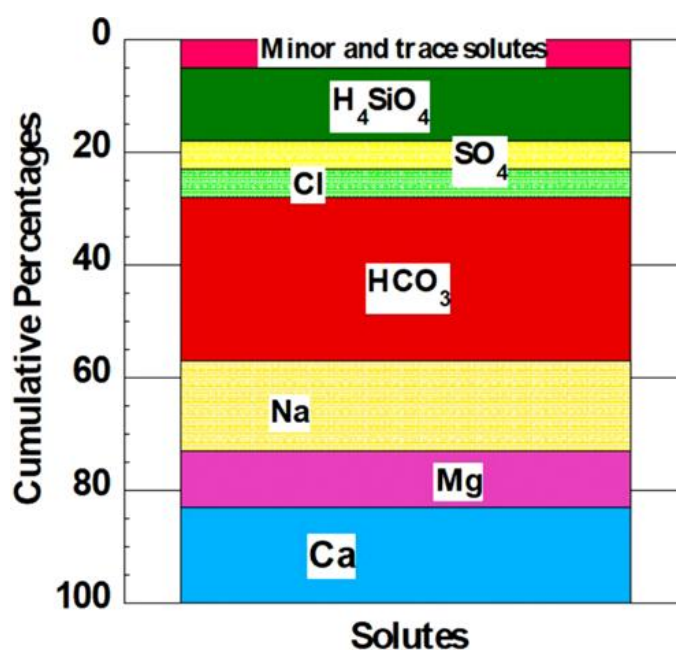


Figure 8 - The three cations (Ca^{2+} , Mg^{2+} , and Na^+), the three anions (HCO_3^- , Cl^- , and SO_4^{2-}) and the neutral silica molecule (H_4SiO_4^0) typically account for over 95 percent of the total mass of dissolved ions in groundwater. The other 84 elements combined are typically less than 5 percent of the total mass.

Elements in groundwater are typically categorized by their concentration relative to the total dissolved mass as either major, minor, or trace. Major elements are those present in a concentration greater than 1 percent of total dissolved solute mass and typically include calcium (Ca^{2+}), sodium (Na^+), magnesium (Mg^{2+}), bicarbonate (HCO_3^{1-}), chloride (Cl^{1-}), sulfate (SO_4^{2-}), and silica (H_4SiO_4^0). Minor elements are defined as having concentrations between 1 percent and 0.1 percent of total dissolved solute mass and are

typically the ions of potassium (K^{1+}), fluoride (F^{1-}), nitrate (NO_3^{1-}), and oxygen gas (O_2^0). Both major and minor solutes are generally expressed in mg/L (milligrams per liter). Trace elements are defined as having concentrations less than 0.1 percent of total dissolved solutes and are typically present in diminishingly low concentrations frequently expressed in $\mu\text{g/L}$ (micrograms per liter).

Figure 9 provides an example of some common trace elements in groundwater in both dry and humid environments in the USA (Ayotte et al., 2011). Because of the wide range of environmental conditions across the USA, these data likely reflect global groundwater solute conditions.

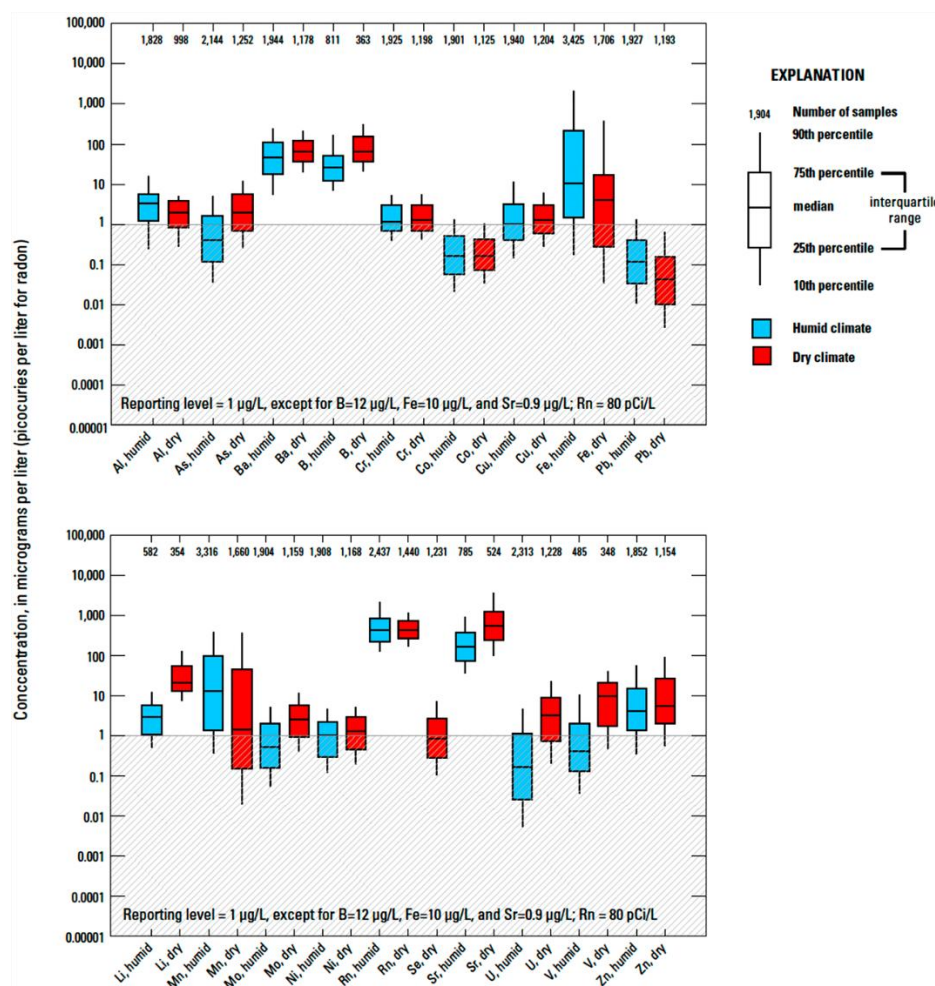


Figure 9 - Concentration, in $\mu\text{g/L}$ (micrograms per liter)—except as noted—of some common trace elements in groundwater under humid (blue) and dry (red) environments. The numerical values along the upper axis are the number of samples at the median (50 percent) value (Ayotte et al., 2011) .

Concentrations of major solutes in most modern chemical analyses are typically expressed as milligrams per liter (mg/L) (mass per volume) or one-thousandth of a gram per liter. In some literature, one can find units of parts per million (ppm) (mass of solute per mass of water plus mass of solutes). As it is generally much easier to accurately measure volume than weight in the laboratory, most analyses are given in mg/L. Some publications utilize the MKS (meter, kilogram, second) system, and results are presented in units of

kg/m³ (kilograms per cubic meter). Some publications use units of mmol/L (millimoles/liter) or µm/L (micromoles/per liter), but these units are not common.

Concentrations are usually expressed in ppm when samples have concentrations of dissolved solids greater than two thousand mg/L; thus, the density is greater than 1.00 g/cm³ and the assumption of a density of 1.00 g/cm³ is not valid. For most groundwaters of less than 1,000 mg/L, the value in ppm is numerically identical to mg/L within the accuracy of measurements but becomes numerically smaller than mg/L as the density increases. Concentration for many trace elements is given in µg/L (microgram per liter), one-millionth of a gram per liter of water, or ppb (parts per billion; [mass of solutes]/[mass of water plus mass of solutes]).

Specific conductance or electrical conductivity is a common measurement that provides a rapid approximation of the mass of solutes present and is expressed in micro-Siemens per centimeter at 25 °C (µS/cm). The value is dependent on temperature, the ionic charge, and the concentration of the dissolved ions. It is worth mentioning that TDS (total dissolved solids)—referred to more correctly as residue on evaporation—is not the same value as total dissolved *solute*s. The total solute is the sum of the solutes in mg/L. Total dissolved solids is an older method of measuring solutes predating modern chemical analyses and does not include half of the mass of the bicarbonate ion carbon that is lost as CO₂ in the analytical procedure; therefore, it is not representative of the total solutes in solution. Concentrations of average global groundwater, seawater, and brine are given in Table 1.

Table 1 - Average global concentration of major (and a few minor) groundwater solutes mg/L (Wood et al., 2022). Mean concentration of ocean water PPM is from Drever (1997). Median concentration of brines (PPM) is from a coastal sabkha in the United Arab Emirates (UAE; Wood et al., 2002). Temperature is in degrees °C, pH in standard units, and specific conductance (Sp. Cond.) is in µS/cm (micro-Siemens per centimeter).

Solutes	Average geospatial groundwater	Ocean water	Median brine UAE
Ca ²⁺	42	411	4,325
Mg ²⁺	13	1,290	6,775
Na ⁺	45	10,760	87,750
K ⁺	3.5	399	3,450
Si	17	0.5	83
HCO ₃ ⁻	214	132	56
Cl ⁻	24	19,300	176,346
SO ₄ ²⁻	31	2,710	3,917
NO ₃ - as N	0.6	1	525
F ⁻	0.24	1.3	0
DO	1.9	0.1	-
TDS	381	35,000	291,951
T (°C)	20	-	31
pH	7.2	8.1	6.6
Sp. Cond. (µS/cm)	553	50,000	224,863

Several different units are used for measuring the activities of radioactive elements; pCi/L (picocuries per liter) is the most common unit in the USA (picocurie per liter of water is 2.22 disintegrations per minute per liter). DPM (disintegration per minute per liter) is also used. However, the Bq/l (Becquerel/liter) is the preferred international unit and represents a rate of radioactive decay equal to 1 disintegration per second per liter. An exception is made for uranium that is measured in concentration units of $\mu\text{g/L}$ owing to its long half-life of ≈ 4.5 billion years; thus, it has an extremely slow rate of disintegration.

Nearly all the 73 elements in the ocean are present in groundwater, but most are in extremely low concentrations and are not detected by normal analytical methods. The analytical limit for typical analyses is approximately 1×10^{-9} m/L (moles per liter). As there are 6.022×10^{23} atoms (Avogadro's number) in one mole (m) of an element, there must be at least 6.0×10^{14} atoms of the element per liter present before it can be detected by most of the common analytical methods.

As a reminder, a *mole* is the weight in grams of 6.022×10^{23} atoms of that element or molecule. For example, a mole of sodium will have 6.022×10^{23} atoms and weigh 22.99 grams (atomic weight of Na), a mole of chloride will weigh 35.453 grams of Cl, and a mole of NaCl (halite) weighs 58.443 grams. When reactions take place in water, the related concentration concept of *molarity* (M) is occasionally used. Molarity (M) is defined as the number of moles of a solute in a liter of solution (weight per volume). A similar and sometimes confusing term, *molality* (m), is defined as the number of moles of solute per kilogram of solution (water and solutes), that is, weight per weight. Molarity (M) and molality (m), like mg/L and ppm, have the same numerical value within analytical error for most fresh groundwater. Conversion of mg/L to Molarity (M) is the value in milligrams divided by the atomic weight of the element in milligrams. Thus, for example, 65 mg/L of calcium is (65/40,078) or 0.001622 M (1.622×10^{-3} M). Chemical reaction equations are generally understood to be written in moles; thus, 2 moles of hydrogen (H) combine with one mole of oxygen (O) to make one mole of water (H_2O).

The concentration distribution of individual solutes in an aquifer system with many samples is commonly illustrated using the *box-and-whisker*, or *box* diagrams (Section 4.2.5), where concentration is on the vertical axis with 75th and 25th greater than percentiles illustrated as the top and bottom of the box and the 90th and 10th percentiles as the whiskers (Figure 10) Also commonly shown is the number of samples used in the analysis, which is typically placed above the top whisker.

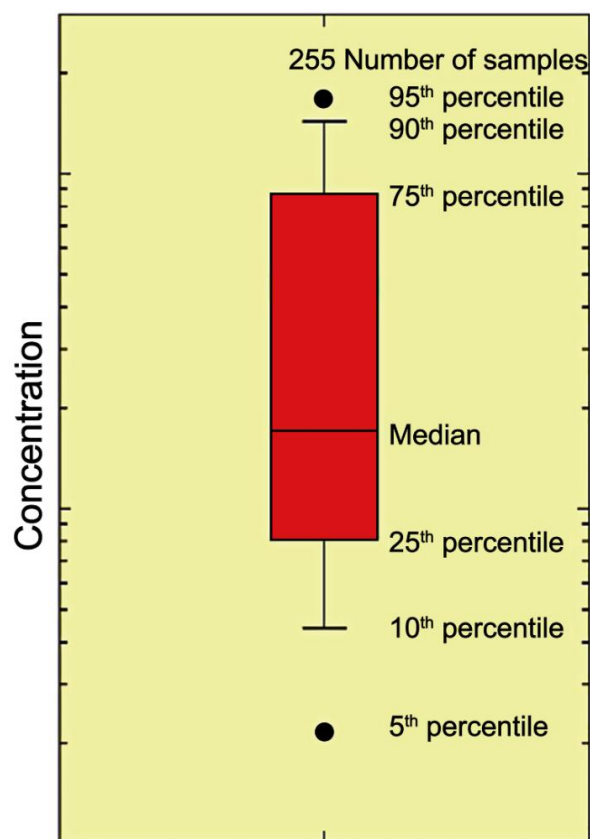


Figure 10 - Box-and-whisker plot of solute concentrations. The median value is the number in which half the concentrations are greater, and half are less. The numerical values at the top are the total number of samples, the horizontal lines indicate concentrations of samples within the 10th, 25th, 50th (median), 75th, and 90th percentiles. For example, the 25th percentile means that 25 percent of the samples have a concentration less than this value (Shand et al., 2007).

In addition to box-and-whisker diagrams, cumulative frequency diagrams provide an additional way to illustrate concentration distribution in large chemical data sets. Data from 7,000 samples from the US Geological Survey (USGS) National Water Quality Assessment (NAWQA) database (retrieved December 15, 2023) are shown in Figure 11. The cumulative frequency distribution of major ions illustrates a significantly different concentration distribution between the individual ions. For example, 5 percent of the samples have a calcium concentration of less than 2 mg/L, and 95 percent have values of less than 150 mg/L (Figure 11). Solute data can be graphically expressed in many ways, some of which are covered in Section 4 of this monograph.

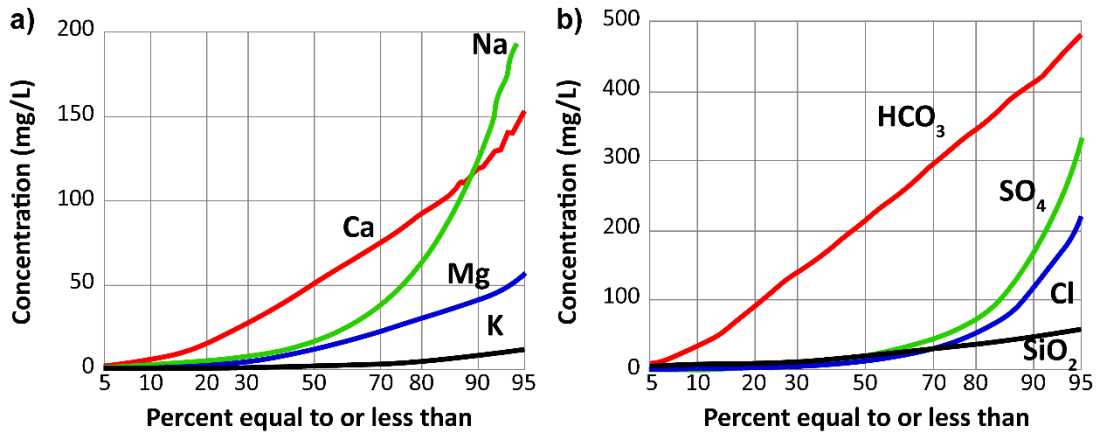


Figure 11 - Cumulative frequency within the 5th to 95th percentile range of a) major cations and b) major anions. The vertical concentration scales are different, 200 mg/L for cations and 500 mg/L for anions. Analyses are from approximately 7,000 representative groundwater samples from the US Geological Survey NAWQA 2023 database.

Large data sets can be displayed on maps, for example several million data points are shown in Figure 12 through Figure 18 to illustrate modeled (predicted) concentration of solutes in groundwater based on GML (geospatial machine learning) for major elements, several minor elements, pH, and temperature (Wood et al., 2022).

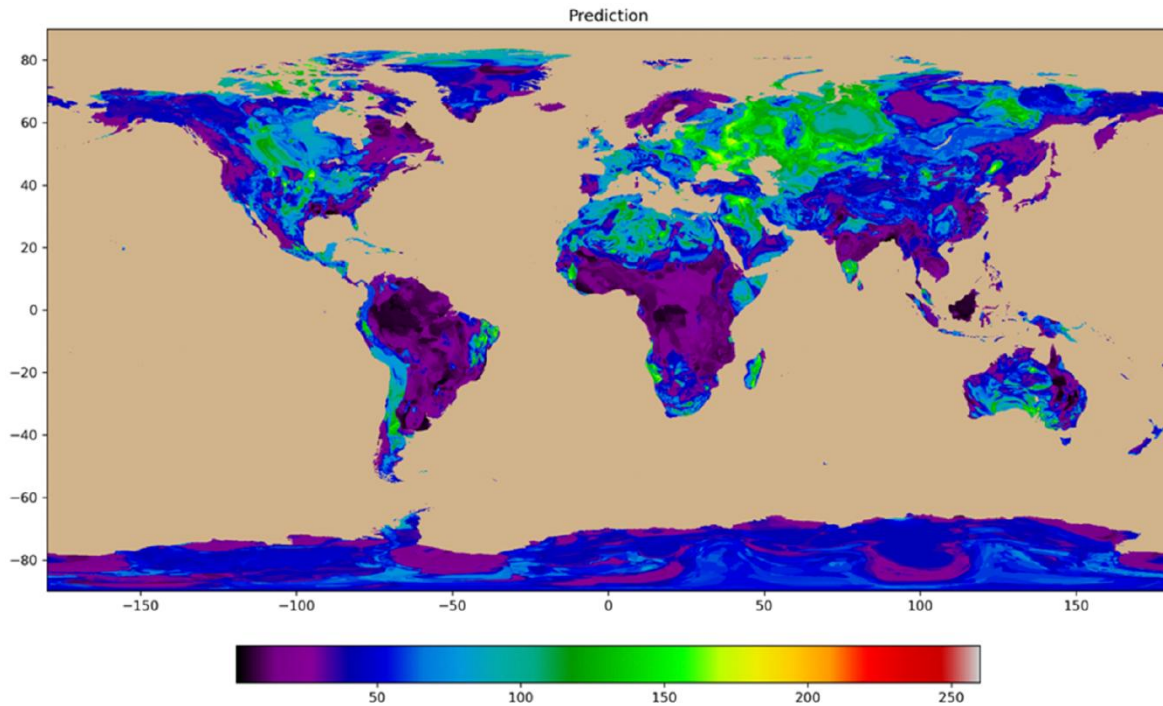


Figure 12 - Geospatial Machine Learning map of modeled calcium concentration distribution in groundwater, in mg/L (reproduced from Wood et al., 2022).

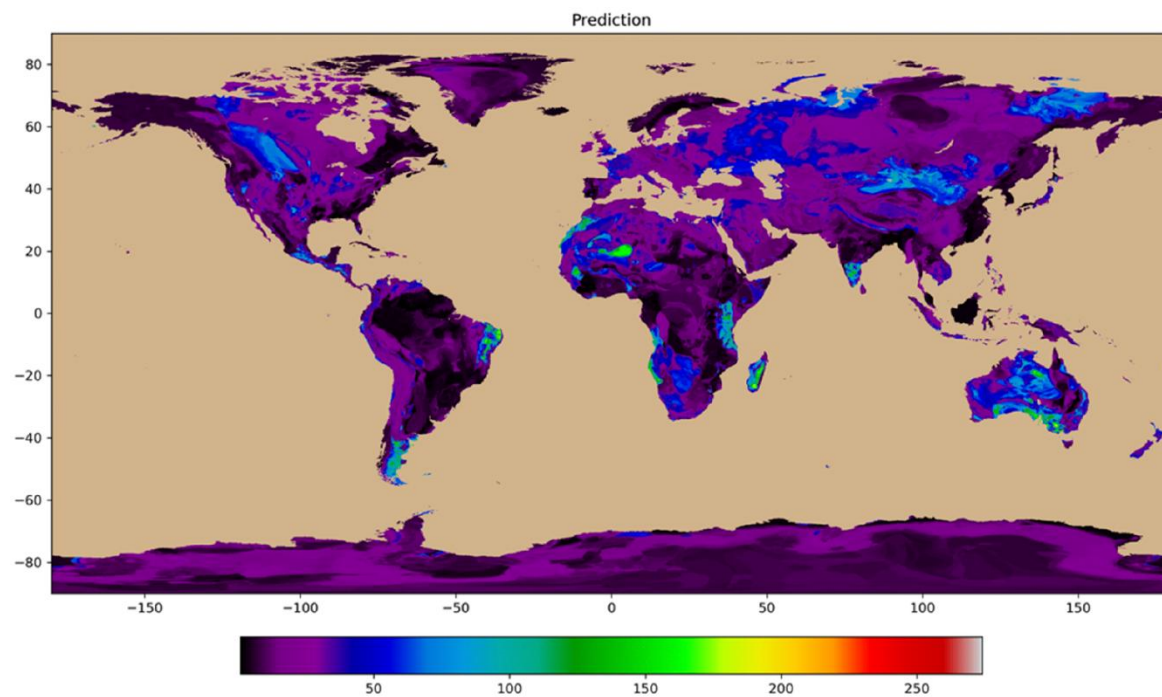


Figure 13 - Geospatial Machine Learning map of modeled magnesium concentration distribution in groundwater, in mg/L (reproduced from Wood et al., 2022).

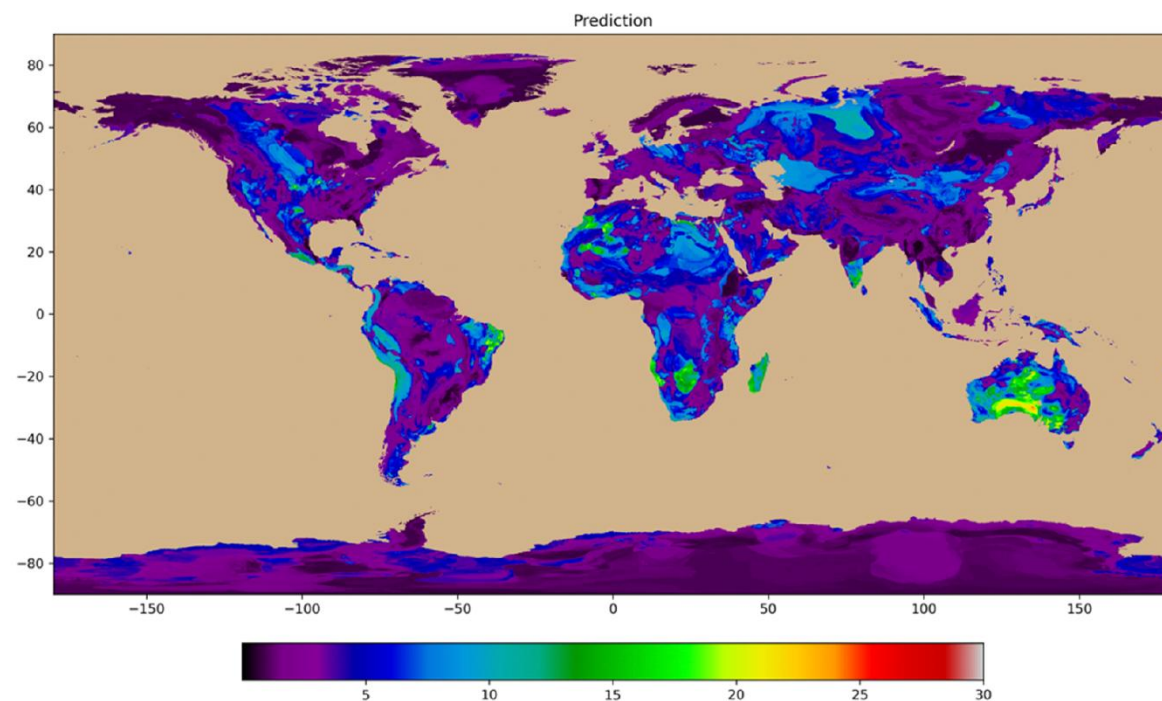


Figure 14 - Geospatial Machine Learning map of modeled potassium concentration distribution in groundwater, in mg/L (reproduced from Wood et al., 2022).

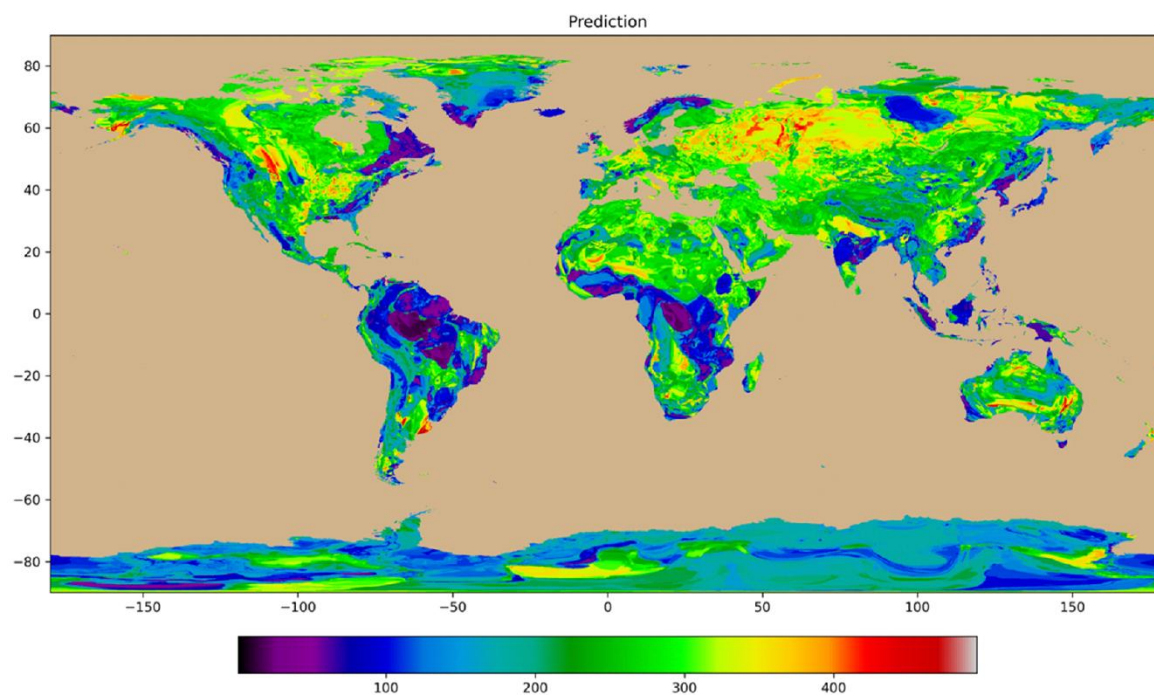


Figure 15 - Geospatial Machine Learning map of modeled bicarbonate (as alkalinity) concentration distribution in groundwater, in mg/L (reproduced from Wood et al., 2022).

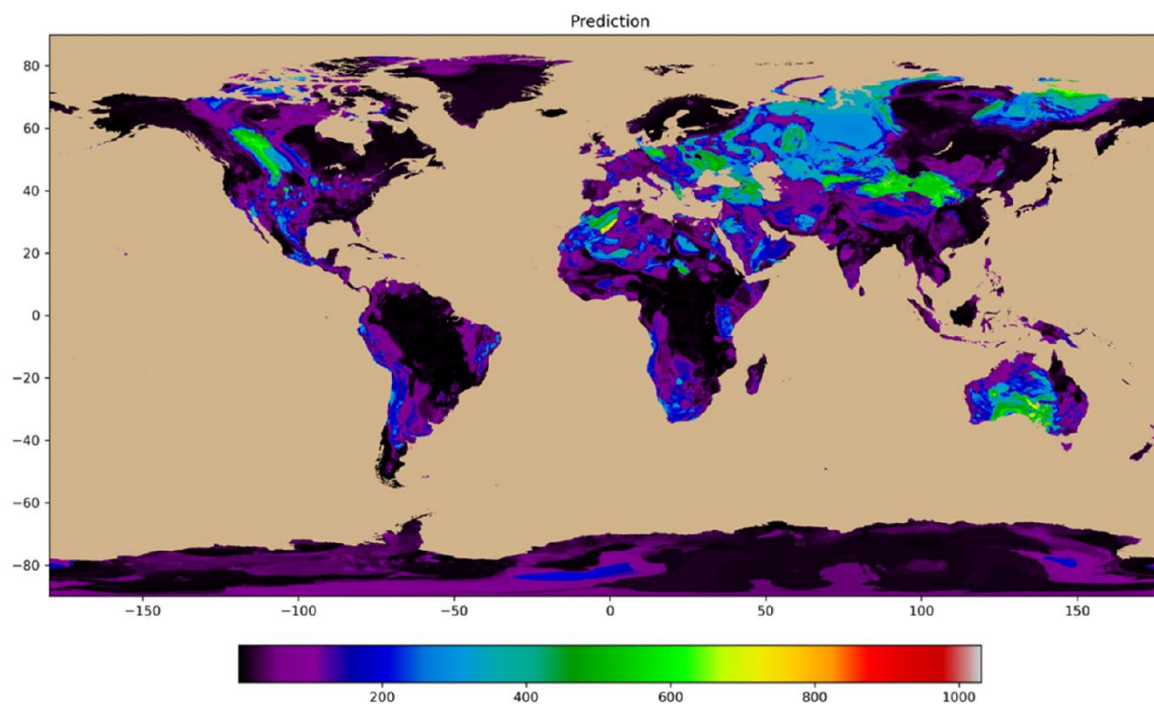


Figure 16 - Geospatial Machine Learning map of modeled sulfate concentration distribution in groundwater, in mg/L (reproduced from Wood et al., 2022).

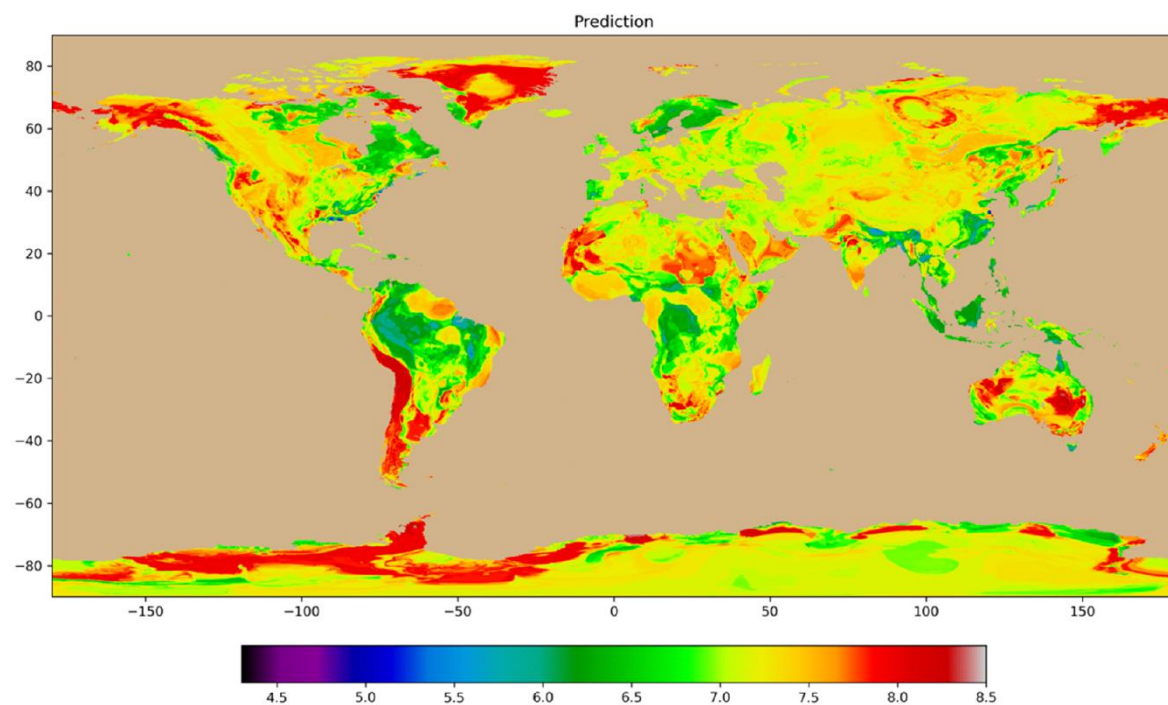


Figure 17 - Geospatial Machine Learning map of modeled pH distribution in groundwater (reproduced from Wood et al., 2022).

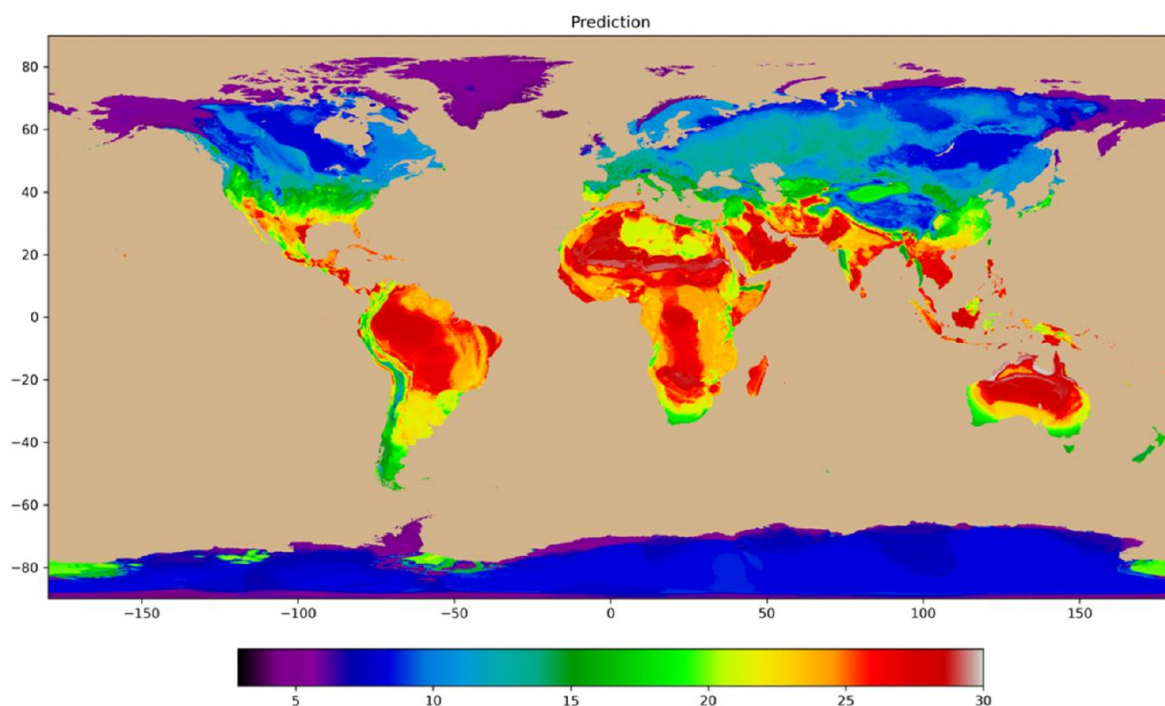


Figure 18 - Geospatial Machine Learning map of modeled groundwater temperature distribution in groundwater, in °C (reproduced from Wood et al., 2022).

The concentration of solutes in groundwater varies due to many geological, geochemical, hydrogeological, and climatic factors. The natural concentration variability in an aquifer in time and space can be visualized as analogous to an undulating surface where the vertical elevations represent concentration (Figure 19).

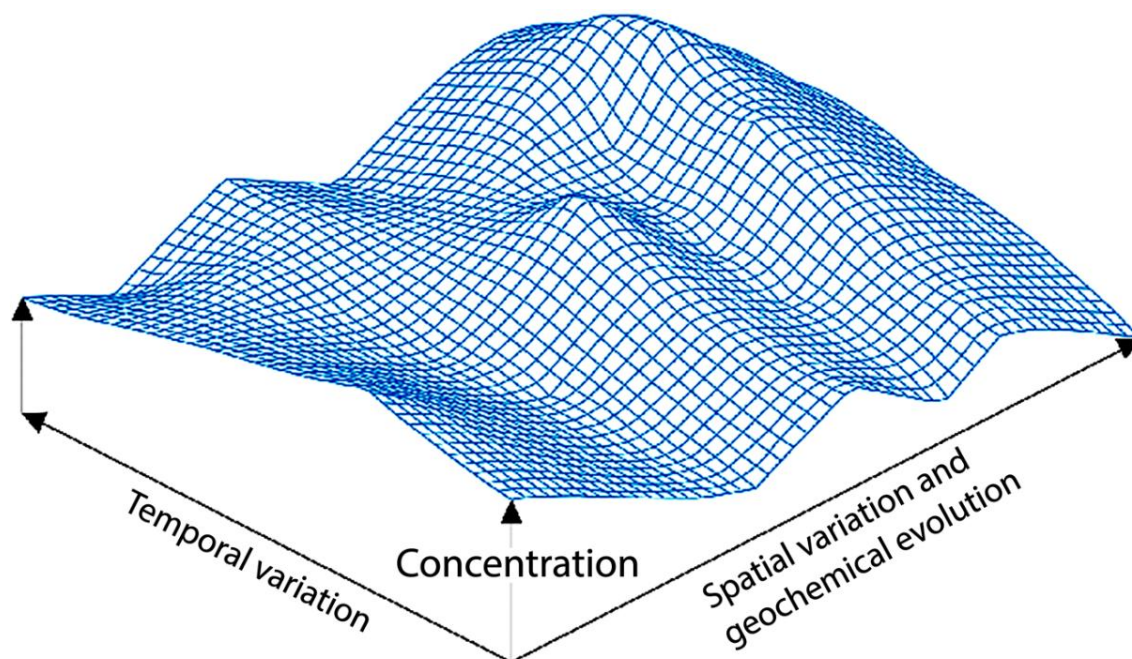


Figure 19 - Solute concentration variation in time and space in an aquifer can be visualized as changes on a topographic surface. The concentrations vary due to variations of landscape, climate, lithology, residence time, recharge, and other factors (modified from Shand et al., 2007).

Gases

The concentration of gases dissolved in groundwater is generally measured in both mg/L and ppmv (parts per million per volume) of groundwater. The partial pressure of an individual gas is also used to measure concentration and is equal to the weight of the individual gas divided by the total weight of gases in the sample (sum of all gases). For example, the dry atmosphere is composed of 780,000 ppm nitrogen, 209,400 ppm oxygen, 9,300 ppm argon, 400 ppm carbon dioxide, and other gases, adding up to 1,000,000 ppm (100 percent). Therefore, the partial pressure of carbon dioxide is $400/1,000,000$ or 0.000400. This value is sometimes expressed as the logarithm to the base 10; thus, (\log_{10}) of 0.000400 is -3.398 (the minus sign in logarithms indicates the numerical value is less than 1).

Atmospheric gases such as nitrogen (N_2), oxygen (O_2), carbon dioxide (CO_2), methane (CH_4), hydrogen (H_2), helium (He), neon (Ne), argon (Ar), and krypton (Kr) are commonly dissolved in groundwater. When groundwater is brought to atmospheric pressure and temperature by pumping, some of these elements will form bubbles and escape to the atmosphere; thus, accurate sampling can be challenging (IAEA, 2013). Noble gases in the atmosphere dissolved in recharge are a valuable tool for the determination of recharge temperatures, as there is a strong correlation between gas solubility and temperature. Gases are also generated within the aquifer system by radioactive decay; for example, radon-222 (^{222}Rn) gas is generated from the decay of radium-226 (^{226}Ra); helium-4 (4He) from decay of uranium-238 (^{238}U); and argon-40 (^{40}Ar) by the decay of potassium-40 (^{40}K).

Groundwater includes several chemically generated gases. Most of the carbon dioxide (CO_2) is generated in the vadose zone by the oxidation of organic plant material by root, insect, fungal, and bacterial respiration. Significant amounts are converted to bicarbonate ions (HCO_3^{1-}) by reaction with water and the mineral framework of the aquifer. A change in redox conditions (Section 2.6.4) is a process that can generate gases from solutes. For example, nitrate (NO_3^{1-}), the oxidized form of nitrogen, can be reduced to neutral nitrogen gas (N_2) that subsequently may escape into the atmosphere, removing nitrogen from the aquifer system. Similarly, sulfate (SO_4^{2-}), the oxidized form of sulfur, can be reduced to hydrogen sulfide (H_2S) gas that can then escape as gas or react with the other minerals present, removing sulfur from the solution. Dissolved organic carbon (DOC) can be converted to methane (CH_4) under reducing conditions and escape from an aquifer as a gas.

The solubility of gases in groundwater is a function of temperature, pressure, and total solutes. The solubility of five gases common to groundwater as a function of solubility and temperature is shown in Figure 20a. Figure 20b depicts the solubility of oxygen as a function of temperature for three different pressures.

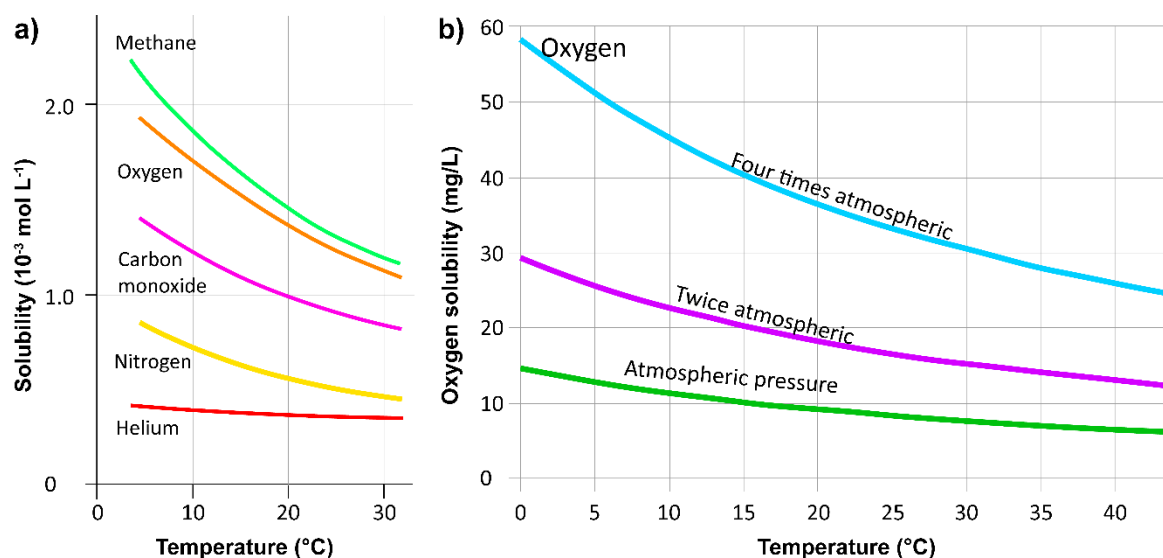


Figure 20 - a) Solubility (in 10^{-3} moles per liter) as a function of temperature for five common gases in groundwater. b) Solubility of oxygen (in mg/L) in fresh groundwater as a function of temperature at three different atmospheric pressures.

Particulates

The transport of particulate material is not commonly considered a part of groundwater hydrogeochemistry. However, particulate transport (referred to in the soil literature as *illuviation*) of organic material and iron hydroxide particles is common in the near-surface of the aquifer system and is critical in forming soils. Bacteria and viruses are common particulate materials that, under certain conditions, are mobile in groundwater systems. This type of transport is not intuitively obvious; however, numerous experiments and observations document the process. For example, the transport of cesium-134 sorbed

on clay particles was documented as clay particles moved downward approximately 25 cm in an aquifer during a 44-day recharge experiment (Goss et al., 1973). Similarly, glass particles containing cesium-137 from the 1986 nuclear accident in Chernobyl, Ukraine, were observed to a depth of approximately 5 cm in the surface profile of the sabkha in Abu Dhabi, United Arab Emirates, in 1999, 13 years after the accident (Figure 21).

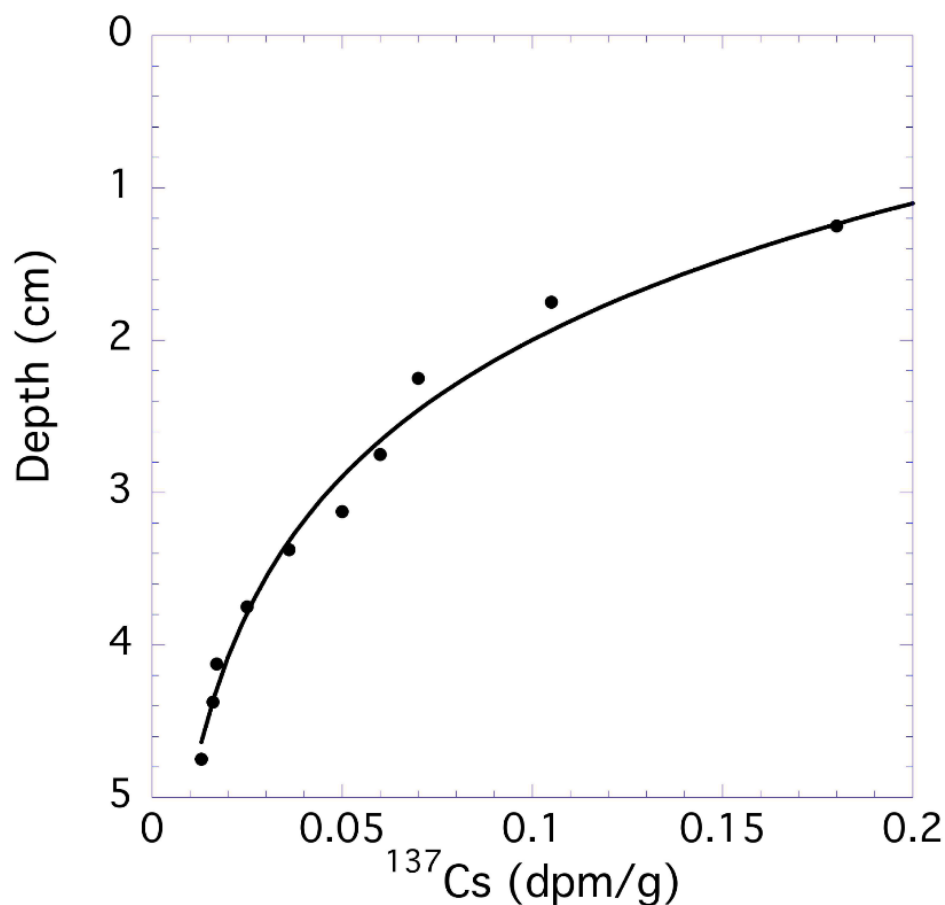


Figure 21 - Depth of penetration of glass spheres in the Abu Dhabi sabkha 13 years after the Chernobyl nuclear accident.

Transport of particulate material, including bacteria and viruses, occurs more readily in fractured and karst aquifers because they typically have larger pore openings than clastic aquifers. Some bacterial transport has been documented over hundreds of meters (Mahler et al., 2000). It has been postulated that particulate organic carbon penetrated at least 22 meters into the unsaturated zone of the Ogallala formation in the Southern High Plains of Texas, USA (Wood & Petraitis, 1984). This karst-like aquifer is composed of carbonate-rich alluvial fan material with increased porosity owing to weathering of the carbonate minerals, permitting the transport of particulate organic material. This material is then oxidized at depth, forming a concentration 60 times that of atmospheric CO₂, that further increases the weathering of carbonate minerals in a positive feedback loop (Figure 22).

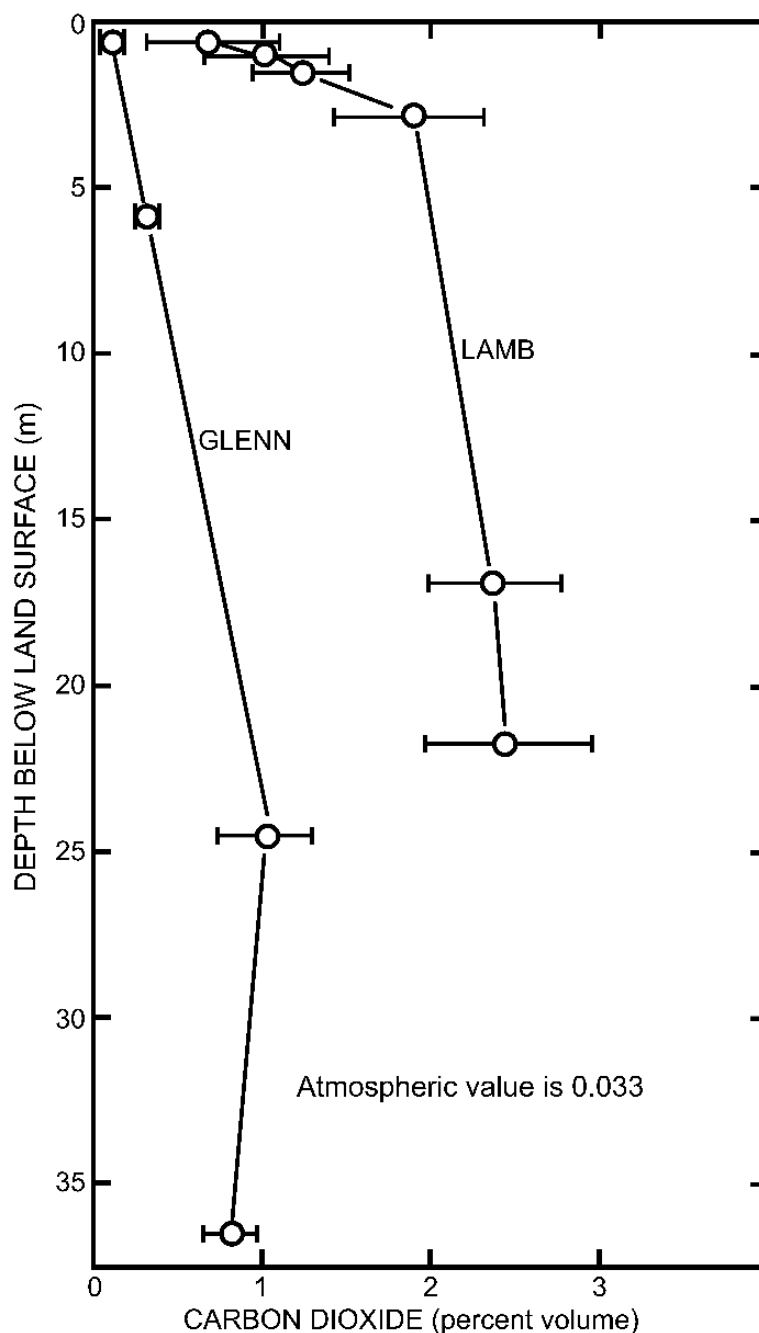


Figure 22 - Concentration (percent volume) of carbon dioxide in the unsaturated zone from two sites—Glenn and Lamb—in the unsaturated zone of the Ogallala formation in the southern High Plains of Texas, USA, illustrating the elevated concentration of carbon dioxide (nearly 60 times greater than atmospheric at the Lamb site; reproduced from Wood & Petraitis, 1984).

1.4 Water Isotopes

Water isotopes can play an important part in our detective story of understanding the history of water and solutes. An isotope of an element has the same number of protons and electrons but differs in the number of neutrons in its nucleus; thus, they have different atomic weights. The presence of isotopes is the reason why one observes fractional atomic weights. For example, the atomic weight of oxygen is 15.9994, not 16.0000, because of the

presence of isotopes other than ^{16}O . Oxygen has 17 known isotopes ranging in weight from ^{12}O to ^{28}O , of which ^{16}O , ^{17}O , and ^{18}O are stable. Hydrogen has seven isotopes ^1H to ^7H , of which ^1H and ^2H are stable; ^2H is sometimes referred to as deuterium (from Greek *deuteros*, meaning “second” or 2 neutrons). The most common radioactive hydrogen isotope, ^3H , is known as tritium (from Greek *tritos* meaning third or 3 neutrons).

The difference in weight means that different isotopes of the same element will behave differently in physical processes. That is, ^{16}O will behave differently than ^{18}O during evaporation or freezing of water. Any phase change from gas to liquid or liquid to solid creates a difference in the abundance of the isotopes remaining in the current phase and the new phase, and this can be very helpful as an indicator of the process the water or solutes may have experienced. You can conceptually think of the lighter isotopes having greater vibration energy per unit mass. For example, the lighter isotopes of oxygen (e.g., ^{16}O) in evaporating water will escape to the atmosphere in preference to the heavier isotopes; therefore, the remaining water will be isotopically heavier with evaporation. In contrast the remaining water is lighter during the formation of ice. The same physics apply to all solutes as they change phases.

Owing to the small mass difference between isotopes, a ratio is used to express the relative difference in isotope mass between the sample and a standard. The analytical value uses the delta (δ) notation and is expressed as ‰ or *per mil* (per thousand) owing to multiplying the ratios by 1,000 as seen in Equation (1).

$$\delta^{18}\text{O} = \left(\frac{\left(\frac{^{18}\text{O}}{^{16}\text{O}} \right)_{\text{sample}}}{\left(\frac{^{18}\text{O}}{^{16}\text{O}} \right)_{\text{standard}}} - 1 \right) 1,000 \quad (1)$$

Thus, when the oxygen isotopes of water are evaluated, they are expressed in terms of delta notation, for example as $5.2 \delta^{18}\text{O}\text{‰}$. Note the convention is to use the heavier of the two isotopes in the numerator when comparing a ratio $^{18}\text{O}/^{16}\text{O}$. One common reference standard for hydrogen and oxygen in water is VSMOW (Vienna Standard Mean Ocean Water); another is VPDB (Vienna Pee Dee Belemnite *americana*), which is named for a fossil in the Pee Dee Formation. It is common—though not universal—to include the reference standard as a subscript on the bottom right of the expression, for example $3.8 \delta^{18}\text{O}_{\text{VSMOW}}\text{‰}$. Identification of the standard is important as the calculated numerical values vary significantly depending on the reference standard.

The global meteoritic line of water is constructed from global precipitation collected at or near sea level from the Arctic through the Equator to the Antarctic and illustrates the impact of temperature (evaporation) on isotope ratio (Figure 23). A figure, with the $\delta^2\text{H}\text{‰}_{\text{VSMOW}}$ on the vertical axis and $\delta^{18}\text{O}\text{‰}_{\text{VSMOW}}$ on the horizontal axis, is commonly used to illustrate the range of water isotopes from a study area. In general, water

isotopes become lighter toward the continental interior (due to rainout as heavier water falls first) with increasing latitude (due to decreasing temperature, as lighter isotopes vibrate faster at a given temperature and thus do not form rain drops as easily) and with increasing elevation (due to a combination of decreasing temperature and rainout).

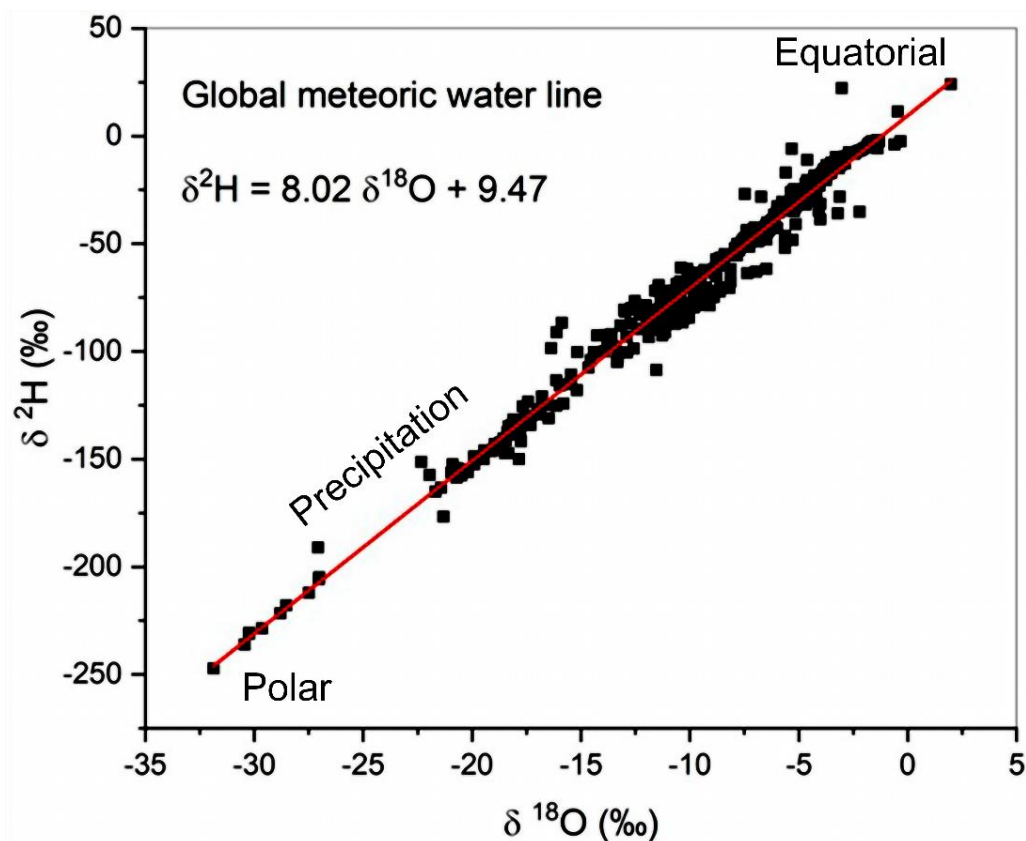


Figure 23 - Global meteoric water line showing the effect of temperature on water isotopic ratios with the isotopically light values from the cold polar areas and the isotopically heavy from the warm equatorial areas reference VSMOW (data from IAEA, 2013).

The meteoric data set (Figure 23) is commonly expressed by the slope of the best fit line, $8.02 = (\delta^2\text{H}/\delta^{18}\text{O})$ and the $\delta^2\text{H}$ intercept of 9.47 at $\delta^{18}\text{O}=0$, expressed as the equation of a line as shown in Equation (2).

$$\delta^2\text{H} = 8.02 \delta^{18}\text{O} + 9.47 \quad (2)$$

Groundwater commonly receives precipitation water that has undergone evaporation, thus it is isotopically heavier and has a smaller slope and different intercept than precipitation (Figure 24).

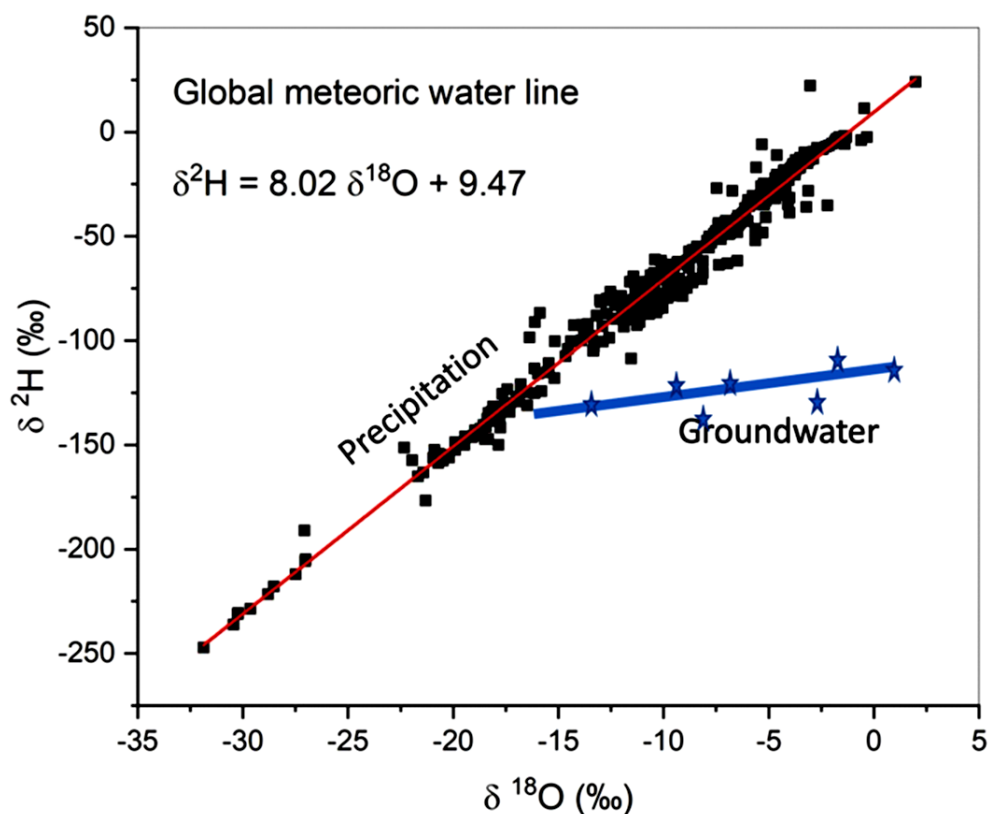


Figure 24 - Isotope ratios of global precipitation and average groundwater. Groundwater is typically isotopically heavier and exhibits a different slope and intercept than local precipitation. This is interpreted as a sign of evaporation of water prior to recharge.

In addition to water isotopes, several stable isotopes of major and minor solutes are commonly evaluated, including $\delta^{13}\text{C}$, $\delta^{15}\text{N}$, $\delta^{34}\text{S}$, and $\delta^{87}\text{Sr}$. It is beyond the scope of this monograph to discuss these and other isotopes in detail. More details can be found in Clark (2015), Cook (2020), and Diamond (2022).

Radioactive carbon-14 (^{14}C ; half-life of 5,730 years) and hydrogen-3 (tritium; half-life of 12.3 years) are two radioactive elements that have been used to date groundwater from the last time it was exposed to the atmosphere. The half-life of an element is the length of time that half of the mass of the element will decay. Thus, after two half-lives, only one-fourth of the original material remains, and after three half-lives, only 12.5 percent of the original material exists. The concept of half-life decay is illustrated in Figure 25. Analytically, the range of years suitable for dating is generally limited to approximately ten half-lives or about 1/1,000 of the original concentration. Thus, in general, ^{14}C has a maximum of about 50,000 years and tritium of about 120 years, depending on the analytical method. Other isotopes have also been used for dating, but they are not common. More details can be found in Clark (2015), Cook (2020), and Diamond (2022).

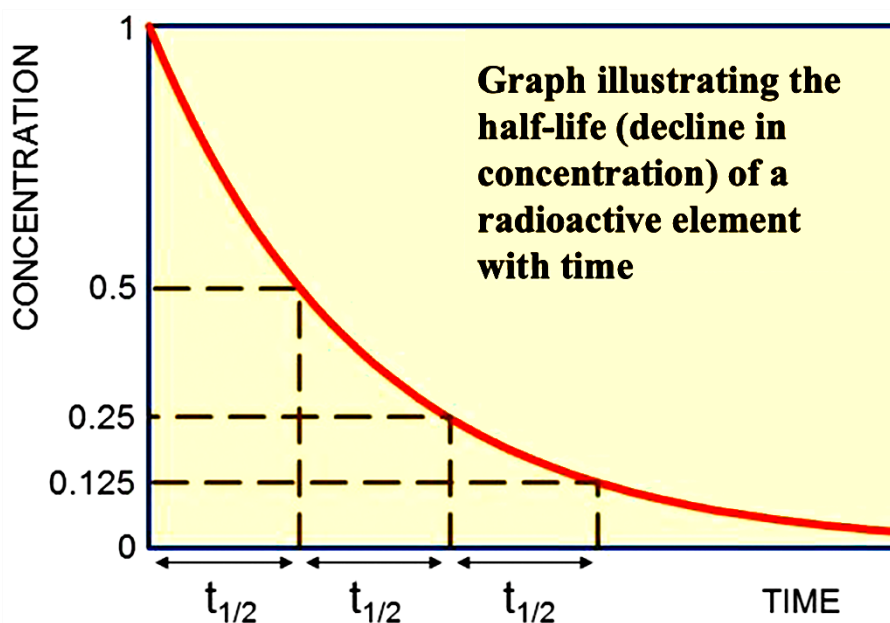


Figure 25 - Half-life is a measure of the decline in concentration with time. Thus, after one half-life, half of the element is gone; after three half-lives, only one-eighth of the original mass remains. After about ten half-lives, the concentration becomes very low ($1/1,000$ of the original) and approaches the analytical detection limit. Thus, limiting its usefulness in dating (modified from Cook, 2020).

Whereas it is analytically relatively easy to acquire the radioactive age of groundwater, it is generally difficult to interpret the results owing to the mixing of the different lengths of flow paths captured in sampling. For example, different ages are commonly encountered in wells with long screens or open intervals and are mixed in the sampled water. Extreme care is necessary in choosing a suitable aquifer system, as dating is generally very sensitive to the heterogeneity of the flow paths and length of recharge events. However, dating can be extremely useful in determining if groundwater is old (no tritium) or young (presence of tritium). This is discussed in Section 8.

The isotopes of solutes and water isotopes have provided an interesting and valuable tool to unravel the history of water and solutes in aquifer systems. However, their study and use are beyond the scope of this monograph; excellent texts devoted to this subject are Clark (2015), Cook (2020), and Diamond (2022).

1.5 Collection of Groundwater Samples

Collecting water samples from an aquifer is commonly limited to springs, baseflow, and existing wells—called *boreholes* or *bores*; in many English-speaking countries. The term bores is used to distinguish drilled wells from shallow hand-dug wells constructed with picks and shovels. In the USA and Canada, most wells are drilled with rotary or percussion methods; thus, the use of the term *wells* rather than *bores* is common. The term *well* is used in this monograph, and the modifier *dug* is only added as necessary. Wells drilled in unconsolidated sediments have metal or plastic casing to keep the formation from collapsing into the well, and some sections of the pipe contain screens to allow water to

enter the well while excluding sediment. The screens are made of stainless steel, bronze, or plastic with different opening sizes to prevent sediment from entering the well with the groundwater. Wells in consolidated sediment or solid rock often have a short surface casing to exclude weathered and broken material, then an open hole with no casing or screen for the remainder of the depth. Collecting a sample from this or a multiple-screened environment integrates the water and solutes from all producing zones. In contrast, sampling from a *piezometer*—a well that is only open to the aquifer over a short vertical interval of a few centimeters—provides a point for collecting a sample reflecting groundwater from a single flow path (i.e., a nonintegrated sample) as shown in Figure 26.

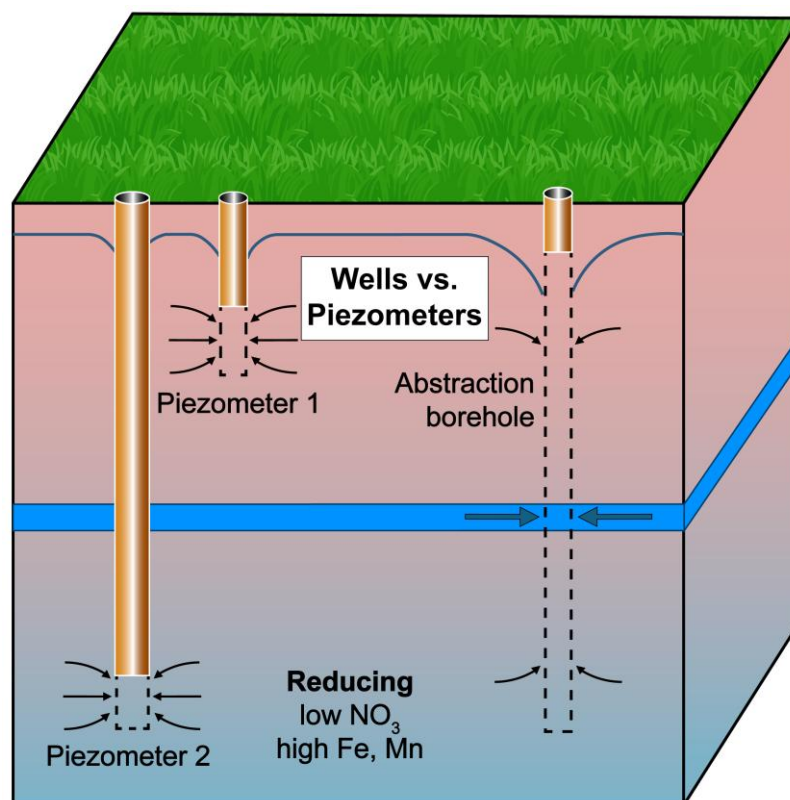


Figure 26 - Sampling from a piezometer—a small vertical opening for water to enter—provides a point sample. Sampling from a well or borehole—large vertical opening for water to enter—represents an integrated or combined sample. The shade of coloring reflects different concentrations in this aquifer. The thin, high, permeable blue-colored bed has substantially different water chemistry that is included in the sample from the well but not the piezometers. Openings of wells and piezometers may be screens in loose uncemented sediments but may be an *open hole* in igneous, carbonate, cemented sandstone, or metamorphic rocks (modified from Shand et al., 2007).

There are two general approaches to sampling for chemical analysis, depending on the goals of the project. One involves collecting the groundwater sample from existing wells, springs, and river base flow; this is by far the most common in regional studies because they are spatially available in many areas and provide a vertically integrated solute sample.

The other approach is to install piezometers at specific depths—*point samplers*—aimed at determining the hydrogeochemical interactions at that point in the aquifer. For most water supply wells, the intake intervals are long and draw water from more than one transmissive zone; each may have a different mineralogical makeup and be of different age. These samples are blended or mixed when the well is pumped so that the composition may be different from the local chemical equilibrium in each layer. The point sampling devices have vertical intakes short enough for collecting water from specific layers so that calculations based on thermodynamic models and age have relevance to the in-situ conditions.

However, the use of piezometers is uncommon in regional studies because of the significant cost of drilling and installing piezometers and the difficulties in sampling from their typically small diameter. In contrast, piezometers are common in groundwater contamination studies. Hence, one of the uncertainties in the integrity of many regional groundwater studies is a lack of knowledge about blending of groundwater in the samples; this uncertainty is only minimally addressed in the hydrogeochemical literature. However, if a given study aims to assess the suitability of the water for drinking or other uses, then knowledge about blending is not needed because sampling results pertain to the usefulness of the blended water produced by the wells.

Trace element collection from a typical steel well with a metal pump and bronze well screen lends itself to potential contamination of some metals; thus, depending on the element in question, it may require specially constructed plastic or stainless-steel well screens and pumps for sampling. Analyses of trace levels of solutes typically require laboratories with special “clean” rooms where technicians wear unique element-free apparel to minimize potential contamination from hair, perspiration, and skin. All reagents are extremely pure, and analyses are conducted with many blanks—known values against which analytical values can be checked.

1.6 Uncertainty

In evaluating any hydrogeochemical system, several types of uncertainty exist:

1. uncertainty of analytical methods and thermodynamic data,
2. uncertainty in describing the heterogeneity of both the flow and the mineral framework, and
3. uncertainty in assumptions about the aquifer boundary conditions and initial conditions in models used to evaluate the hydrogeochemistry.

Chemical and isotope analyses have an analytical uncertainty that is generally stated in isotope analyses but seldom in solute analyses. Analytical uncertainty in chemical concentration is generally incorporated in the precision of the reported value. Values should not be given as 503.25 mg/L Cl, but rather 505 mg/L or 500 mg/L, depending on the analytical method. In general, analyses are commonly given to two decimals for analyses

between 1 and 0.01 mg/L, one decimal for analyses between 1 and 10 mg/L, no decimal between 10 and 100 mg/L, and to the nearest 5 mg/L for analyses greater than 100 and less than 1,000. This range, however, depends on the analytical methods.

An individual solute analysis can be checked by electrical balance to see if it contains a large analytical error or is missing a significant ion. That is, the cations (positively charged ions) must equal the anions (negatively charged ions) because a solution is electrically neutral. This calculation uses the relation shown in Equation (3).

$$\left\{ \frac{(\text{sum of cations} - \text{sum of anions})}{(\text{sum of cations} + \text{sum of anions})} \right\} 100 = \% \text{ difference} \quad (3)$$

To perform this error analysis, the concentrations in milligrams per liter (mg/L) must be converted to milliequivalents per liter (meq/L) using the conversions presented in Table 2. The factor for a solute in Table 2 is then multiplied by the observed concentration in mg/L to convert to meq/L. For example, 160 mg/L of bicarbonate is equal to 2.6224 meq/L

Table 2 Factors for conversion of mg/L to meq/L for selected ions: multiply milligrams per liter by the appropriate factor to obtain milliequivalents per liter.

Species	Factor
Bicarbonate	0.01639
Bromide	0.01252
Calcium	0.04990
Chloride	0.02821
Magnesium	0.08229
Nitrate	0.01613
Potassium	0.02558
Sodium	0.04350
Strontium	0.02283
Sulphate	0.02082

The values in this table were calculated by dividing the valence charge (either plus or minus) by the atomic weight in grams. For example, the bicarbonate ion (HCO_3^-) has a charge of one (1) divided by its atomic weight (61.0168 g), providing the value of 0.01639. Using this approach, you can calculate a conversion factor for any solute not in the table.

Acceptable analyses are usually less than ± 5 percent for typical groundwater concentrations. For brines, most analyses should be less than 1 percent error, but for rainfall and other dilute solutes, it is common to accept a 10 percent to 15 percent error and above that the sample is not used in the study. Another quick check for gross error associated with common groundwater analyses is that the numerical value of specific conductance in $\mu\text{S}/\text{cm}$ divided by 100 is approximately equal to the cations (or anions) in meq/L. Thus, for a specific conductance of 350 $\mu\text{S}/\text{cm}$, one would expect cations or anions to be approximately 3.5 meq/L.

In aquifer systems, the analytical and thermodynamic data uncertainties are generally small relative to spatial uncertainty caused by the heterogeneous nature of the

aquifer's skeletal framework, amount of recharge, and other variables that influence groundwater chemistry. Spatial uncertainty can never be known; however, in cases where sample values exhibit a normal distribution, uncertainty can be assessed by the standard deviation. That is, approximately 95 percent of the sample values will fall within a range of two standard deviations from the mean. Thus, the standard deviation provides some guidance for estimating variability within the groundwater system, as do graphical methods that incorporate space or time.

The statistic r^2 is typically used to evaluate graphical correlations (that is, *goodness of fit*) and is an equivalent approach to standard deviation. In some instances, with large data sets (giga-, terra-, or petabyte sizes), machine learning (artificial intelligence) may generate correlations between samples that standard statistics developed for small data sets may not reveal.

Cumulative frequency analysis is commonly used to illustrate the concentration range of larger data sets (Figure 27a). Both mean (average) and median (middle value of the data set) can be used in describing the central tendency of solute concentration depending on the distribution of concentration values. Mode—the range of values that appears most often in a range or series of *bins*—is a third method to express concentrations and is expressed graphically using a histogram (Figure 27b).

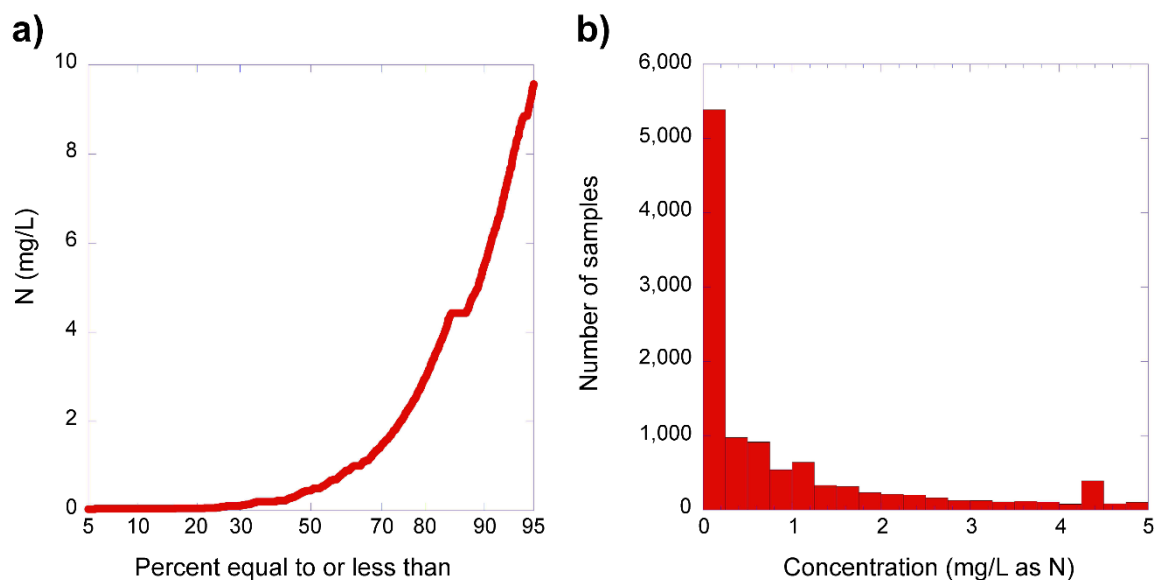


Figure 27 - a) Cumulative frequency of nitrogen in groundwater. The mean for this data set is 2.23 mg/L and the median is 0.46 mg/L. The curved line illustrates a non-normal distribution. b) Histogram of the same data with the less than 0.20 mg/L bin (mode) having the greatest number of samples consistent with the observed median of 0.46 mg/L. Clearly median or mode is a better indicator of true value than mean in this case.

If the values are normally distributed, the mean, along with the standard deviation, may be the preferred statistic to describe the general central concentration. However, most groundwater solute data are not normally distributed, so reporting the median with the 10th and 90th percentile is a better description of the solute concentration.

Whatever statistical method is employed, one needs to be cautious to ensure that the method is suitable, as centralizing statistics like mean and median are designed to represent central values that may obscure important spatial or temporal information associated with a gradient. Many commonly used statistical tests like mean and standard deviation assume a normal distribution; however, in most groundwater systems solute concentrations are not normally distributed, rather they tend to exhibit a logarithmic distribution. Of the major ions, only bicarbonate concentration is typically normally distributed (the straight line in Figure 11). Seldom are concentrations of minor or trace elements normally distributed, so care must be taken in the use of mean values.

When modeling a hydrogeochemical system, uncertainties associated with the assumed boundary and initial conditions are difficult to evaluate analytically. However, it is common practice to show a range of probable outcomes based on different assumptions about the nature of boundary and initial conditions.

In field-based problems, one is typically faced with a physically heterogeneous aquifer system, poorly known initial conditions, and limited resources to address the questions; thus, it is necessary to make assumptions when modeling the system. The fundamental question of how well the assumptions fit the aquifer is frequently a matter of professional judgment that depends on the intended purpose of the analysis and the resources available to address the question. It is common practice to show a range of probable outcomes based on a range of assumptions. Most water resources problems aim to solve the problem to the highest degree of acceptable certainty with the least cost—referred to as *the elegance of the solution*. Judicial matters in the USA provide some societal guide to the level of certainty, including: beyond a reasonable doubt (i.e., the kind of evidence required in a capital criminal trial); or a preponderance of clear and convincing evidence (i.e., the level of evidence used in a civil trial and most scientific arguments). In public health or safety questions, an ethical perspective requires use of the highest level of certainty—*beyond a reasonable doubt*.

2 Sources and Mechanisms Controlling Solutes

After the review of basic chemistry and hydrology presented in Section 1, we can now look at the origin of solutes in groundwater from a hydrogeochemical perspective, that is, integrating flow and chemical reactions. Solutes in groundwater aquifer systems are from three general sources:

- solutes remaining from the time of deposition that is, the so-called relic, fossil, legacy, or connate;
- solutes introduced or lost from the surface (precipitation, rivers, lakes) and from adjacent, underlying, or overlying geologic formations and loss or gains by aeolian activity; and
- solutes generated or lost by mineral precipitation, mineral solution, ion exchange, adsorption, desorption, ultrafiltration, radioactive decay, or by a gas phase entering the aquifer and being converted to a solid or conversion of solutes to a gaseous phase that escapes the aquifer.

2.1 Advective Flow and Diffusion as Transport Mechanisms

Solute in groundwater are transported into and out of aquifers largely by advective flow with many flow paths of different lengths in a series of topographically driven flow cells where atmospheric recharge occurs at several topographically higher points and discharge occurs at rivers or springs in topographic lows. The length of a flow path depends on the topography, distribution of hydraulic conductivity, amount of recharge, thickness of the aquifer, and hydraulic gradients (Figure 28).

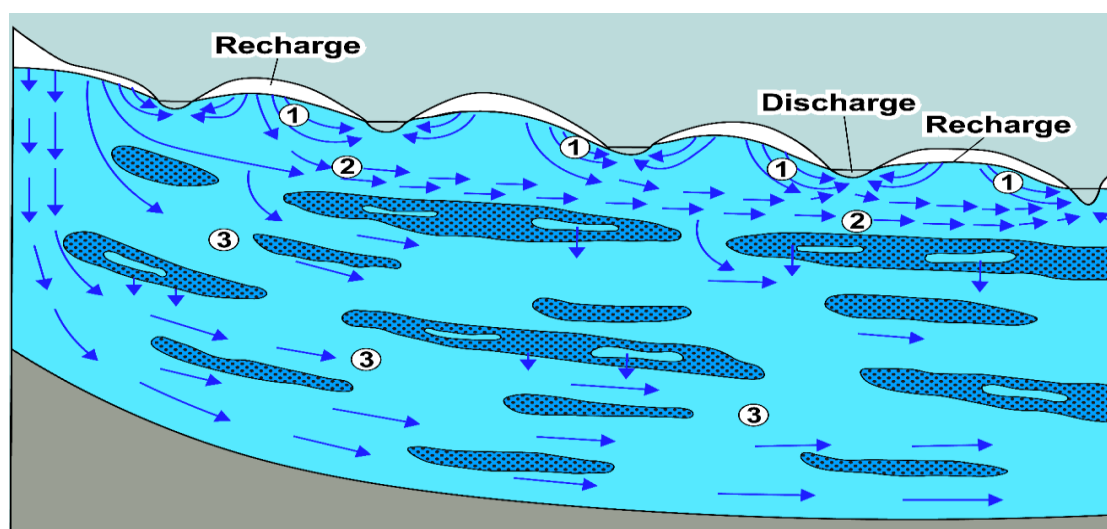


Figure 28 - Cross section through heterogeneous regional aquifer illustrating different groundwater flow paths associated with recharge and discharge. Different flow paths result in different velocities, where (1) indicates local flow with short travel times, (2) longer flow paths with intermediate travel times, and (3) regional flow with long flow paths and travel times. Their different ages and different hydrogeochemical environments result in different solute compositions and concentrations. In locations where water traveling substantially different paths converges, the different water ages and chemistries mix, potentially confounding the interpretation of the sample results (modified from Alley et al., 1999).

In addition to advective flow, diffusion can be a major transport mechanism in many aquifer systems. It is common for a high concentration of solute, that was present at the time the aquifer was deposited in seawater, to be held in a low-flow velocity portion of the aquifer (clay zone or aquitards). Vibrating ions are constantly colliding with one another, bouncing around like billiard balls. Some careen away from the mass into the surrounding water with a lower solute concentration. Over time, more ions enter the area of low solute concentration as they move away from the concentrated solute in the low-flow zone (Figure 29). The rate at which diffusion occurs in water is a function of temperature, the size and charge of the ion, the presence of other ions, and the concentration gradient. More details on the diffusion process are given in Section 7.4.

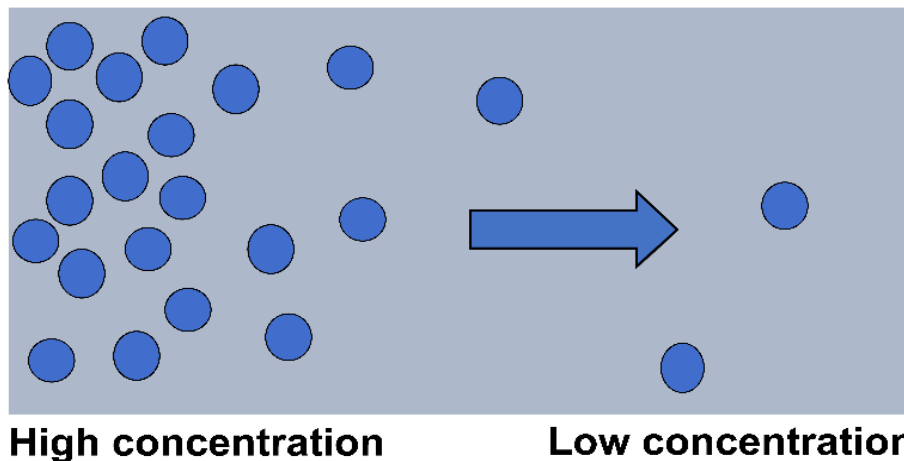


Figure 29 - Diagram illustrating diffusive movement of solutes from zones of high concentration to zones of lower concentration. Arrow indicates the net direction of movement.

Consider a condition in which a thick glacial sand outwash deposited by melting glaciers overlies a clay deposited in a marine environment. Owing to the high concentration of legacy marine solutes in the clay, solute diffusion will occur from the clay into the glacial outwash (Figure 30).

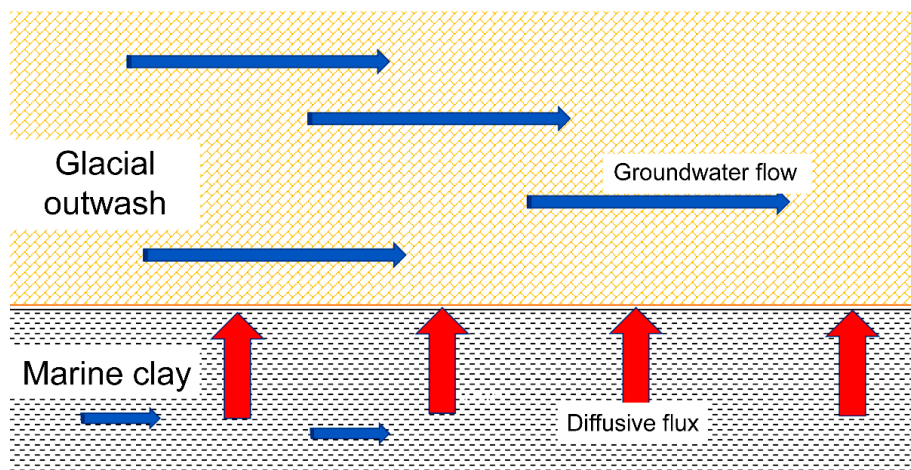


Figure 30 - Diffusive flux (mass per unit area per unit time, e.g., $\text{kg/m}^2/\text{yr}$) red arrows from an underlying marine clay with an elevated concentration of solutes into an overlying glacial outwash aquifer with a low concentration of solutes.

Whether advection or diffusion dominates, the mixing in an aquifer depends largely on the water flux through the aquifer system. A typical groundwater flux is given as cubic meters/square meter/year ($\text{m}^3/\text{m}^2/\text{y}$). Some confusion occasionally occurs in groundwater flow owing to the cancelation of the meter units that results in units of velocity (m/y), which is sometimes referred to as the *Darcy velocity*, but it is a flux. In general, the greater the water flux, the greater the impact of advective processes; the lower the flux, the greater the impact of diffusive processes. In most aquifer systems, solute transport occurs through both processes, although one is usually dominant.

2.2 External Solute Source: Precipitation, River, Lakes, and Contiguous Aquifers

Advective solute transport from rainfall is nearly universal as solutes generated from wet and dry atmosphere aerosols are always present and may be the dominant solute source in some mature, semi-arid, and arid aquifer systems. In addition, nearly all elements are present in the atmospheric deposition in both particulates and solutes as they originate from ocean spray, fires, volcanos, continental dust, and lightning. If you live in an area where snowfall occurs, you can gain an intuitive feeling of the amount of atmospheric particulate material by observing the change in the color of snow from bright white to dirty gray after several days. This particulate material is dissolved, adding to the solutes in precipitation. Atmospheric solutes are concentrated many times before being recharged, depending on the amount of evaporation and transpiration thus, 1 mg/L in the atmosphere can easily become 10 to 15 mg/L in the groundwater recharge.

Maps of the total annual depositional flux (kilograms per hectare per year) for many ions in the continental USA are available from the National Atmospheric Deposition Program ([NADP](#), 2020). Significant spatial variability in depositional flux exists between various ions consistent with different sources, nucleation rates, crystal size, settling rates, and so on (Figure 31). The year-to-year variability for the same ion depends largely on variations in annual precipitation flux.

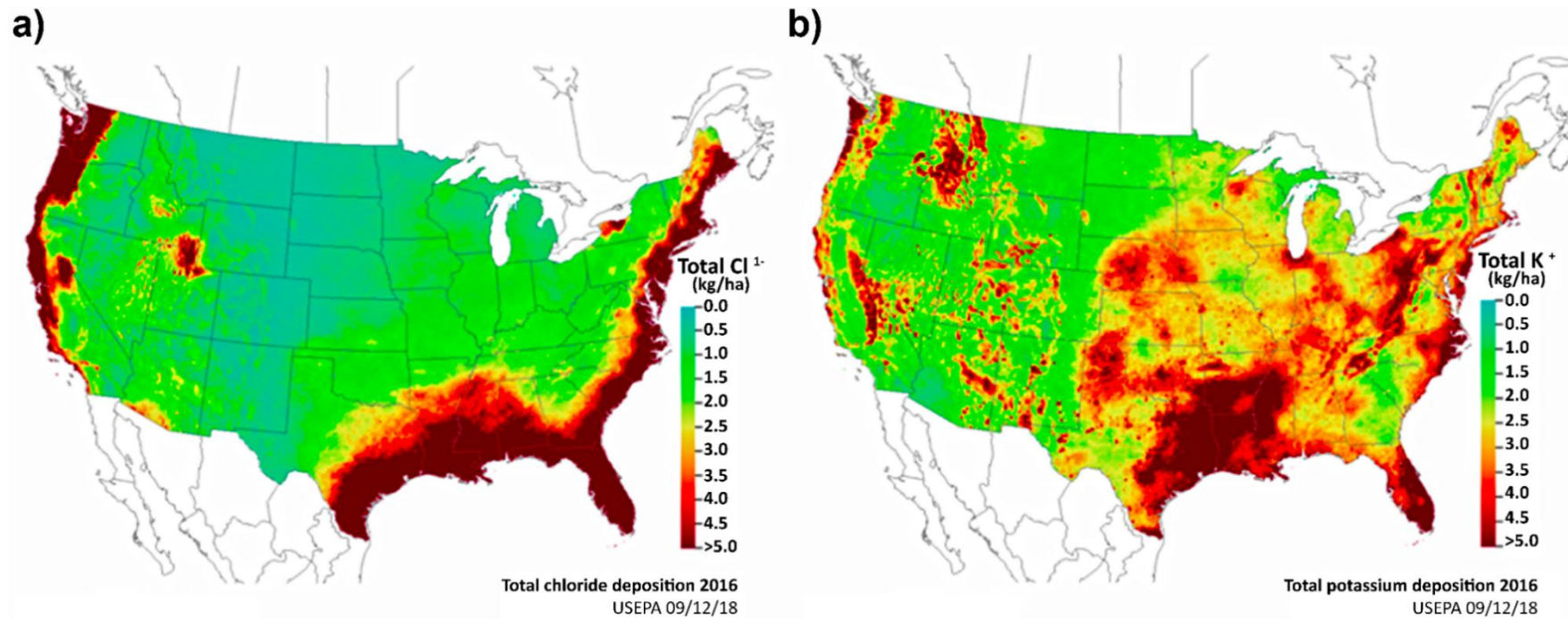


Figure 31 - Maps of total (wet plus dry) atmospheric precipitation deposition flux (kg/ha/y) of a) chloride and b) potassium on the continental USA in 2016. These maps illustrate the spatial variation in deposition, which suggests different sources and other factors (National Atmospheric Deposition Program, NADP, 2020).

The solute impact on groundwater from precipitation can be estimated by a CF (concentration factor) defined for a specific area, as shown in Equation (4).

$$\frac{\text{precipitation flux} - \text{storm runoff flux}}{\text{groundwater recharge flux}} = CF \quad (4)$$

For example, assume that a semi-arid area has an annual precipitation flux of 500 mm, annual storm runoff flux of 100 mm, and annual groundwater recharge flux of 20 mm, then $CF = (500-100)/20$. Thus, a solute in precipitation is concentrated by a factor of approximately 20. That is, 1 mg/L chloride in precipitation becomes 20 mg/L chloride in recharging groundwater.

In semi-arid and arid areas where significant water is lost to evapotranspiration, a concentration factor of 50 to 100 is not uncommon. The concentration factor from three different environments in the USA varies from 7.5 to 43 (Table 3). Thus, in some aquifer systems, atmospheric precipitation may represent the dominant source of solutes to the groundwater.

Table 3 - Concentration of chloride in precipitation by evapotranspiration before recharge to the groundwater. The concentration factor as expressed in Equation (4) varies widely over the continents (modified from Manna et al., 2019).

Chloride	Grand River Basin, Central Michigan	San Susana, California	Southern High Plains of Texas and New Mexico
Concentration in Precipitation	0.2 mg/L	3.2 mg/L	0.58 mg/L
Concentration factor	7.5	20	43
Concentration in Recharge	1.5 mg/L	64 mg/L	25 mg/L

Aquifers also gain water and solutes from hydrologically connected rivers (so-called losing streams) and/or lakes. That is, if the hydraulic head (hydraulic head is analogous to water level) of the river or lake is greater than that of the groundwater, then water and solutes are transported from the surface water feature into the groundwater system. This solute source is more common in immature landscapes such as recently glaciated or active karst areas.

Aquifers commonly receive solutes from overlying, underlying, or adjacent formations. For example, when fresh water meets a brine or ocean water it is forced to the surface and solutes are transported from underlying formations to a shallow coastal aquifer as shown in Figure 32.

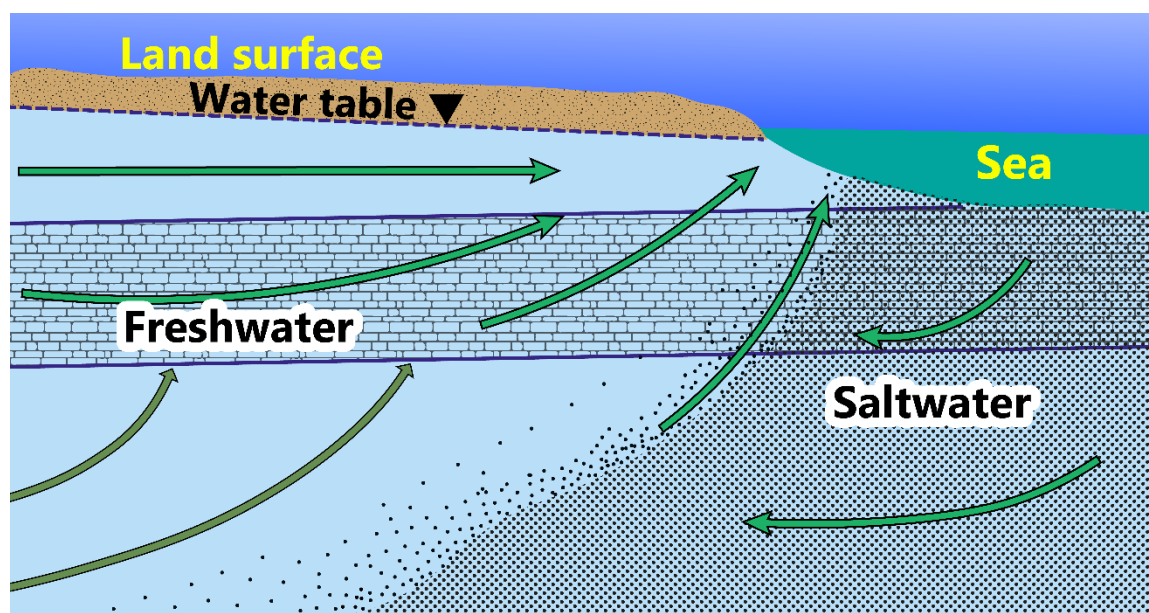


Figure 32 - Example of advective flow transporting solutes from underlying freshwater aquifers up to a shallow coastal aquifer (modified from Cooper, 1964).

2.3 Internal Solute Sources: Fossil, Relic, Legacy, or Connate

Geologic deposits that evolved as aquifers were formed in various depositional environments—including alluvial fans, fluvial, aeolian, lake, glacial, and marine environments—most of which initially contained solutes at the time of deposition. Some of these may remain and are referred to as the relic, fossil, legacy, or connate solutes. In some cases, the relic solutes have been flushed out by discharging groundwater flow; in others, some solutes remain. Because it requires a large water flux to remove solutes, relic solutes generally have a more significant impact in flow systems with low water flux or low hydraulic conductivity (i.e., permeability; the ability to transmit water) rather than systems with larger flux and higher hydraulic conductivity.

The amount of washing, flushing, or replacement with water depends on the length of time the system has been an active aquifer, the groundwater recharge rate, hydraulic conductivity, and topography; many millions of years may be required to remove the relic solutes. Relic solutes are typically identified in younger systems, in arid to semi-arid areas with less groundwater discharge through them, or in *aquitards*—areas of low permeability within an aquifer, usually with a significant clay content (Figure 33).

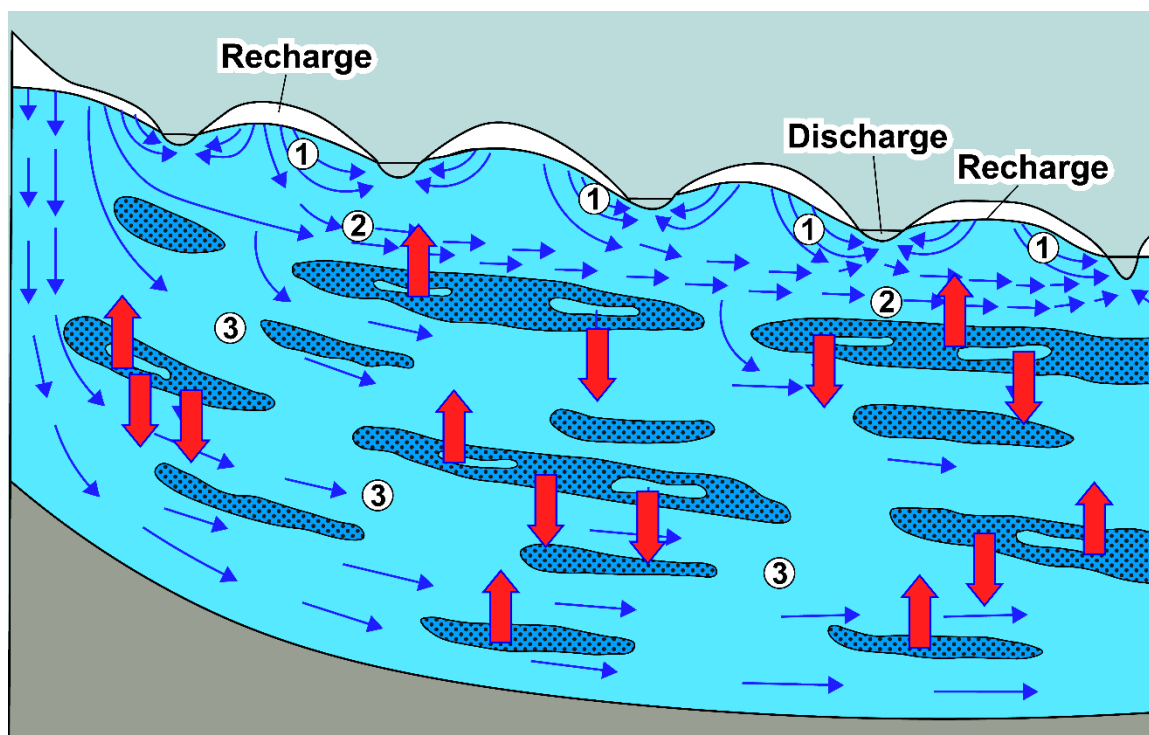


Figure 33 - Low permeability lenses (aquitards) in regional systems can be a major source of relic solutes (red arrows) that are added to the active groundwater flow system by advection and diffusion. Numbers indicate 1 local, 2 intermediate, and 3 regional flow systems (modified from Alley et al., 1999).

Aquitards have bulk hydraulic conductivity much lower than the surrounding aquifers, and therefore, water flux in aquitards is much lower than in aquifers. Diffusion is commonly the primary transport mechanism for moving solutes to the aquifer. The solute input from aquitards is ignored in many studies; however, to fully understand the evolution of solutes, it is crucial to recognize any influences of the aquitards in the aquifers.

2.4 Internal Solute Source: Radioactive Decay

Radioactivity is a process by which unstable neutrons in the atomic nucleus decay with the release of gamma rays, photons, electrons, protons, alpha, or beta particles (Figure 34). The decay of neutrons in the nucleus is shown in two ways:

1. a neutron decays into an electron (beta particle) and a proton, or
2. two neutrons combine that also combine with two protons to form an alpha particle that is ejected from the nucleus.

Radioactive elements occur naturally in many rocks and can add new elements to the groundwater that are products of the decay process.

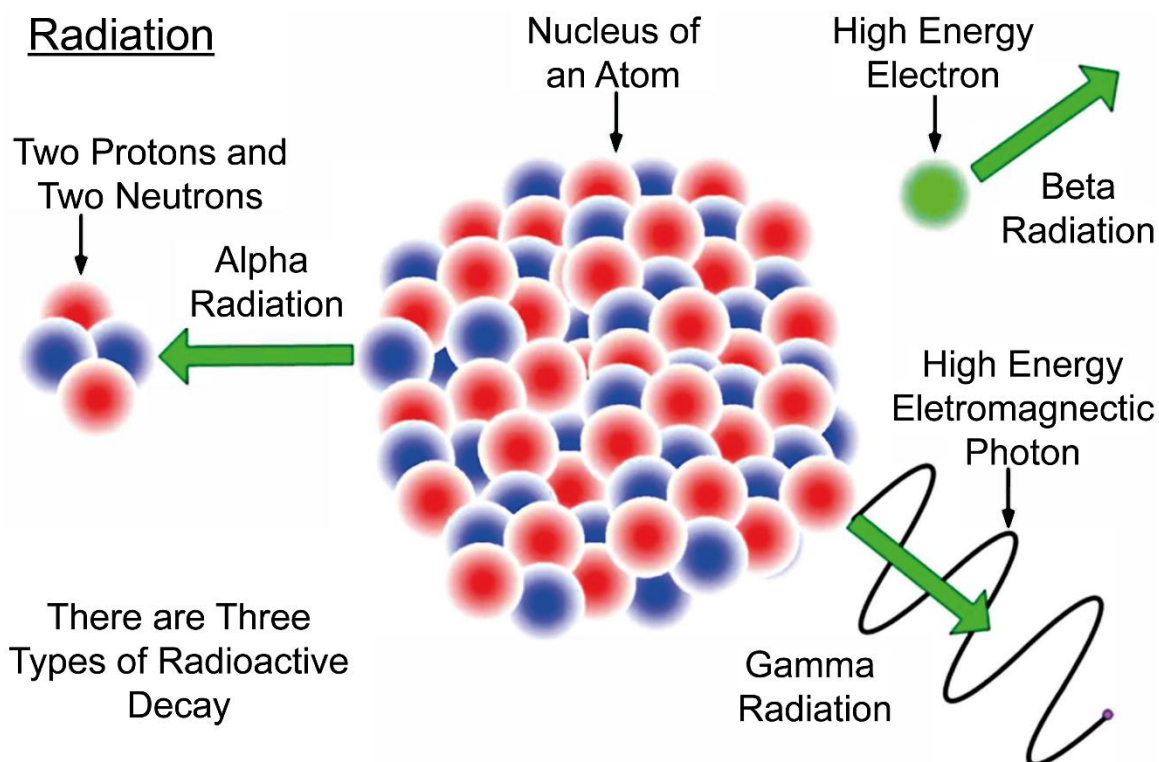


Figure 34 - Some of the common types of radiation—alpha particle (helium atom), beta (electron), gamma, and photons—emitted in radioactive decay (reproduced from Vitug, 2019).

The rate of decay and formation of prodigy elements—older literature refers to these as "daughter" elements or products—is a function of the element's half-life or the time required for half of the element to decay. Some elements have a long half-life, such as uranium-238 with a half-life of 4.5 billion years, whereas the half-life of other elements is much shorter, carbon-14 is a few thousand years, tritium (^3H) a few years, radon-222 a few days, and others a few seconds. Radioactivity is commonly measured in groundwater as gross alpha mainly based on the dominance of alpha decay in the decay series of uranium-238 (Figure 35), which is the primary source of radioactivity in most groundwater.

The Uranium-238 Decay Chain

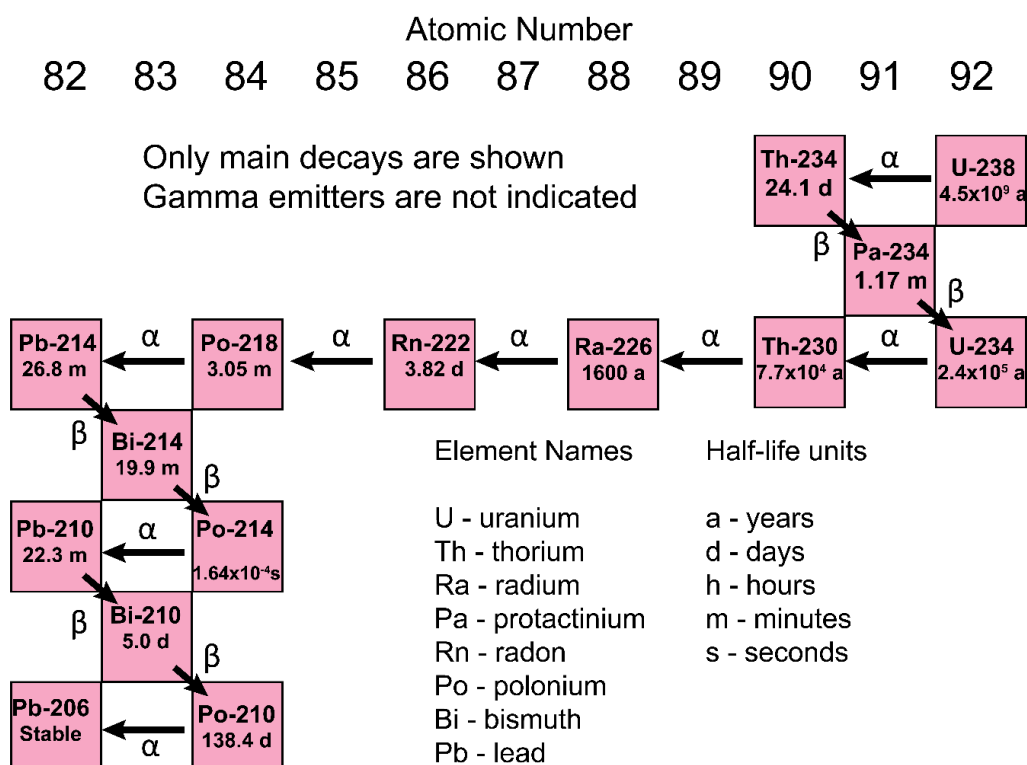


Figure 35 - Uranium-238 decay sequence illustrating the elements atomic number, and their atomic weight and half-life generated by radioactive decay with the release of alpha (α) and beta (β) particles. (U.S. Geological Survey; The Uranium 238 Decay Chain <https://pubs.usgs.gov/of/2004/1050/uranium.htm> Accessed 1 November 2024)

Recall that it is the number of protons that determines the element. An example of the decay of uranium-238 is given in Figure 35, where its unstable nucleus (92 protons and 146 neutrons) ejects an alpha particle (2 neutrons with 2 protons, i.e. ^4He), thus decreasing the atomic mass by 4 and atomic number by 2 and creating the element thorium-234 (90 protons and 144 neutrons). Thorium-234 is unstable, with a neutron decaying and adding a proton to the nucleus and emitting a beta particle (electron), thus creating a new element: protactinium-234 (91 protons and 143 neutrons). Protactinium-234 is unstable, with a neutron decaying, adding a proton to the nucleus and emitting a beta particle, thus creating a new isotope, uranium-234 (92 protons and 142 neutrons). The uranium-234 is unstable and releases an alpha particle, decreasing the atomic mass by 4 and atomic number by 2, creating the element thorium-230 (90 protons and 138 neutrons). This decay continues down the series with the loss of protons until becoming the element lead-206 (82 protons and 124 neutrons) which has a stable nucleus. Some decays also release energy through gamma rays and photons that do not change the mass or atomic number. An explanation of the nuclear physics causing this neutron instability is beyond the scope of this monograph.

2.5 Internal Source of Solutes: Weathering

Weathering of the aquifer framework is an important source of groundwater solutes in carbonate (limestone and dolomite) aquifers, in clastic aquifers that contain abundant carbonate minerals, and in young glacial and alluvial fan aquifers and other deposits that contain many unweathered, mechanically-broken crystals and rock fragments. Whereas many minerals are present in most geologic terrains, only a few; calcite, dolomite, pyrite, gypsum, anhydrite, several feldspars, and amphiboles control the solute concentration of most major ions.

The amount of these minerals may seem insignificant, for example, as easily weathered pyrite may be less than 0.01 percent of the mass of the aquifer but control the sulfate ion concentration and pH. For example, in weathered till of Alberta, Canada, gypsum was only 0.34 percent of the bulk rock but controlled the sulfate concentration in groundwater (Hendry et al., 1986). In short, bulk mineralogy may not be a good indicator of the potential for early geologic solute evolution, because solubility may be more critical. Whereas much of the geogenic weathering is by the action of carbonic and sulfuric acid reacting with the rocks and minerals, the process of hydrolysis—weathering independent of pH—is also a critical weathering mechanism as observed by weathering of halite, gypsum, anhydrite, and a few silicate minerals like the olivine mineral forsterite.

Hydrothermal systems typically have elevated trace and minor element concentrations, but the fluxes are small relative to most groundwater systems and generally have only local impact.

In general, more than 50 percent of solutes in groundwater are derived from wet and dry aerosols, relic solutes, and bicarbonate derived from the weathering of organic material and not from rock–water interaction (Wood, Sanford, Cherry, & Wood, 2023). Dissolution of the aquifer framework also occurs, as there is a correlation between the solute concentration and composition lithology (rock types) of aquifers as shown in Figure 36. The general source of solutes weathered from the aquifer framework is given in Table 4.

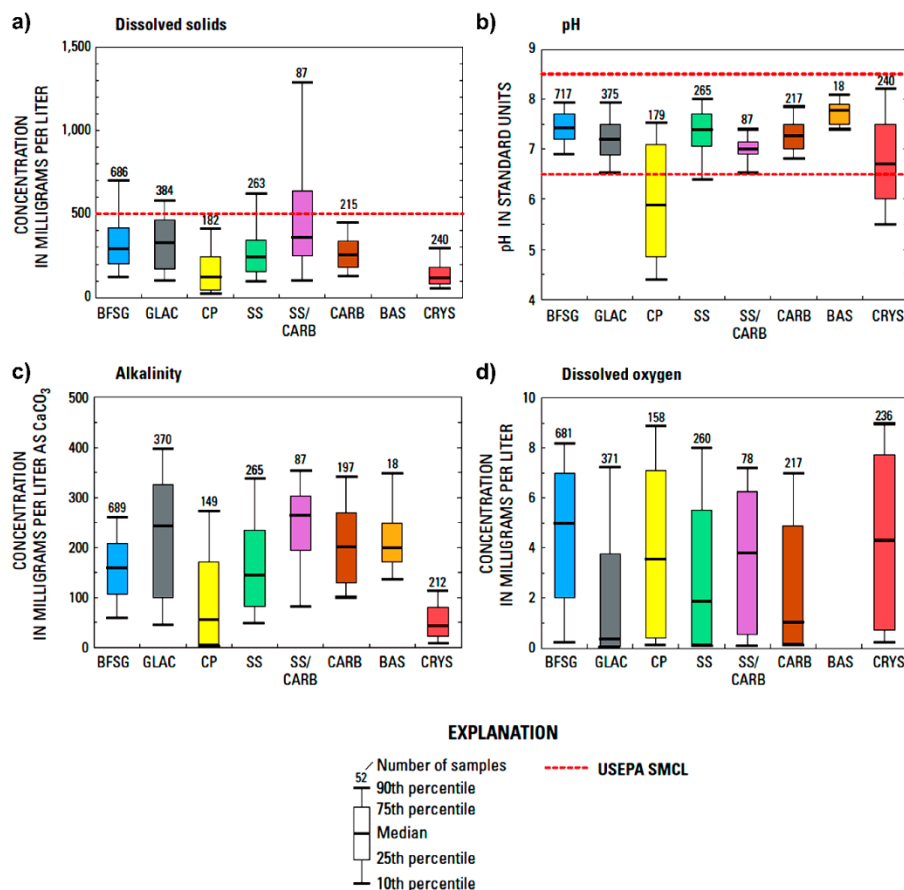


Figure 36 - Variability of solute composition and concentration of groundwater from different aquifer lithology. Dissolved solids, pH, alkalinity, and oxygen from aquifers composed of basin fill (BFGS), glacial (GLAC), coastal plain (CP), sandstone (SS), sandstone and carbonate (SS/CARB), carbonate (CARB), basalt (BAS), and crystalline rock (CRYS) of groundwater from domestic wells in the USA. SMCL is Secondary Maximum Contaminant Level. (reproduced from DeSimone et al., 2009).

Table 4 - Major sources of geogenic solutes in groundwater.

Element	Dominant source of major geogenic solutes in groundwater
Na	Solution of feldspar, ion exchange (clays), rainfall, relic/fossil water
Mg	Solution of dolomite, ferromagnesian minerals (olivine, amphibole, pyroxene, biotite), ion exchange
Ca	Solution of calcite, dolomite, plagioclase, gypsum
HCO ₃	Oxidation of organic matter and subsequent dissolution of calcite, dolomite, silicate minerals
SO ₄	Solution of gypsum/anhydrite, oxidation of pyrite
Cl	Rainfall, mixing with relic/fossil water
Si	Solution of silicate minerals

2.6 Equilibrium Variables

In hydrogeochemistry, the concepts of chemical equilibrium and thermodynamics are commonly the basis for the analysis or description of the chemical state of the solutes. Therefore, it necessary to assess the degree of disequilibrium for each mineral component of the aquifer. Until now, this monograph has largely avoided equations as they are off-putting to many readers. As famously stated by the physicist Stephen Hawking when

talking about his popular book *A Brief History of Time*, “Someone told me that each equation I included in the book would halve the sales.”

Chemical equations are just a shorthand way of writing chemical reactions, and the associated math is equivalent to the checkbook accounting of adding and subtracting. In chemistry, this accounting method is given the exotic name *stoichiometry* (Greek "stoicheion" meaning "element" and "metron" meaning "measure,"). For example, an equation may state that one mole of methane (CH₄) and four moles of oxygen (O) can react to form one mole of carbon dioxide (CO₂) and two moles of water (H₂O) as shown by Equation (5).



The equal sign represents equilibrium in the equation and separates the reactants on the left from the products on the right. By convention, reactants are always on the left of the equal sign, and products are always on the right. Thus, one can determine the direction in which the reaction will progress with loss of thermal energy, hence the name *thermodynamics*: temperature (thermal) change (dynamics).

The chemical system is in equilibrium when the amount of an ion leaving a mineral by weathering and forming a solute is equal to the amount of solute being precipitated as the mineral; thus, the solute no longer increases in concentration with time. For example, consider the common reaction of Ca²⁺ with CO₃²⁻ in solution equilibrating with the mineral calcite (CaCO₃). There is a forward reaction forming CaCO₃, thus, removing Ca²⁺ and CO₃²⁻ from the solution, and a reverse reaction dissolving CaCO₃ that adds Ca²⁺ and CO₃²⁻ to the solution. When the forward and reverse reactions are equal, the system is said to be in *chemical equilibrium* (Figure 37).

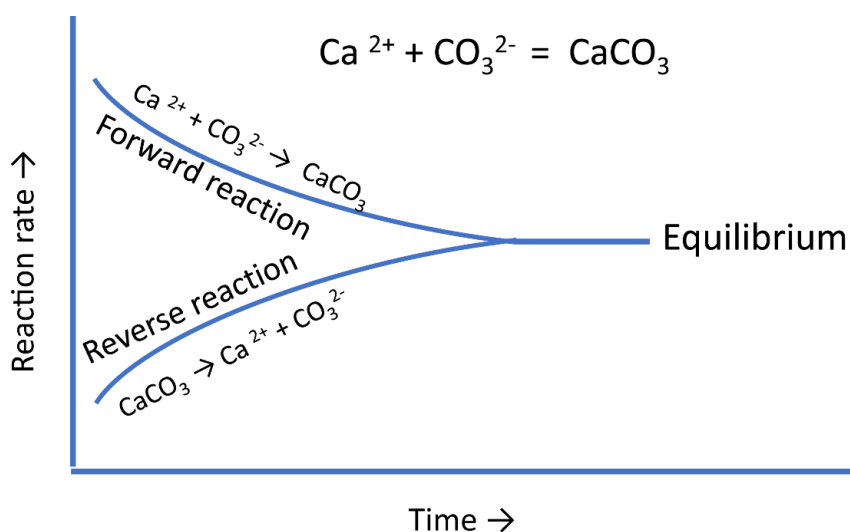


Figure 37 - Conceptual diagram illustrating the equilibrium process with time of calcium and carbonate solutes and the mineral calcite with the forward reaction precipitating calcite and reverse reaction dissolving calcite and reaching an equilibrium where the rates of formation and dissolution are equal and the concentration is not changing with time.

The weathering of the aquifer skeletal framework is the subject of most groundwater geochemistry textbooks. Hydrogeochemists are frequently interested in whether the observed solute concentration in groundwater is in equilibrium with a given mineral in the aquifer. That is, will the groundwater dissolve more of the mineral and add solutes, precipitate some of the minerals from the solution, removing solutes, or have no effect on the solute concentration?

This question can be addressed by conducting a chemical analysis of the solutes in the water and by considering six fundamental factors—the mineral's intrinsic solubility plus the following five environmental variables:

1. temperature,
2. pressure,
3. pH—the amount of ionized hydrogen (H^+) in solution,
4. Eh—a measure of the potential of excess or deficiency of electrons in solution, and
5. thermodynamic activity, or *effective* concentration of the solutes in the surrounding solution.

2.6.1 Mineral Solubility: A Fundamental Thermodynamic Property

The amount of mass that can be weathered from a specific mineral under specific environmental conditions is controlled by the mineral's intrinsic solubility. In general, this is controlled by the type of chemical bonding—how tightly the elements are held together in a mineral—that determines its resistance to weathering, that is, the time necessary to dissolve.

In general, there are three types of bonds: ionic, covalent, and metallic. An ionic bond is formed when valence electrons are transferred from one atom to the other to complete the outer electron shell. For example, the sodium (Na) atom gives up its valence electron to complete the outer shell of the chlorine (Cl) atom forming halite NaCl (Figure 38). These are generally weak bonds resulting in greater solubility.

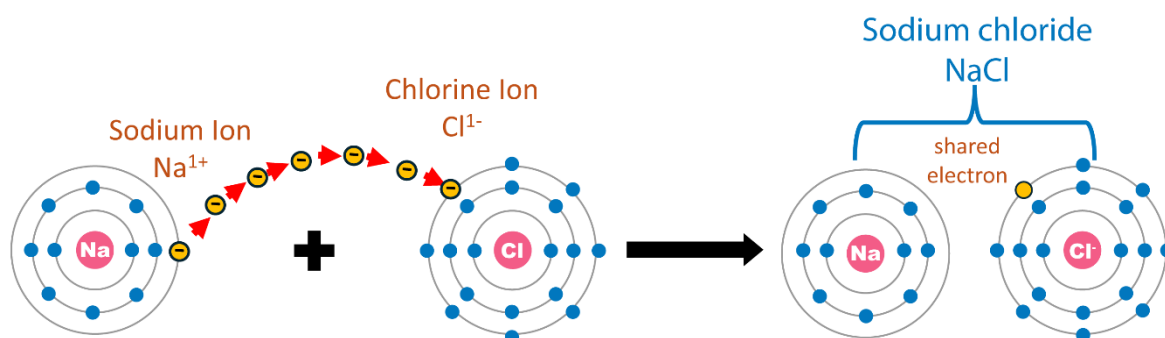


Figure 38 - Ionic bonding occurs when an ion with an extra electron in the orbital subshell for example (Na^+) is shared with an atom that is deficient in an electron its subshell for example (Cl^-) so that both atoms are in a stable electron subshell, in this case it forms the mineral halite (Box 1 explains the shells).

A covalent bond is formed when the valence electrons from one atom are shared between two or more other atoms. One example is the four oxygen atoms and one silica atom in quartz. These are strong bonds so quartz is poorly soluble and not as readily released to the solution. Various ways of illustrating covalent bonds are shown in Figure 39.

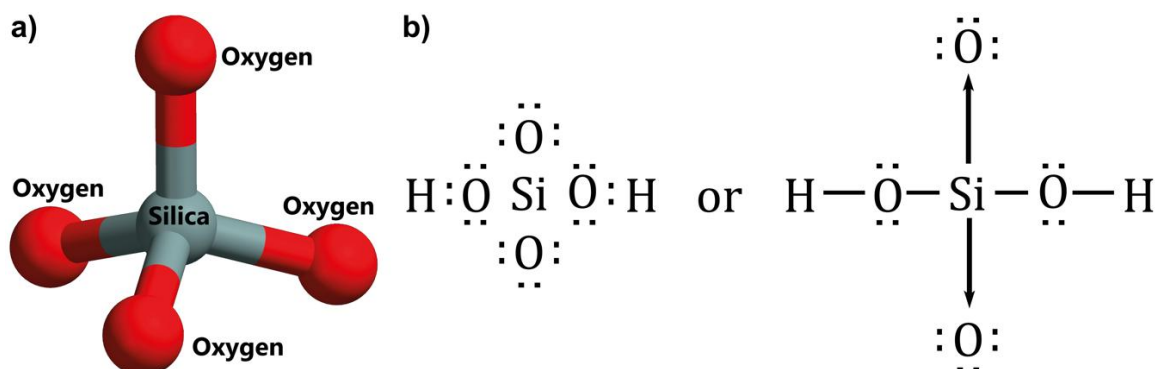


Figure 39 - Different ways of graphically illustrating covalent bond-sharing electrons using silicon (Si), oxygen (O), and hydrogen (H) atoms in a) the SiO_4 molecule (quartz) and b) the H_2SiO_4 molecule (dihydrogen orthosilicate) as examples.

A metallic bond is formed when the valence electrons are not associated with a particular atom or ion but exist as a "cloud" of electrons around the ion centers, which is why metals are such good conductors of electricity. The time required for some minerals to dissolve into a solution are given in Table 5. This time is a surrogate measure of solubility.

Table 5 - Approximate time calculated for a hypothetical sphere of 1 mm diameter to dissolve in a dilute water solution at pH 5 at 25 °C (reproduced from Lasaga et al., 1994).

Mineral	Time (years)
Quartz	34,000,000
Kaolinite	6,000,000
Muscovite	2,600,000
Epidote	923,000
Microcline	921,000
Albite	575,000
Sanidine	291,000
Gibbsite	276,000
Enstatite	10,100
Diopside	6,800
Forsterite	2,300
Anorthite	112
Dolomite	1.6
Calcite	0.1
Gypsum	Short
Halite	Very short

The rate of release of silicate ions to solution for five common silicate minerals is shown in Figure 40. This exponential decline in the rate of approach to equilibrium is typical of most minerals. The study of this reaction time is referred to as kinetics that, are a

function of many factors, including the surface area of the reacting mineral, activation energy, Arrhenius factor, gas constant, and temperature (Lasaga, 1984).

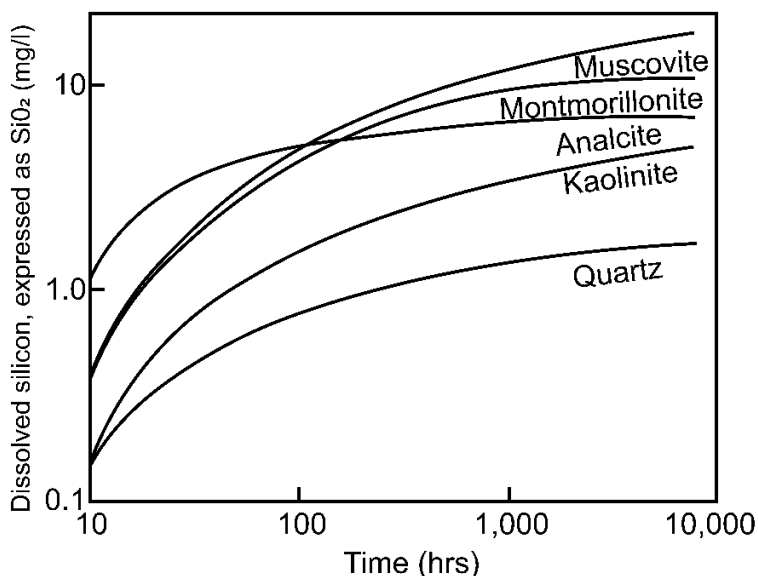
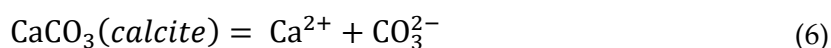


Figure 40 - Release of silica in distilled water from different minerals with time at 25 °C (reproduced from Bricker, 1967).

Each mineral has its intrinsic value for solubility that is referred to as the equilibrium constant and is given the notation (K_{eq}). The K is for *Konstante*, the German word for constant. The equilibrium constant K_{eq} is the thermodynamic activity of the products (material on the right side of a reaction) divided by the thermodynamic activity of the reactants (material on the left side) of a reaction at a specified temperature, pressure, pH, Eh, and thermodynamic activity. By convention, the equilibrium constant is written for the dissolution reaction in which the mineral is the reactant, and the ions are the products. For example, one mole of the mineral calcite (CaCO_3) dissolves into its component products of one mole of Ca^{2+} and one mole of CO_3^{2-} ions as shown by Equation (6).



The equilibrium constant for this expression is the thermodynamic activity of the products [Ca^{2+} and CO_3^{2-}], divided by the thermodynamic activity of the reactant [CaCO_3] as represented by Equation (7).

$$K_{eq} = [\text{Ca}^{2+}][\text{CO}_3^{2-}]/[\text{CaCO}_3] \quad (7)$$

In Equation (7), the square brackets [] indicate thermodynamic activities or effective concentration—more generally, *activity* (activity is discussed in Section 2.6.5). Table 6 provides examples of K_{eq} for some common aquifer minerals. For the example shown in Equation (7), the K_{eq} of calcite is the activity of Ca^{2+} multiplied by the activity of CO_3^{2-} divided by the activity of CaCO_3 . The activity of a solid (in this case, CaCO_3) is always 1.

Table 6 - Equilibrium constants of some common minerals at 25 °C (Freeze & Cherry, 1979; solubility data from Seidell, 1958). More current values are available in the code PHREEQC (Parkhurst & Appelo, 2013).

Mineral	Dissociation reaction	Equilibrium constant K_{eq}	Solubility at pH 7 (mg/L)
Gibbsite	$Al_2O_3 \cdot 2H_2O + H_2O = 2Al_3^+ + 6OH^-$	10^{-34}	0.001
Quartz	$SiO_2 + 2H_2O = Si(OH)_4$	$10^{-3.7}$	12
Hydroxyl apatite	$Ca_5OH(PO_4)_3 = 5Ca^{2+} + 3PO_4^{3-} + OH^-$	$10^{-55.6}$	30
Amorphous silica	$SiO_2 + 2H_2O = Si(OH)_4$	$10^{-2.7}$	120
Fluorite	$CaF_2 = Ca^{2+} + 2F^-$	$10^{-9.8}$	160
Dolomite	$CaMg(CO_3)_2 = Ca^{2+} + Mg^{2+} + 2CO_3^{2-}$	$10^{-17.0}$	90* 480†
Calcite	$CaCO_3 = Ca^{2+} + CO_3^{2-}$	$10^{-8.4}$	100* 500†
Gypsum	$CaSO_4 \cdot 2H_2O = Ca^{2+} + SO_4^{2-} + 2H_2O$	$10^{-4.5}$	2,100
Sylvite	$KCl = K^+ + Cl^-$	$10^{+0.9}$	264,000
Epsomite	$MgSO_4 \cdot 7H_2O = Mg^{2+} + SO_4^{2-} + 7H_2O$	-----	267,000
Mirabilite	$Na_2SO_4 \cdot 10H_2O = 2Na^+ + SO_4^{2-} + 10H_2O$	$10^{-1.6}$	280,000
Halite	$NaCl = Na^+ + Cl^-$	$10^{+1.6}$	360,000

*Partial pressure of $CO_2 = 10^{-3}$ bar.

†Partial pressure of $CO = 10^{-1}$ bar.

For simple equations, a numerically equivalent expression is the *solubility product*. The constant K_{sp} is often used in the geochemical literature on this topic. For example, the solubility product for the same reaction for calcite is written as Equation (8).

$$K_{sp} = [Ca^{2+}][CO_3^{2-}] \quad (8)$$

As noted above, it is assumed that the activity product of a pure solid mineral is always 1 and is not included in the expression for solubility product K_{sp} (Table 6). That is, K_{sp} is a shortcut for using K_{eq} . However, mineral solids may be significantly different from pure. $CaCO_3$, for example, has varying amounts of Sr^{2+} and Mg^{2+} substituting for Ca^{2+} . Despite this, condition 1 is commonly used because analytical uncertainty of several parameters controlling the reaction may be greater than adjusting for impurity.

In the above descriptions of equilibrium constant and solubility product, it has been assumed that the products and reactant are formed instantly without delay. This instant formation is generally not the case, as many minerals require weeks or years to establish equilibrium depending on environmental factors that are discussed in Sections 2.6.2 through 2.6.5. This delay in reaching equilibrium is referred to as kinetics and is discussed in Section 2.7.

2.6.2 Temperature: An Environmental Thermodynamic Property

Temperature is an essential environmental control on the dissolution of minerals as all equilibrium constants and solubility products are temperature dependent. The average global temperature for active groundwater systems is approximately 20 °C, for aquifers less than 12 meters below the surface but is dependent on the amount of solar radiation. Heat applied by solar radiation at a given location varies throughout the year, as shown by the daily surface temperature for one year on a sabkha in the Arabian Gulf approximately 50 km northwest of the city of Abu Dhabi (Figure 41). Owing to the storage of heat by the

minerals on the surface, the surface temperature is greater than the air temperature. This surface temperature is the thermal input to the aquifer, not air temperature.

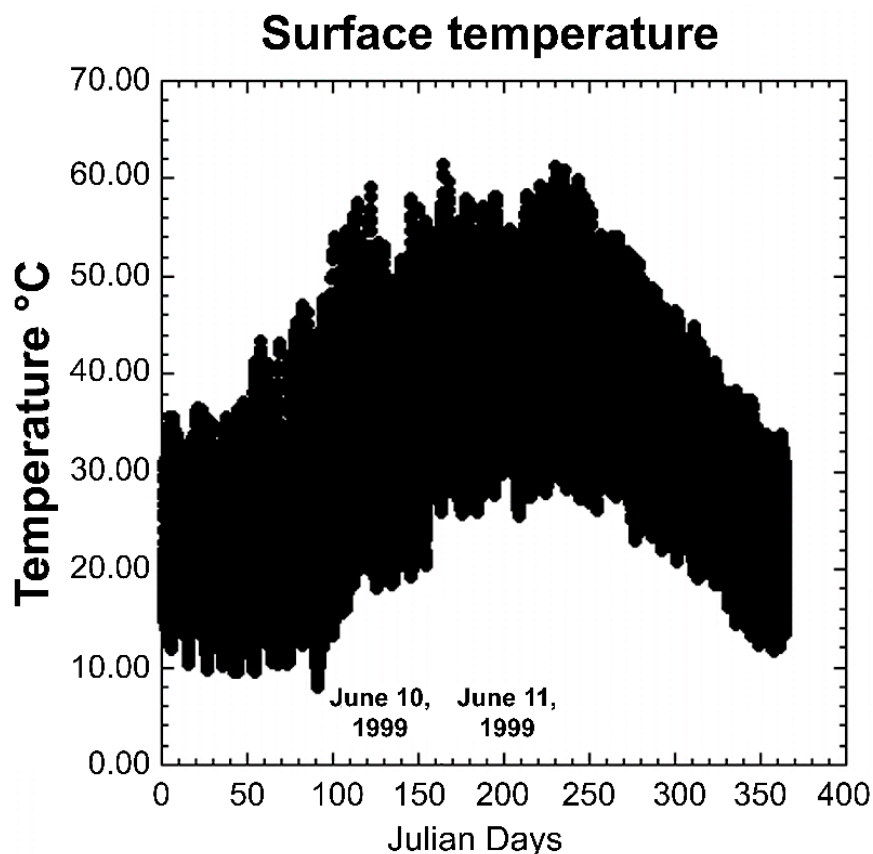


Figure 41 - Daily earth surface (not air) temperature ranges for a year on the coastal sabkha in the United Arab Emirates. The vertical axis represents temperature in degrees Celsius; the horizontal axis represents time in days. The average surface temperature for this period of record is 31 °C, which is nearly identical to shallow groundwater (30.5 °C).

Figure 42, shows a wave of warmer summer temperature propagating downward by conduction and finally disappearing at approximately 12 m depth after one year. The depth of penetration of the temperature wave is a function of the thermal conductivity of the water and aquifer framework, but is typically in the range of 12 to 15 m.

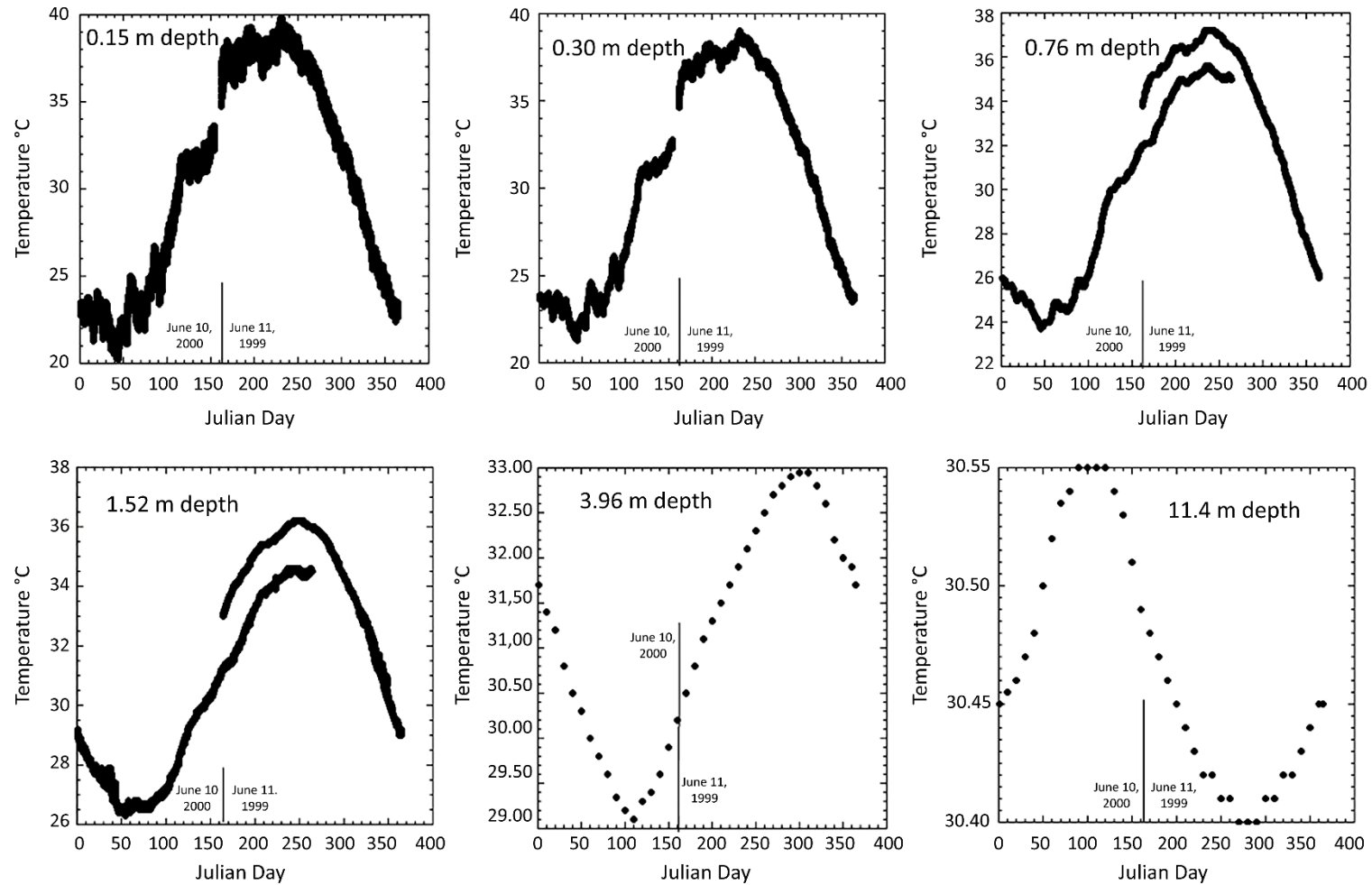


Figure 42 - Annual temperature variation at six depths below land surface in the coastal sabkha of the United Arab Emirates. The vertical axis represents temperature, and the horizontal axis represents the time since the start of measurements. The deeper the measurement, the more the maximum temperature is shifted to occur later, and the difference between maximum and minimum temperature is smaller. Data collected from June 11, 1999 through September 21, 2000 are plotted as the number of their Julian day on the x axis, thus data from January 1 to June 10 of 2000 appear before data from June 11 to December 31 of 1999, and data from June 11, 2000 to September 21, 2000 plot on the same x axis ordinate as data from June to September of 1999 (from Wood, 2021).

In shallow groundwater, the annual maximum groundwater temperature occurs later in time relative to the surface, and the seasonal fluctuation in temperature is less pronounced with depth (Figure 42). For example, at 0.15 m depth, the maximum groundwater temperature occurs only a few days after peak surface temperature, and the groundwater temperature has an extensive annual range of 20 °C (Figure 42). At 11.4 m depth, the maximum groundwater temperature occurs approximately 355 days after peak surface temperature, and the annual temperature range is small, being only 0.15 °C (Figure 42).

Temperatures of groundwater deeper than the annual depth of influence by solar radiation increase with depth owing to the thermal gradient from the Earth's interior. Depending on the location, the thermal gradient adds approximately 2.5 °C per 100 m of depth (25 °C/km) in the upper 40 km of the Earth's crust. Therefore, even in the center of ancient cratons, high-temperature water exists at depth. For example, brine from a 5 km depth in the middle of the Canadian Shield would typically be around 125 °C and is liquid only due to the high pressure at that depth. The pressure at 5 km depth in the continental crust is approximately 150 megapascals or about 1500 atmospheres. Shallow groundwater near geologically recent igneous intrusions may be greater than several hundred degrees centigrade (°C) and is the source of nearly all geothermal springs and geysers.

Groundwater typically moves from recharge areas of elevated topography and generally lower temperatures to discharge areas of lower elevation with higher temperatures. Thus, it is common for the water temperature to increase along the flow path. Consequently, minerals that exhibit normal solubility dissolve with distance along the flow path even though they may have been at equilibrium in the recharge area—thus increasing solute concentration as illustrated with halite (NaCl; Figure 43, panel D). Conversely, minerals with retrograde solubility become less soluble and will precipitate with increasing temperature (calcite, gypsum, anhydrite, and dolomite Figure 43, panels A, B, and C). This decreasing solubility with temperature is commonly observed in coffee machines and tea kettles that build up a calcium carbonate deposits over time.

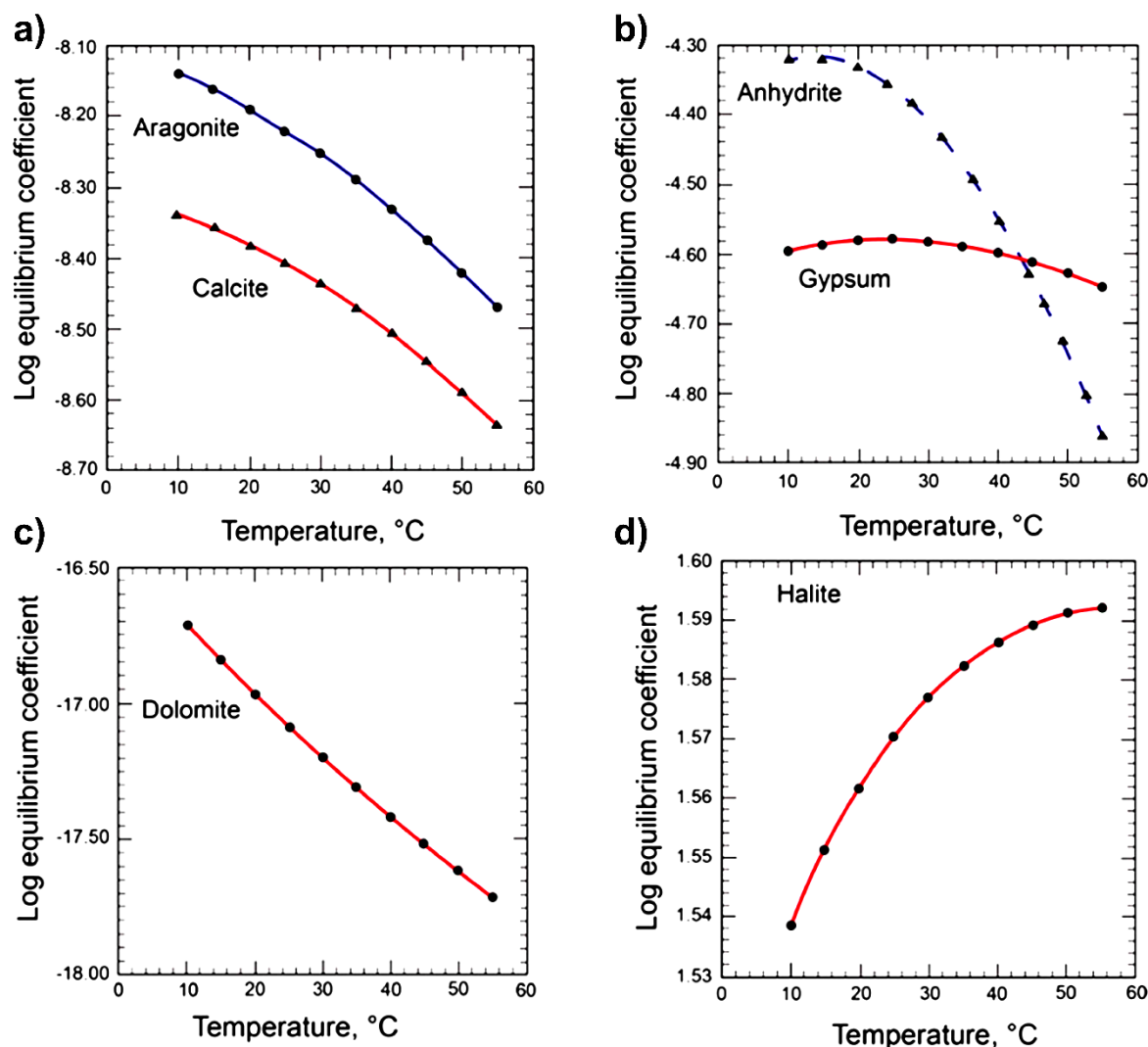


Figure 43 - Equilibrium constants (vertical axis) as a function of temperature (horizontal axis) illustrate the retrograde solubility (decreasing solubility with increasing temperature) in panels (a), (b), and (c) of the common minerals calcite, aragonite, dolomite, gypsum, and anhydrite in contrast to the normal solubility of halite (increasing solubility with increasing temperature) shown in panel (d) (from Wood, 2021).

2.6.3 pH: An Environmental Thermodynamic Property

An additional environmental thermodynamic variable controlling the dissolution and precipitation of many minerals is pH, which measures the amount of hydrogen (H^+) ions present in a solution. The more (H^+) present, the more acidic the solution becomes, and the lower the numerical value of pH.

The formal definition of pH is *the negative logarithm of effective concentration (activity) of hydrogen ions (H^+)*—an unintuitive way of defining pH, as most people do not think in terms of negative logarithms. Usually, one thinks the higher the concentration, the higher the numerical value. In the case of pH, it is the reverse with high numerical value representing lower concentration of H^+ . An activity of 10^{-3} molar solution of hydrogen ions yields a pH of 3 and a solution of much lower molar hydrogen ion activity of 10^{-9} yields a pH of 9. The pH is a log scale with each value being ten times more (or less) acidic than the

next value. A pH of 7 is considered neutral as water contains equal molar activity of 10^{-7} hydrogen ions (H^+) and 10^{-7} hydroxyl ions (OH^-). If the pH is 5 (10^{-5} molar H^+ ions), the hydroxyl (OH^-) must be 10^{-9} molar OH^- ions. Typical groundwater is usually near a pH of 7 (Figure 44).

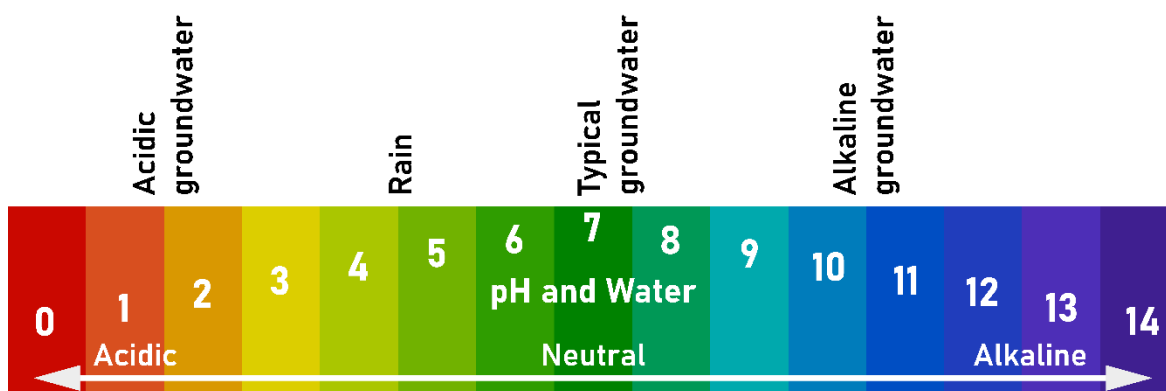


Figure 44 - Range of pH from acidic, pH = 0, to alkaline, pH = 14. Most groundwater is between 6 and 8, with a geospatial global mean of 7.2.

The rate of dissolution and precipitation of most carbonate and silicate minerals is strongly pH dependent. An example of one of the most common pH-controlled dissolution/precipitation reactions is that involving the mineral calcite ($CaCO_3$). The concentration of calcium (Ca^{2+}) ion and bicarbonate (HCO_3^-) ion—two major ions in most groundwaters (Table 1)—is controlled by the concentration of CO_2 in the vadose zone that may be several tens or a hundred times greater than atmospheric. When water from atmospheric precipitation intersects the increased carbon dioxide in the unsaturated zone it reacts forming carbonic acid (H_2CO_3) that creates a thermodynamically undersaturated condition with respect to the mineral calcite ($CaCO_3$). As a result, calcite dissolves, increasing the concentration of both calcium and bicarbonate ions in the resulting groundwater. The reaction of one mole of carbon dioxide (CO_2) with one mole of water (H_2O) forms one mole of carbonic acid (H_2CO_3) that dissociates into one mole hydrogen ions (H^+) and bicarbonate ions (HCO_3^-). The hydrogen reacts with the calcite ($CaCO_3$) to form calcium ions (Ca^{2+}) and additional bicarbonate (HCO_3^-) ions as expressed in Equation (9).

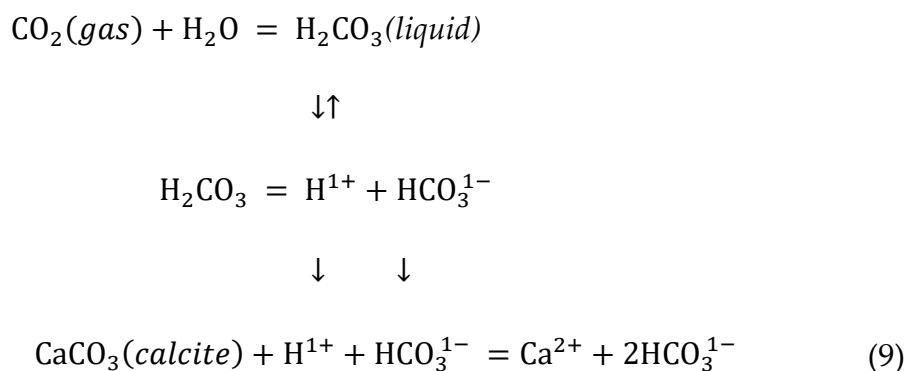


Figure 45 shows the concentration of each of the carbon solute species (vertical axis) as a function of pH (horizontal axis), where H_2CO_3 is the dominant species at pH below 4.5, HCO_3^- is the dominant species between pH 6 and 10, and CO_3^{2-} is the dominant species with a pH greater than 10. The graph shows that the more hydrogen in the molecular formula, the lower the pH at which it is the dominant species.

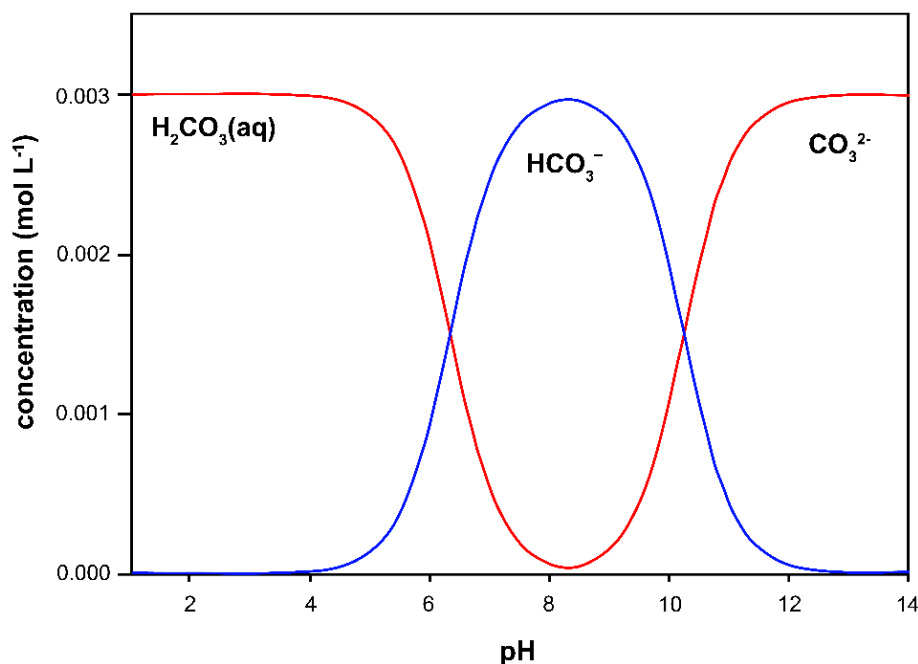
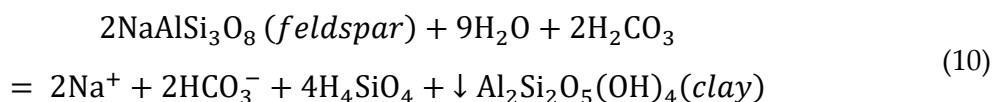


Figure 45 - Graph illustrating the concentration of the major dissolved carbon species as a function of pH. The greater the pH, the less hydrogen in the formula; thus, HCO_3^- is the most dominate carbon species in groundwater with a typical pH between 6 and 8.

The hydrogen ion is very reactive and dissolves most silicate minerals, as shown by the reaction in which two moles of silicate feldspar mineral albite ($\text{NaAlSi}_3\text{O}_8$) are weathered to two moles of Na^+ , two moles of HCO_3^- , four moles of H_4SiO_4^0 , and one mole of kaolinite clay ($\text{Al}_2\text{Si}_2\text{O}_5(\text{OH})_4$) as shown in Equation (10). The down arrow in front of the kaolinite means that it forms as a solid and is removed from solution.



The distribution of silica species in solution at the common groundwater pH of less than 8 is mainly in the form of H_4SiO_4^0 (Figure 46) but is frequently expressed in analytical tables as SiO_2 or Si. The actual molecular form depends on the pH of the environment; thus, the greater the numerical value of pH, the less hydrogen in the formula— H_4SiO_4^0 , $\text{H}_3\text{SiO}_4^{1-}$, and $\text{H}_2\text{SiO}_4^{2-}$ (Figure 46)—and the distribution as a function of pH is similar to the carbon species (Figure 45).

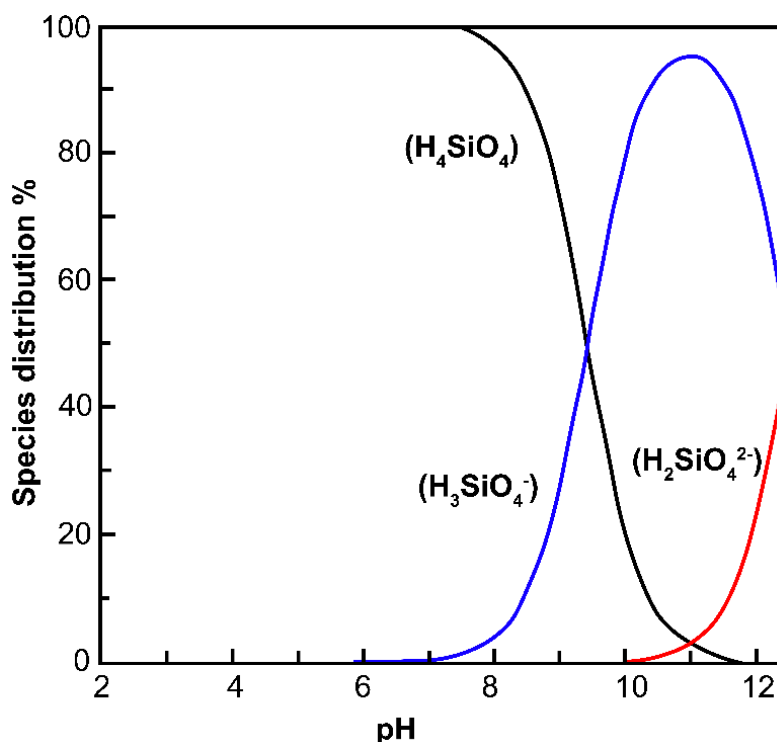


Figure 46 - Distribution of silica species as a function of pH at 25 °C in water. The greater the pH, the less hydrogen in the formula: H_4SiO_4^0 , $\text{H}_3\text{SiO}_4^{1-}$, $\text{H}_2\text{SiO}_4^{2-}$; thus, silica in most groundwaters with a pH of 7.2 is in the uncharged form of H_4SiO_4^0 .

Sulfuric acid weathering is also important in some systems containing pyrite (FeS_2). For example, one mole of pyrite (FeS_2) is oxidized by 3.5 moles of oxygen to form one mole of sulfuric acid (H_2SO_4) that dissociates into two moles of SO_4^{2-} and two moles of H^+ ions, as shown by Equation (11). The hydrogen ion attacks the bonding of the crystal and weathers the minerals. It has been the author's observation that, in general, the mass of weathering by sulfuric acid is much less than carbonic acid weathering in typical groundwaters.



Some weathering—not related to hydrogen ions—occurs by hydrolysis, where the electrical attraction of the asymmetrically charged water molecule attaches to the mineral and then pulls it away as the water responds to a hydraulic gradient thus removing ions from the crystal lattices. For example, hydrolysis occurs in the weathering of the mineral halite (NaCl). In the presence of water, one mole of NaCl dissociates into one mole of sodium ions and one mole of chloride ions without free hydrogen ions Equation (12).



An additional example is one mole of the silicate mineral forsterite (Mg_2SiO_4) reacts with water to create one mole of H_4SiO_4 , two moles of Mg^{2+} , and and 4 moles of OH^{1-} ions from the mineral framework, as shown by Equation (13).



2.6.4 Eh (Redox): An Environmental Thermodynamic Variable

The Eh or redox potential is an additional thermodynamic variable controlling solution for elements with variable valences. Oxidation is a process in which a substance loses electrons whereas reduction is a process in which a substance gains electrons. The word *redox* is a combination of the words *reduction* and *oxidation*.

The oxidation/reduction or redox potential is given the symbol Eh and is commonly measured in volts or millivolts (mV). In oxidized water with oxygen concentrations above 1 or 2 mg/L, the redox potential will be positive at 300 to 500 mV. Eh in reduced environments it will commonly be below 100 mV or negative. You can think of Eh as a measure of the potential to change the valence of an element (change the electrical charge) by adding or removing an electron. This is important as ions of an element with different valence charge have vastly different solubilities. For example, the solubility of iron depends on pH, Fe^{3+} occurs at lower pH and has a solubility of approximately 10^{-10} molar thus tends to precipitate as hydroxide, whereas Fe^{2+} occurs at higher pH and is more soluble with a solubility of approximately 10^{-3} molar.

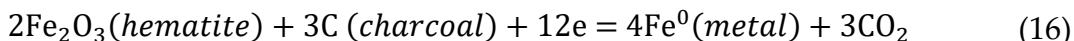
Oxidation and reduction must occur together in a reaction; that is, one element must give up an electron and one element must receive an electron. For example, one mole of methane (CH_4) is oxidized to one mole of carbon dioxide (CO_2) and two moles of water (H_2O) by the reduction of two moles of oxygen (O_2) as shown by Equation (14).



Carbon with a minus 4 valence (C^{4-}) in methane is oxidized to carbon with a plus 4 valence (C^{4+}) in carbon dioxide, while the two uncharged oxygen (O_2^0) molecules (four atoms) are reduced to O^{2-} by donating 8 electrons. Redox reactions are sometimes written to include the electron to illustrate the process. For example, the reduction of Mn^{4+} to Mn^{2+} by adding 2 electrons (e) can be written as Equation (15) showing that it is a redox reaction and a balance of charges. It is important to recognize that there are no free electrons; this is just a useful convention for illustrating an equation in which electrons are involved.



Many naturally occurring metal ores are present near the Earth's surface as oxides, and the pure metals are extracted for industrial use by a reduction process. For example, the common iron ore mineral hematite (Fe_2O_3), where the iron is +3 (Fe^{+3}), has traditionally been reduced to metallic iron (Fe^0) (no valence charge) by reacting with carbon (charcoal) at high temperatures. The carbon provides electrons to reduce the Fe^{+3} to Fe^0 , and carbon C^0 in charcoal is oxidized to +4 valence in CO_2 as shown by Equation (16).



Values of Eh are typically plotted against pH, as illustrated in Figure 47. Eh/pH stability fields for various minerals are shown in Figure 48. For example, ferrous ion (Fe^{2+}) is many times more soluble in groundwater with a low Eh, than ferric iron (Fe^{3+}). Many important minor and trace elements like iron, manganese, arsenic, manganese, chromium, uranium, and mercury have variable valence; thus, they are redox-sensitive. Sulfur, carbon, and nitrogen are common elements in groundwater that are Eh-sensitive. Table 7 gives guidance on common reduction equations.

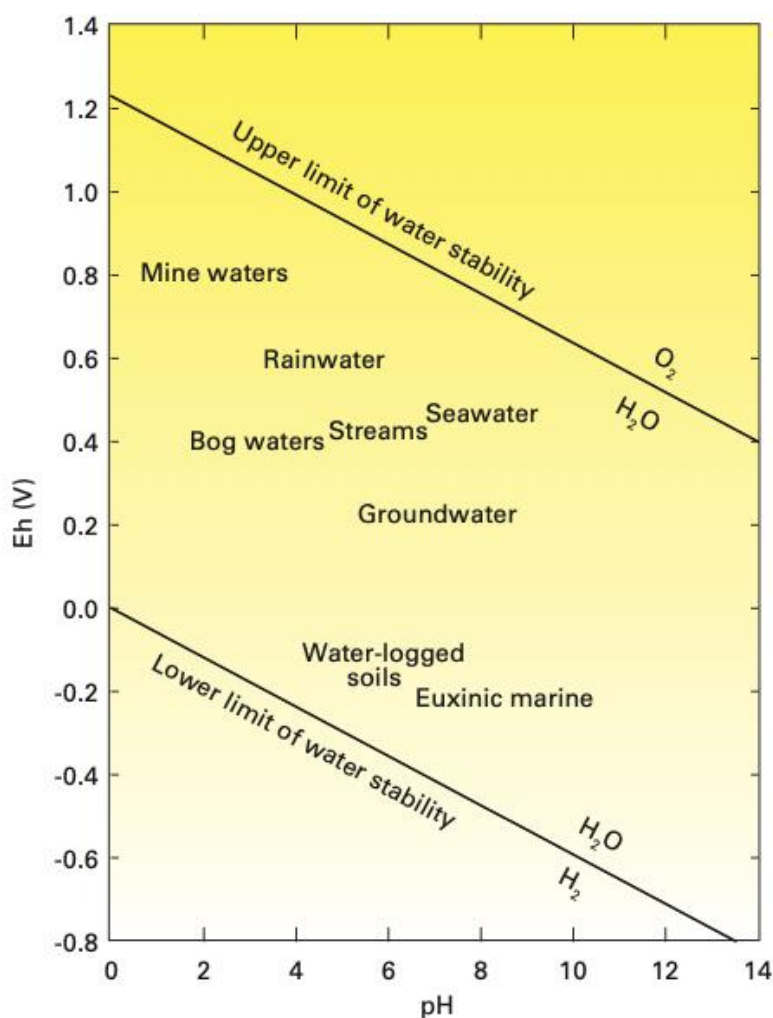


Figure 47 - Diagram showing various naturally occurring environments as a function of Eh versus pH (reproduced from Shand et al., 2007).

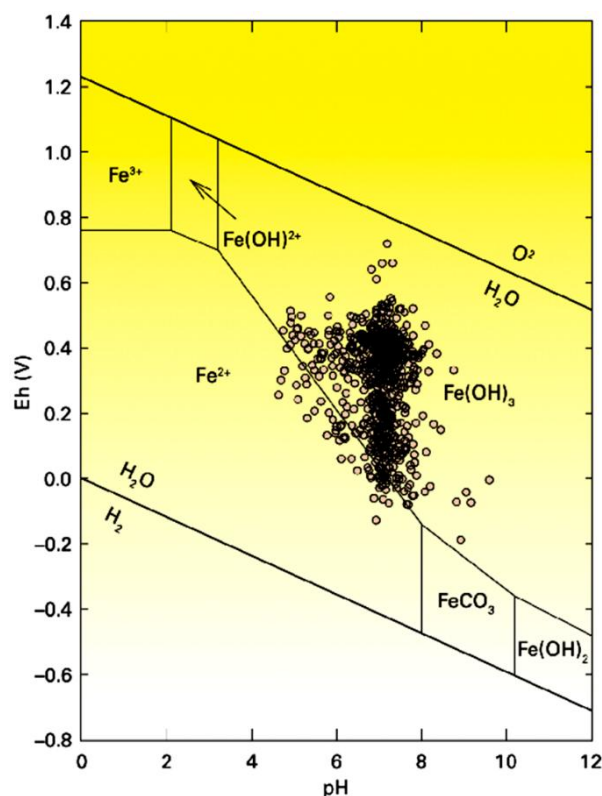


Figure 48 - Eh-pH diagram showing the stability fields for iron (Fe) species with groundwater samples from England and Wales. In this illustration most aquifer water is in equilibrium with ferric hydroxide $\text{Fe}(\text{OH})_3$, consistent with an oxidized environment (reproduced from Shand et al., 2007).

Table 7 - Several redox reactions of common groundwater solutes (reproduced from Jurgens et al., 2009).

Anoxic	NO_3^-	$2\text{NO}_3^- + 12\text{H}^+ + 10\text{e}^- \rightarrow \text{N}_{2(\text{g})} + 6\text{H}_2\text{O};$ $\text{NO}_3^- + 10\text{H}^+ + 8\text{e}^- \rightarrow \text{NH}_4^+ + 3\text{H}_2\text{O}$
Anoxic	Mn(IV)	$\text{MnO}_{2(\text{s})} + 4\text{H}^+ + 2\text{e}^- \rightarrow \text{Mn}^{2+} + 2\text{H}_2\text{O}$
Anoxic	Fe(III)/ SO_4	Fe(III) and/or SO_4^{2-} reactions as described in individual element half reactions
Anoxic	Fe(III)	$\text{Fe}(\text{OH})_{3(\text{s})} + \text{H}^+ + \text{e}^- \rightarrow \text{Fe}^{2+} + \text{H}_2\text{O};$ $\text{FeOOH}_{(\text{s})} + 3\text{H}^+ + \text{e}^- \rightarrow \text{Fe}^{2+} + 2\text{H}_2\text{O}$
Anoxic	Fe(III)- SO_4	Fe(III) and SO_4^{2-} reactions as described in individual element half reactions
Anoxic	SO_4	$\text{SO}_4^{2-} + 9\text{H}^+ + 8\text{e}^- \rightarrow \text{HS}^- + 4\text{H}_2\text{O}$
Anoxic	CH_4 gen	$\text{CO}_{2(\text{g})} + 8\text{H}^+ + 8\text{e}^- \rightarrow \text{CH}_{4(\text{g})} + 2\text{H}_2\text{O}$

In general, Eh values are important in aquifer systems that contain significant amounts of labile organic material without oxygen. Most major aquifer systems contain several mg/L of oxygen (the median is 2.7 mg/L; Table 1), and the redox reactions are important in only limited areas within these systems, typically in and around aquitards. Figure 47 illustrates the range of Eh/pH values typically found in aquifers and other water-related environments. Figure 48 illustrates the variability of iron species as a function of Eh and pH from aquifer systems in England and Wales (Shand et al., 2007). At the pH and Eh values of those aquifer systems most of the water is in equilibrium with iron species $\text{Fe}(\text{OH})_3$, not Fe^{2+} .

The hydrogeochemical role of bacteria in groundwater is generally important in controlling the concentration of solutes by creating microenvironments where pH and Eh are altered. Microbes are usually more abundant and chemically meaningful in geologically young systems where organic sediments contain abundant, easily degraded proteins, lipids, and carbohydrates. They are less critical in older, more refractory organic materials such as coal, where long-chain cellulose, tannins, and lignins are the dominant organic components. As a rule of thumb, solute analyses of iron or manganese in the solution above approximately 0.2 mg/L indicate reducing conditions in the aquifer.

2.6.5 Thermodynamic Activity: An Environmental Thermodynamic Property Activity as a function of ionic concentration

Thermodynamic activity is the final fundamental environmental variable that is considered in our quest to evaluate equilibrium. Thermodynamic activity is another way of saying *effective concentration*, that is, the concentration of solutes available for reaction.

Several conditions reduce the measured analytical concentrations that are available to react, such as total amount of dissolved solids, the size and charge of the ions, temperature, and other factors. The influence of dissolved solids can be envisioned as the other ions in the solution getting in the way of the two reactive ions and preventing them from coming together as readily (Figure 49). To adjust the measured analytical concentration to the effective concentration, a thermodynamic activity coefficient is commonly used, and typically, given the small Greek letter *gamma* (γ). The thermodynamic activity of an ion is the analytical concentration multiplied by the activity coefficient. For example, if the analytical value of Ca^{2+} in groundwater is 50 mg/L and the activity coefficient (γ) is 0.80, the effective concentration for the ion would be 50 mg/L multiplied by 0.80 or 40 mg/L.

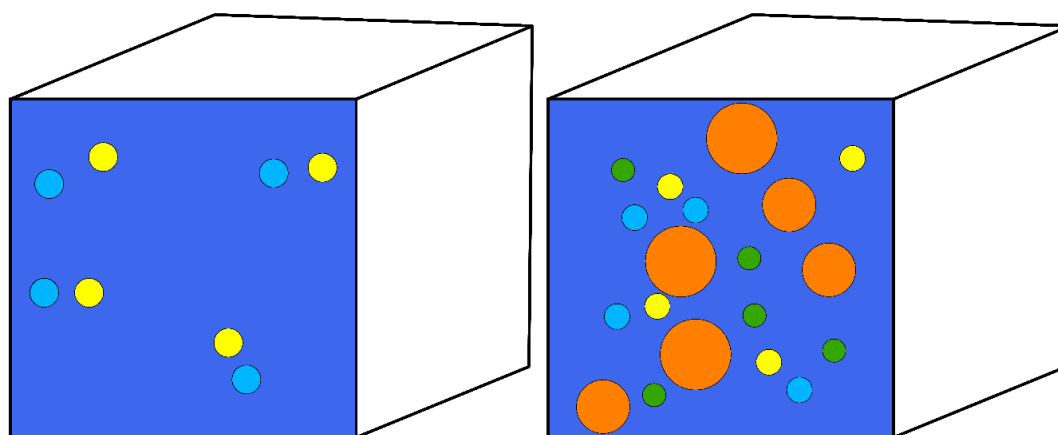


Figure 49 - Conceptual illustration of the role of solutes in the activity of the solution. Both boxes have the same number of blue and yellow symbols representing ions that can easily interact. The box on the right has additional orange and green symbols representing ions that interfere with the reactions between yellow and blue solutes by physically preventing the blue and yellow ions from coming in contact with each other. Thus, the effective concentration or activity of blue and yellow ion is less in the box on the right due to the total amount of dissolved solids.

Several geochemical models are used to calculate thermodynamic activity; the two most common are Debye-Hückle and Pitzer (Parkhurst & Appelo, 2013). Deciding which one to use for a given case depends on several factors but is primarily based on the total dissolved solids (TDS). For dilute solutions below approximately 3,000 mg/L TDS, the Debye-Hückle relation is commonly selected; for solutions with higher TDS, the Pitzer equations are commonly utilized. An example of activity coefficients (γ) with increasing ionic strength calculated with the Debye-Hückle relation is illustrated in Figure 50. Details related to calculating the thermodynamic activity using the Debye-Hückle equation are given in [Box 2](#).

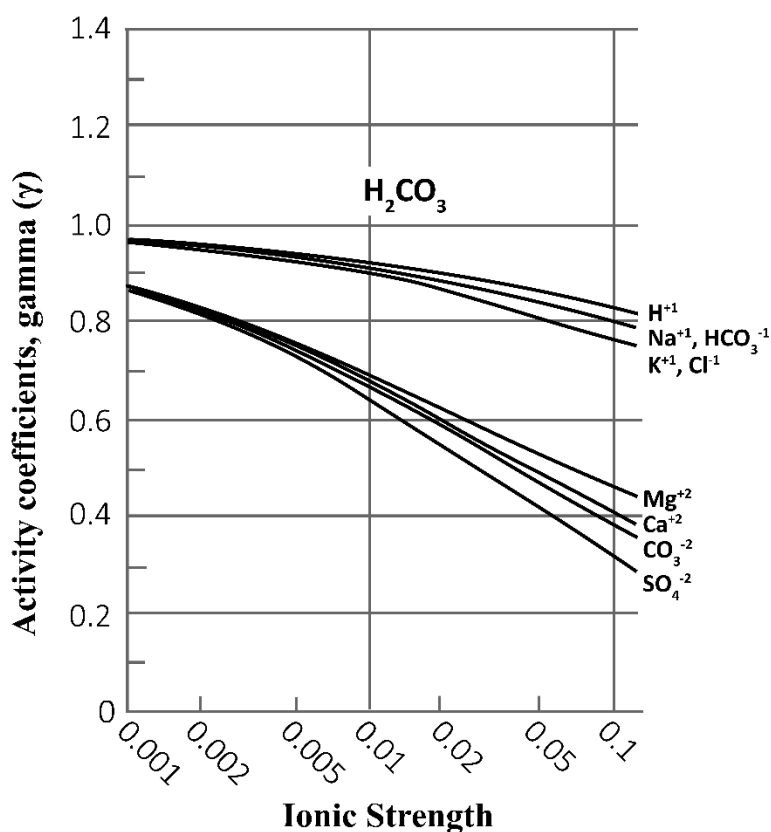


Figure 50 - Activity coefficient (vertical axis) as a function of ionic strength (horizontal axis) for a variety of common major ions using the Debye-Hückle equation. Where labels are indicated on the same line, Na^{+1} is the upper curve and HCO_3^{-1} is the lower curve; while K^{+1} and Cl^{-1} follow the same curve (modified from Freeze & Cherry, 1979).

In addition to total dissolved solids, the size and charge of the ions, and temperature, several additional factors control the thermodynamic activity of solutes that may be important in the evaluation of trace elements, including ion pairs, complex ions, and oxyanions.

Ion pairs

Ion pairs are uncharged molecules formed from a pair of oppositely charged ions attracted to each other by the difference of valance charge—a simple attraction of opposite charges (Figure 51).

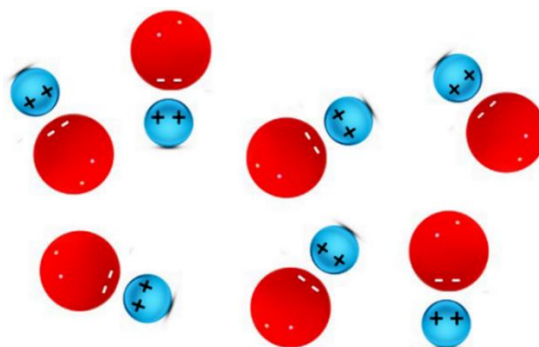


Figure 51 - Ion pairs where solutes are attracted by opposite charges, thus removing them from effective concentration; however, the bonding is not strong enough to form a compound.

For example, Ca^{2+} and SO_4^{2-} ions interact to form a CaSO_4^0 ion pair. CaSO_4^0 is neutral in charge and is typically shown with a zero superscript (⁰) to distinguish it from the mineral anhydrite with the same composition. The ion pair CaSO_4^0 exists in solution and is not a solid Equation (17).



An equilibrium constant, much like that with a mineral, can be used to calculate the concentration of ion pairs. Ion pairs effectively reduce the concentration reducing the thermodynamic activity of a solution. They typically have a much smaller impact than the ionic strength in controlling the effective concentration.

Complex ions

The formation of complex ions is another factor that decreases the effective concentration of an ion in solution. Conceptually, they are like ion pairs in that they remain in ionic form but inhibit ions from reacting by forming covalent bonds with the two atoms sharing electrons. Complex ions typically have a metal cation (positive charge) at the center that forms covalent bonds with several anions (negative charges) surrounding them thus, neutralizing the solute and preventing reaction with other ions (Figure 52). Many trace metals exhibit this type of bond (Section 3).

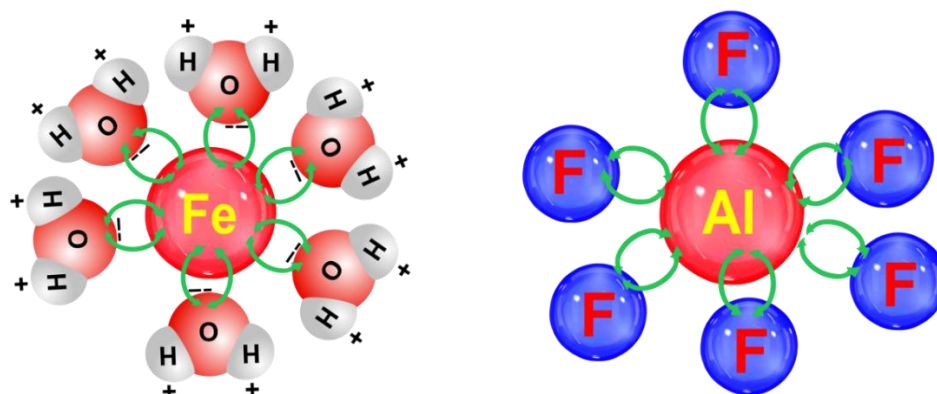


Figure 52 - Examples of covalent bonding (green arrows) generating complex ions with an iron ion (Fe) surrounded by water molecules and aluminum ion (Al) surrounded by fluoride (F) ions, thus reducing their effective concentration.

Oxyanions

Oxyanions are another way an element remains in ionic form yet is removed from reaction—reducing its activity. They are like complex ions but involve oxygen ions with the core element. An oxyanion has the general formula A_xO^{y-z} , where A represents an element, O is an oxygen atom, and x, y, and z are integer values representing the number of moles. Covalent bonding between the central atom and the oxygen atoms, with some common examples from groundwater, includes carbonate (CO_3^{2-}), nitrate (NO_3^-), and sulfate (SO_4^{2-}) ions. For example, covalent bonded sulfate ions are in the form illustrated in Figure 53. Thus, C, N, and S nearly always react in solutions via their oxyanion form rather than as a lone charged ion. Several trace elements, including arsenic, exhibit this type of bond.

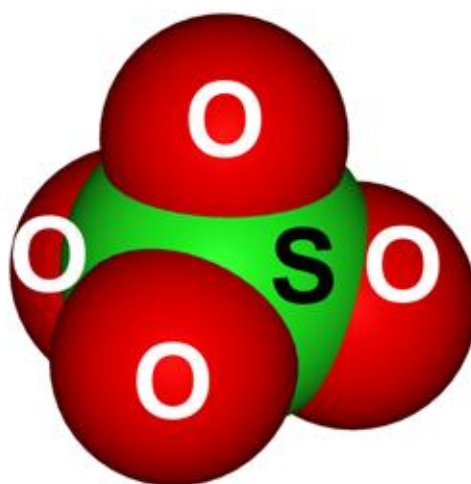


Figure 53 - Illustration of an oxyanion with the sulfur ion in the center forming a covalent bond with four oxygen ions. The chemical formula for this oxyanion is SO_4^{2-} .

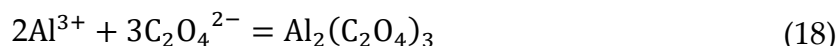
Several suffixes and prefixes are used in the nomenclature of these species. The most common oxyanion has the suffix *-ate* such as sulfate (SO_4^{2-}), nitrate (NO_3^{1-}), or carbonate (CO_3^{2-}). Additionally,

- removing one oxygen from the *-ate* oxyanion changes the suffix to *-ite*;
- removing one oxygen from the *-ite* oxyanion requires adding the prefix *hypo-*; and
- adding one oxygen to the *-ate* oxyanion requires adding the prefix *per-*.

Oxyanions form in higher concentrations in solutions where the pH is elevated. The hydroxyl ions (OH^-) present in higher pH solutions increase competition for positive sorption sites on the aquifer mineralogical framework, thus keeping the oxyanion in solution rather than being sorbed on the aquifer framework.

An additional factor controlling the transport of solutes like oxyanions and complex ions is an organic chelate, where organic coordinate bonds (covalent bonds where one atom shares two electrons) hold a metal ion and prevent it from interacting with other ions. These are compounds; for example, oxalic acid ($H_2C_2O_4$) acts as a chelating agent and is

important in transporting poorly soluble aluminum and iron in soil development (Drever & Vance, 1994) Equation (18).



Equations controlling the thermodynamic activity of ion pairs, ion complexes, oxyanions, and chelate ions are typically calculated in geochemical computer programs such as PHREEQC (Parkhurst & Appelo, 2013) because their effects are tedious to calculate by hand.

2.6.6 Equilibrium Calculations

With this background in thermodynamics, we can now address our questions.

1. Will the minerals in the aquifer dissolve and increase solute concentration?
2. Or, will the solutes precipitate as minerals and reduce the solute concentration?

These questions can be addressed by performing a calculation of the ion activity product (IAP) from a chemical analysis of the solutes that is then compared with the known equilibrium constant (K_{eq}) of the mineral under the environmental conditions of the aquifer. For most groundwater evaluations pressure can generally be ignored if the aquifer is less than 500 m deep and no gasses are involved in the reactions.

Returning to the example of equilibrium of groundwater with the mineral calcite, it is desirable to be able to determine the effective concentration from the chemical analysis using the activity coefficient. The concentrations are expressed in moles per liter (moles/L) of Ca^{2+} and CO_3^{2-} ions. Multiply the activity coefficient adjusted for ion pairs, complexes, and so on to obtain the K_{IAP} . Thus, if the temperature is 25 °C, the activity of Ca^{2+} in solution is 40 mg/L (1×10^{-3} moles/L), and activity of CO_3^{2-} is 61 mg/L (1×10^{-3} moles/L), then the $K_{\text{IAP}} = [\text{Ca}^{2+}][\text{CO}_3^{2-}]$ is 1×10^{-6} . This value is then compared to the known value of K_{eq} for calcite at the known temperature ($10^{-8.4}$ from Table 6). The ratio of $\frac{K_{\text{IAP}}}{K_{\text{eq}}}$ typically expresses this calculation and is generally referred to as the *saturation index* (SI). There are three potential outcomes of this ratio:

- 1) = 1 solute is in equilibrium with respect to the mineral;
- 2) >1 solute is supersaturated with respect to the mineral and may precipitate; or
- 3) < 1 solute is undersaturated with respect to the mineral and may dissolve.

In our example, $(1 \times 10^{-6} \text{ moles/L}) / (10^{-8.4} \text{ moles/L}) = 251$, which is much greater than 1 and thus the solution is supersaturated with respect to CaCO_3 , and will likely precipitate calcite (CaCO_3) from solution.

Owing to analytical uncertainties in both K_{IAP} and K_{eq} , there is a range of error in most calculations; SI ratios between 0.9 and 1.1 are generally considered at equilibrium. The logarithm to the base 10 of the ratio is commonly used, and the saturation index is expressed as $\log_{10} \frac{K_{\text{IAP}}}{K_{\text{eq}}}$, which in this case is 2.4.

If there are different molar ratios in the equation, there is an additional step in the calculation. For example, in the case of the IAP for the mineral fluorite $[\text{CaF}_2] = [\text{Ca}^{2+}] + [2 \text{F}^-]$, there are two fluorite atoms for every calcium atom; convention states that the activity of fluoride would be squared, that is, $[\text{Ca}^{2+}][\text{F}^-]^2$. The general formula can be expressed as shown by Equation (19).



In Equation (19), a moles of element A plus b moles of element B is in equilibrium with c moles of element C plus d moles of element D; so $\text{IAP} = \frac{[C]^c[D]^d}{[A]^a[B]^b}$. Thus, in the balanced chemical equation, the concentration of the products and reactants is always raised to the power of their coefficients. All these calculations and much more are performed in geochemical codes like PHREEQC (Parkhurst & Appelo, 2013) or similar programs. The reader should become familiar with using PHREEQC as it is a very powerful and useful code that comes with many examples of geochemical conditions although the input and output are a bit clunky. It is [available at no cost from the USGS](#) and makes the required thermodynamic calculations. The PHREEQC program and its supporting data input system were written for the Microsoft Windows operating system. However—as there are many Mac users—There is a MacPHREEQC version with instructions for downloading and running an example using a Macintosh operating system given in [Box 3](#).

2.7 Kinetics of Precipitation

When minerals fail to precipitate from the solution, even if they are thermodynamically supersaturated, it is referred to as a *kinetic delay*. A kinetic delay typically occurs when an incompatible ion, in terms of charge or size, blocks the orderly deposition of the ions building the crystalline mineral (Figure 54). For example, the sulfate ion is believed to inhibit the formation of dolomite, resulting in significant thermodynamic oversaturation that may last for years in groundwater.

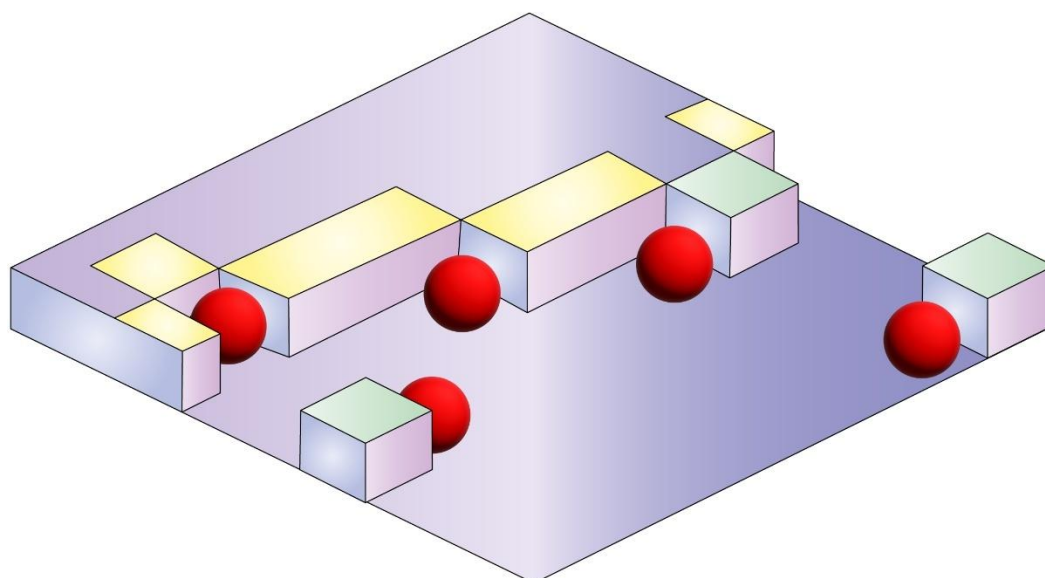


Figure 54 - Kinetic blocking in which ions of different sizes or charges prevent ions from fitting into orderly positions in crystal structures. The red spherical shaped ions illustrate the lack of fit with the rectangular shaped ions that form the crystal, which prevents crystal growth and thus, blocks removal of solutes from solution.

2.7.1 Cation Exchange and Adsorption

Most clay minerals have many ion exchange sites occupied by various cations, commonly Ca^{2+} , Mg^{2+} , Na^+ , and K^+ but less commonly NH_4^+ and H^+ . These exchange sites are the result of a negative electrical charge of the crystal structure of clays owing to an aluminum ion with a 3+ charge substituting in the crystal for a silica ion with a 4+ charge. Positively charged cations from the solution are, thus attracted and held on the crystal surface by this coulombic charge attraction. For equal concentrations, cation exchange takes place in the following order: $\text{Ca}^{2+} > \text{Mg}^{2+} > \text{K}^+ > \text{Na}^+$, which is a function of charge density where Ca^{2+} has the highest and Na^+ the lowest affinity for the clay surface; however, the actual exchange order is controlled by individual cation concentration. If for example Na concentration is highly elevated in solution it will occupy all the exchange sites.

The CEC (cation exchange capacity) can be expressed as the total number of moles of exchange sites per unit mass (kilograms) of rock or per unit volume (cubic meters) of rock. Many sedimentary aquifers were formed in a marine environment; thus, their initial ion exchange sites were filled with sodium, which is several tens of times more concentrated in seawater than other positively charged cations. Thus, these clays have the potential to exchange calcium in solution for sodium on the crystal site (Figure 55). If sodium is added to the water and calcium is removed, the process is sometimes called *natural softening* as it mimics commercial water-softening techniques.

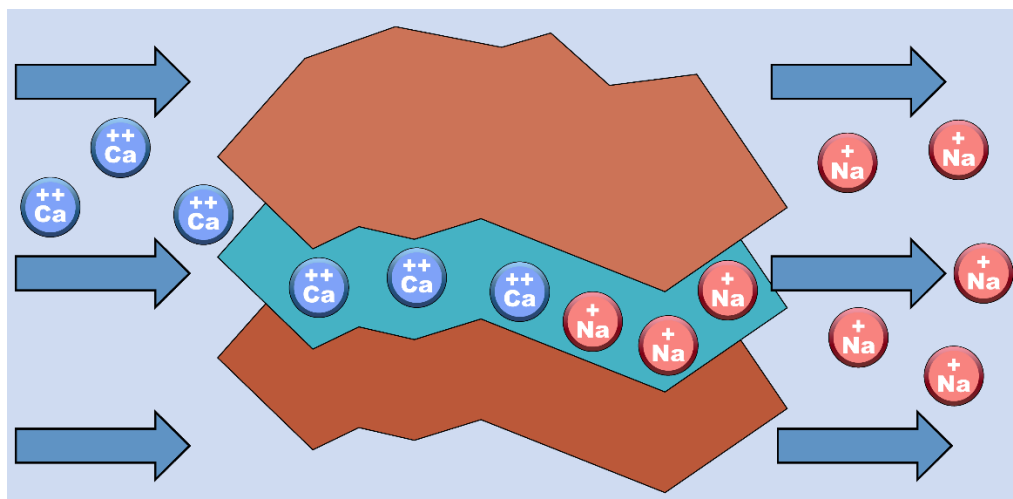


Figure 55 - Layers of clay minerals illustrating ion exchange. Calcium (Ca) in solution is replacing sodium (Na) on mineral exchange sites within a clay, resulting in sodium going into solution and removing calcium from solution. Ions in solution are labeled with white letters while those attached to ion exchange sites are labeled with black letters. This is nature's way of softening water.

The exchange capacity of some systems is substantial, thus requiring a significant number of exchangeable ions to remove the initial sorbed ion. In addition, ion exchange may increase the pH if the removal of the calcium ion from the solution forces thermodynamic undersaturation of the groundwater with respect to calcite—which is then dissolved, consuming hydrogen and creating bicarbonate ions. Thus, the pH may increase to 9 or 10 instead of a pH of around 7, which is typical for groundwater of most systems.

Total solutes can increase with the calcium for sodium exchange as the calcium removal shifts the calcium carbonate equilibrium, causing more calcite (CaCO_3) to dissolve, adding calcium and bicarbonate ions and removing hydrogen ions. As the solution of calcite adds calcium, this allows additional ion exchange, driving it towards a sodium bicarbonate water that is higher in solute concentration than the original water. Sodium bicarbonate minerals are much more soluble than calcium bicarbonate, allowing the increase of bicarbonate ion concentration. Sections 4.3 and 7.2 of this monograph include examples of ion exchange.

2.7.2 Adsorption — A Process of Removing Solutes

Adsorption, sometimes known as *chemisorption*, is the attraction of opposite charges or covalent sharing of electrons. This *adsorption* contrasts with *absorption*; in the latter, an ion enters the matrix—for example, gas absorbs in a liquid.

Physical adsorption of ions from solution onto the mineral framework often results from a charge on the mineral surface created by an iron or manganese hydroxide coating (Figure 56) or by substituting an aluminum ion with a 3+ charge for a silica ion with a 4+ charge in the crystal structure. Thus, it is much like ion exchange except usually H^+ or OH^- is exchanged from the solid to the solution to maintain electrical neutrality of the solution. This sorption is sometimes referred to as *Langmuir sorption* after the Nobel Prize-winning chemist Irving Langmuir, who quantified the process (Irving Langmuir is also the

uncle of Don Langmuir, who wrote the outstanding geochemistry text *Aqueous Environmental Geochemistry*).

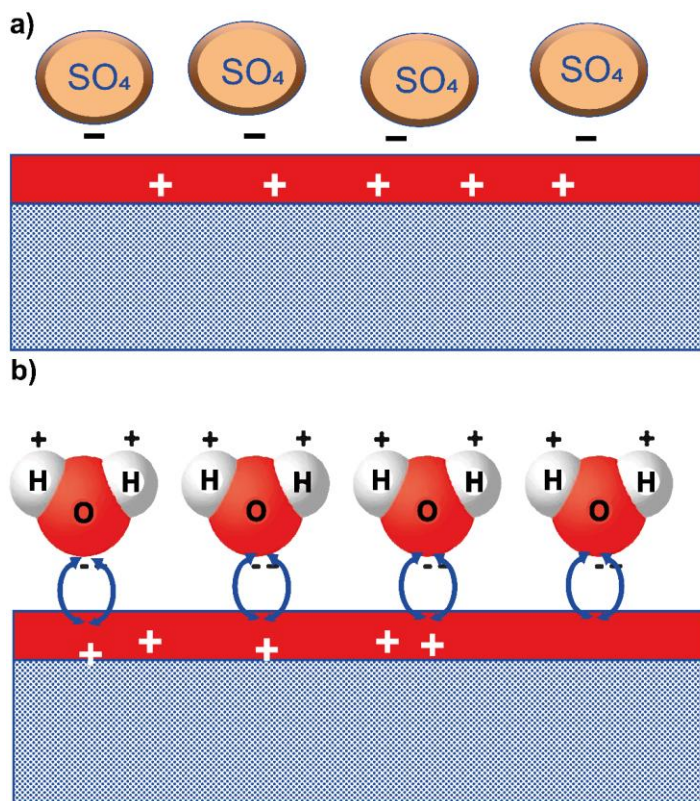


Figure 56 - Conceptual model of charged ions being attracted to a mineral surface by a) ionic charge difference and b) ions sharing electrons (covalent bonding) with a mineral surface.

Solute mass involved in sorption is usually small per unit mass of the aquifer material and is usually only detected in mass balance evaluation of trace elements. However, sudden changes of temperature, pH, or Eh from anthropogenic contamination can mobilize a significant mass of previously sorbed ions. Adsorption can cause significant delay in transport from the time of input of an ion into an aquifer system until the time it is discharged.

2.8 Hydrodynamic Dispersion in Transport

Hydrodynamic dispersion is a function of both physical mixing owing to different flow path length (resulting from different pore sizes and shapes) and chemical diffusion. Much intellectual effort has been applied in developing an advective-diffusion equation and dispersion coefficients that capture both processes. Consider the physical condition depicted in Figure 57, where water and solute flow takes place from left to right. At a specific time, the flow starts, the red minerals begin to dissolve, and the solutes from these minerals take different paths through the sand. Thus, their arrival time varies; the solute is diluted by mixing and this dilution is referred to as *hydrodynamic dispersion*.

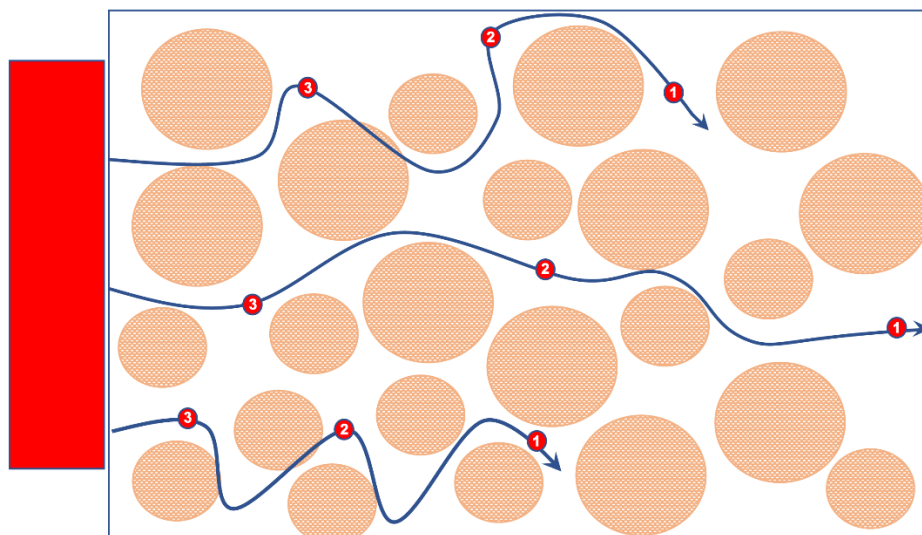


Figure 57 - Schematic diagram showing individual flow lines in a porous medium with a snapshot of individual solutes (red dots) released at times 1, 2, and 3. This illustrates that different paths traveled by solutes have different lengths and velocities which results in different amounts of time to traverse the volume of porous medium shown here. This variability dilutes the solute at the leading edge of the contaminant plume and is referred to as hydrodynamic dispersion by advection.

If a vertical cylindrical column containing nearly uniform glass beads is initially filled with distilled water and a conservative non-reactive solute (chloride) of known but low concentration (C_0) is continuously introduced at the top of the column, and the concentration (C) of this solute is continually measured as water discharges from the bottom of the column the measurement will be zero at first and then gradually rise until it equals the input concentration.

The concentration of solute at the end of the column is shown as the ratio of the concentration to the initial concentration ($\frac{C}{C_0}$) in Figure 58. In this type of experiment, measuring the volume discharged from the column in terms of pore volumes is convenient. A pore volume is the volume of pore spaces of the material under consideration (Section 6.2 for more explanation). In a perfectly isotropic system with no hydrodynamic dispersion, each flow path is the same length. In this condition, $\frac{C}{C_0}$ will be zero until one pore volume is replaced, then $\frac{C}{C_0}$ will abruptly be 1 and the plot of the solute concentration versus pore volume would be a vertical line on the graph (Figure 58). This is referred to as *plug flow* (dashed blue line in Figure 58a). However, in natural systems, there are always flow paths of different lengths, and the $\frac{C}{C_0}$ curve is a reclined S-shape-like the black dashed line in Figure 58a, rather than a vertical line and, for a conservative ion that does not react, $\frac{C}{C_0}$ will always be 0.5 at 1 pore volume. The experiment that produced the data shown in Figure 58a was run for 0.5 hours using a dilute solution to minimize chemical diffusion.

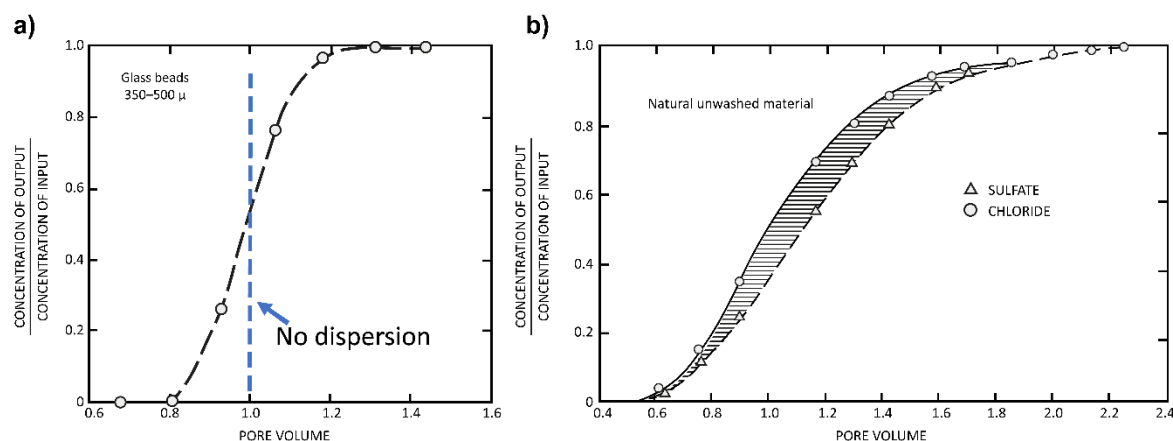


Figure 58 - a) Graph showing the relationship between the concentration ratio (C/C_0) of a conservative solute at the outflow of a laboratory column and the number of pore volumes that have passed through the column. The column is homogeneously packed with glass beads of 350- to 500-micron diameter. b) Graph showing the relation between the concentration ratio of both a conservative solute (circles) and reactive solute (triangles) in a heterogeneous medium-grained sand, indicating more pore volumes are necessary to move the reactive tracer through the column than a conservative solute.

The greater the heterogeneity of size and shape of pore openings, the greater the range in length of flow lines and the more stretched out the reclined S-shaped curve will be. For example, the column used to generate the data shown in Figure 58b is filled with well-sieved medium sand with a broader range of sizes and shapes than the glass beads used in the column that produced the data shown in Figure 58a. A dilute solution of sodium chloride and sodium sulfate ions were used as solutes where sulfate was known to sorb on the iron oxide of the sand grains. In this case, the S-shaped curve is elongated because more pore volumes are required to move the solute out of the column.

If there is a reaction between the solute and the medium filling the column, the $\frac{C}{C_0}$ of the reactive solute will be delayed or retarded (bottom curve Figure 58b) relative to the conservative solute (top curve) because some of the solute is temporarily delayed by sorbing to the medium. In this example, the sorption of sulfate ion (SO_4^{2-}) on the iron hydroxide coating on the sand grains caused a loss of sulfate ion compared with the conservative chloride ion that was not sorbed. The mass of SO_4^{2-} sorbed to the solid at any time (as indicated by number of pore volumes) is directly related to the area between the two curves (Figure 58b).

2.9 Solute Control in Open and Closed Systems

In addition to the source of solutes (Figure 3) controlling the groundwater solute concentration and composition, they also depend on the chemical *openness* of the groundwater system. In a totally open system, all solutes enter and leave; in a totally closed system, all solutes remain in the system, with only water leaving. Partially open or *leaky* systems (Figure 59) are typically of interest in semi-arid and arid areas where concentration increases to the point of mineral precipitation which selectively removes solutes and, thus, alters the ratios of the remaining solutes. For example, calcium is commonly removed by

precipitation of calcite, leaving a sodium-enhanced solution; precipitation of gypsum removes both calcium and sulfate, changing the concentration of the remaining solution for both ions. The amount of change of the solute ratios depends on the leakage ratio—that is, the ratio of mass solute leaving a system volume divided by the mass of solute entering the volume—which will always be less than 1.0 in a leaky system.

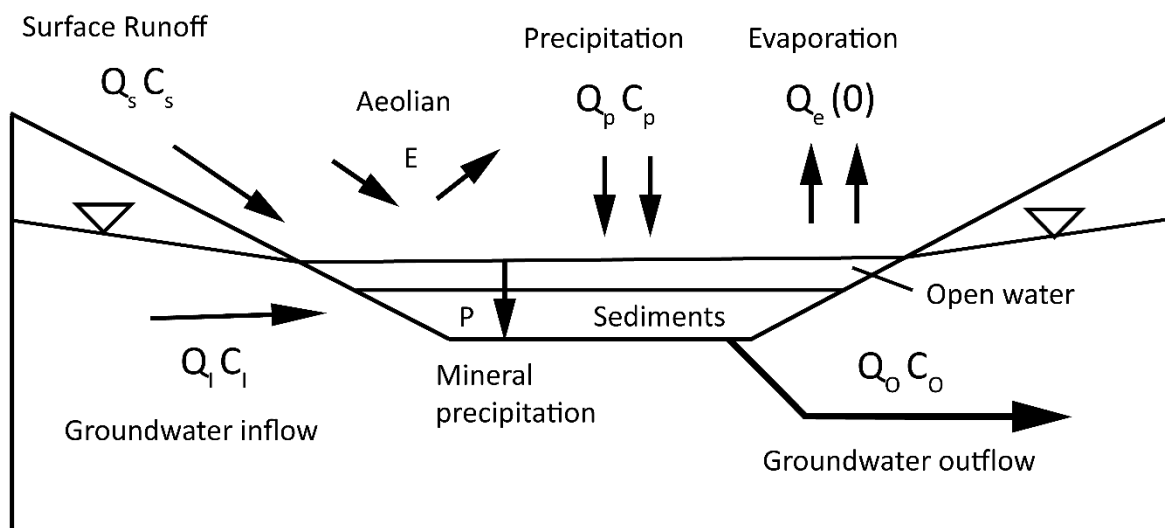


Figure 59 - Conceptual mass-balance model for a leaky sediment basin illustrating water and solute input and loss, where Q represents water flux and C represents concentration in that flux. The product of Q and C for each input and output component is the mass flux for that component. P represents mineral precipitation and E represents aeolian process that can introduce or remove chemical elements from the system (reproduced from Wood & Sanford, 1990).

The continental surface of the Earth has many topographically closed basins receiving groundwater, such as the Caspian Sea in Eurasia, the Great Salt Lake in North America, Lake Eyre in Australia, Lake Titicaca in South America, and Lake Chad in Africa. Groundwater and surface water that flow into these basins is subsequently evaporated, which removes water but not the solutes, thus concentrating solutes that form mineral precipitates and brines. These and hundreds of smaller closed basins cover approximately 18 percent of the Earth's continental surface (Hammer, 1986), some of which are leaky and contribute solutes to the downgradient groundwater.

Given a starting composition for a closed system, the solute evolution to an equilibrium condition can be predicted for each ion (Hardie & Eugster, 1970); that is, a specific and characteristic assemblage of minerals is determined by mineral solubility and the starting solute composition. The solute ratios control which solute is limiting when precipitation of a mineral begins and which other solute will continue to increase in concentration with continued evaporation. The evolution of solute concentration and minerals precipitating in a partially open or leaky system (Wood & Sanford, 1990; Sanford & Wood, 1991) is significantly different than in a closed system and is highly dependent on the degree of leakage (Figure 60).

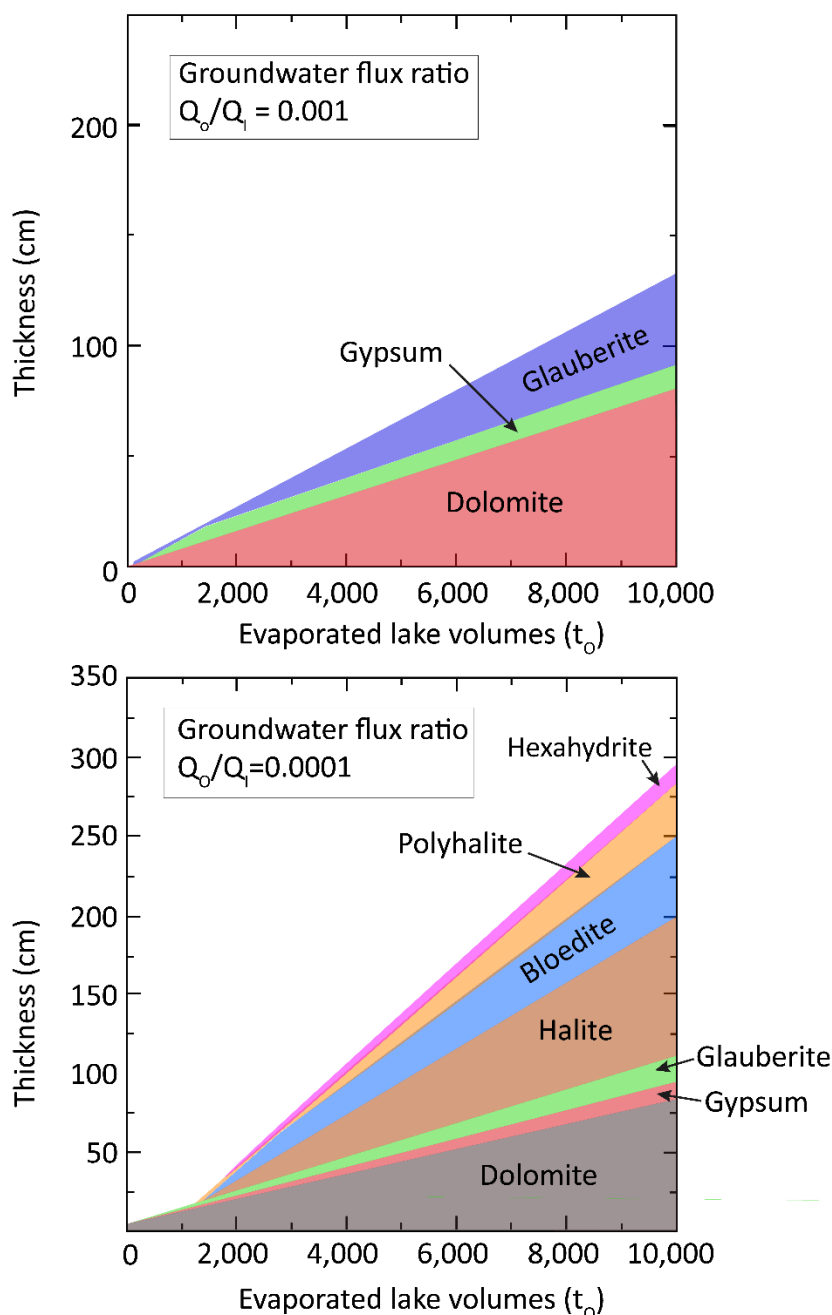


Figure 60 - Example of the mineralogical change and thickness associated with the same Southern High Plains groundwater solute input chemistry but different flux leakage ratio at 25 °C. a) Thickness of the three minerals formed in a “leaky” basin with an output/input flux ratio of 0.001. b) Thickness of seven minerals formed in a “leaky” basin with an output/input flux ratio of 0.0001. The large difference in the number of minerals and their thickness depends only on the leakage flux ratio of the basin. Solute changes follow a pattern dependent on the leakage ratio (Wood & Sanford, 1990).

The solute loss from a leaky system has profound control over the suite and thicknesses of evaporite minerals formed in the basin and in the remaining groundwater solutes; that is, it is possible to attain a great thickness of a single mineral rather than a thin covering of many minerals as groundwater is evaporated. For example, changing only the leakage ratio, not the solute input composition, illustrates how widely different solutes and

mineralogy can develop (Figure 60). Thus, with the same input composition, saline lakes in a region can have significantly different brine chemistry and mineral deposits. The solute evolution for systems with two different leakages is shown in Figure 61, dramatically illustrating the impact of different leakages on solute evolution.

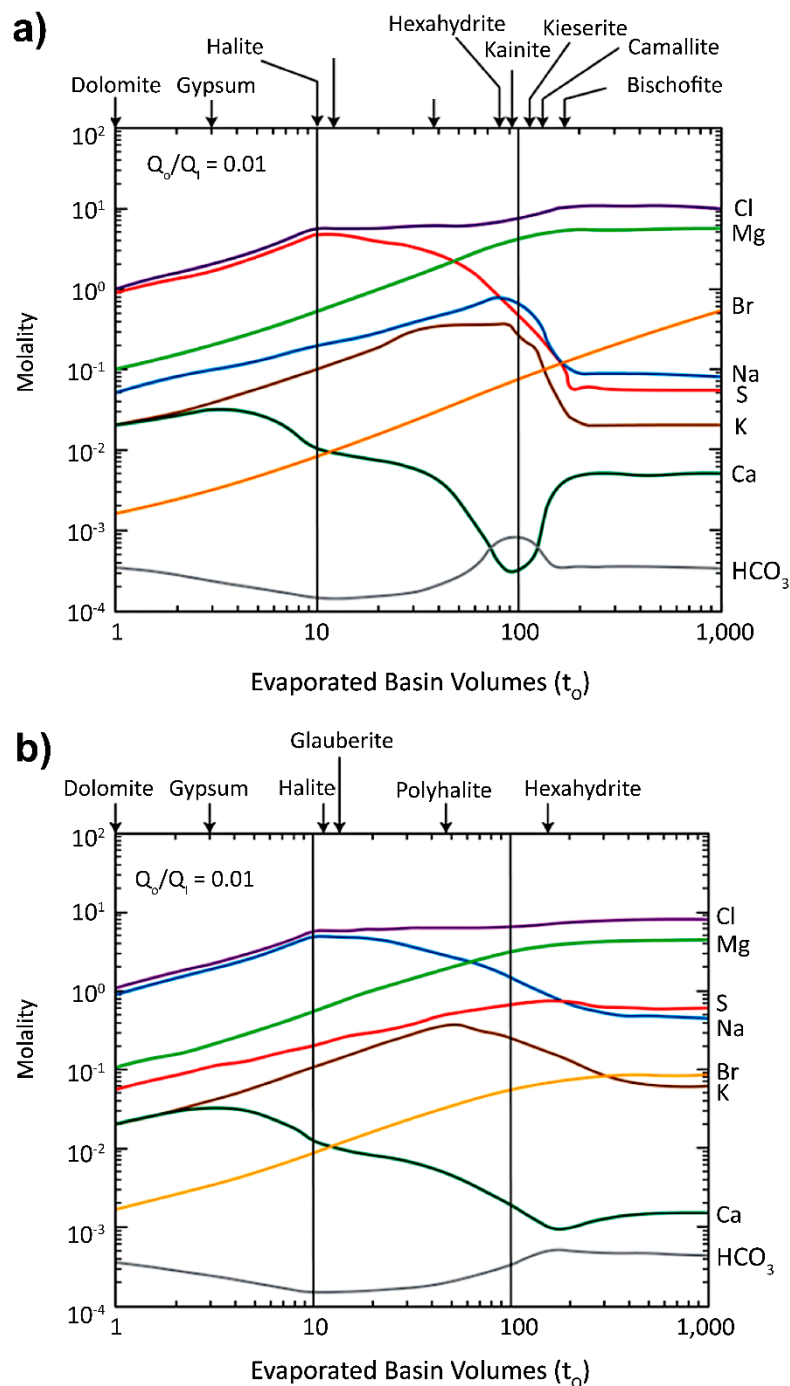


Figure 61 - a) Solute evolution of marine water driven by evaporation from an open system with a leakage of 0.01 as the various minerals are precipitated. Labels at the top of the graph indicate when each mineral begins to precipitate. b) Solute evolution of marine water from a more closed system with a leakage ten times less than that shown in (a), i.e., 0.001. There is a large difference in the type of mineral precipitated and the time of onset of precipitation in the evolutionary sequence given different leakage ratios (Sanford & Wood, 1991).

2.10 Ultrafiltration (Reverse Osmosis) as a Physical Control on Solute

Ultrafiltration, hyperfiltration, reverse osmosis, or salt sieving are different names for the exclusion of ions as water is forced through a membrane of low-permeability material such as clay or shale (Figure 62). This process neither adds nor removes total solutes directly, but it can alter the groundwater composition and concentration at locations upstream and downstream of the ultrafiltration membrane. The process can change solute concentration in the system by changing thermodynamic conditions and causing additional mineral dissolution downstream or precipitation upstream of the membrane (Wood, 1976; Neuzil & Pearson, 2017).

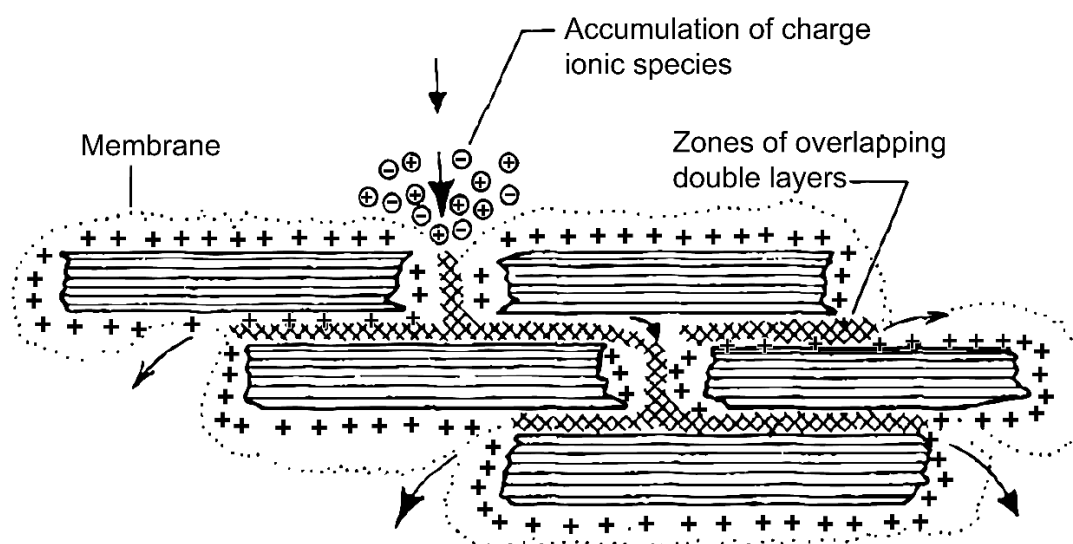


Figure 62 - Mechanism of ultrafiltration (i.e., ion filtration) in aquifer systems, with water flow from the top towards the bottom of the figure as indicated by the arrows and charged ions being excluded by the charge field created by the ions between the clay particles represented by striped zones. The charge field is strongest (double layers) between adjacent clay particles (Wood, 1976).

Many common clay minerals have an electrical charge owing to the substitution of 3+ aluminum ions for a 4+ silica ions in their structure. The unbalanced charge attracts a surrounding coating of cations thus, when the clay particles are compressed the charges on the cations form a charge field in the adjacent pore spaces. This charge field inhibits charged ions from being transported through the pore spaces; however, uncharged molecules can pass through.

Thus, one observes an increased ion concentration on the recharging side and a lower solute concentration on the discharge side of the membrane (Figure 62). Ions like chloride, magnesium, and sodium that form highly soluble minerals can thus accumulate on the upgradient side and increase in concentration. This increase in concentration may cause ions to exceed their mineral solubility, resulting in the precipitation of some ions on the upgradient side and the dissolution of minerals on the downgradient side, thus changing both the solute concentration and the mineral ratios. Neuzil and Person (2017, p. 4938) concluded:

Our analysis suggests ultrafiltration in geologic membranes is complex, and its effects can be counterintuitive; conditions evolve over long periods, salinity changes tend to be self-limiting, and salinity increases and decreases may not occur where expected.

Ultrafiltration's effects may not be recognized, but their presence can change how groundwater flow environments are interpreted and understood, especially in deeper basins with shale lithologies (Section 5.6 provides an example of ultrafiltration).

2.11 Section Wrap-up

Initial inspection of the literature on an aquifer system can aid in focusing on the most probable solute sources and sinks. If the system is young and only a few volumes of recharge water have passed through it, then legacy solutes may be a significant source of current day solutes.

In younger systems, much of the solute mass may be controlled by mineral weathering. As weathering progresses, the mineralogical framework becomes more important if it is readily soluble—such as carbonate or sulfate minerals— or in alluvial fans, river deposits, or glacial deposits that have many broken and exposed chemical bonds. Recently fractured rocks are more reactive than older fractures because surfaces become less reactive once coated with weathering products. In mature clastic aquifers, where the relatively unreactive quartz or other low soluble silicates dominate, the mineralogical framework limits the source of solutes from weathering, and atmospheric aerosols may be an important source of solutes.

In aquifers of topographically low areas near streams, oceans, or lakes, one might expect solutes to enter from underlying aquifers. Thus, the primary source of solutes to aquifers—atmospheric, weathering, and solutes from adjacent or underlying aquifers, or relic solutes—are commonly controlled by climate and hydrogeologic properties, not by geochemical processes.

Over geologic time, all aquifers are open to both water and solutes; so weathering dissolves and removes most minerals except for highly resistant quartz, leaving nearly pure quartzite aquifers that are occasionally observed in the geologic record. Additionally, solute flux from the diffusion of the internal low permeability zone declines with time as their soluble mass is depleted. Each aquifer environment is unique concerning recharge flux, precipitation concentration, solute flux from outside the aquifer, relic solutes, mineral composition, and age since active flow started that controls the solute sources and sinks. Thus, predicting in detail how groundwater solutes will evolve is exceptionally challenging because tectonics, chemistry of the atmosphere, and climate change through time.

[Exercise 1](#)  provides an opportunity to explore the intrinsic and environmental controls on the thermodynamics that control mineral equilibrium.

3 Geogenic Trace Elements Related to Human Health

We continue our discussion of the origin of solutes and shift our emphasis from major ions to trace elements that are known to be of concern for human health. Globally, over five billion individuals rely on groundwater for drinking and household needs. Although groundwater is generally a pathogen-free, safe, and reliable source of drinking water for billions of people, some common geogenic minor and trace elements may pose potential human-health concerns, with the greatest number of people being affected by the geogenic solutes arsenic and fluoride. Elevated arsenic and fluoride concentrations (colorless, odorless, and tasteless) currently affect more than one hundred million people across the globe through groundwater.

The United States Environmental Protection Agency (USEPA), the World Health Organization (WHO), and others have established human-health benchmark values (HHBs) to aid in the evaluation of health risks. Benchmarking is an advisory management approach; although not mandatory, maximum contaminant level (MCL) is a concentration that can be legally enforced. In this section, the hydrogeochemistry of twelve common health-related geogenic trace elements are examined — Mn, As, Rn, Sr, U, Fl, Mo, Pb, Sb, Se, Zn, and Li—that occur at concentrations greater than HHBs in more than 1 percent of water samples from the US Principal Aquifers (Ayotte et al., 2011). Because the US Principal Aquifers cover a large range of climates and lithologies, it is assumed the findings would likely be similar globally.

Large-scale differences in concentration of trace elements in groundwater reflect several hydrologic conditions and geochemical processes, including ion competition, alkalinity, complexation, redox, pH, TDS, and temperature. For example, trace elements that commonly exist as cations—including cadmium (Cd), cobalt (Co), copper (Cu), lead (Pb), nickel (Ni), and zinc (Zn)—are more likely to stay in solution at lower pH. This condition results from a greater concentration of positively charged hydrogen ions (H^+) competing for negative ($-$) sites on the aquifer mineral framework, thus preventing cation sorption and allowing these solutes to remain in solution.

Conversely, trace elements such as arsenic (As), uranium (U), chromium (Cr), selenium (Se), and molybdenum (Mo) that form negative oxyanion complexes with oxygen ions are more likely to remain in solution as the pH increases. They occur in greater concentrations in groundwater in arid regions with higher pH and more oxygen than in humid regions. This condition occurs because competition from the negatively charged hydroxyl ion (OH^-) for positive sites on the aquifer mineral framework prevents the negatively charged oxyanions from attaching to the aquifer framework, thus remaining in solution.

Much of the following descriptive information is taken from the NAWQA database of principal aquifers in the USA (DeSimone et al., 2014; and Ayotte et al., 2011). As part of

our puzzle-solving approach in this monograph, we look at the geochemical and hydrogeologic processes that control the concentration of these elements (Figure 63). The USGS's principal aquifers have been evaluated for important major, minor, and trace elements that clearly illustrate the widespread occurrence of some geogenic elements of human health concern (Figure 64). A summary of the data is presented in Table 8.

Unconsolidated and semiconsolidated sand and gravel aquifers

-  Sand and gravel aquifers north of the limit of Quaternary continental glaciation and east of the Rocky Mountains. The aquifers are mostly in glacial deposits – Gray is combined with color of underlying aquifer
-  1 Basin and Range basin-fill aquifers
-  2 Rio Grande aquifer system
-  3 California Coastal Basin aquifers
-  4 Pacific Northwest basin-fill aquifers
-  5 Columbia Plateau basin-fill aquifers
-  6 Snake River Plain basin-fill aquifers
-  7 Puget Sound aquifer system
-  8 Willamette Lowland basin-fill aquifers
-  9 Northern Rocky Mountains Intermontane Basins aquifer system
-  10 Central Valley aquifer system
-  11 High Plains aquifer
-  12 Pecos River Basin alluvial aquifer
-  13 Mississippi River Valley alluvial aquifer
-  14 Seymour aquifer
-  15 Surficial aquifer system
-  16 Unconsolidated-deposit aquifers (Alaska)
-  17 South Coast aquifer (Puerto Rico)
-  Coastal Plain aquifer systems in semiconsolidated sand
- 18 Coastal lowlands aquifer system
- 19 Texas coastal uplands aquifer system
- 20 Mississippi embayment aquifer system
- 21 Southeastern Coastal Plain aquifer system
- 22 Northern Atlantic Coastal Plain aquifer system

EXPLANATION

Sandstone aquifers

-  23 Colorado Plateaus aquifers
-  24 Denver Basin aquifer system
-  25 Lower Cretaceous aquifers
-  26 Rush Springs aquifer
-  27 Central Oklahoma aquifer
-  28 Ada–Vamoosa aquifer
-  29 Early Mesozoic basin aquifers
-  30 New York sandstone aquifers
-  31 Pennsylvanian aquifers
-  32 Marshall aquifer
-  33 Cambrian–Ordovician aquifer system
-  34 Jacobsville aquifer
-  35 Lower Tertiary aquifers
-  36 Upper Cretaceous aquifers
-  37 Upper Tertiary aquifers

Sandstone and carbonate-rock aquifers

-  38 Edwards–Trinity aquifer system
-  39 Valley and Ridge aquifers – Carbonate-rock aquifers are patterned
-  40 Mississippian aquifers
-  41 Paleozoic aquifers

Carbonate-rock aquifers

-  42 Basin and Range carbonate-rock aquifers
-  43 Roswell Basin aquifer system
-  44 Ozark Plateaus aquifer system
-  45 Blaine aquifer
-  46 Arbuckle–Simpson aquifer
-  47 Silurian–Devonian aquifers
-  48 Ordovician aquifers
-  49 Upper carbonate aquifer
-  50 Floridan aquifer system
-  51 Biscayne aquifer
-  52 New York and New England carbonate-rock aquifers
-  53 Piedmont and Blue Ridge carbonate-rock aquifers
-  54 Castle Hayne aquifer
-  55 North Coast Limestone aquifer system (Puerto Rico)
-  56 Kingshill aquifer (Virgin Islands)

Igneous and metamorphic-rock aquifers

-  57 Southern Nevada volcanic-rock aquifers
-  58 Pacific Northwest basaltic-rock aquifers
-  59 Snake River Plain basaltic-rock aquifers
-  60 Columbia Plateau basaltic-rock aquifers
-  61 Hawaiian volcanic-rock aquifers – Locally overlain by sedimentary deposits
-  62 Piedmont and Blue Ridge crystalline-rock aquifers

Other

-  Rocks that are minimally permeable but may contain locally productive aquifers

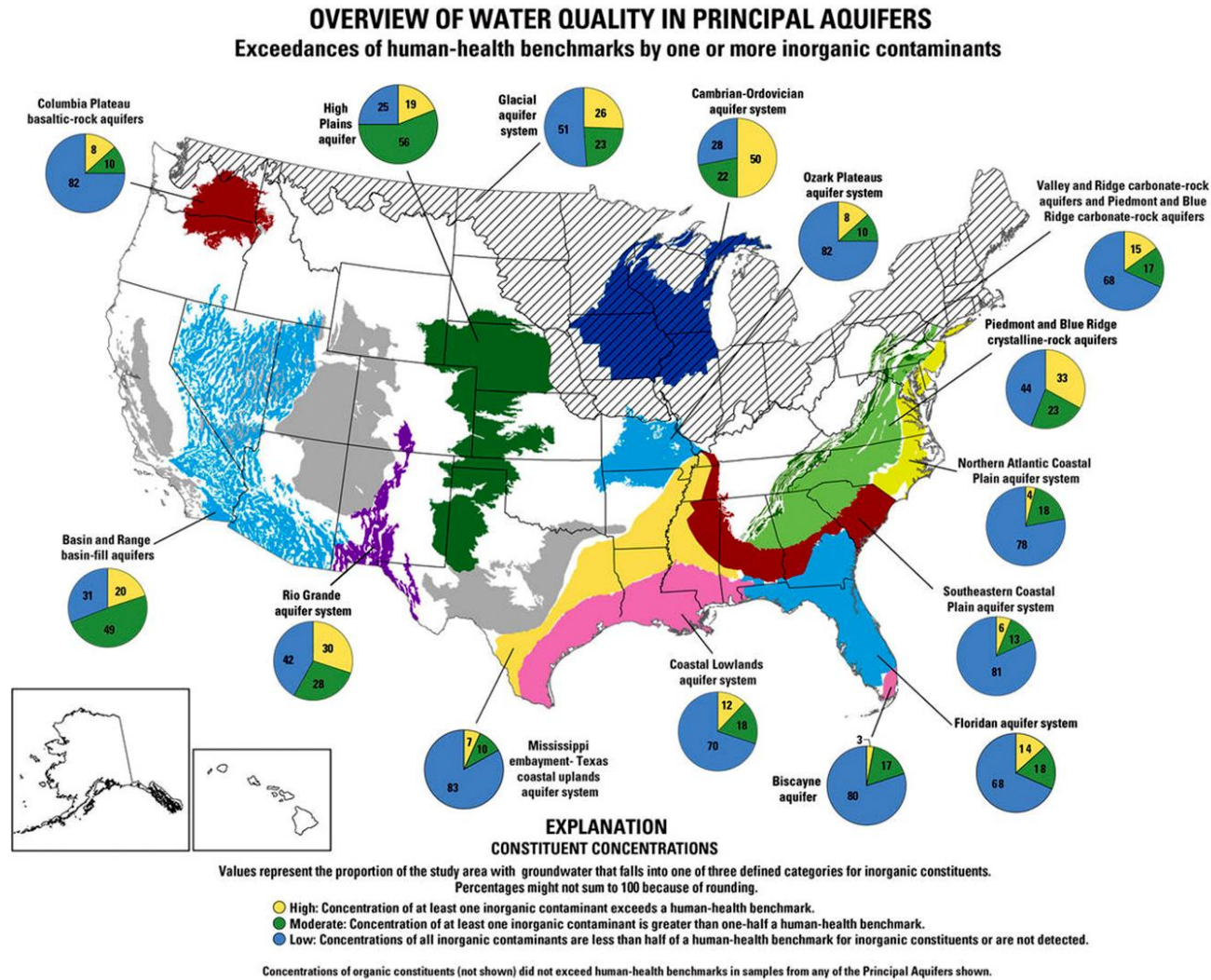


Figure 64 - Map of the USA showing water quality overview of principal aquifers that exceeded the human-health benchmarks (HHBs). The blue of each circle represents the percentage of low concentration; green the percentage of medium; and yellow the percentage of high concentrations of human-health elements. The numerical values in each circle refer to the number of samples. The white areas lack principal aquifers (reproduced from DeSimone et al., 2014).

Table 8 - The 11 geogenic elements that most frequently exceeded the USEPA Maximum Contaminant Levels for human-health benchmarks in the USA (HHBs; DeSimone et al., 2014). HBSL is a non-enforceable, health-based, screening level benchmark developed by the US Geological Survey to supplement USEPA standards and guidelines. Work by Lindsey and others (2021) suggests that lithium should also be included.

Contaminant	Human-health benchmark		Number of wells sampled	Percentage of samples with concentrations greater than the benchmark	Number of Principal Aquifers with one or more exceedances of the benchmark
	Value	Type			
Contaminants from geologic sources					
Manganese	300 µg/L	HBSL	3,662	6.9	25 of 41
Arsenic	10 µg/L	MCL	3,074	6.7	20 of 37
Radon	*4,000 pCi/L (300 pCi/L)	Proposed AMCL (Proposed MCL)	3,120	3.6	15 of 41
Strontium	4,000 µg/L	HBSL	1,956	1.7	10 of 29
Uranium	30 µg/L	MCL	3,258	1.6	12 of 37
Fluoride	4 mg/L	MCL	3,655	<1	8 of 41
Molybdenum	40 µg/L	HBSL	3,036	<1	8 of 37
Lead	15 µg/L	Action level	3,035	<1	3 of 37
Antimony	6 µg/L	MCL	3,026	<1	4 of 37
Selenium	50 µg/L	MCL	3,036	<1	4 of 37
Zinc	2,000 µg/L	HBSL	2,979	<1	3 of 37

3.1 Manganese (Mn)

Manganese, long recognized as a nuisance for staining white porcelain fixtures and clothing, has been recognized to impair the intellectual development of children. Although manganese is beneficial to human health in trace quantities, it can be injurious at concentrations greater than 300 µg/L, mainly affecting the respiratory tract and nervous system and causing hallucinations and forgetfulness. Infants may be susceptible to manganese exposure through drinking water.

Manganese can be noticeable in water at concentrations as low as 50 µg/L as it gives the water an unpleasant taste, odor, and black color. Approximately 7 percent of domestic (i.e., private) wells in the US have concentrations of manganese at levels that may present a potential human health risk (McMahon et al., 2019). This statistic is based on 43,334 samples collected in the continental USA. Their distribution is shown in Figure 65.

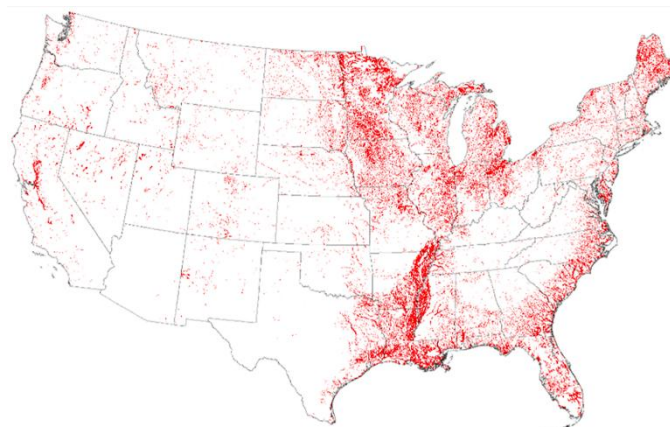


Figure 65 - Distribution of 43,334 manganese analyses from groundwater in the continental USA (reproduced from McMahon et al., 2019).

McMahon and others (2019) found elevated levels of manganese in groundwater above the human-health benchmark along the Mississippi Valley, the eastern coast, and the Great Lakes area (Figure 65). Elevated manganese in groundwater occurs most frequently in anoxic zones near rivers, where the overlying soil is rich in organic carbon or where nitrogen fertilizer has been applied to poorly buffered soil. Manganese oxide is ubiquitous in sediments and associated with iron hydroxide but only becomes mobile and solubilizes when the redox conditions are lowered. The solubility of manganese Mn^{4+} —the more oxidized of two major ionic species—is relatively low in typical groundwater conditions, whereas the reduced species Mn^{2+} is more soluble.

3.2 Arsenic (As)

Arsenic (As) is likely the most important health-related geogenic solute and has been identified in elevated concentrations in more than seventy countries (Podgorski & Berg, 2020; Smedley & Kinniburgh, 2002). Intuitively, one thinks of arsenic as one of the most toxic elements, mainly owing to the infamous mystery genre trope where arsenic poison in the tea is a favorite murder weapon of seemingly kindly old ladies. While there is little doubt about the lethal properties of arsenic, the concentrations observed in most aquifers are not generally sufficient to cause death. However, consumption of elevated concentrations over extended periods may lead to significant skin disorders, cardiovascular diseases, respiratory problems, complications of the gastrointestinal tract, liver and spleen ailments, kidney and bladder disorders, and other health-related conditions. Arsenic in groundwater used for irrigation is a significant problem for rice production as it accumulates in rice more than in other major grain crops.

The regulatory community has had significant discussions about the current value of HHBs. In the USA, the HHB value for arsenic is currently set to 10 $\mu\text{g/L}$; approximately 7 percent of the wells sampled exceeded this value (DeSimone et al., 2014). Figure 66, illustrates a significant portion of the population is impacted by elevated concentrations of arsenic—but with few identified health consequences, it remains a challenge for epidemiologists and proponents of lower HHBs.

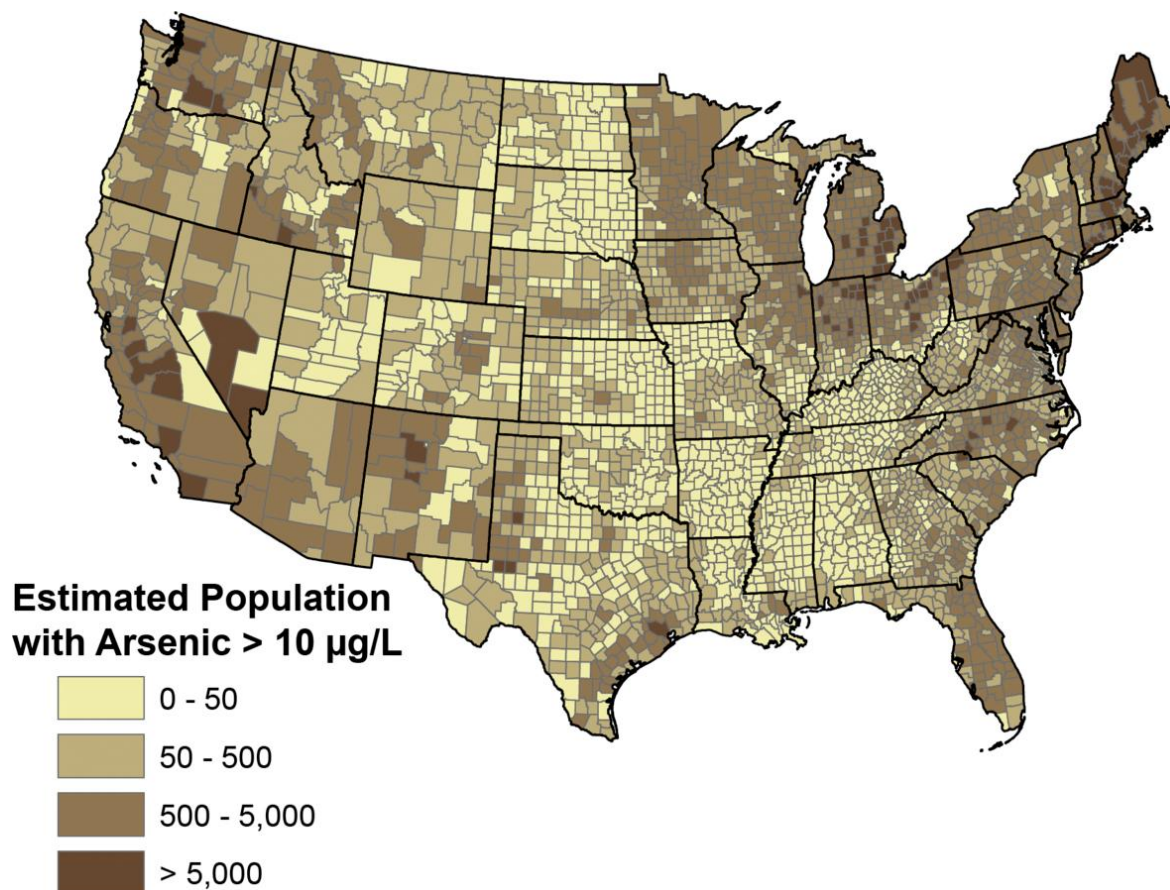


Figure 66 - Population impacted by arsenic in groundwater in the continental USA (DeSimone et al., 2014).

Arsenic ions exist in groundwater as an oxyanion representing two oxidation states: arsenite [+3] as in (AsO_3^{3-}) and arsenate [+5] as in (AsO_4^{3-}). Arsenic is mobilized in groundwater by three different geochemical mechanisms:

1. reduction and, thus, mobilization of iron oxide oxides that have previously sorbed arsenic;
2. desorption by elevated pH > 8.5; and
3. oxidation of arsenopyrite or other arsenic-bearing minerals.

As a result of these different mechanisms, arsenic is found in a wide range of environmental conditions, including geothermal. Arsenic-containing minerals commonly exist in rock-forming minerals of sulfides, oxides, phosphates, and carbonates. Its most widespread mineral occurrence is as a substitute for the sulfur (S) ion in the crystal lattice of the common sulfide mineral pyrite (FeS_2) and released to the groundwater as pyrite dissolves. The concentrations of arsenic in different principal aquifers in the continental USA are presented in Figure 67.

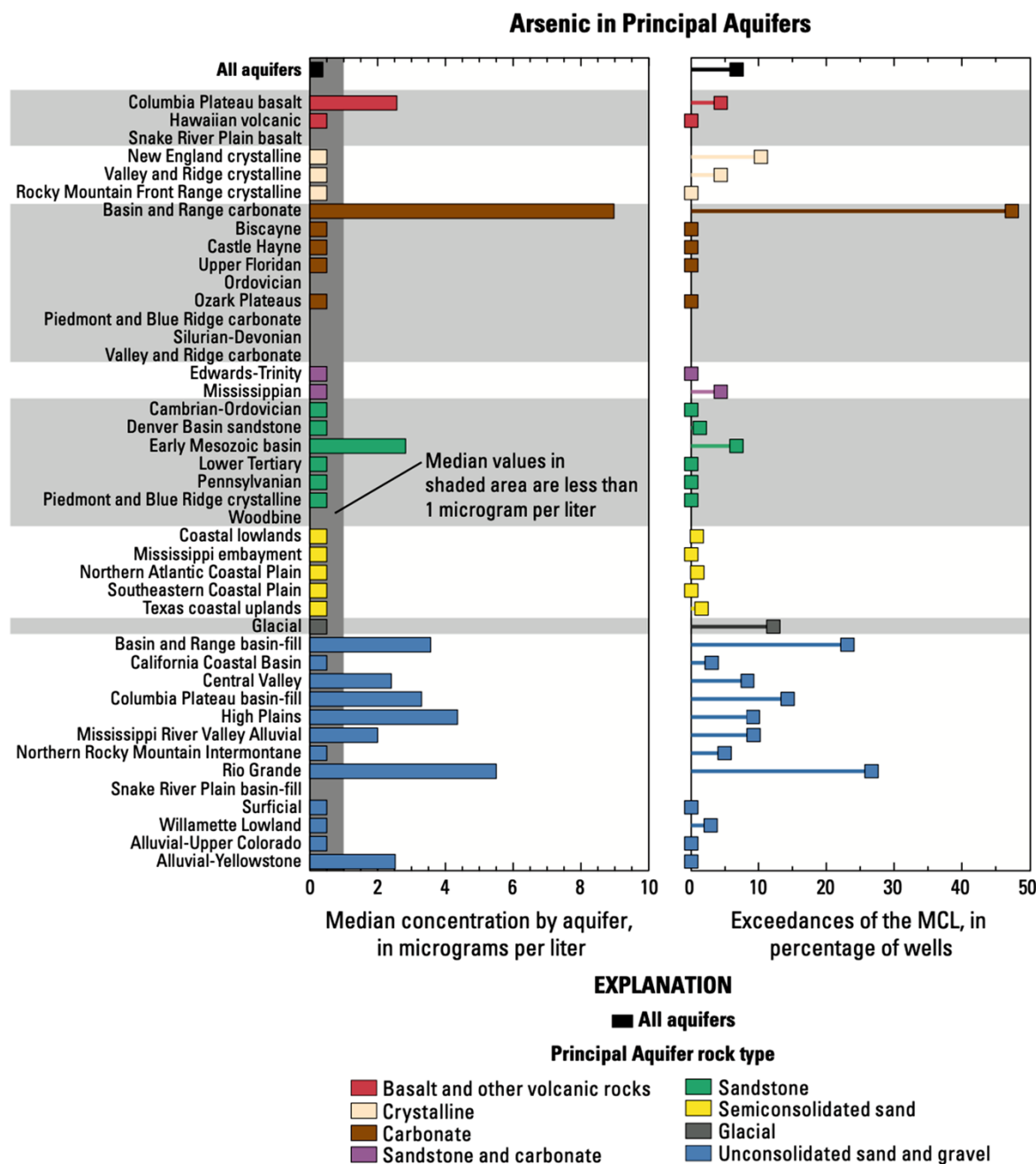


Figure 67 - Arsenic concentration ($\mu\text{g/L}$) and exceedance of the MCL in principal aquifer systems in the USA (reproduced from DeSimone et al., 2014).

Podgorski and Berg (2020) provided a global prediction map of groundwater arsenic concentrations exceeding $10 \mu\text{g/L}$ using a random forest machine-learning model (Figure 68).

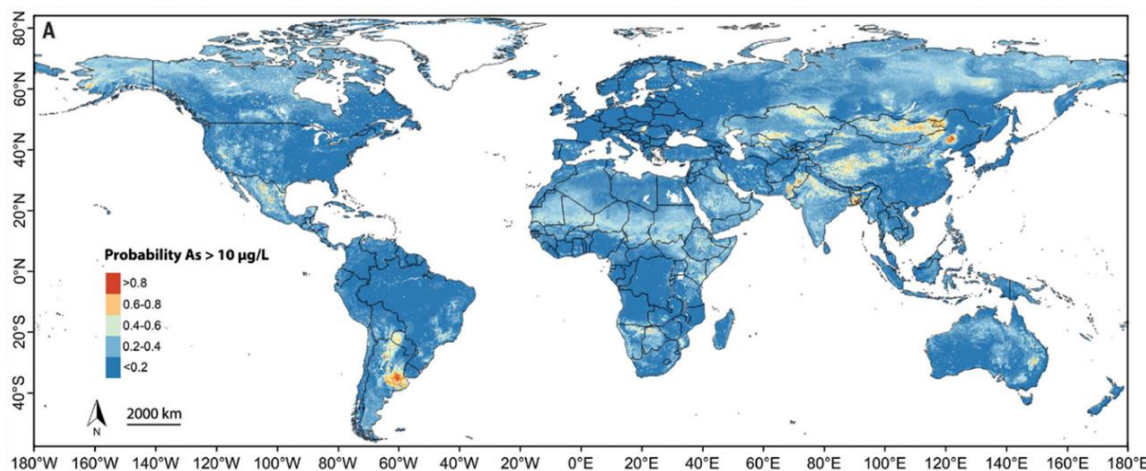


Figure 68 - The modeled probability of arsenic concentration in groundwater exceeding 10 µg/L for the entire globe (Podgorski & Berg, 2020).

The geogenic concentration of arsenic in shallow groundwater was shown to be elevated in much of Bangladesh (Figure 69). UNICEF (2018) provided some guidance on arsenic in groundwater.

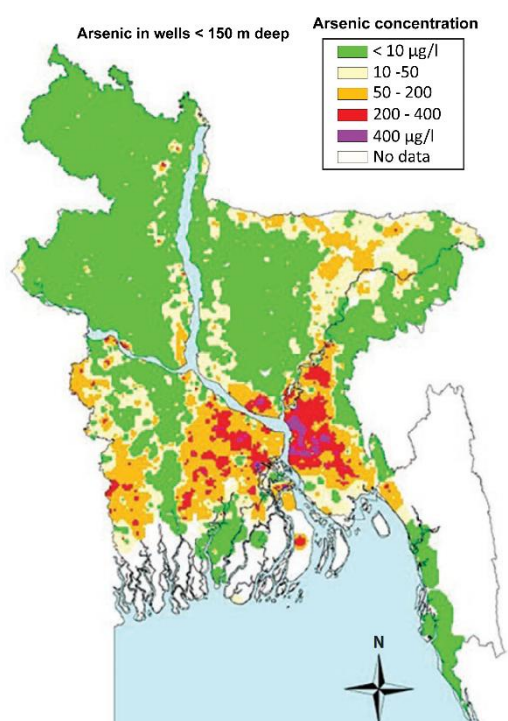


Figure 69 - Concentration µg/L of arsenic in groundwater of Bangladesh (reproduced from Ravenscroft & Lytton 2022).

3.3 Radionuclides of Uranium (U), Radium (Ra), Radon (Rn), Polonium (Po), and Lead (Pb)

Groundwater frequently contains measurable quantities of geogenic radioactive elements—radionuclides—including isotopes of uranium (U), radium (Ra), radon (Rn), polonium (Po), and lead (Pb-210). Radionuclides in drinking water sources concern

human health because of their radioactivity, carcinogenic properties, and because several are chemically toxic. Most of the geogenic radionuclides in groundwater originate from the radioactive decay series of elements: uranium-238 and thorium-232 (Figure 70).

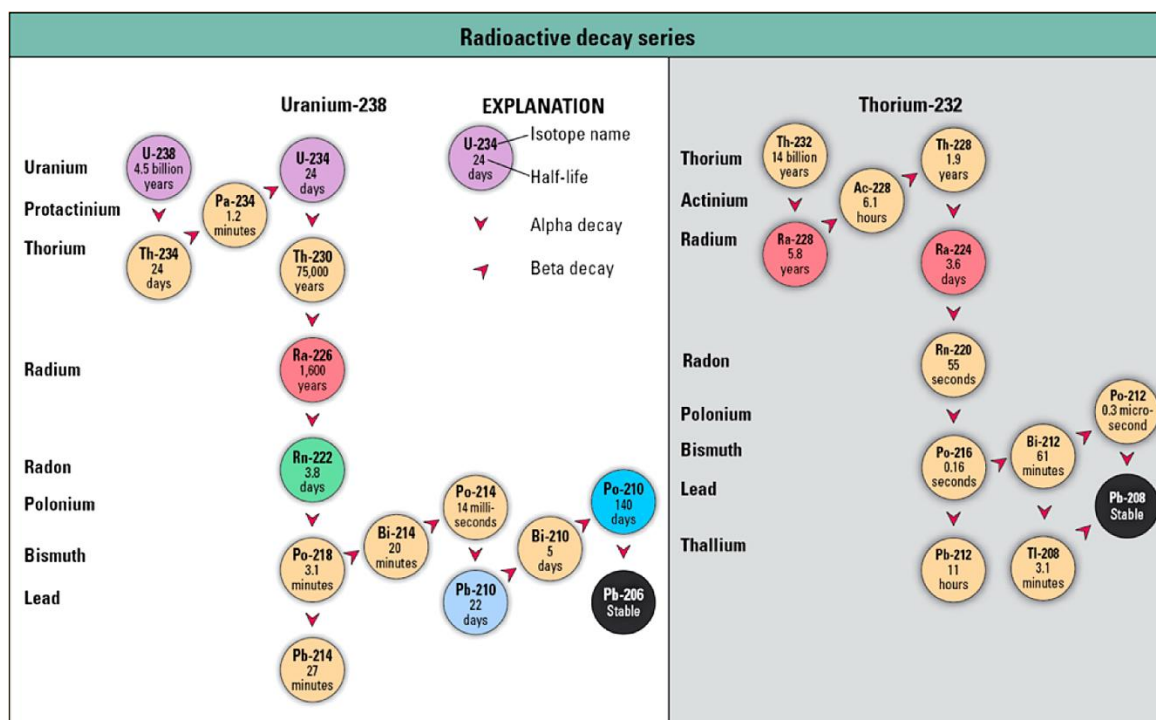


Figure 70 - Radioactive decay series for ²³⁸U and ²³²Th illustrating the radioactive isotopes ²²²Rn, ²²⁴Ra, ²²⁶Ra, ²²⁸Ra, ²¹⁰Pb, and ²¹⁰Po that occur in groundwater. Some can pose health concerns in drinking-water sources. These are indicated by purple, red, and green circles. ²¹⁰Po (dark blue) and ²¹⁰Pb (light blue) can, under some circumstances, become important (reproduced from DeSimone et al., 2014).

Radioactive isotopes in water typically are measured by the amount of radioactive released from their decay, which is referred to as *activity*. Several different units are used for measuring the activities of isotopes; in the USA, picocurie per liter of water is the most used unit (Section 1.4). However, the preferred international unit is the Becquerel (Bq): 1 Bq represents a rate of radioactive decay equal to 1 disintegration per second per liter. However, uranium is an exception and is measured in µg/L—a concentration rather than an activity, primarily because of its long half-life (4.5 billion years), thus low activity. Nearly all the uranium in groundwater is uranium-238.

DeSimone and others (2014) identified critical radionuclides that, under certain conditions, can be health concerns including uranium-238, and its prodigies radium-226 and radon-222. Radium-228 and radon-224 from the thorium-232 decay series have very short half-lives (Figure 70) and are not commonly observed in groundwater.

Uranium in the reduced state (+3, +4) is insoluble and typically stays in the solid phase. In contrast, the oxidized species (+6 as the UO₂²⁺ ion) is mobile and is a solute in most groundwaters. Thus, uranium is more likely to stay dissolved in oxygenated groundwater with an elevated pH. The presence of high concentrations of bicarbonate or

sulfate that complex the UO_2^{2+} ion also increases the concentration. Radon-222 is a noble gas with no charge. Thus, the geochemistry of the environment does not significantly affect it, and it is dissolved in groundwater over a wide range of pH, dissolved solids, and redox conditions.

Uranium-238 has a half-life of 4.5 billion years, whereas radon-222 has a half-life of less than 4 days. This difference in half-life means that uranium-238 can travel long distances from its source mineral in aquifer rocks or sediments before it decays. Conversely, radon-222 can travel only a short distance from its source before it decays. Finally, radon-222—a dissolved gas—can escape from the water, whereas uranium—a dissolved charged solute—cannot. This difference in geochemistry is illustrated in their respective concentrations in Figure 71.

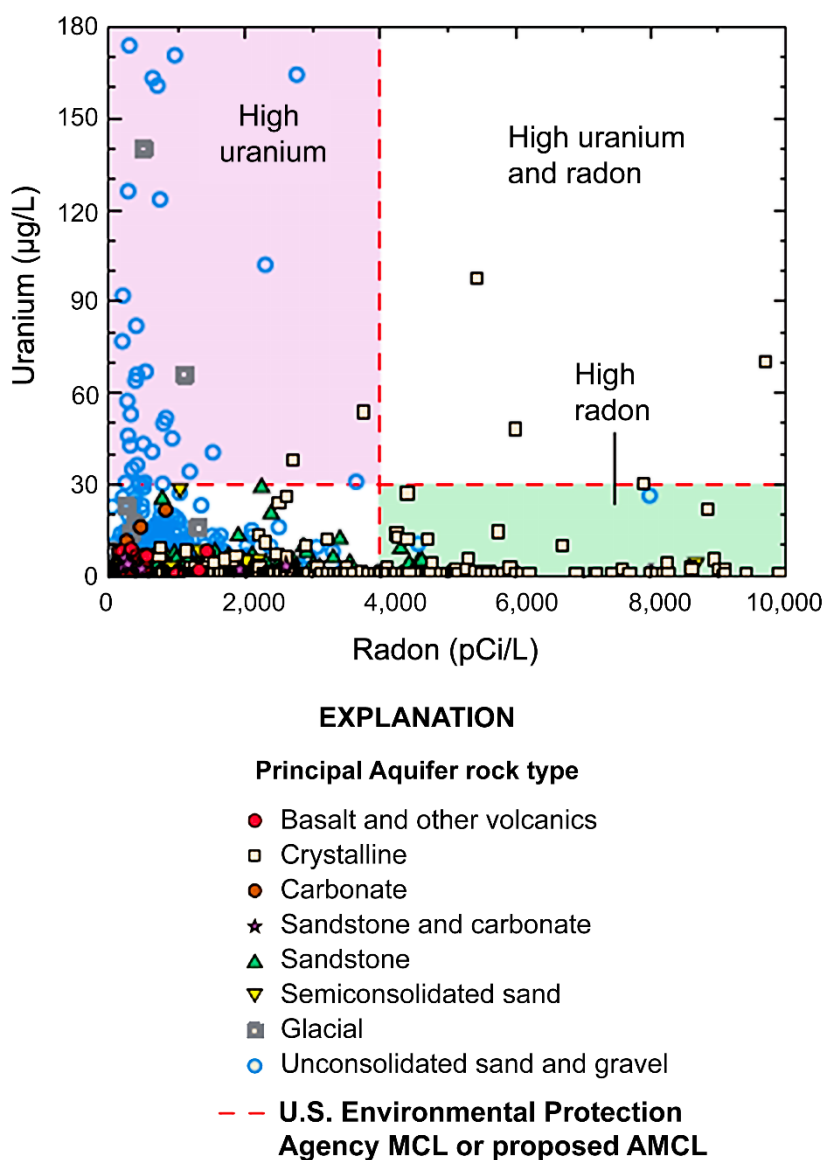


Figure 71 - Differences in geochemical properties and half-life between uranium and radon result in concentration differences in the same groundwater environment. High concentrations of uranium and radon do not often co-occur (reproduced from DeSimone et al., 2014).

Radon is ubiquitous in many clastic and granitic aquifer systems and is an acknowledged health risk, but it does not have an HHB. Two alternative maximum contaminant levels (AMCLs) have been proposed for radon—300 pCi/L and 4,000 pCi/L—that would include 25 to 50 percent of samples from wells in the crystalline rock aquifers. Approximately 3.5 percent of wells sampled nationally were above this level (DeSimone et al., 2014). Sampling locations of radon in groundwater in the USA are shown in Figure 72.

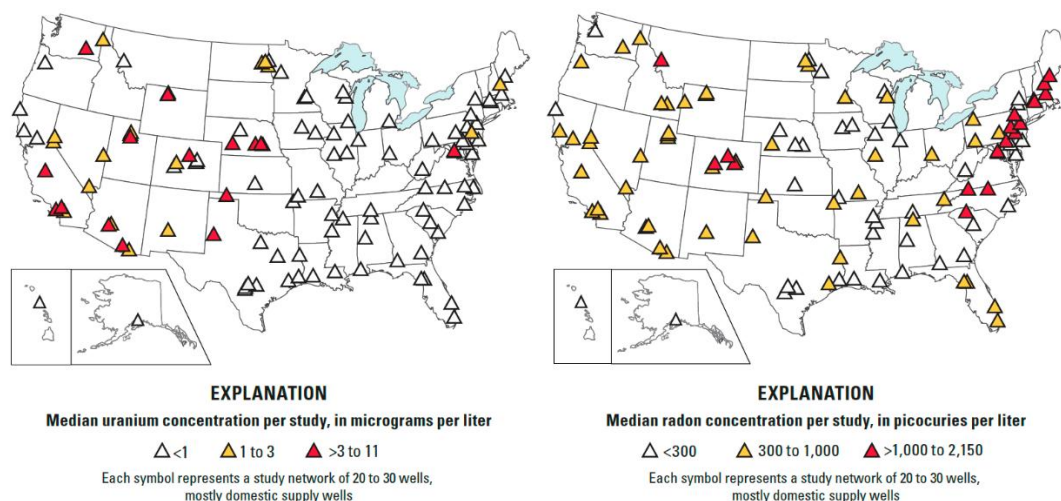


Figure 72 - Concentration of a) uranium (µg/L) and b) radon (pCi/L) in groundwater of the USA (reproduced from DeSimone et al., 2014).

The concentration of uranium in aquifers is reflected in its concentrations in soils (Figure 73)—a factor that influences groundwater concentrations.

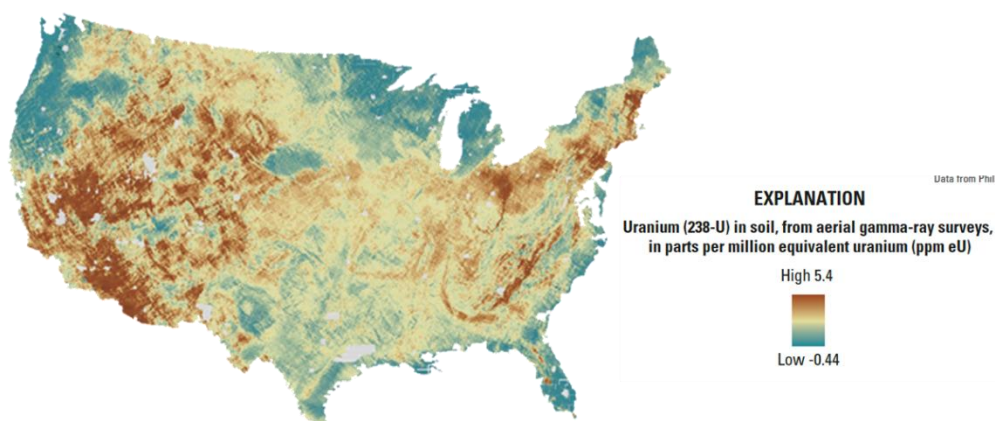


Figure 73 - Range of concentration (PPM) of uranium in soils of the continental USA (reproduced from DeSimone et al., 2014).

Uranium was detected in concentrations greater than 1 µg/L in 35 percent of wells sampled in the aquifers used for drinking water but exceeded the US EPA MCL of 30 µg/L in only 1.6 percent of samples nationally (DeSimone et al., 2014). Although weakly carcinogenic, uranium is chemically toxic. Uranium is a common trace element in many

rock types; however, it is mainly concentrated in felsic crystalline rocks such as granites and rhyolites as well as sediments derived from these rocks.

Owing to uranium's higher solubility in its oxidized forms, its mobility in groundwater depends on redox conditions. Uranium sorption is also pH dependent and it can form complexes with carbonate, phosphate, and sulfate anions that keep it in solution over a broader range of conditions. Under natural geochemical conditions, uranium's two main oxidation states are +4 and +6. In groundwater, uranium is mainly present in its most mobile oxidized form of uranyl +6 as UO_2^{2+} , typically in hydroxyl and carbonate complexes. A global review of uranium in groundwater is given by Vengosh and others (2022).

High radon concentrations in groundwater were found primarily in the eastern half of the USA, where older granitic rocks are abundant (Figure 74). Knowing the half-life of radon-222 is so short—3.8 days—it is reasonable to wonder how its activity can be so high in well water when the parent uranium concentration in the aquifer framework is low. Wood and others (2004) demonstrated that radium-226—the immediate precursor of radon-222 in the uranium-238 decay series—is mobilized and sorbed on iron hydroxide in fractures near the wells, which allows a build-up of high activity of radon-222 in the groundwater near the well.

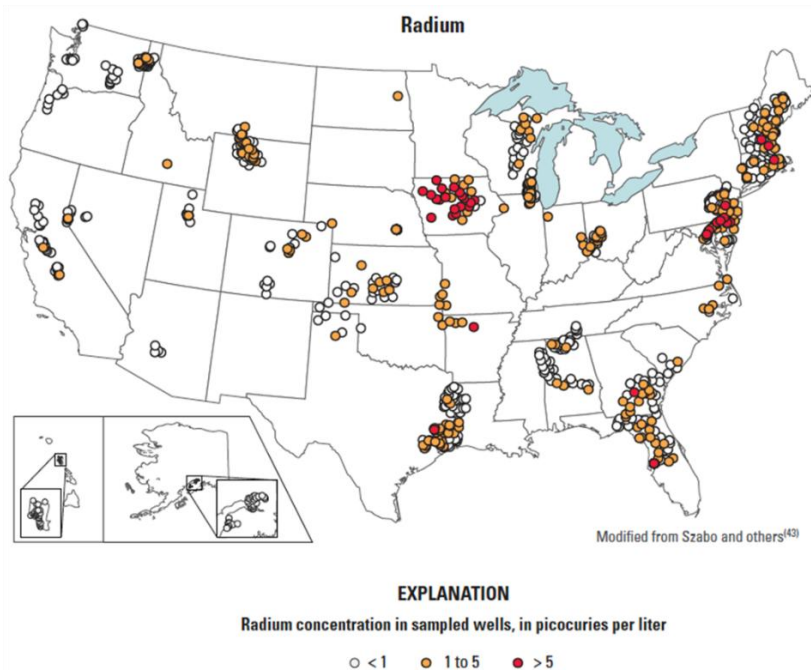


Figure 74 - Radium concentration (pCi/L) in groundwater in the USA (reproduced from DeSimone et al., 2014).

The concentrations of uranium and radon in all principal aquifers are presented in Figure 75.

Radium-226 and radium-228 are the two most common isotopes of radium and both are carcinogenic. Radium dissolved in drinking water is a human-health concern because it accumulates in bone and other tissues, thereby increasing lifetime cancer risks. The US EPA HHB for radium is 5 pCi/L for the combined concentration of radium-226 and radium-228.

Nationally, 3.2 percent of 1,270 wells for which samples were analyzed for radium-228 and (or) radium-226 had concentrations greater than the MCL for combined radium (DeSimone et al., 2014). Radium, a typical cation, can enter groundwater by the dissolution of aquifer materials, by ion exchange and desorption from rock or sediment surfaces, and by release from minerals during radioactive decay. Radium has only one oxidation state and is thus not redox-sensitive. Elevated concentrations were more common in groundwater in the north-central USA than in other regions (Figure 76).

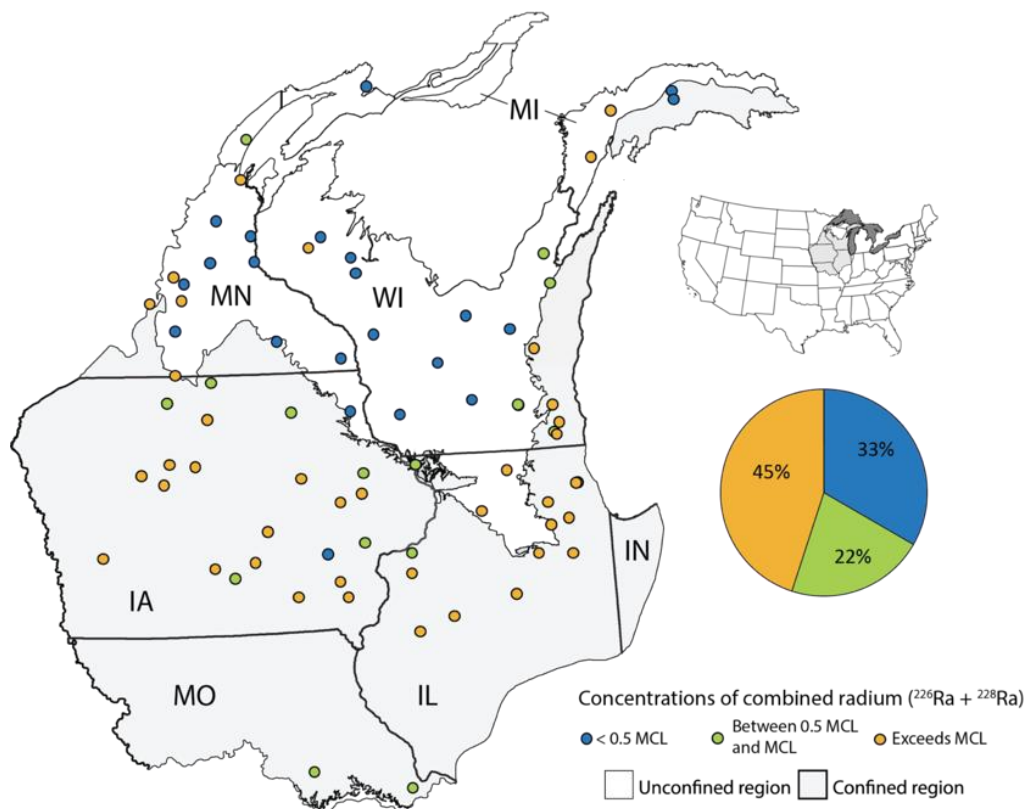


Figure 76 - Concentration and distribution of radium in groundwater in north-central USA. Forty-five percent of samples exceeded MCL, 33 percent of samples were less than 0.5 MCL, and 22 percent of samples were between 0.5 and MCL (reproduced from DeSimone et al., 2014).

Lead-210 (found in 3.7 percent of 1,263 samples) and polonium-210 (found in 1.5 percent of samples) in 19 principal aquifers may exceed the HHB (Szabo et al., 2020; Figure 77).

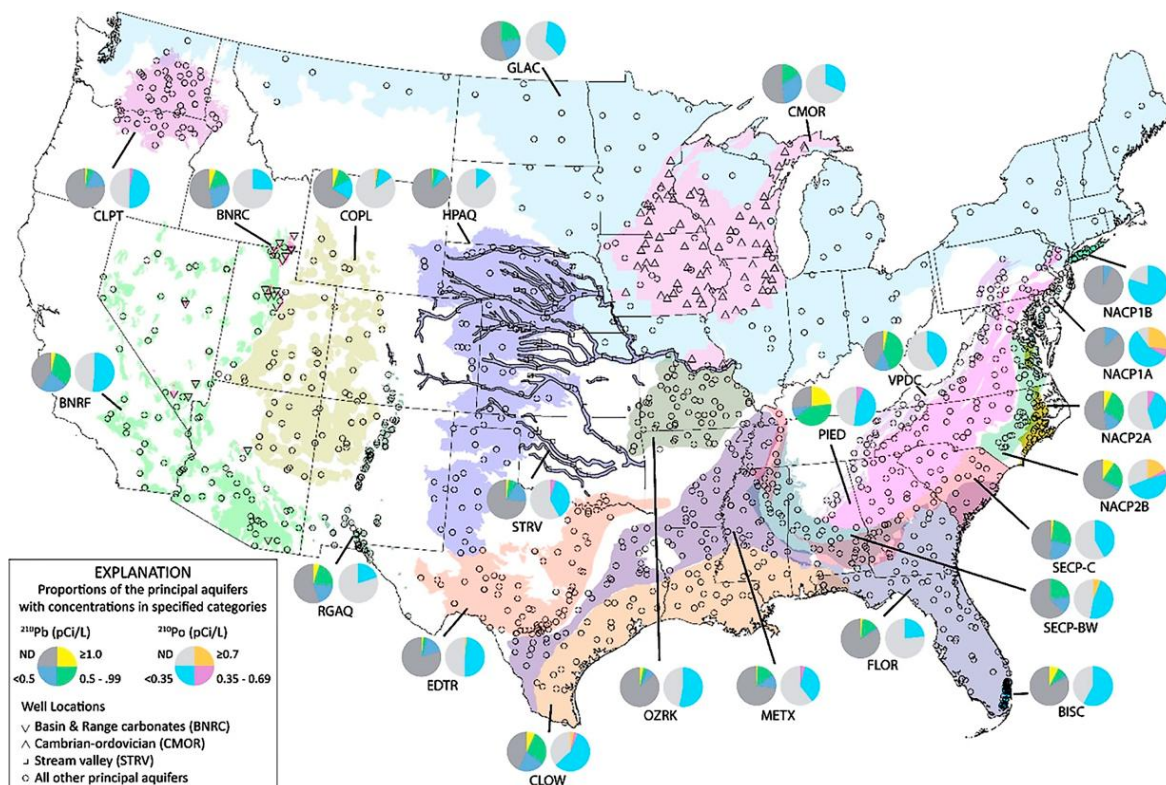


Figure 77 - Distribution of radioactive lead-210 and polonium-210 in the Principal Aquifers of the USA (reproduced from Szabo et al., 2020).

Lead-210 concentrations greater than or equal to 1.0 pCi/L occurred most frequently where acidic groundwaters inhibited adsorption and where lead carbonate complexes were present—enhancing lead mobility (Szabo et al., 2020). Polonium-210 concentrations greater than or equal to 0.7 pCi/L occurred almost exclusively in confined coastal plain aquifers where groundwaters were reducing with high pH (> 7.5) and high sodium/chloride (Na/Cl) ratios (Szabo et al., 2020). In high-pH environments or low redox conditions, aqueous polonium-210 is poorly sorbed and remains in solution (Figure 78).

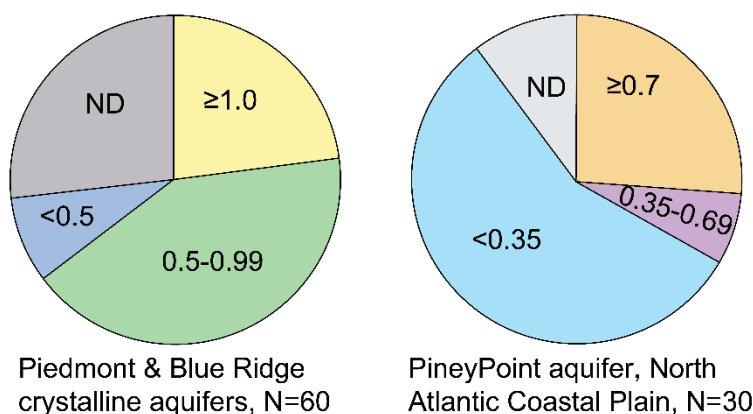


Figure 78 - Concentration of lead (²¹⁰Pb) in two contrasting geologic environments (reproduced from Szabo et al., 2020).

3.4 Strontium (Sr)

Strontium (Sr) is a ubiquitous element in most groundwaters and exhibits similar geochemical properties to calcium and can replace calcium in the bone, disrupting the typical bone structure. The US EPA HHB for strontium is 4,000 $\mu\text{g/L}$. Elevated concentrations in groundwater typically occurred in carbonate aquifers associated with the minerals strontianite (SrCO_3) and celestite (SrSO_4) and it is a trace component in the minerals calcite, gypsum, and anhydrite (Musgrove, 2021). The distribution of strontium concentrations in groundwater in the Principal Aquifers of the continental USA is illustrated in Figure 79.

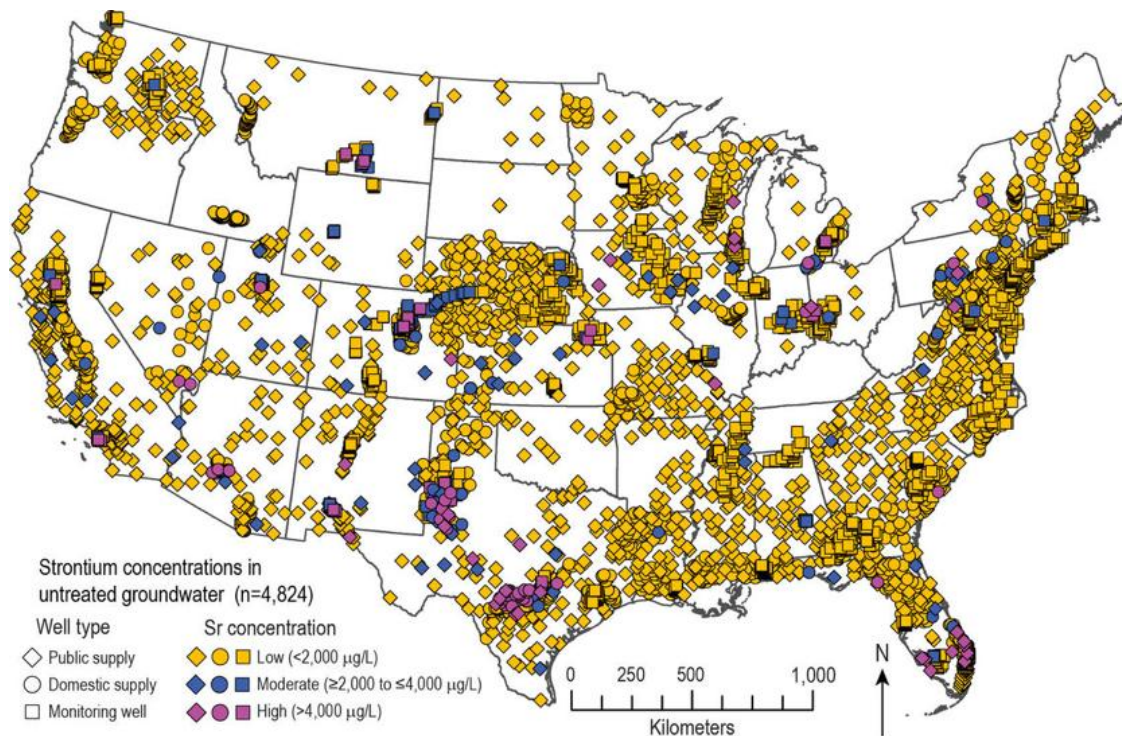


Figure 79 - Strontium concentration ($\mu\text{g/L}$) in groundwater in the Principal Aquifers of the continental USA (reproduced from Musgrove, 2020).

Figure 79 reveals that moderate and high concentrations of strontium are limited to only a few areas. This distribution of strontium concentrations within the Principal Aquifers of the continental USA is illustrated by box-and-whisker plots in Figure 80.

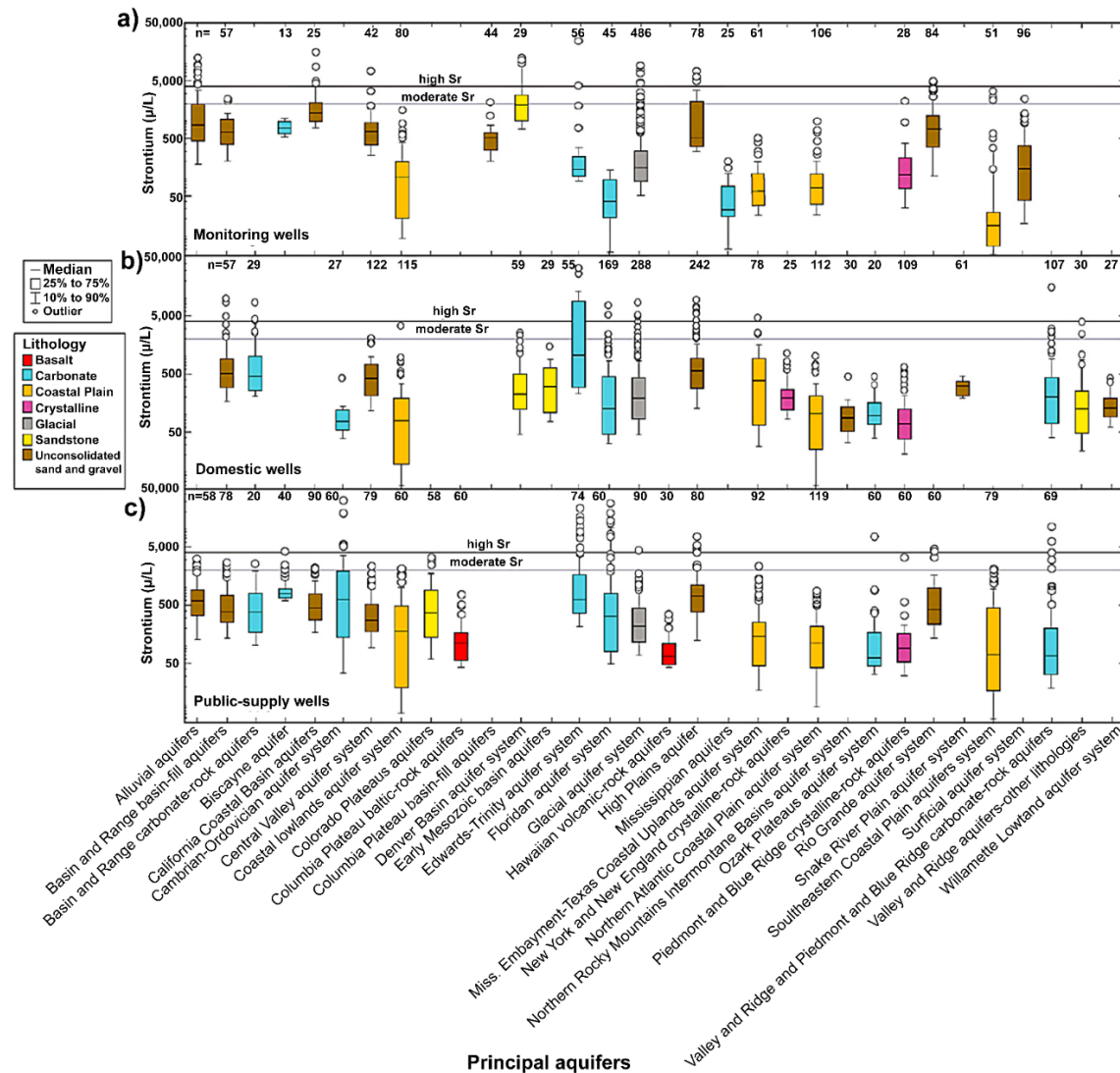


Figure 80 - Box-and-whisker plots of strontium concentration (mg/L) in a) monitoring, b) domestic, and c) public supply wells in Principal Aquifers in the continental US (reproduced from Musgrove, 2020).

3.5 Fluoride (F)

Fluoride (F) is another ubiquitous element essential in human development. Fluoride was shown to be widespread in groundwater in the continental USA based on 38,105 samples (Figure 81). A concentration of 0.7 mg/L fluoride in drinking water is beneficial to human health in preventing dental cavities—and it is added to many municipal water supplies to reach that level. However, high concentrations (> 4 mg/L) can damage tooth enamel and cause skeletal fluorosis; US EPA recommends a limit of a maximum of 4 mg/L. However, the World Health Organization (WHO) recommends an HHB maximum limit of 1.5 mg/L.

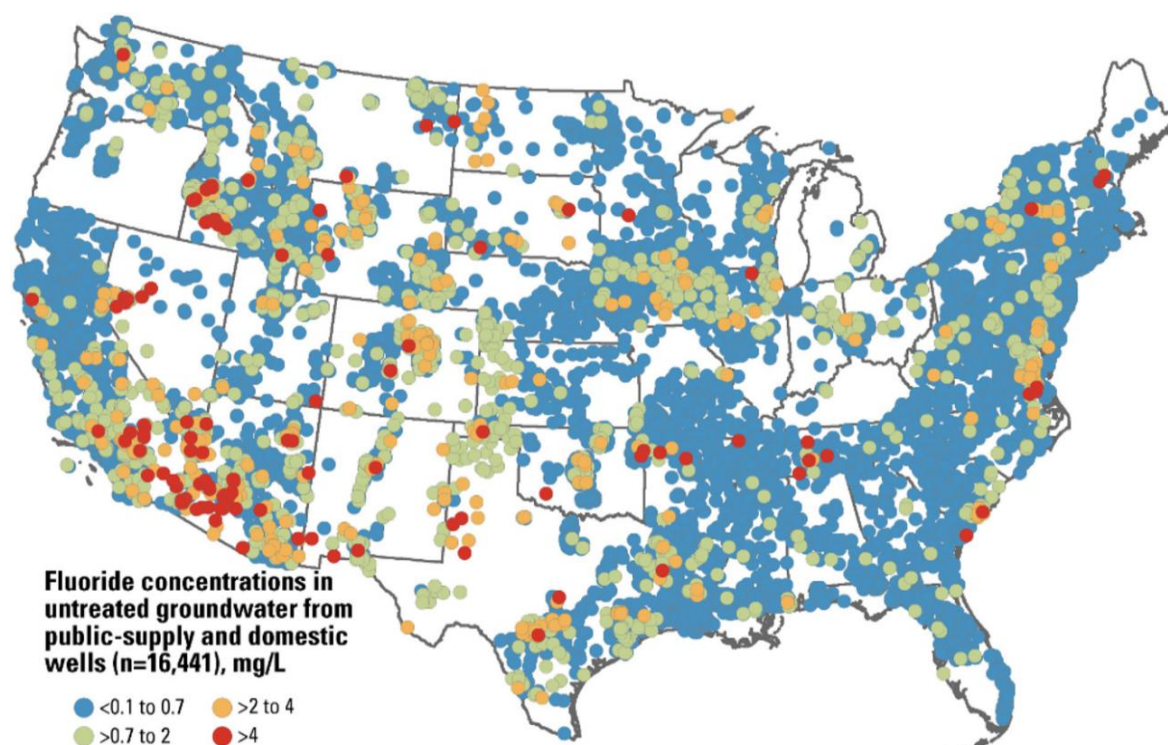


Figure 81 - Fluoride concentration (mg/L) in the Principal Aquifers of the continental USA (reproduced from McMahon et al., 2020).

From the dataset of 38,105 samples, 14.5 percent had fluoride concentrations greater than 0.7 mg/L, 4.3 percent had fluoride greater than 2 mg/L, and 1.6 percent had fluoride greater than 4 mg/L (McMahon et al., 2020; Figure 81). Fluoride was shown to be elevated in aquifers containing volcanic ash and aquifers with an elevated pH (Figure 82).

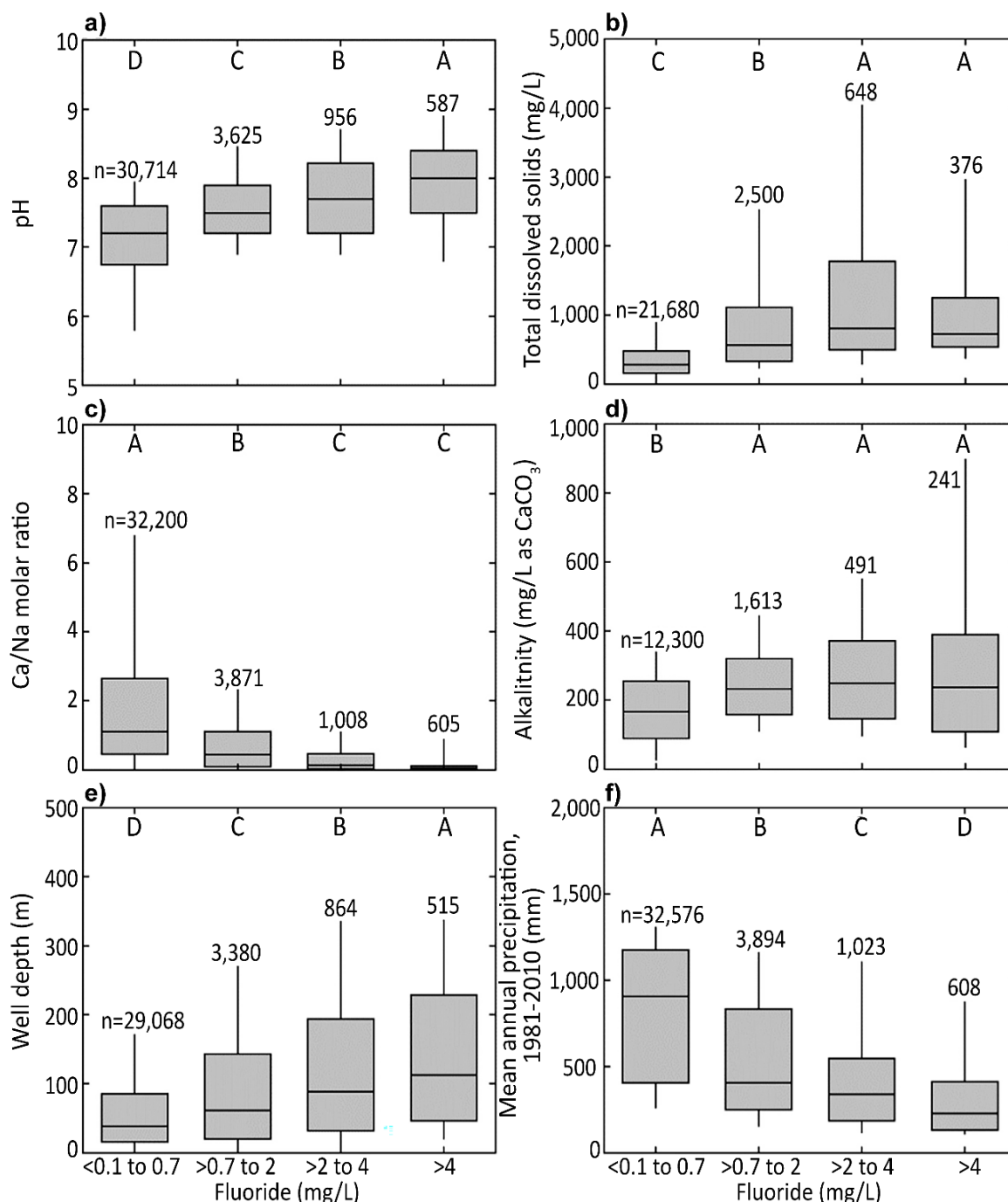


Figure 82 - Box-and-whisker plot of the distribution of fluoride concentration (mg/L) in the samples shown in Figure 81 for selected environmental factors: a) pH, b) total dissolved solids, c) Ca/Na molar ratio, d) alkalinity, e) well depth, and f) mean annual precipitation (reproduced from McMahon et al., 2020).

McMahon and others (2020) showed an association between elevated concentrations of fluoride and increased water temperature controlled by regional heat flow (Figure 83), consistent with that shown for global groundwater by Edmunds and Smedley (2013) and Nordstrom and Smedley (2022). In addition, the high solubilities of the mineral fluorite, as well as processes such as anion exchange and complexing, were shown to enhance the concentration of fluoride in groundwater.

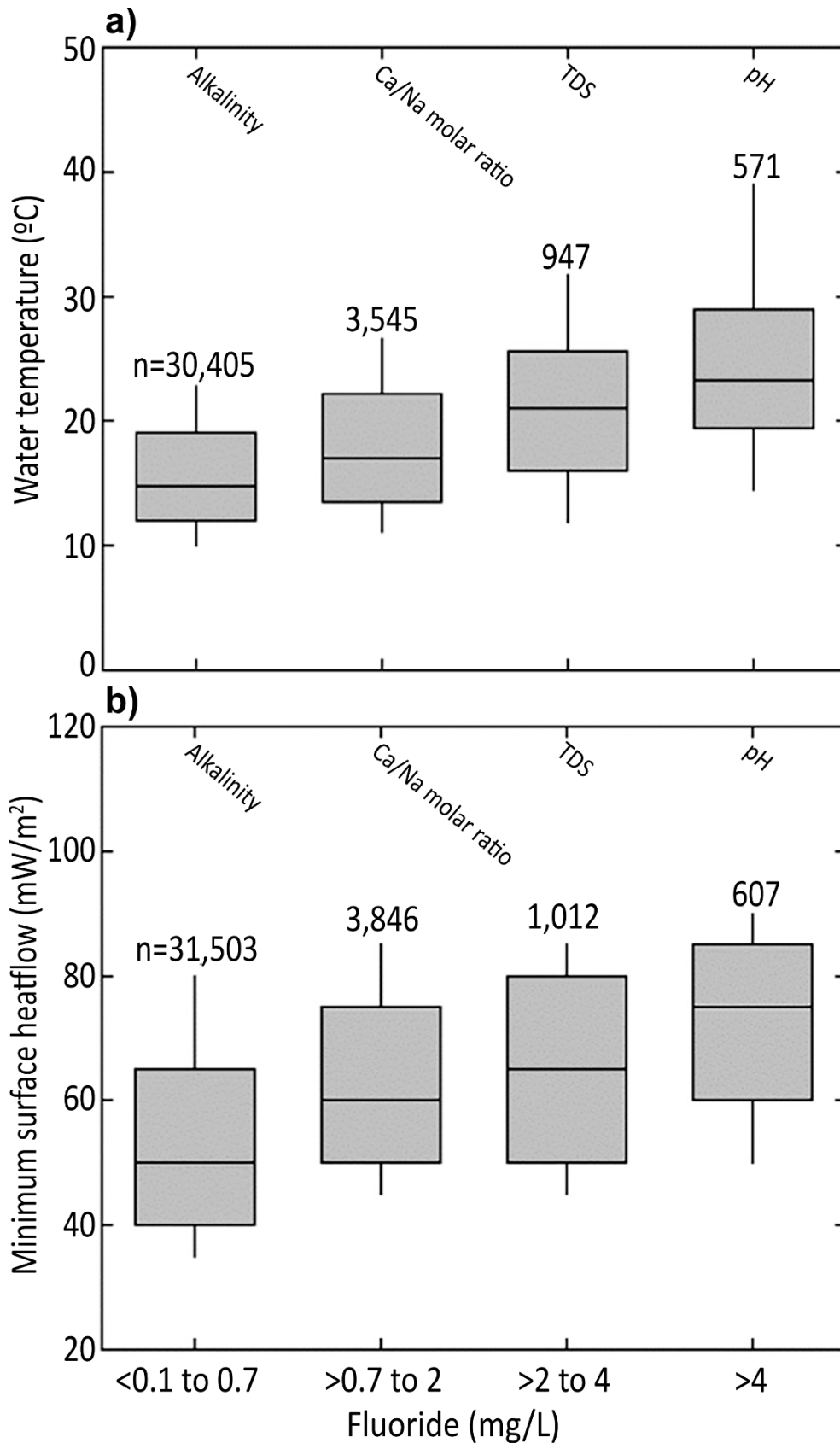


Figure 83 - Relation of fluoride concentration (mg/L) with a) water temperature and b) heat flow. Box-and-whisker plots of the distribution of fluoride concentration (mg/L) for selected environmental factors of alkalinity, Ca/Na molar ratio, total dissolved solids (TDS), and pH (modified from McMahon et al., 2020).

Globally, widespread elevated concentrations of fluoride occur, as shown in Figure 84.

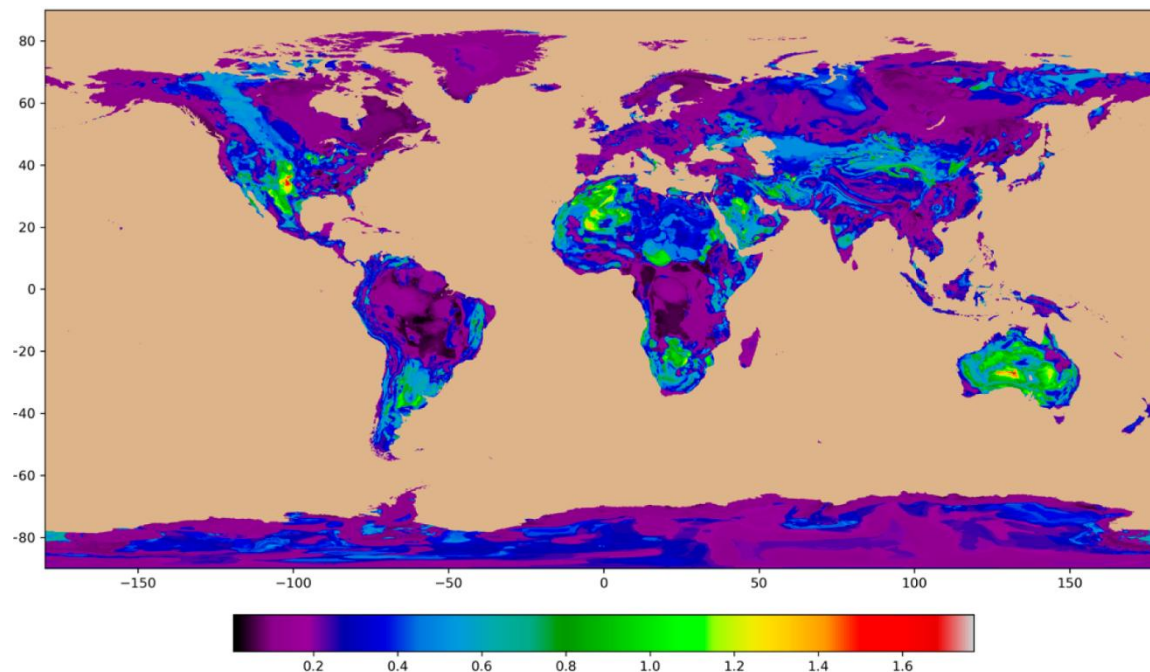


Figure 84 - Modeled global fluoride concentration in groundwater, mg/L (reproduced from Wood et al., 2022).

3.6 Molybdenum (Mo)

Molybdenum (Mo) is an essential trace element for human health; enzymes containing molybdenum catalyze basic metabolic reactions in the carbon, sulfur, and nitrogen cycles. Thus, Mo is an important component in the evolution of life on Earth.

The US EPA has established an HHB of 40 $\mu\text{g/L}$ for Mo. A review of molybdenum (Smedley & Kinniburgh, 2017) provided insight into the global distribution of its concentration in natural waters, including groundwater. Ayotte and others (2011) and DeSimone and others (2014) focused on groundwater in the USA (Figure 85 and Figure 86, respectively). They found the median value of 3,063 samples was 1.0 $\mu\text{g/L}$, with higher values in dry versus humid climates.

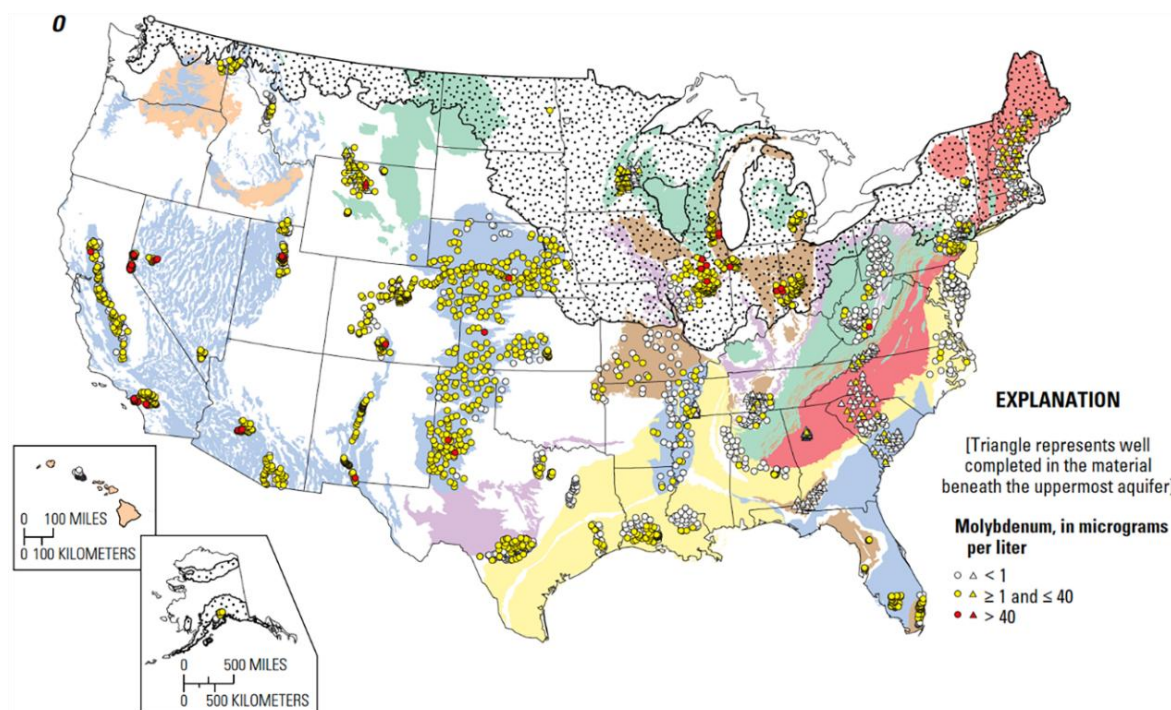


Figure 85 - Range of molybdenum concentration, in $\mu\text{g/L}$, in Principal Aquifers of the USA. Shading indicates major aquifer provinces as defined in the legend associated with Figure 63 (reproduced from Ayotte et al., 2011).

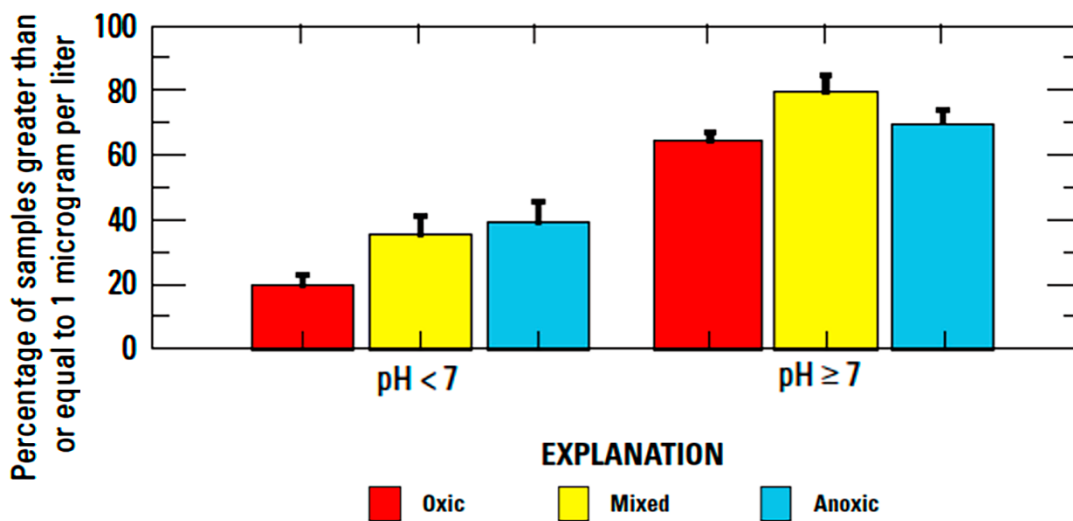


Figure 86 - Percentages of samples equal to or greater than $1 \mu\text{g/L}$ of molybdenum as a function of pH and redox conditions in groundwater of the continental USA (reproduced from Ayotte et al., 2011).

Molybdenum exists in three important oxidation states (+4, +5, +6) in the groundwater environment, enabling Mo to participate in many redox reactions. Molybdenum commonly forms an oxyanion in groundwater that is affected by redox and pH (Figure 86). The concentration of molybdenum in groundwater generally increased from oxic to anoxic redox conditions with increasing pH.

3.7 Lead (Pb)

The US EPA set the MCL goal for lead in drinking water at zero (0) as lead is toxic and can harm human health at low exposure levels; lead can bioaccumulate in the body over time and be distributed to the brain, liver, kidneys, and bones, and be stored in the teeth and bones. Lead in bone is released into the blood during pregnancy and becomes a source of exposure for the developing fetus.

Young children, infants, and fetuses are particularly vulnerable to lead because lead's physical and behavioral effects occur at lower exposure levels in children than in adults. No level of exposure to lead is known to be without harmful effects. Lead concentrations above the 15 $\mu\text{g}/\text{L}$ action level were found in three of 37 Principal Aquifers in the USA, but in less than 1 percent of all wells analyzed (DeSimone et al., 2014). Figure 87 illustrates the spatial distribution of lead in the groundwater of the USA.

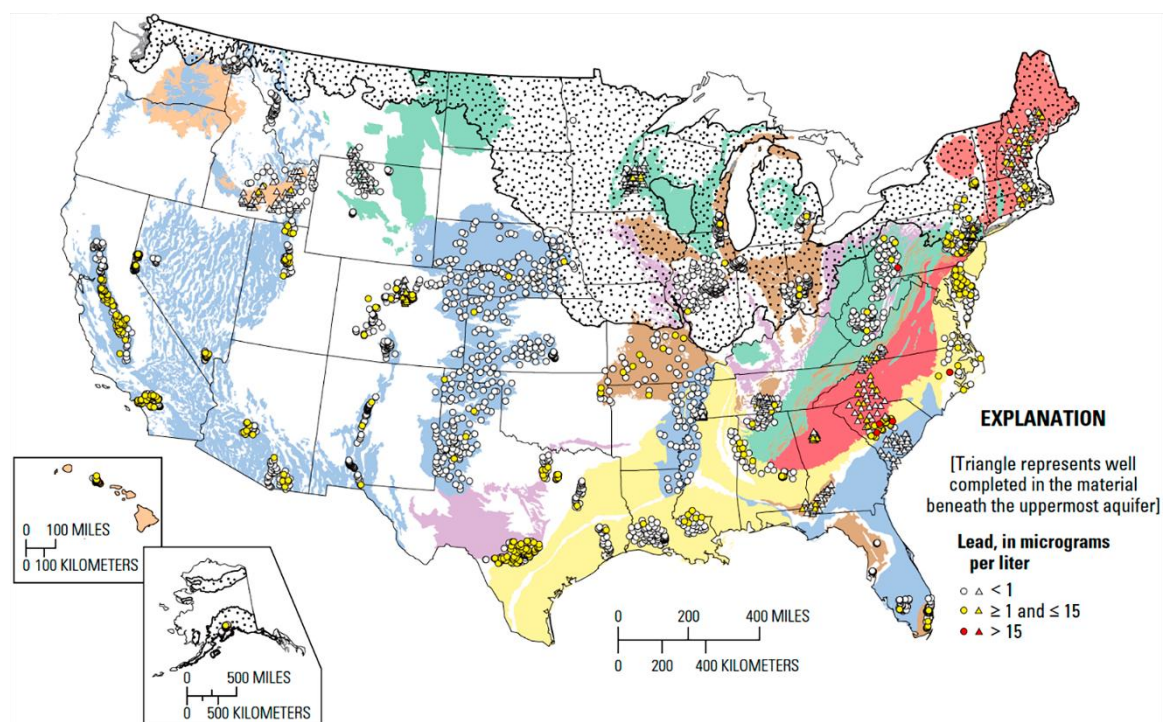


Figure 87 - Lead concentration ($\mu\text{g}/\text{L}$) in groundwater of the Principal Aquifers of the USA. Shading indicates major aquifer provinces as defined in the legend associated with Figure 63 (reproduced from Ayotte et al., 2011).

Lead is an element that commonly exists as a positively charged ion. Thus, it is more likely to sorb onto aquifer rocks and sediments at higher pH as there is less positively charged hydrogen ion (H^+) competing for the negative surface charge of the metal oxide coatings and clay minerals. Therefore, lead in groundwater is more likely to occur under low-pH conditions (Ayotte et al., 2011; Figure 88).

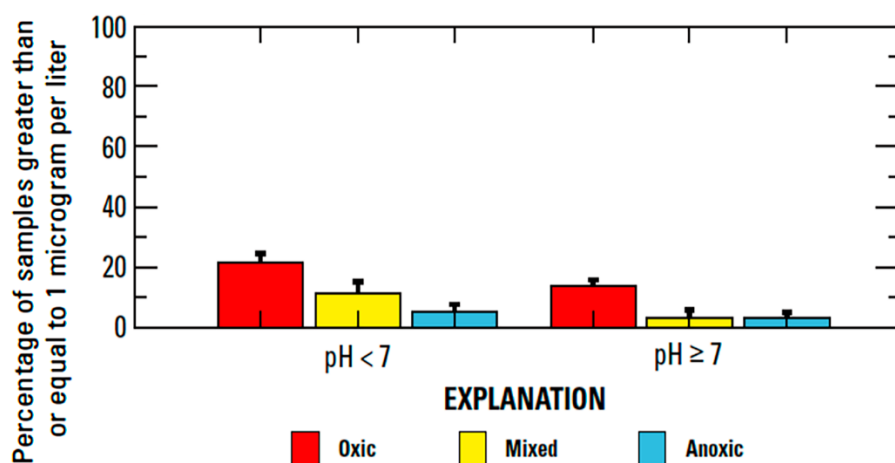


Figure 88 - Diagram of the percentages of samples equal to or greater than 1 (μg/L) Pb as a function of pH and redox conditions in the groundwater of the continental USA (reproduced from Ayotte et al., 2011).

3.8 Antimony (Sb)

The US EPA found antimony to potentially cause nausea, vomiting, and diarrhea in humans exposed to levels above the HHB (6 μg/L) for relatively short periods. However, no reliable data concerning health effects from long-term exposure to antimony in drinking water are available. The distribution of antimony in groundwater in the USA is shown in Figure 89, where most sample concentrations were less than 1 μg/L (Ayotte et al., 2011).

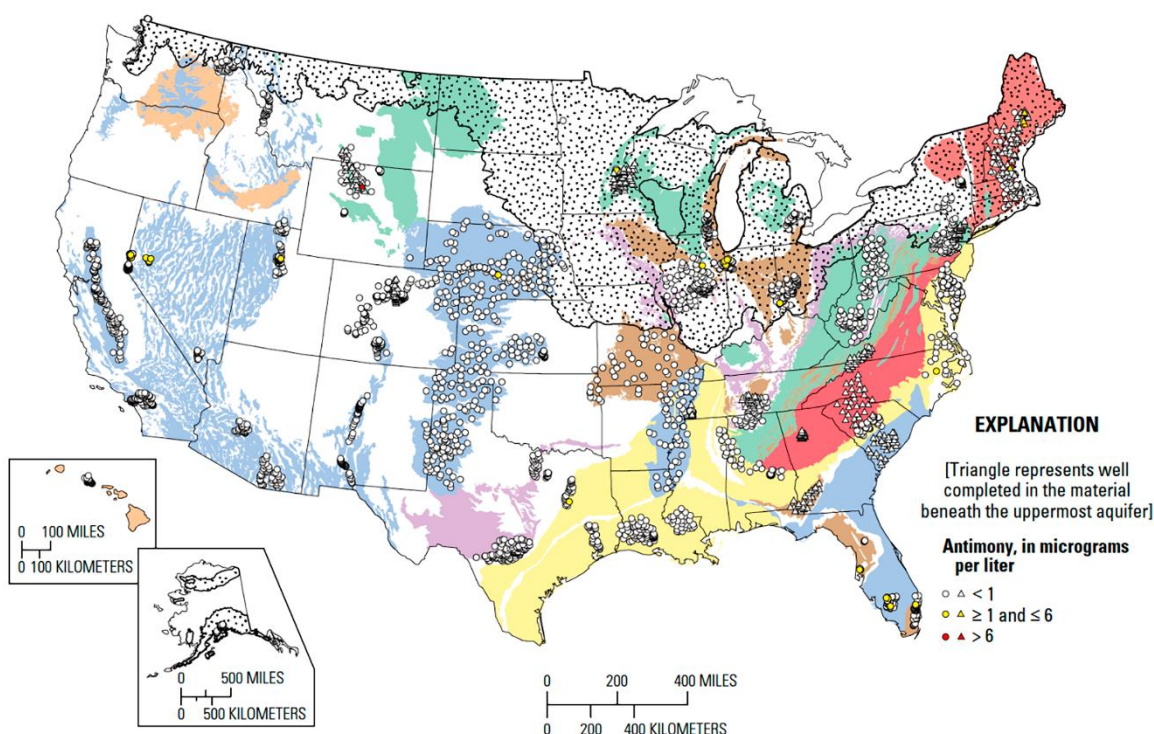


Figure 89 - Antimony concentration (μg/L) in the groundwater of the USA. Shading indicates major aquifer provinces as defined in the legend associated with Figure 63 (reproduced from Ayotte et al., 2011).

Antimony was shown to be low in all lithologic groups in the US (Figure 90; Ayotte et al., 2011).

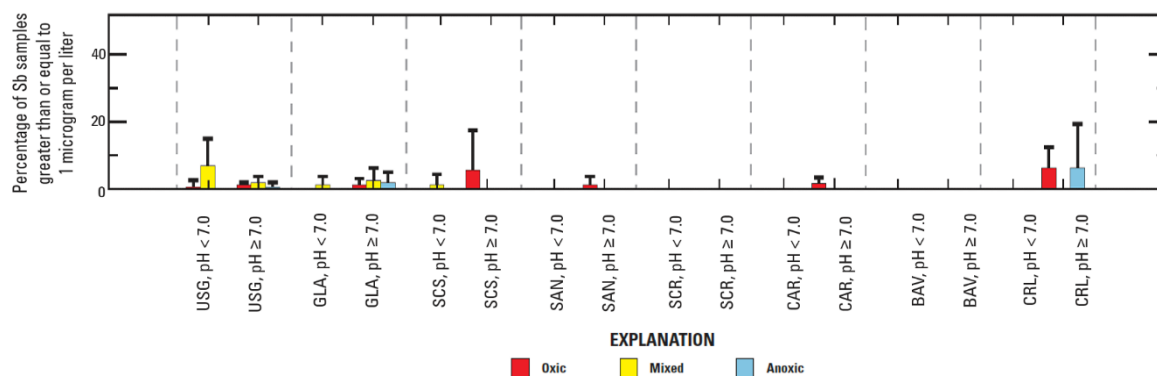


Figure 90 - Percentage of samples greater or equal to 1 $\mu\text{g/L}$ of antimony (Sb) from groundwater of the continental USA as a function of pH and redox conditions (reproduced from Ayotte et al., 2011).

Antimony exists in two oxidation states (+3 or +5). In the mineral stibnite (Sb_2S_3), the oxidation state is +3; antimony also forms pentafluoride (SbF_5) where its oxidation state is +5.

Oxidation of sulfide minerals is the most predominant geochemical mechanism for releasing antimony into groundwater, and its concentration is determined by its oxidation state. Oxyhydroxides of iron, manganese, and aluminum minerals are recognized as zones of naturally occurring removal mechanisms for antimony in groundwater. Trivalent antimony is more mobile in acidic than in basic conditions, whereas pentavalent is more mobile in elevated pH, consistent with the competition from H^+ and OH^- ions.

3.9 Selenium (Se)

The US EPA's HHB for selenium is 50 $\mu\text{g/L}$, whereas the WHO guideline is 40 $\mu\text{g/L}$. Selenium, as a micronutrient, is needed to maintain good health and is found in multivitamins and supplements. However, short-term oral exposure to high concentrations of selenium may cause nausea, vomiting, and diarrhea. Long-term oral exposure to high concentrations of selenium may result in selenosis, which may cause hair loss, nail loss, or neurological symptoms such as numbness in the hands or feet.

Selenium is particularly problematic for livestock and wildlife because it bioaccumulates and can be toxic at elevated levels. Selenium accumulates in the western aster (*Symphyotrichum ascendens*), a wildflower which is responsible for many selenium livestock poisonings. The distribution of selenium in groundwater in the USA is given in Figure 91 (Ayotte et al., 2011).

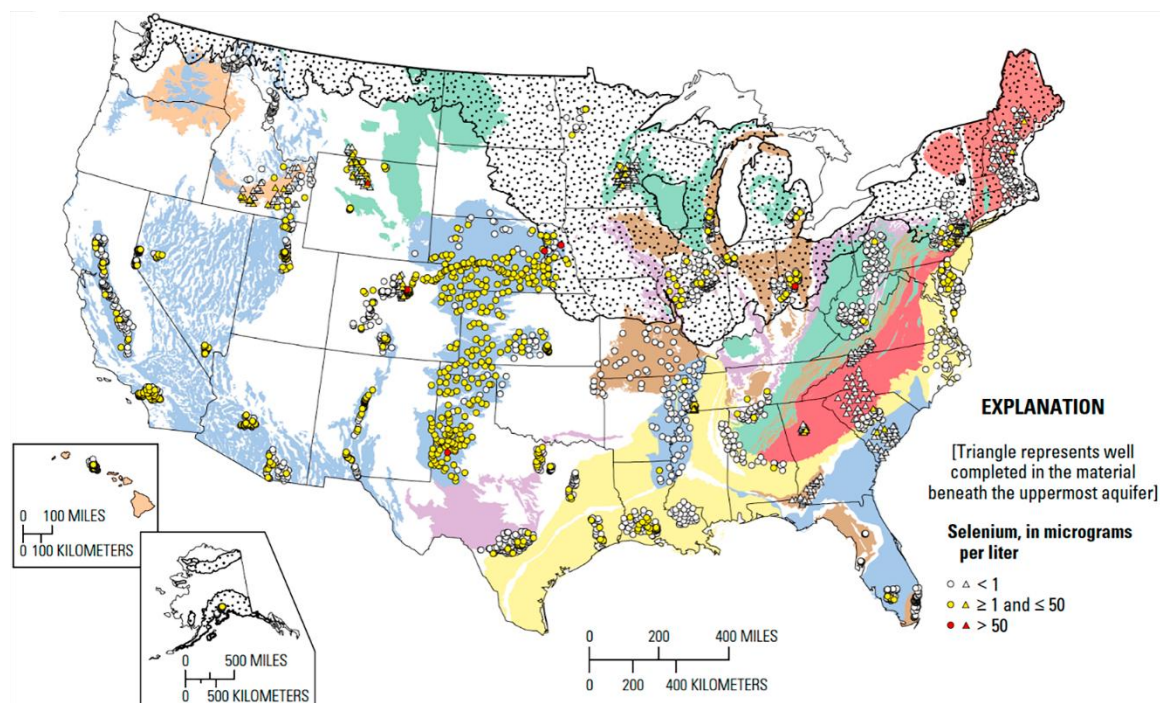


Figure 91 - Selenium concentration $\mu\text{g/L}$ in groundwater of the USA. Shading indicates major aquifer provinces as defined in the legend associated with Figure 63 (reproduced from Ayotte et al., 2011).

Selenium is often a trace element substituting for sulfur in pyrite (FeS_2). At typical groundwater pH values (7.0 to 9.5), only anionic forms of selenium (Se^{+4}) HSeO_3^- or (Se^{+6}) SeO_4^{2-} are typically found. As selenium oxides are negatively charged, it is likely to increase in groundwater as the pH increases; because the OH^- ions are competing for the positive sorption sites on the solids, thus keeping it in solution at elevated pH.

3.10 Zinc (Zn)

The HHB for zinc is set at 2,000 mg/L as short-term consumption of elevated zinc concentrations can cause stomach cramps, nausea, and vomiting. Ingesting high zinc levels for several months may cause anemia, damage the pancreas, and decrease high-density lipoprotein (HDL) cholesterol levels. Zinc is a ubiquitous element occurring in many rocks in the Earth's crust and is commonly found in mineral deposits along with copper and lead. Sphalerite, a zinc/iron sulfide mineral— $(\text{Zn},\text{Fe})\text{S}$, is the primary ore mineral for zinc. However, its presence as a trace element substituting for iron in other minerals is the most likely source of most of the zinc in groundwater. Zinc ions in groundwater act largely as cations and thus are more mobile in low pH waters. Figure 92 shows the distribution of zinc in the groundwater of the US Principal Aquifers (Ayotte et al., 2011).

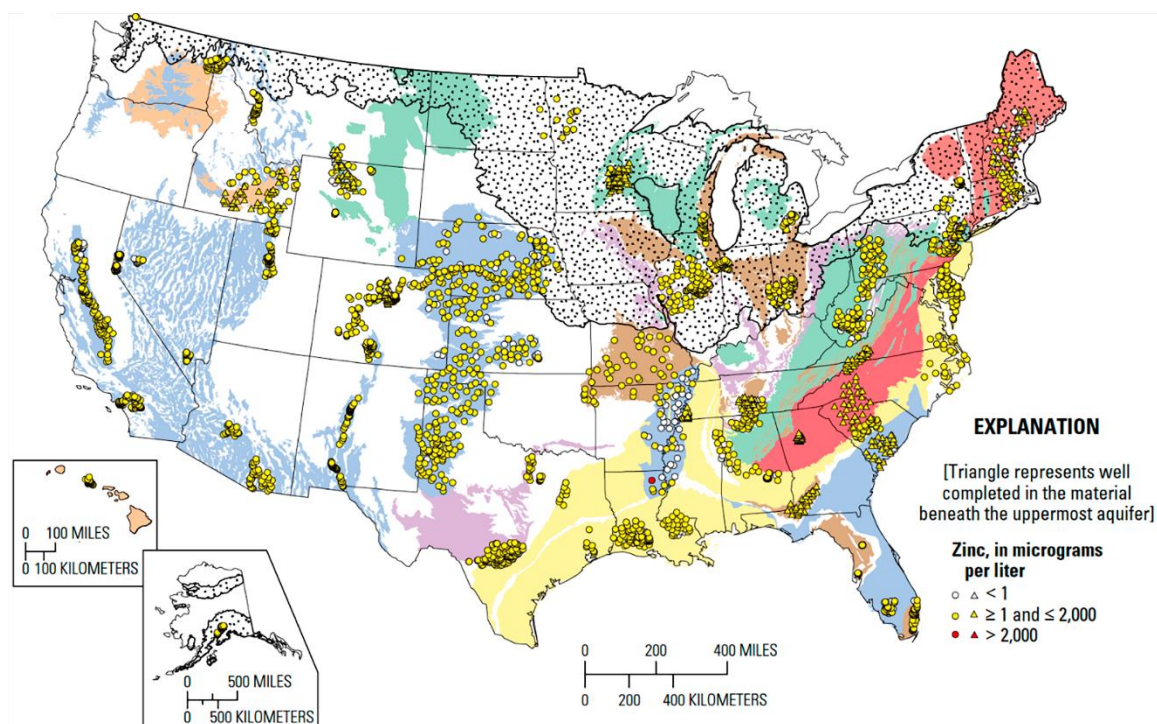


Figure 92 - Concentration of zinc ($\mu\text{g/L}$) in groundwater in Principal Aquifers of the USA. Shading indicates major aquifer provinces as defined in the legend associated with Figure 63 (reproduced from Ayotte et al., 2011).

3.11 Lithium (Li)

Lithium in low concentrations is ubiquitous in groundwater in the USA (Figure 93; Lindsey et al., 2021). Although helpful in treating mental health disorders, lithium can cause adverse health effects, primarily by impairing thyroid and kidney functions. Presently, lithium is not regulated in drinking water in the USA; however, the US EPA (2021) proposed a HBSL for lithium in drinking water of $10 \mu\text{g/L}$. Lindsey and others (2021) reported that approximately 45 percent of public-supply wells and 37 percent of USA domestic-supply wells have concentrations of lithium above this HBSL. Lithium is also a critical element in the rapidly developing use of high-efficiency batteries; thus, it is important to have a geogenic background value before anthropogenic activity impacts the lithium concentration in groundwater.

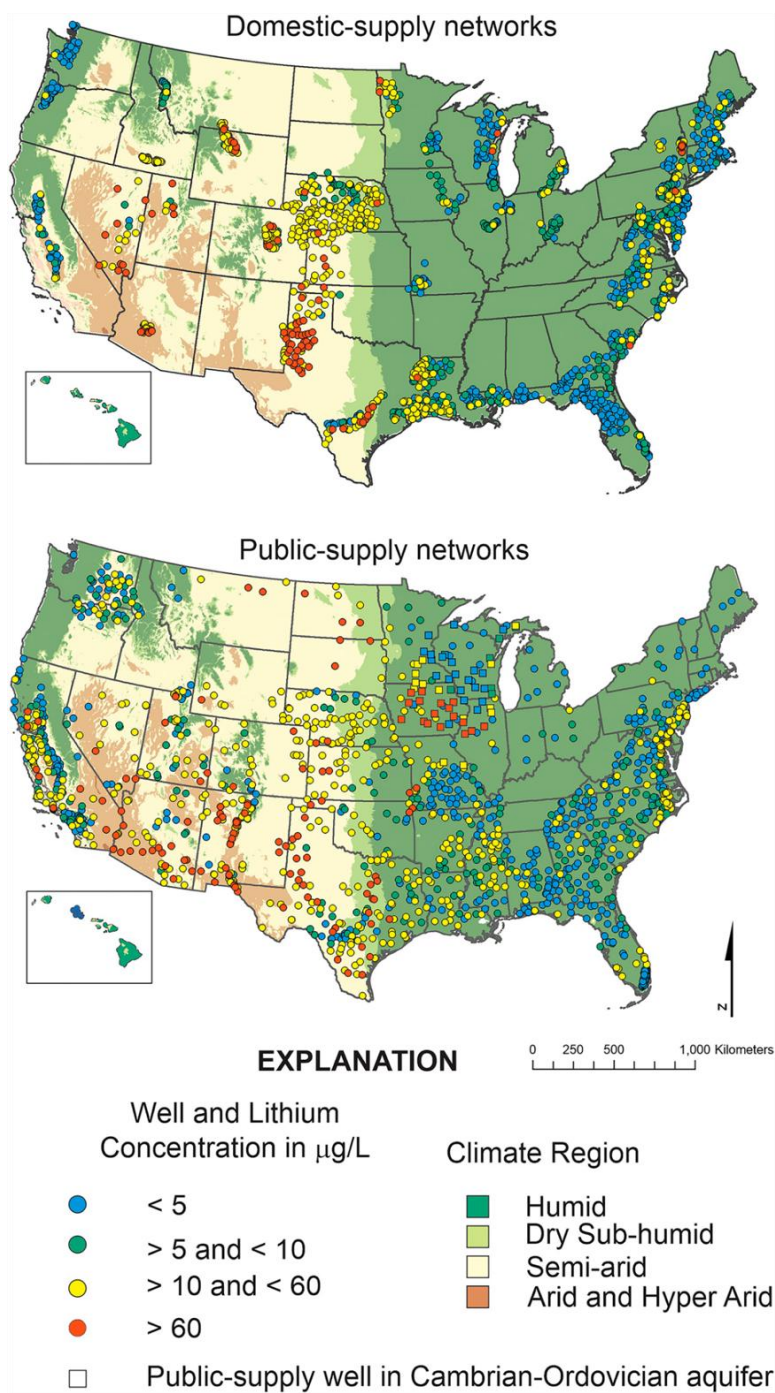


Figure 93 - Lithium concentration ($\mu\text{g/L}$) as a function of climate in groundwater in the USA (reproduced from Lindsey et al., 2021).

Lindsey and others (2021) reported lithium concentrations in groundwater from 1,464 public-supply wells and 1,676 domestic-supply wells in the USA (Figure 94). Concentrations nationwide ranged from <1–396 $\mu\text{g/L}$ (median of 8.1) for public-supply wells and <1 to 1,700 $\mu\text{g/L}$ (median of 6 $\mu\text{g/L}$) for domestic-supply wells (Lindsey et al., 2021). Concentrations were highest in arid regions and older groundwater—particularly in unconsolidated clastic aquifers and sandstones—and lowest in carbonate-rock aquifers, consistent with differences in lithium abundance among primary lithologies and rock

weathering (Figure 94 and Figure 95; Lindsey et al., 2021). The median concentration for public-supply wells in the unconsolidated clastic High Plains aquifer was 24.6 µg/L. Other unconsolidated clastic aquifers in the arid USA West had exceedance rates comparable to the High Plains aquifer. The lithium-bearing mineral spodumene—LiAl(SiO₃)₂—may be present in felsic volcanic rocks.

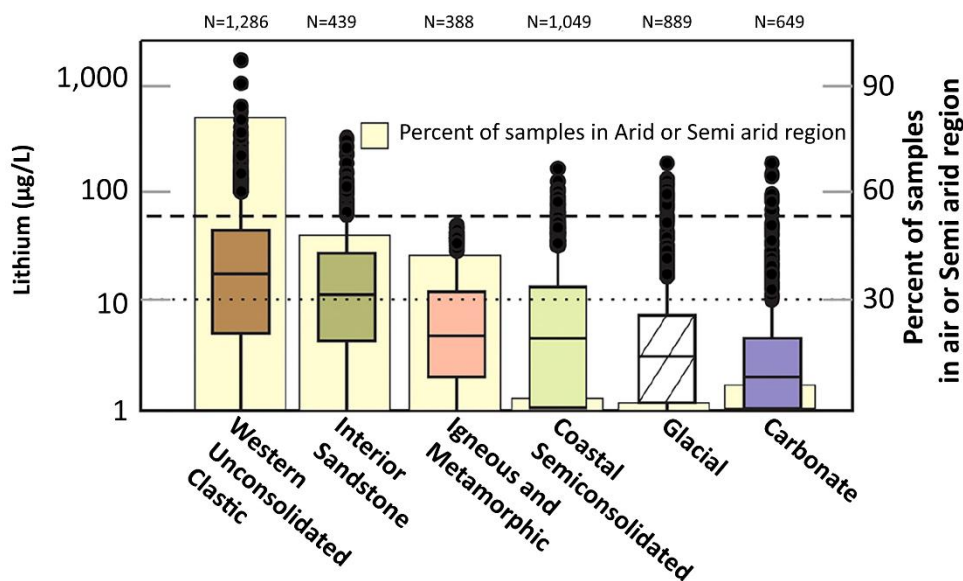


Figure 94 - Box-and-whisker diagrams of lithium concentration (µg/L) in groundwater of different depositional environments in the USA. The light yellow indicates the percent of samples from arid and semi-arid areas, while the central color is correlated to the lithotype indicated on the x-axis as indicated on maps of Lindsey et al., 2021. The dashed line is the 60 µg/L drinking water only threshold while the dotted line is the USEPA proposed 10 µg/L HBSL (reproduced from Lindsey et al., 2021).

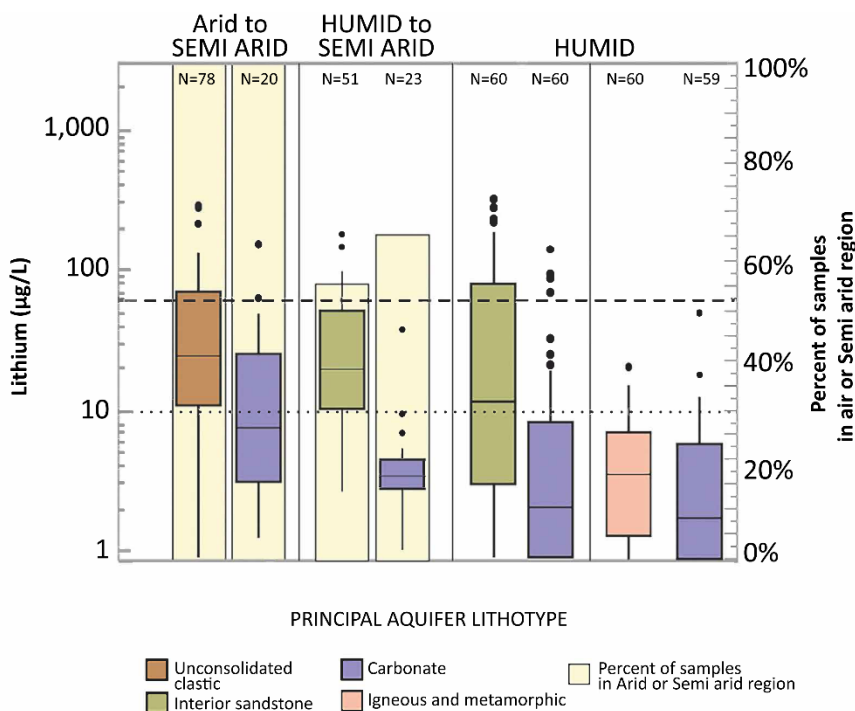


Figure 95 - Box-and-whisker diagram of lithium concentration (µg/L) in the groundwater of noncarbonate (left of each pair) and carbonate (right of each pair) rocks in different climates in the continental USA (reproduced from Lindsey et al., 2021).

3.12 Nuisance Elements

The US EPA has established Secondary Maximum Contaminant Levels (SMCLs) that establish nonmandatory water quality standards for fifteen items. The US EPA does not enforce these SMCLs as they are established to assist public water systems in managing their drinking water for aesthetic considerations such as taste, color, and odor. These items are not considered a risk to human health, although some have negative health impacts (Table 9).

Table 9 - Secondary maximum contaminate level (SMCL) established by the [US EPA Secondary Drinking Water Standards: Guidance for Nuisance Chemicals](#)⁷.

Contaminant	Secondary MCL	Noticeable Effects above the Secondary MCL
Aluminum	0.05 to 0.2 mg/L	Colored water
Chloride	250 mg/L	Salty taste
Color	15 color units	Visible tint
Copper	1.0 mg/L	Metallic taste; blue-green staining
Corrosivity	Non-corrosive	Metallic taste; corroded pipes/fixtures staining
Fluoride	2.0 mg/L	Tooth discoloration
Foaming agents	0.5 mg/L	Frothy, cloudy; bitter taste; odor
Iron	0.3 mg/L	Rust color; sediment; metallic taste; reddish/orange staining
Manganese	0.5 mg/L	Black to brown color; black staining; bitter metallic taste
Odor	3 TON (threshold odor number)	“Rotten-egg”, musty, or chemical smell
pH	6.5–8.5	Low pH: bitter metallic taste; corrosion High pH: slippery feel; soda taste; deposits
Silver	0.1 mg/L	Skin discoloration; graying of the white part of the eye
Sulfate	250 mg/L	Salty taste
Total Dissolved Solids, TDS	500 mg/L	Hardness; deposits; colored water; staining; salty taste
Zinc	5 mg/L	Metallic taste

3.13 Iron (Fe)

Iron—with its two oxidation states: Fe^{2+} (soluble in reducing and low pH conditions) and Fe^{3+} (with poor solubility in elevated pH and oxygenated waters)—is an essential element for living organisms and is involved in a wide variety of metabolic processes, including oxygen transport, deoxyribonucleic acid (DNA) synthesis, and electron transport. The US EPA secondary MCL for iron is 300 $\mu\text{g/L}$, above that level, Fe can give water a disagreeable metallic taste, and, when used to make tea and coffee, produces a black appearance with an unpleasant taste.

3.14 Hydrogen Sulfide (H_2S) and Methane (CH_4)

While neither hydrogen sulfide (H_2S) nor methane (CH_4) are on the US EPA list of HHB or SMCL, they can be nuisance gases. Some groundwater from reducing conditions exhibits a concentration of H_2S gas—with a “rotten-egg” smell—that, in higher concentrations, can be lethal to humans and pets as it is heavier than oxygen and will settle in low areas, replacing oxygen in the atmosphere of a residence.

Methane gas is neither toxic nor accountable for human health problems in groundwater. However, it can de-gas from the water, creating an explosive environment in poorly ventilated or confined areas. These gases are usually minor in most aquifer systems and can be removed by external aeration.

3.15 Section Wrap-up: Selected Trace Geogenic Elements

As the Principal Aquifers of the USA represent a wide variety of lithology and climate environments (Table 10), one would expect to see a similar presence of geogenic trace health elements in aquifer systems globally. Three generalized conclusions from the USA data can be made that are likely applicable to other areas of the Earth.

1. At least one inorganic constituent exceeded a human-health benchmark in all 15 Principal Aquifers studied.
2. Arsenic, fluoride, and manganese commonly exceeded human-health benchmarks in the 15 Principal Aquifers studied.
3. At least one radioactive constituent exceeded a human-health benchmark in a small percentage of samples (1 to 10 percent) in the Principal Aquifers studied.

[Exercise 2](#) explores the factors that determine the concentration of trace elements.

Table 10 - Summary of the percentages of exceedances of HHB or non-health guidelines (ug/L) in samples across the US by major aquifer groups. The total number of these elements with ≥ 1 percent exceedance is shown at the bottom of the table: unconsolidated sand and gravel (USG); glacial unconsolidated sand and gravel (GLA); semi-consolidated sand (SCS); sandstone (SAN); sandstone and carbonate rock (SCR); carbonate rock (CAR); basaltic and other volcanic rock (BAV); crystalline rock (CRL) (from Ayotte et al, 2011).

Element	Benchmark or guideline (ug/L)	Major aquifer group															
		USG		GLA		SCS		SAN		SCR		CAR		BAV		CRL	
		N	%	N	%	N	%	N	%	N	%	N	%	N	%	N	%
Aluminum	200	1,226	1.0	485	1.0	301	3.0	229	1.7	166	0.60	195	0.00	31	0.00	193	1.0
Antimony	6	1,318	0.0	498	0.0	338	0.00	256	0.39	186	0.00	189	0.00	30	0.00	194	0.00
Arsenic	10	1,507	12	512	6.8	373	0.80	282	1.4	189	1.1	229	1.3	81	6.2	223	5.4
Barium	2,000	1,376	0.07	513	0.0	343	0.29	283	0.35	189	0.00	189	0.00	35	0.00	194	0.00
Beryllium	4	1,318	0.00	511	0.0	338	0.29	258	0.78	186	0.00	189	0.00	31	0.00	194	0.52
Boron	1,000	552	3.4	274	1.1	181	0.00	86	0.00	--	--	--	--	30	0.00	51	0.00
Cadmium	5	1,351	0.37	511	0.00	338	0.00	274	1.1	186	0.00	189	0.00	81	0.00	194	0.00
Chromium	100	1,367	0.07	491	0.00	338	0.00	275	0.00	188	0.00	190	0.00	80	0.00	194	0.00
Copper	1,300	1,372	0.7	501	0.00	339	0.00	280	0.00	189	0.00	189	0.00	80	0.00	194	0.00
Iron	300	1,769	12	1,190	29	570	29	389	32	222	7.7	480	19	232	3.4	279	9.3
Lead	15	1,355	0.0	498	0.00	339	1.2	277	0.36	187	0.00	189	0.00	81	0.00	194	0.00
Manganese	300	1,700	12	1,148	20	564	9.8	376	17	219	3.2	463	1.9	228	2.6	278	3.6
Molybdenum	40	1,368	2.4	499	2.0	339	0.00	257	0.78	188	0.53	189	0.00	30	0.00	194	0.00
Nickel	100	1,369	0.00	502	0.00	341	0.29	262	2.3	189	0.00	189	0.00	30	0.00	194	0.00
Radon	300	1,481	77	763	54	243	39	358	65	136	44	431	61	192	43	273	92
Selenium	50	1,395	0.29	511	0.20	342	0.00	282	0.35	189	0.00	183	0.00	74	0.00	190	0.00
Silver	100	1,297	0.00	506	0.00	339	0.00	264	0.00	184	0.00	169	0.00	35	0.00	194	0.00
Strontium	4,000	483	5.2	259	1.2	155	0.00	59	3.4	98	26	140	0.71	31	0.00	84	0.00
Thallium	2	366	0.00	202	0.00	154	0.00	57	0.00	--	--	--	--	--	--	58	0.00
Uranium	30	1,409	8.7	640	0.47	339	0.00	336	0.30	187	0.53	318	0.31	33	0.00	279	3.9
Zinc	2,000	1,335	0.07	494	0.00	308	0.00	238	0.00	178	0.00	190	0.00	70	0.00	193	0.00
Number of elements with $\geq 1\%$ exceedance		9		8		5		8		5		4		4		6	

4 Graphical Display of Hydrogeochemical Data

Individuals acquire and process information differently by listening, reading, writing, or visual presentations. To illustrate a concept, converting data tables to visual representation is frequently helpful; diagrams provide a quick summary of essential data or show a relation. That is, *a diagram may be worth a hundred tables*. Additionally, one of the unstated values of a graph may be its value in eliminating or confirming the hypothesis to a researcher. Thus, plotting data in different ways can provide insight into the process and statistical distribution of the data; therefore, graphs can be an important tool for learning about a system.

Graphs should make large datasets coherent, challenge the reader to think about the substance of the plot, and be closely integrated with statistical and written descriptions—but avoid distorting the data. Common data-management spreadsheets such as Microsoft Excel or Apple Numbers provide a variety of excellent general-purpose graphs that can be used to illustrate solute concentration, ratios, relations, or other critical information. Using these graphs has the advantage that most individuals are familiar with them. Other programs, such as KaleidaGraph, provide a variety of additional, easy-to-plot statistical graphs and alternative ways of presenting data. There are several excellent books on the philosophical background of presenting data graphically, such as Tufte (1997) and Turkey (1977). Cleveland (1985) presents a more how-to-do-it approach, and there are many helpful online instructions for constructing specific graphs.

Graphs can display large amounts of numerical data or portray the relationships between concentration, solute ratios, groundwater flow lines, or other variables. The choice of the type of graphical illustration depends on the background of the intended audience and the purpose of the illustration. Are you attempting to classify different types of solutes in water? Provide a visible result of a statistical analysis? Contrast or correlate a solute change along the flow path? Show the chemistry of different portions of an aquifer? Support or refute a conceptual model? Illustrate change with time? Replace a data table in the main body of a report?

In general, three fundamental types of illustrations are typically used to display groundwater solute data, those that:

1. show variations in space or time (e.g., plan, cross-section, or fence diagrams of the aquifer at a specific location with time or in relation to flow paths) illustrating concentration or solute ratio changes laterally or vertically in an aquifer by use of *contours* or color *heatmaps*;
2. display ionic ratios and/or concentrations of individual analyses for a small number of analyses by use of *bar graphs*, *pie diagrams*, *stick diagrams*, among others to give a visual representation of the solute data; and
3. display the statistical distribution of many samples.

It is critical to be mindful of the audience and be careful not to include too many variables; otherwise, the graph can quickly become confusing and thus defeat the purpose. The magazine *Scientific American* does an excellent job of illustrating concepts, and much can be learned from graphical presentations by looking at several of its articles. Further, the captions tell a story, so the reader can get a quick overview of the article by looking at the figures and reading the captions. This is an excellent approach for publications intended for popular consumption; that is, write the report around the graphs rather than just adding the graphs to the report.

4.1 Principals of Graph Design

The features of graph construction are legends, scales, plotting symbols, keys, tick marks, panels, and markers that together form a graph. The goal is to convey a concept, make the data come alive, and speak to the reader. Too often, to conserve space and reduce the number of figures, one observes a single graph with several variables on each axis so that it is nearly impossible to follow. It is beyond the scope of this manuscript to go into the details contained in the books like those already mentioned: Cleveland (1985), Tufte (1997), and Turkey (1977). Rather, the goal is to provide an overview of some of the basic ways hydrogeochemical data can be presented.

Graphs are best kept simple, so the concept is quickly grasped, much like a slide in a presentation. Use several graphs rather than cluttering up one graph. Recall the views of Oliver Wendell Holmes Jr.: "*For the simplicity that lies this side of complexity, I would not give a fig, but for the simplicity that lies on the other side of complexity, I would give my life,*" or as Leonardo Da Vinci stated, "*Simplicity is the ultimate sophistication.*" Thus, illustrations such as the Durov diagram and fence diagrams should generally be restricted to specialized professional audiences.

One of the most common poor practices in plotting the concentration of trace and minor elements with low concentration is obscuring the data with a value of zero by putting zero on the edge of the graph (Figure 96).

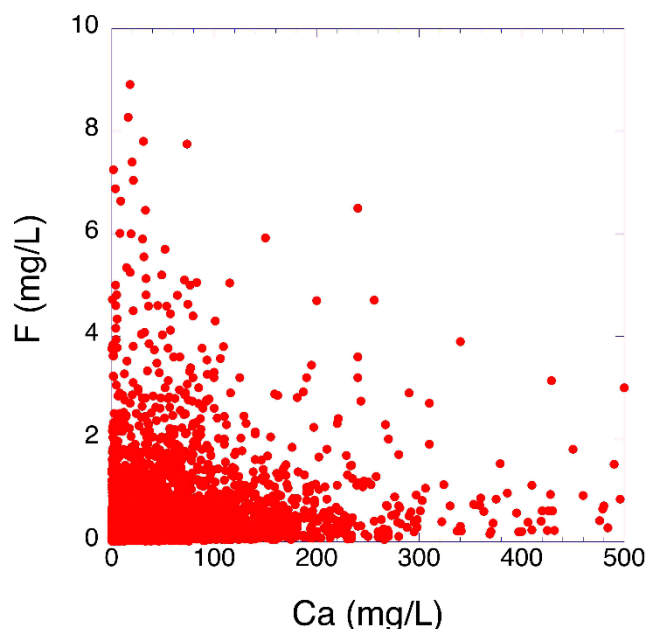


Figure 96 - Groundwater solute data plotted with no offset from zero on the horizontal or vertical axis. This obscures the large number of data points that have a value of zero.

The same data are plotted in Figure 97 with the axis offset. This figure reveals a great deal of fluoride data have a value of 0 and is thus determined. The offset shows the values of 0.0 and have been determined. If a data point is on the y axis it could be that it was not determined. This is particularly important in trace elements that tend to be low in concentration and near the edge of the graph. The data are open to question if they are plotted without the offset.

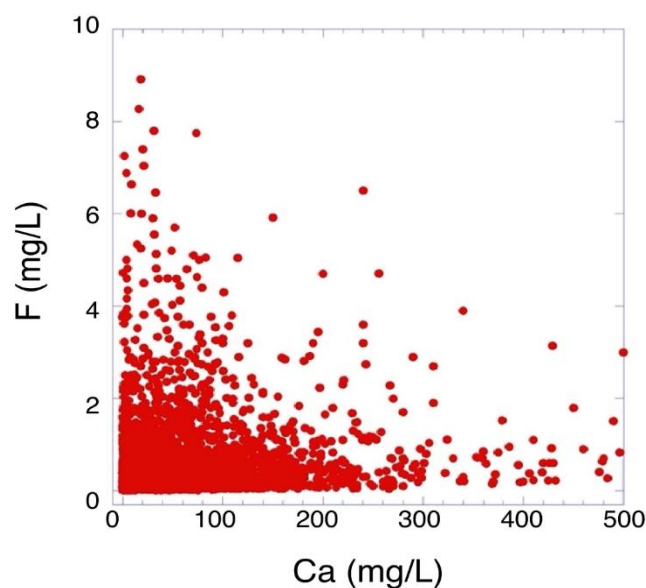


Figure 97 - Same data as Figure 96 but with both solutes plotted with an offset to better illustrate the large number of points at which one of the parameters is at zero.

As solute data are generally log-normally distributed, the data may be plotted on a logarithm scale (Figure 98) for both parameters and this may provide some insight into the origin of the solutes.

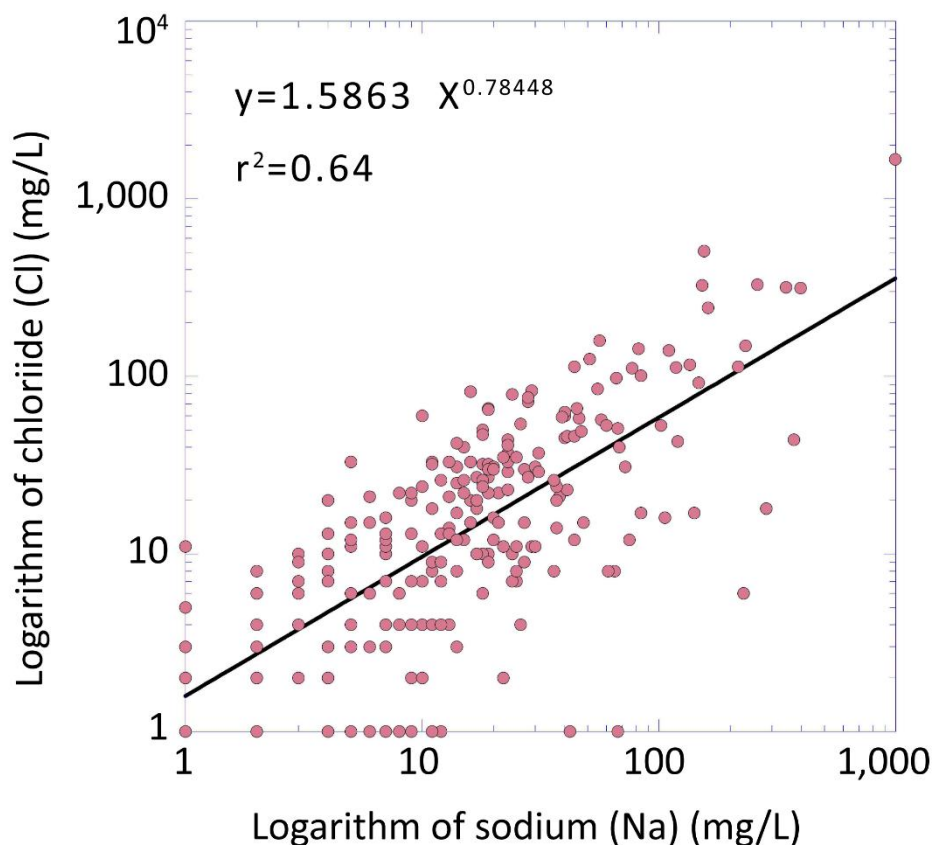


Figure 98 - The logarithm of chloride (Cl) concentration plotted against the logarithm of sodium (Na) concentration of 250 typical groundwater samples illustrating the fit of a power curve. The r^2 of 0.64 is a measure of the goodness of fit of the data to the curve, with 1.0 being a perfect fit.

Solute ratios or concentration can be plotted directly on a map; thus, with a simple glance, the differences and similarities over a large geographical area are quickly seen (Figure 99). To add an additional parameter, such as total dissolved solutes, the diameter of the pies can be increased or decreased.

OVERVIEW OF WATER QUALITY IN PRINCIPAL AQUIFERS

Exceedances of human-health benchmarks by one or more inorganic contaminants

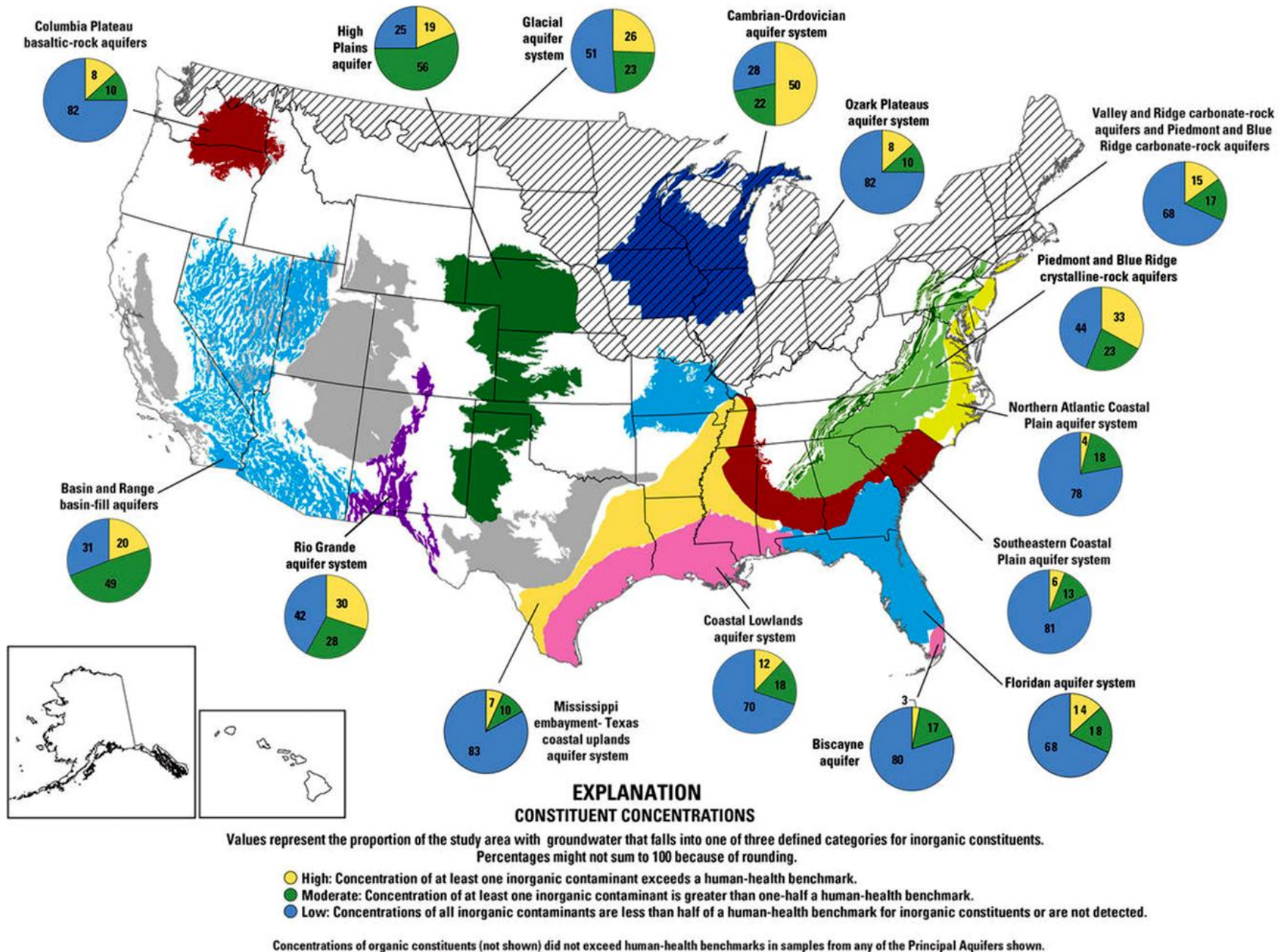


Figure 99 - Map of the USA showing water quality overview of solutes in principal aquifers that exceeded the human-health benchmarks (HHBs). The blue of each circle represents the percentages of low concentration.

4.1.1 Heat Map

A heat map, where the intensity of a color indicates the concentration, is another common way of expressing the geospatial distribution of a parameter, as is shown by the distribution of domestic wells supplying drinking water in Figure 100.

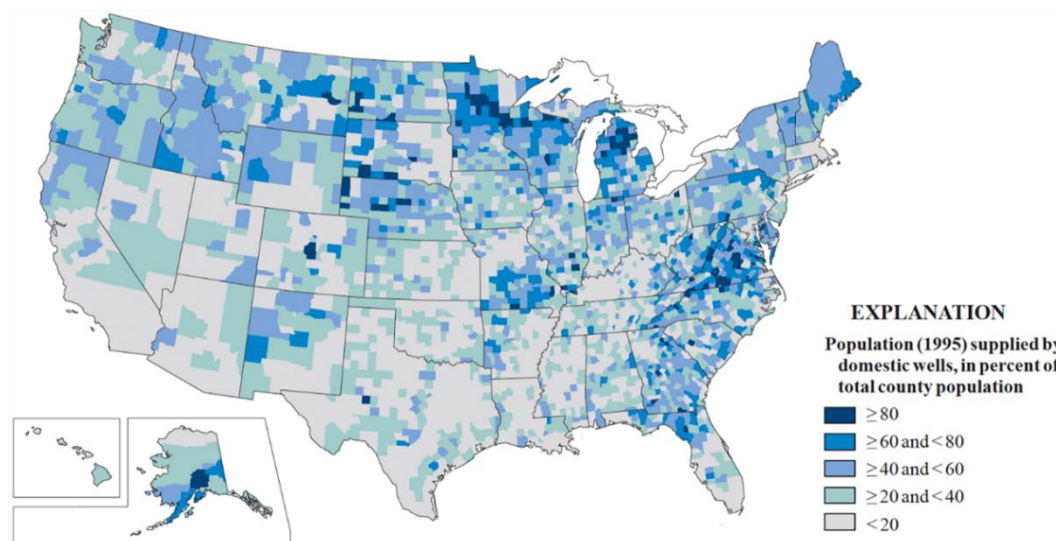


Figure 100 - Domestic wells that supply drinking water in the USA are shown with different color intensities as a function of their quantities (reproduced from DeSimone et al., 2009).

4.1.2 Contour Map

If a geospatial gradient is present, a common presentation format is a contour map of the solute. For example, the specific conductance map of an aquifer system in the Emirates of Abu Dhabi, UAE. Figure 101 illustrates an increase in specific conductance with the direction of flow – something that might not be apparent from a table of data (Figure 101).

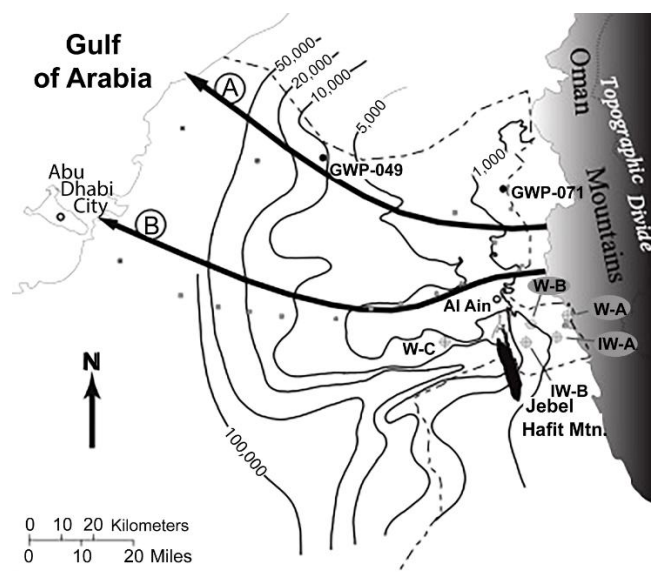


Figure 101 - Contour of specific conductance ranging from 1,000 to 50,000 mS in an aquifer in Abu Dhabi, UAE (reproduced from Imes & Wood, 2007). A contour graph is typically used to illustrate solute gradient within an aquifer.

4.1.4 Cumulative Frequency

Several types of diagrams are used in the statistical summary of a large set of solute data. The cumulative frequency diagram is often used to show:

- whether the data are statistically normally distributed—that is, the mean and median are the same value—and
- the distribution of the data (Figure 103).

In Figure 103, all solutes except bicarbonate and perhaps silica appear to curve upward with increasing concentration; thus, they are not normally distributed, indicating that some common statistical expressions, such as mean and standard deviation, are inappropriate to describe the distribution. One of the advantages of a cumulative frequency diagram is being able to identify the type of statistical distribution that represents the data at a glance without applying an elaborate statistical test to the data.

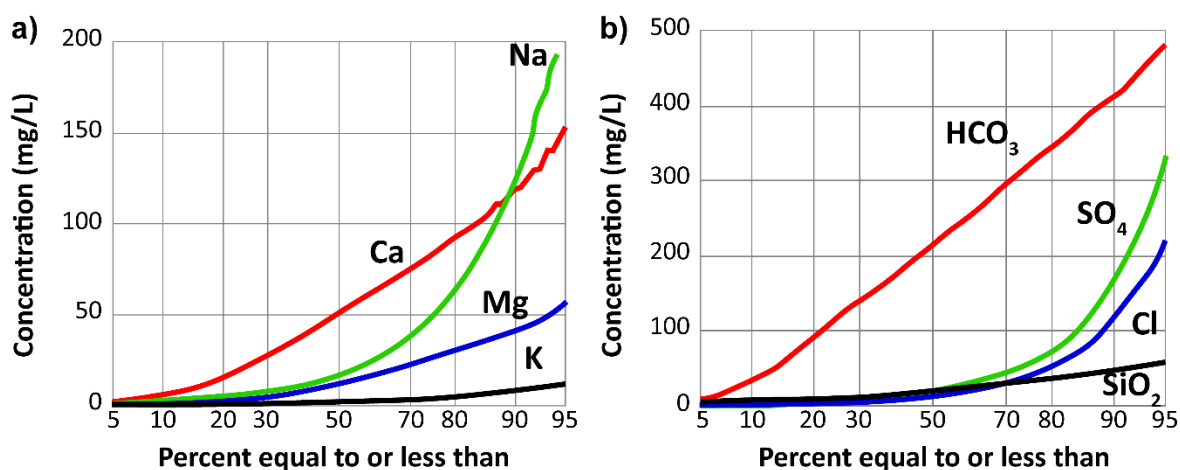


Figure 103 - Cumulative frequency within the 5 to 95 percentile range of a) major cations (positive charge) and b) anions (negative charge) plus SiO₂, in mg/L from thousands of groundwater analyses (data from USGS NAWQA database).

4.1.5 Box-and-Whisker Plot

A common way to express large data sets of non-normally distributed data is with a box-and-whisker plot of concentrations (Figure 104 and Figure 105). The median value is the number in which half the analyses are of greater concentration and half are less. The numerical values at the top are the total number of samples; the horizontal lines within each box—10, 25, 50 (median), 75, and 90—are percentiles. The Microsoft Excel program includes 5th and 95th percentiles as shown by dots (Figure 104). The 5th percentile means that 5 percent of the samples have a concentration less than this value, and the 95th indicates the portion that has a concentration less than 95 percent of this value.

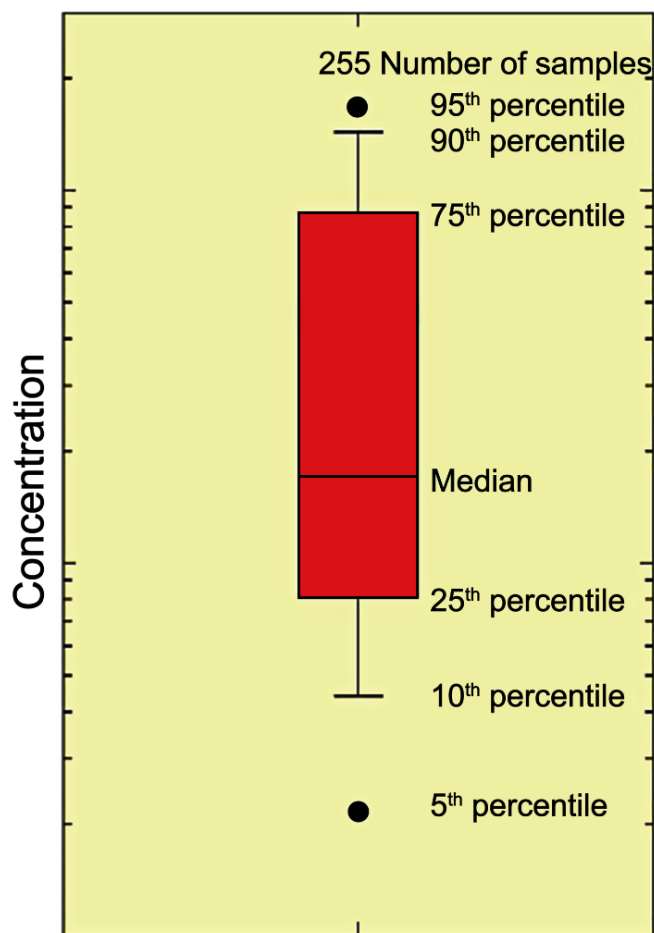


Figure 104 - Box-and-whisker plot of concentrations of solutes illustrating significant statistical reference points (reproduced from Shand et al., 2007).

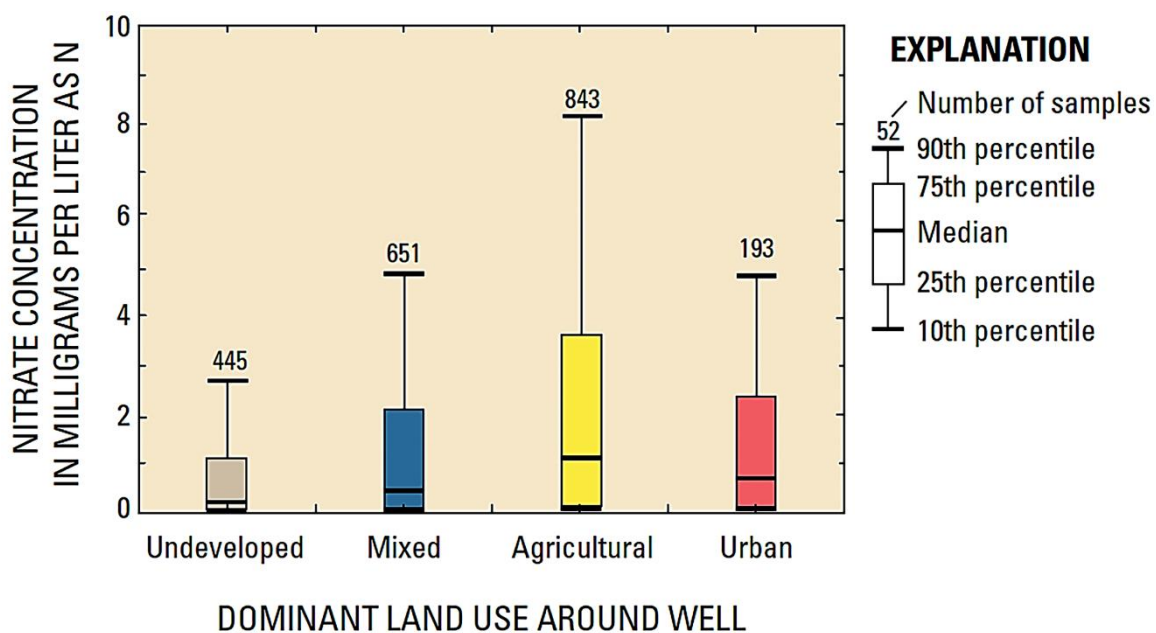


Figure 105 - Illustration of a box-and-whisker display of concentrations of nitrate varying with land use surrounding the sampled wells. Concentrations were highest in wells surrounded by agricultural land use and lowest in wells in undeveloped areas (reproduced from DeSimone et al., 2009).

4.1.6 Histogram

The frequency of a specific concentration range, also called a *bin*, is often presented in a histogram (Figure 106) and is commonly used to illustrate the broad range of solute concentration in large data sets. This type of presentation clearly illustrates if the data are normally distributed—that is, equal numbers of samples on either side of a central value. In the case shown in Figure 106, the calcium concentration is not normally distributed.

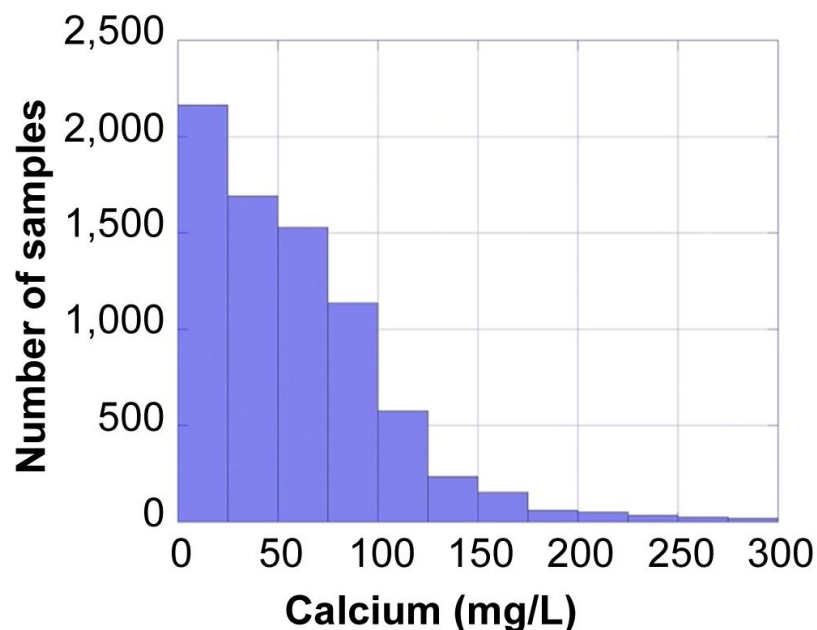


Figure 106 - Typical histogram illustrating the number of analyses of calcium in a large groundwater database for each concentration range or bin (data from the USGS NAWQA).

4.1.7 Pie Diagram

Pie diagrams are another graph frequently used to illustrate the distribution of solutes in data sets or an individual analysis. This type of diagram is commonly used to illustrate budgets in nontechnical literature; accordingly, the general audience is familiar with them. In Figure 107a, they illustrate the percentage of major solutes in global groundwater and the area of the pie pieces show the solutes are dominated by calcium and bicarbonate ions. Thus, it provides a visual contrast between global groundwater and the analyses of brine in Abu Dhabi, UAE, which is dominated by sodium and chloride (Figure 107b). This type of diagram can also be made in different diameters to indicate total solute concentration if the ionic ratios are similar but concentrations are different.

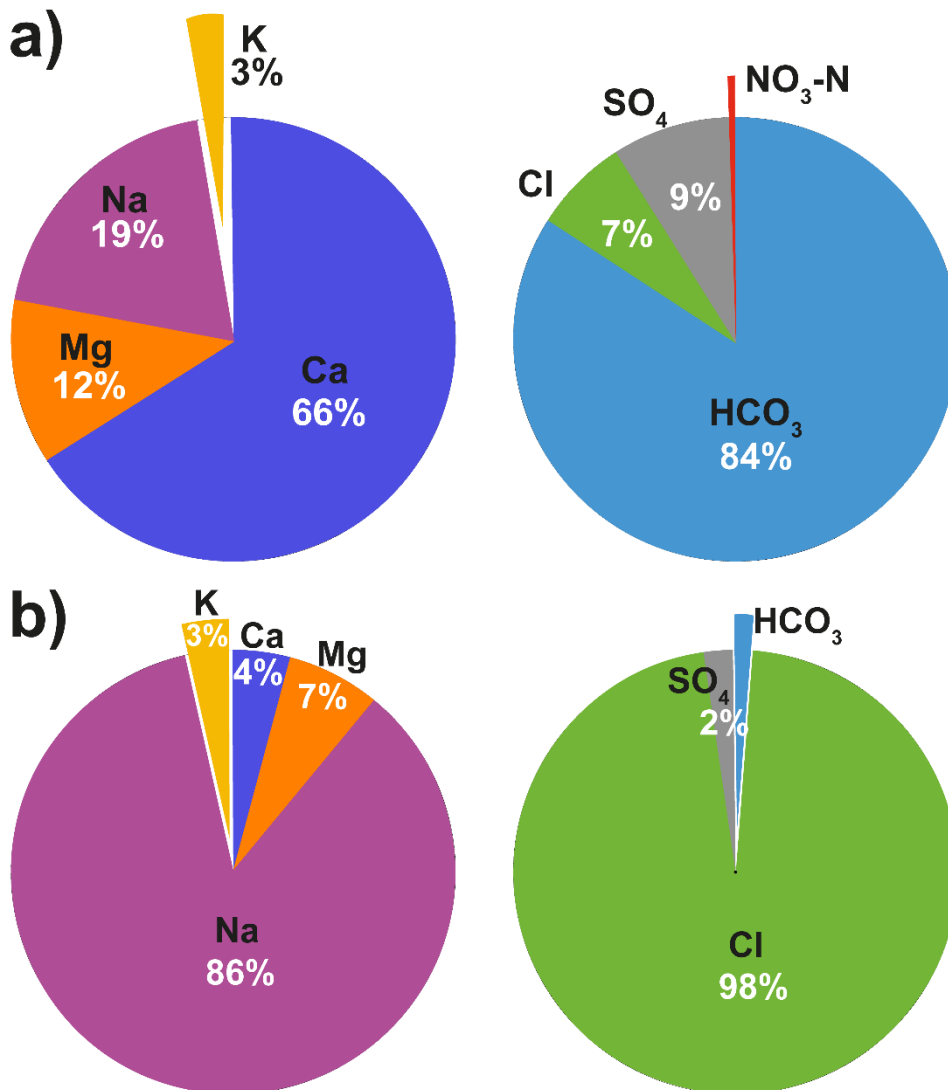


Figure 107 - a) Analyses of mean global groundwater represented by circles subdivided based on percent of cations and anions in milligrams per liter. b) Percentage of cations and anions in brine from the Abu Dhabi coastal sabkha (Table 1). This presentation format is commonly used in literature intended for general audiences as many people are familiar with pie diagrams being used to describe economic development.

4.1.8 X–Y Linear Graph

The most common and simple graphical technique to illustrate a relation between two ions, is an x–y graph, where two parameters are plotted against one another. For example, one might plot sodium concentration in mg/L against chloride concentration in mg/L to illustrate the relation between these two elements (Figure 108).

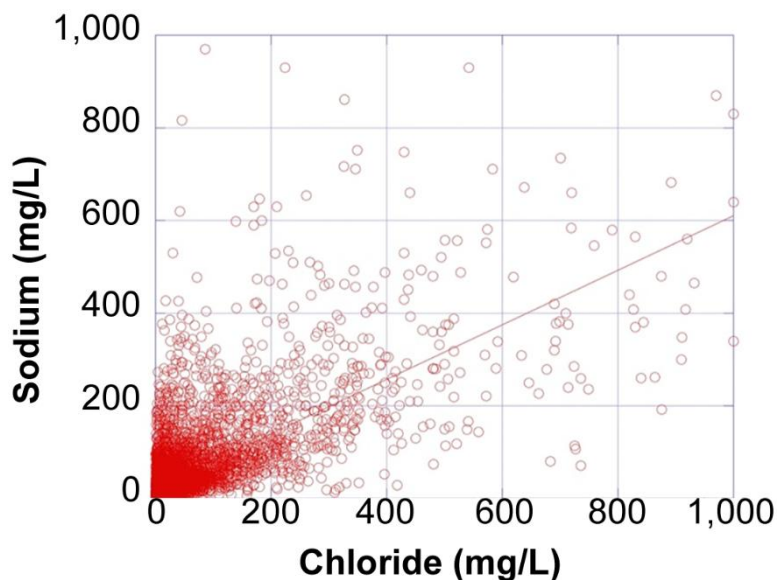


Figure 108 - An x–y graph of thousands of samples of global groundwater sodium concentration in mg/L against chloride concentration in mg/L in the same water sample. Typically, x–y linear graphs are used to illustrate relations between two solutes. There is no offset on either axis as the goal is to show the correlation over large concentration ranges. The diagonal line represents the best-fit of a linear correlation.

4.1.9 Bar Diagram

The bar diagram is another common type of illustration, as these are used in general-purpose newspaper and magazine articles dealing with budgets, military hardware, wins of sports teams, and other topics that most people are familiar with (Figure 109).

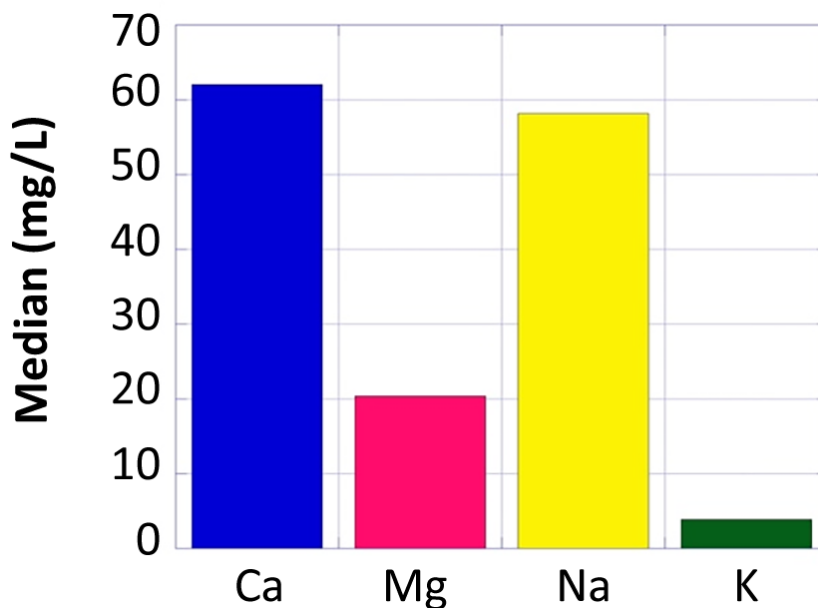


Figure 109 - Typical bar diagram showing the median concentration of cations in groundwater from the USA (from the USGS NAWQA database).

Many methods of graphic representation convert analyses in mg/L to milliequivalents per liter (meq/L) by multiplying concentration in milligrams per liter by a conversion factor (Table 2). This conversion puts data in a form that more clearly reflects the potential for chemical reaction rather than the relative concentration and provides an estimation of the electrical balance, thus, a measure of the accuracy of the analysis.

4.1.10 Stacked Diagram

A variation of the bar diagram is the stacked bar diagram (Figure 110). This approach is used to compare the solute makeup of several different analyses.

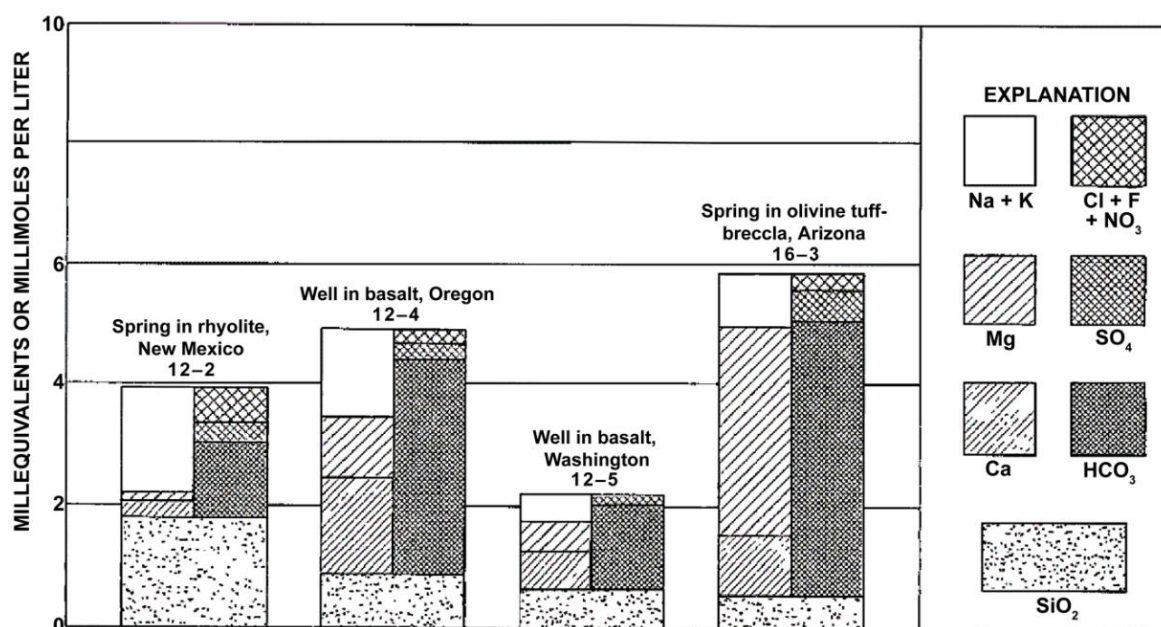


Figure 110 - Stacked bar diagram where vertical scale is concentration in milliequivalents per liter (reproduced from Hem, 1985). This type of graph is typically used to illustrate solutes between or within different aquifers

4.1.11 Trilinear Diagram

A method to identify different groundwater solute types is shown in a trilinear—also called the Piper—diagram (Figure 111). Data from water sample analyses are converted to a percentage of meq/L and plotted in the lower left and lower right triangles, then the plotted points are projected onto the upper diamond-shaped portion of the graph. The five common water types (Calcium-Chloride, Sodium-Chloride, Sodium-Bicarbonate, Magnesium-Bicarbonate, and Mixed-Type) are visually identified by their position in the figure as highlighted with colors in Figure 111.

Several free software applications are available to plot this diagram in Excel. When analyses are plotted, different types of weathering of silicates, forms of carbonates, ion exchange, and so on show up in different parts of the diagram; thus, trilinear diagrams provide a useful reference for discussing the origin of different solutes. In some settings, associating location identifiers with points on a trilinear diagram can reveal the evolution of water from one type to another along flow paths.

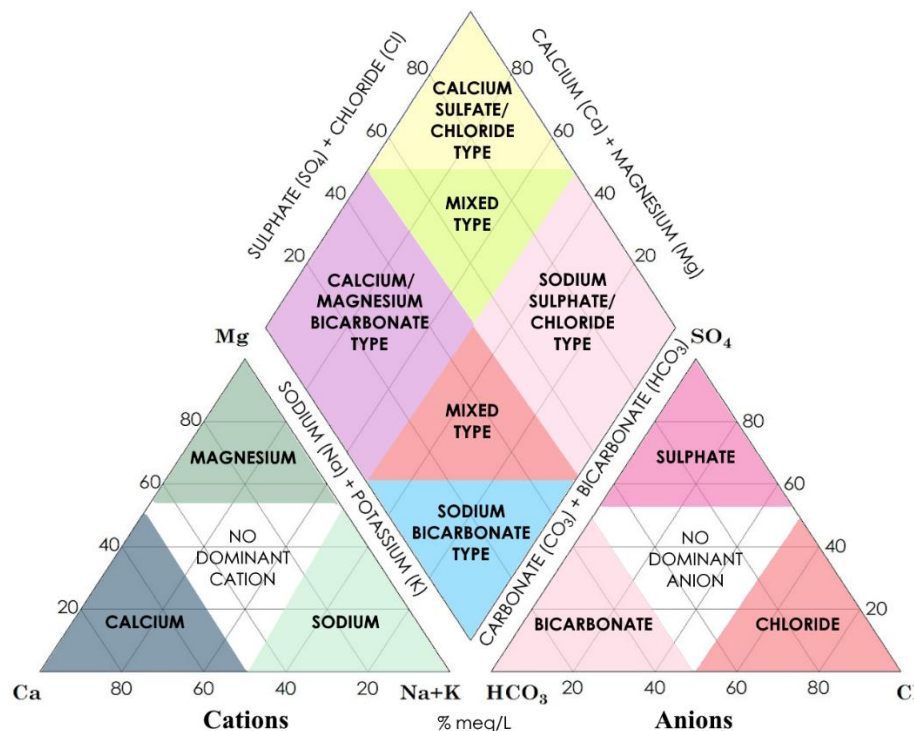


Figure 111 - Trilinear (Piper) diagram that illustrates common solute types. The upper diamond integrates the ions from the bottom left triangle (cations) and lower right triangle (anions).

4.1.12 Stick Diagram

The vector, or stick, diagram is another method of expressing solute ratios and concentrations (Figure 112). The diagram renders a visual difference within and between individual analyses with respect to both the ionic ratios and concentrations by comparing the overall shape and length of the arrows. Again, data are typically plotted in meq/L.

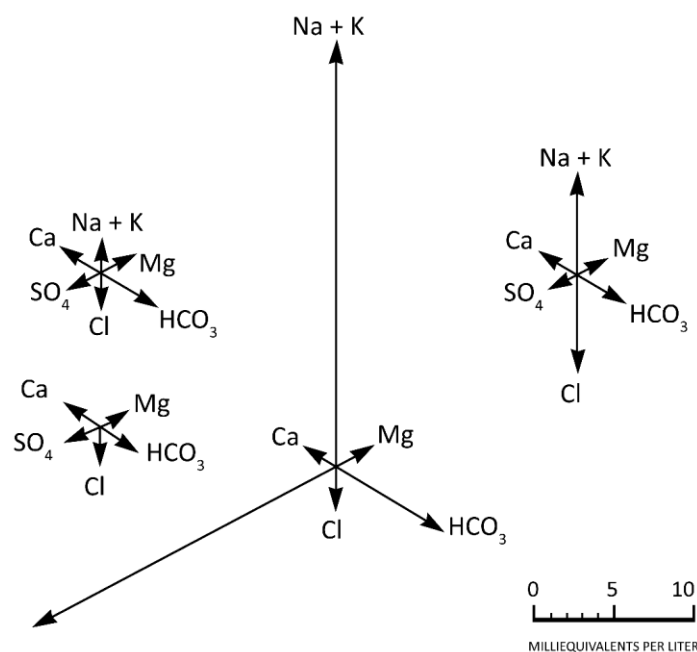


Figure 112 - Vector, or stick, diagram where the length of the line is a function of the concentration in milliequivalents per liter (reproduced from Hem, 1985).

4.1.13 Stiff Diagram

The Stiff diagram is similar the vector, or stick, diagram in that it depends on shape and size to reflect ionic ratios and concentration (Figure 113). Individual analyses in meq/L can be plotted on a map that will illustrate the different solute types, as the eye can readily recognize the subtle differences in shapes that would be difficult to recognize in a data table. Several online applications are available to plot this diagram in Microsoft Excel.

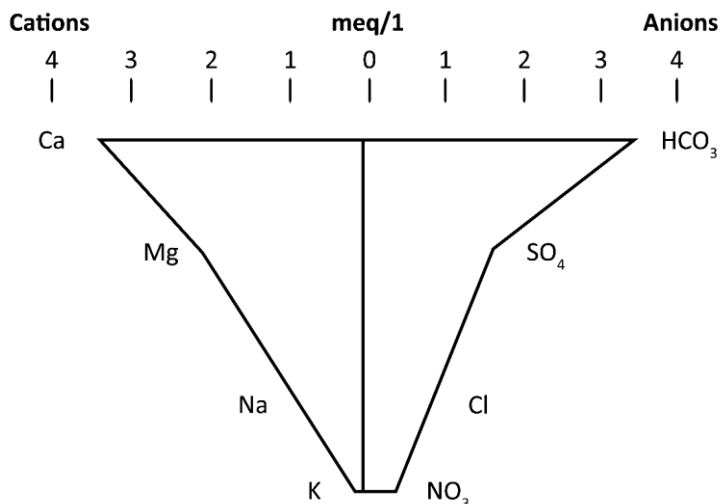


Figure 113 - Analyses represented by patterns of both anions and cations, sometimes referred to as the Stiff diagram (reproduced from Hem, 1985). Like the stick or vector diagram, the shape provides a visual means of discerning the type and concentration of solutes in a water sample in milliequivalents per liter.

4.1.14 Scholler Diagram

A Scholler diagram (Figure 114), facilitates display of multiple samples which may come from different locations on a single diagram that is commonly used to illustrate similarities and differences of solute ratios between or within aquifers. Several free software applications are available to plot Scholler diagrams in Microsoft Excel.

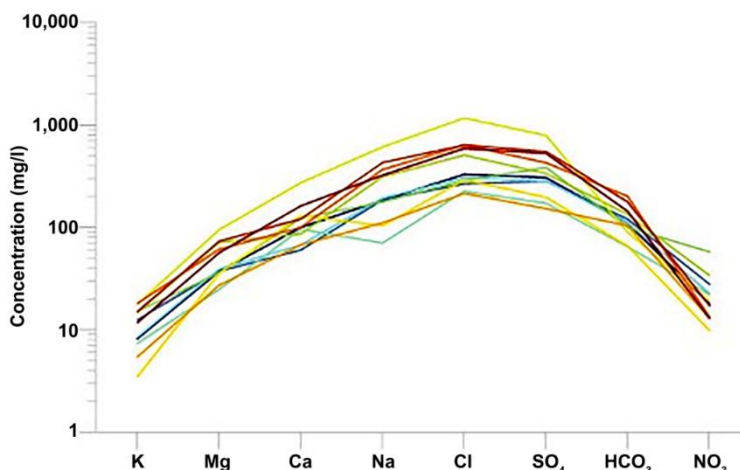


Figure 114 - A Scholler diagram may use milliequivalent/liter, mg/L, or logarithm of mg/L on the vertical axis, with each color representing samples from a different well. It is commonly used to illustrate similarities or differences in solute concentration between or within aquifers.

4.1.15 Durov Diagram

The Durov diagram is one of the more complete but complicated display methods (Figure 115). It is often used in more detailed geochemical studies showing ionic ratios and concentrations. While more complete than other diagrams, it is generally less well suited for general audiences because its axes of different scales may confuse readers. It should generally be avoided for oral presentations unless your audience is familiar with the diagram.

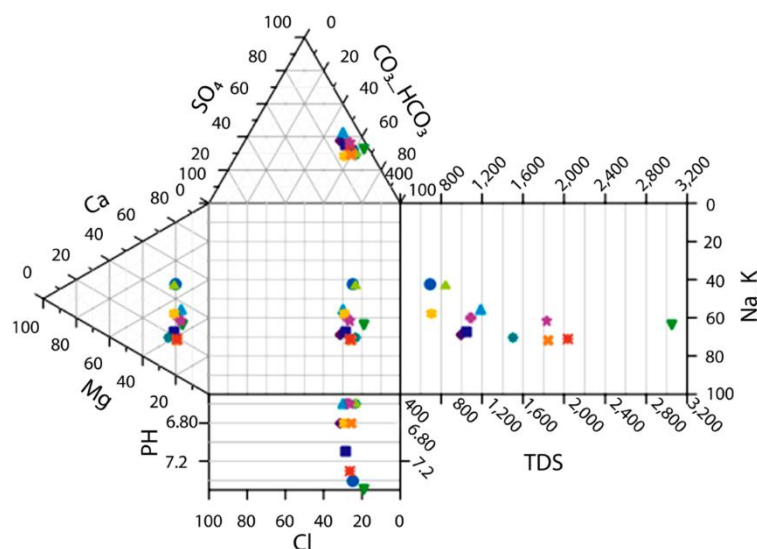


Figure 115 - Typical Durov diagram (reproduced from [Grapher Help](#), n.d.).

4.2 Section Wrap-up

As stated in the introduction, graphical analyses can effectively illustrate solute concentration from statistical data, relations between ions, changes along a gradient or flow line, or other physical features. More importantly, they can provide insight into processes controlling an aquifer system's solute concentration and ratios.

[Exercise 3](#) examines the use of different types of graphical presentations.

5 Field Examples of Different Hydrogeochemical Sources and Processes

As stated in Section 2, solutes in groundwater have one of the following origins.

1. Solute may remain from the environment of aquifer deposition, that is, relic, legacy, fossil, or connate solutes.
2. Solute may be introduced by rainfall recharge, seepage from surface water bodies such as rivers and, lakes, and transport from adjacent, underlying, or overlying formations.
3. Solute may be generated by the reaction of groundwater with the mineral framework of the aquifer or by radioactivity, that is, rock-water interaction.

Solute in aquifer systems result from a combination of these sources, as nearly all systems received some solute mass from both precipitation recharge and weathering in the vadose zone. However, one or two processes frequently dominate or control the solute mass in the aquifer, at least in the immediate area where the aquifer exists. In Section 5, some field examples are explored in which different solute sources or processes are dominant. These examples describe water types using the terms such as Calcium-Chloride, Sodium-Chloride, Sodium-Bicarbonate, Magnesium-Bicarbonate, and Mixed-Type, based on the position of their major ion chemistry when presented in a trilinear diagram which is explained in Section 4.1.11.

Chemical evaluation of regional groundwater systems in North America started with the realization of its significance in the occurrence of uranium minerals in the Colorado Plateau in the 1950s and the recognition of geochemical facies in groundwater in the 1960s (Back, 1960, 1966). Back and others (1993) provided a historical perspective. Similarly, the Regional Aquifers Systems Analysis (RASA) program of the USGS in the 1980s was designed to define regional geohydrology and establish a framework of background information on geology, hydrology, and geochemistry of 25 of the major USA aquifer systems. Sun and others (1997) provided an overview of the RASA program. These works are excellent field studies on regional geochemistry and can be read with great benefit. However, in the more recent context of the drive to understand global nutrient and carbon flux systems under the sustainability paradigm, a global understanding of hydrogeochemistry is required.

5.1 Aquifer Solute Dominated by Atmospheric Precipitation: The Southern High Plains Aquifer of Texas and New Mexico, USA

The Southern High Plains aquifer of Texas and New Mexico, USA, is an example of atmospheric input of solutes that significantly impacts total solutes in groundwater (Figure 116).



Figure 116 - Playa lakes in Southern High Plains of Texas and New Mexico aquifer after a rain illustrate the subdued topography and some of the 20,000 shallow playa lakes that provide groundwater recharge to the underlying Ogallala aquifer (High Plains Underground Water District, 1984).

The Ogallala and Blackwater Draw Formations dominate the Miocene through the Pliocene alluvial fan/aeolian water-table aquifer (Wood & Osterkamp, 1987; Osterkamp & Wood, 1987). The mineralogical skeletal framework is hydrologically mature and composed mainly of quartz and silicates with numerous zones of secondary calcrete and occasional volcanic ash in the Pleistocene aeolian deposits. The system is believed to have been an active aquifer since its creation in the Miocene time, about 23 million years ago.

Precipitation in the Southern High Plains of this semi-arid area ranges from 330 mm/y in the southwest to 560 mm/y in the northeast and averages approximately 500 mm/y (Figure 114). The potential evaporation averages approximately 1,900 mm/y (Figure 117) with an average temperature of approximately 16 °C. The groundwater recharge is approximately 12 mm/y (Wood & Sanford, 1995b). The groundwater gradient is approximately 1.9 m/km easterly, and, in the past, discharged to springs along the eastern escarpment; however, since significant groundwater development started in the late 1930s, the discharge has been primarily through pumping, and most of the springs are no longer active. The average regional hydraulic conductivity is between 20 to 25 m/d with a storage coefficient of 0.18.

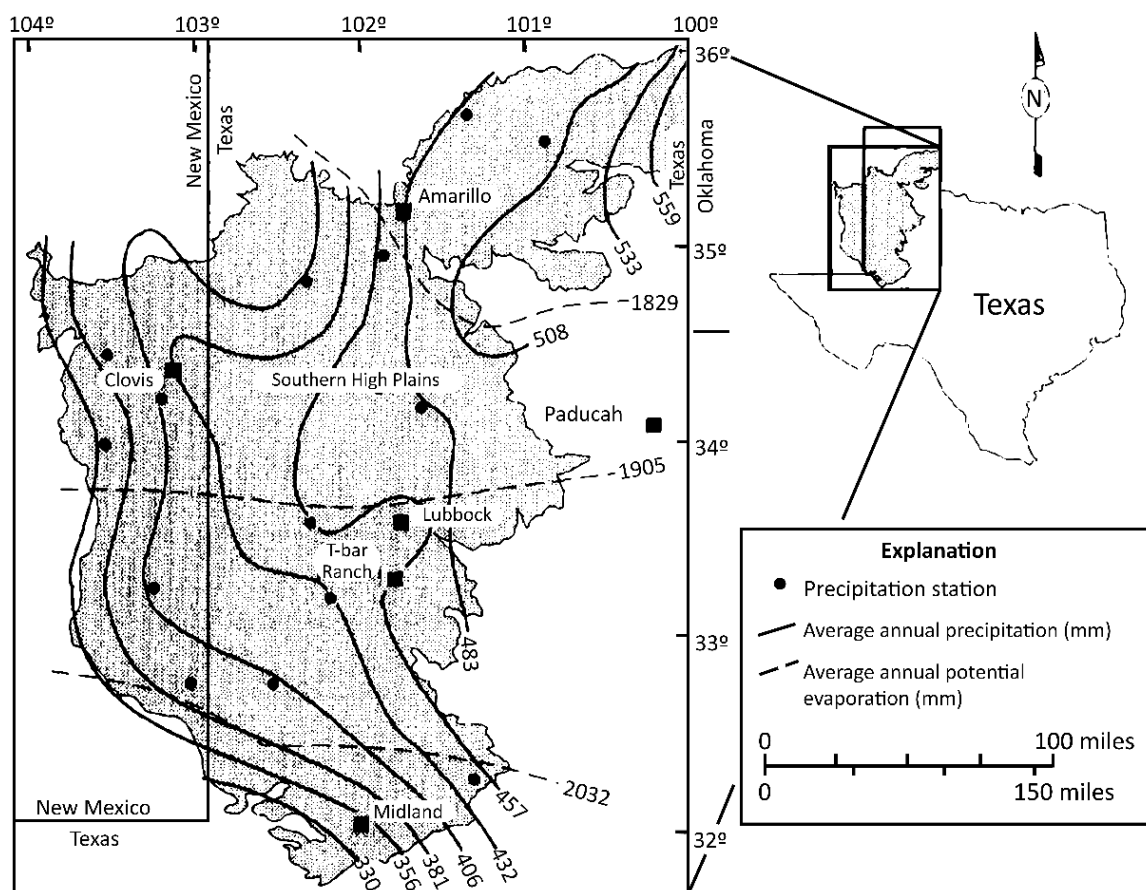


Figure 117 - Precipitation and average annual potential evaporation on the Southern High Plains Aquifer system of Texas and New Mexico, USA. (reproduced from Wood & Sanford, 1995b).

The Southern High Plains exhibit essentially no surface water outflow; over 98 percent of the area is drained internally by the approximately 20,000 small *playa* lakes (Figure 116). The system is hydrologically transient and chemically open, with intermittent recharge occurring mainly in and around playa basins that retain water only for a few days/weeks after precipitation events. The hydraulic head in the aquifer is higher than the underlying sedimentary sequence; thus, there is no advective outflow from the groundwater to the lakes. In addition, there is no flow from adjacent formations due to extensive erosion on the east, west, and north sides of the aquifer system. The elevated hydraulic head prevents brine in the underlying Paleozoic basins from entering the aquifer.

As with any aquifer system, the solutes can originate outside of the aquifer, be a relic within the aquifer, or come from the weathering of the aquifer material. The aquifer material was deposited in a freshwater alluvial fan and – given the millions of years that it has been an active aquifer – seems unlikely to have significant amounts of relic solutes. Given the nature of its mineralogy and the low solubility of silicate minerals, it seems likely that the solutes originated from outside the aquifer – primarily from precipitation. Minor elements such as fluoride, lithium, and uranium are likely derived from weathering the much younger Pleistocene (2.6 million to 12 thousand years ago) volcanic ash in the system’s upper part.

The water is a calcium magnesium bicarbonate type that averages approximately 300 to 350 mg/L total solutes (Table 11, line 4). Assuming steady-state hydraulic conditions, the calculated (wet and dry) atmospheric deposition (Table 11, line 2) was used with a concentration ratio (CR) of 43 to calculate the annual atmospheric solute input (Table 11, line 3). The concentration ratio is the average chloride in groundwater divided by the flux-weight concentration in precipitation, as it is assumed there is little runoff in this system (Wood, 2019).

Table 11 - Percent of potential atmospheric solute deposition in groundwater of the Southern High Plains aquifer.

1 Ions	Ca	Mg	Na	K	HCO₃	Cl	SO₄	NO₃
2 Average atmospheric values (mg/L)	1.74	0.22	0.64	0.76	5.64	0.58	2.60	1.88
3 Calculated atmospheric deposition to groundwater (Concentration Ratio=43) (mg/L)	75	9	28	33	243	25	112	81
4 Observed groundwater concentration (mg/L)	50	26	34	5	255	25	49	11
5 Percent of atmospheric solutes in groundwater	148	37	81	623	95	99	226	715

The percent concentration of atmospheric deposition relative to groundwater (Table 11, line 5) for the ions Ca²⁺, K⁺, SO₄²⁻, and NO₃⁻ exceeds 100 percent, suggesting that atmospheric deposition potentially provides more mass to the aquifer system than observed in the groundwater, resulting in an accumulation in the skeletal mineral framework, vegetation, aeolian erosion, or loss as a gas. Net loss by aeolian activity seems unlikely as the system is currently aggrading. The ongoing formation of calcrete removes Ca²⁺ and HCO₃⁻. Further, SO₄²⁻ and some calcium may be lost to anhydrite that is precipitated with calcite in the abundant calcrete in the system.

Under steady-state conditions, one would assume that NO₃⁻ and the K⁺ ions would enter the groundwater associated with vegetation decay. However, they may be stored in the thick unsaturated zone or have been volatilized and transported out of the system by the frequent prairie fires that historically occurred in the area. As the system is generally oxygenated, the loss of nitrogen by reduction to nitrogen gas seems unlikely.

Additional analysis is required to completely understand solute chemistry (Wood & Sanford, 1995b). The point, however, is to demonstrate that atmospheric deposition likely dominates this system's potential source of solutes and provides insight into geochemical processes. The impact of solutes in precipitation in regional groundwater solutes is also illustrated in the Murray Basin in Australia—another important extensive regional hydrologic system (Herczeg et al., 2001).

5.2 Aquifer Solute Dominated by Rock Weathering: Upper Grand River Basin, Central Michigan, USA

The glacial/consolidated rock Saginaw Aquifer in central Michigan, USA that underlies the Upper Grand River drainage basin (Figure 118) is typical of many basins in the glaciated areas of the northern hemisphere. The aquifer consists of a combination of Pleistocene-age glacial deposits and Holocene alluvium that unconformably overlies and is hydraulically connected to the Pennsylvania-age Saginaw Formation of sandstone, shale, limestone, and minor continental coal deposits (Vanlier et al., 1973).

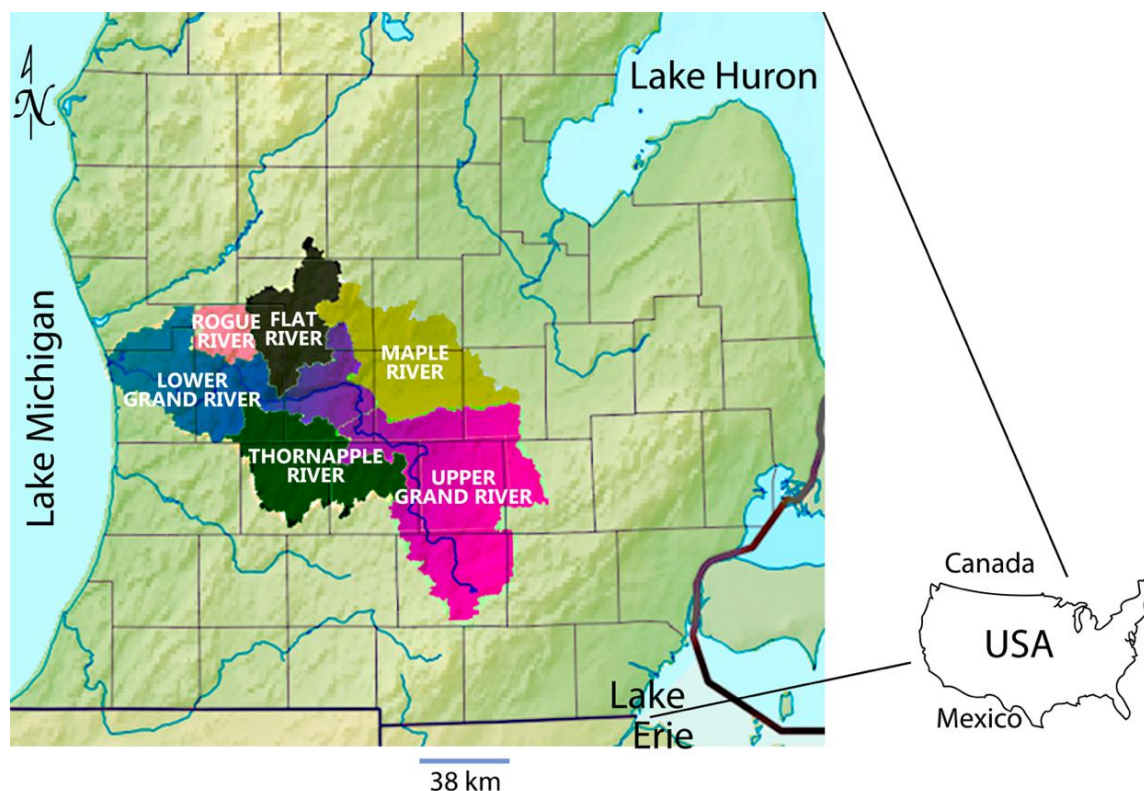


Figure 118 - Several smaller drainage basins define the glacially deposited Grand River Basin, Michigan, USA. The Upper Grand River unconsolidated glacial aquifer is largely underlain by the consolidated Saginaw Aquifer that is comprised of sandstone, shale, limestone, and minor continental coal deposits.

The glacial deposits of tills, moraines, outwash, eskers, and kames that overlie the incised Pennsylvania-age Saginaw Formation are dominated by fragments from igneous, metamorphic, and sedimentary rocks containing quartz, feldspar, hornblende, pyroxene, mica, calcite, dolomite, gypsum. The aquifer system is of variable thickness, averaging approximately 125 m, with modest topographic relief of a few tens of meters and a largely integrated drainage in the Grand River Basin. The Saginaw Formation has a regional hydraulic conductivity of 6 to 8 m/d (Holtschlag et al., 1996). This aquifer system overlies the low permeability Bayport Limestone of the Mississippian age that acts as a hydrologic cap to the thick sequence of nearly 5,000 m of Paleozoic limestones, sandstones, shales, and salt of the underlying Michigan Basin.

As there are only a few small (100 m by 100 m) outcrops of the Saginaw Formation in this drainage area, nearly all groundwater recharged to the system is through the overlying glacial and alluvium deposits. The glacial sediments act as a water table aquifer, whereas the Saginaw Formation acts as a confined/semi-confined aquifer in most places. There is a large deep (> 35 m) cone of depression underlying much of the urban Lansing metropolitan area as a result of extensive pumping. The system is chemically open and in a transient flow condition as the groundwater head is continually lowered owing to withdrawal exceeding recharge. Precipitation in the Upper Grand River basin is approximately 760 mm/y with an average annual temperature of 10 °C.

As with any system, the solutes can be external to the aquifer or internal as relic and weathering. The glacial aquifer material was deposited in a freshwater environment and does not have oceanic relic solutes. As the Pennsylvanian-age formation was likely exposed to rainfall much of the last 200 million years since deposition, it seems unlikely to have significant marine relic solutes. However, some exchange sites in low-permeability shale could contain oceanic solutes. This aquifer contains calcium–magnesium bicarbonate-type water with a total solute of approximately 350 mg/L (Table 12). With an average rainfall flux of 0.760 m³/m²/y and atmospheric depositional data (NADP↗, 2020), the individual solute concentration (C_{depo}) was calculated for each ion (Table 12, line 2). A concentration ratio of 7.5 was used to estimate atmospheric deposition input to the groundwater (Table 12, line 3).

Table 12 - Percent of atmospheric solute deposition in groundwater from the Upper Grand River Basin Aquifer.

1 Ions	Ca	Mg	Na	K	Cl	SO₄	NO₃
2 Average atmospheric deposition (mg/L)	0.46	0.86	0.20	0.07	0.20	0.26	2.61
3 Calculated atmospheric deposition to groundwater (Concentration Ratio=7.5) (mg/L)	3.5	6.4	1.5	0.5	1.5	2.0	20
4 Observed groundwater concentration (mg/L)	82	28	14	2.2	6.1	38	1.0
5 Percent of atmospheric solutes in groundwater	4	23	11	23	24	5	1,954

The percent of atmospheric deposition relative to observed groundwater (line 5 in Table 12) suggests that the atmospheric deposition would only satisfy between 20 to 30 percent of the observed Mg²⁺, K⁺, and Cl⁻ and that most of the mass of these solutes must come from other sources. However, there is a significant atmospheric depositional load of nitrate (Table 12, line 5) as a combination of NO₃⁻, HN₃, and NH₄ that is not reflected in groundwater, suggesting a significant loss of nitrogen prior to groundwater recharge.

The chloride concentration from atmospheric precipitation is approximately 1.5 mg/L (i.e., the product of 0.2 mg/L and CR of 7.5). Thus, the groundwater's remaining 4.6 mg/L chloride (6.2 mg/L – 1.5 mg/L) likely originates from ascending brines. These groundwater data are from relatively deep wells that were sampled in the 1950s and 1960s before the widespread use of sodium chloride for winter highway deicing. These brines would include a small flux of Ca²⁺, Mg²⁺, Na⁺ K⁺, and SO₄²⁻ typical of the Michigan Basin

brines (Wilson & Long, 1993), which are associated with the large cone of depression in the Saginaw and consequent upward head gradient of lower formations.

The amount of Ca^{2+} , Mg^{2+} , Na^+ , K^+ , and SO_4^{2-} introduced from brines must be small, based on the chloride/cation ratio; thus, it is concluded that a significant portion of the solutes in this aquifer originates from weathering of the mineral framework. Although bicarbonate analyses from atmospheric precipitation are not available, most would likely be generated in the unsaturated zone by the reaction of CO_2 with carbonate rock fragments that would also yield Ca^{2+} , Mg^{2+} , Na^+ , and K^+ from reaction of carbonic acid on the freshly broken feldspar, mica, amphiboles, and pyroxenes minerals. Sulfate is likely derived from the weathering of anhydrite incorporated in the carbonate rock fragments.

Detailed analysis is required to fully understand the local solute chemistry (Wood, 1976). The point, however, is that water-rock interaction is consistent with the hypothesis that solute sources are primarily internal in these geologically young glacial deposits.

5.3 Aquifer Solutes Dominated by Ion Exchange: Atlantic Coastal Plain, US

Calcium ion exchange for sodium on clay exchange sites is believed to control the origin of sodium bicarbonate-type water in aquifers of the Atlantic Coastal Plain (Back, 1966; Figure 119). This exchange occurs by converting a calcium-bicarbonate type recharge water to a sodium-bicarbonate type water by ion exchange and mixing with seawater to form a sodium-bicarbonate-chloride type water (Figure 120).



Figure 119 - Map of a portion of the United States Atlantic Coastal Plain in which groundwater is impacted by ion exchange (reproduced from Back, 1966) (1 mile = 1.62 km).

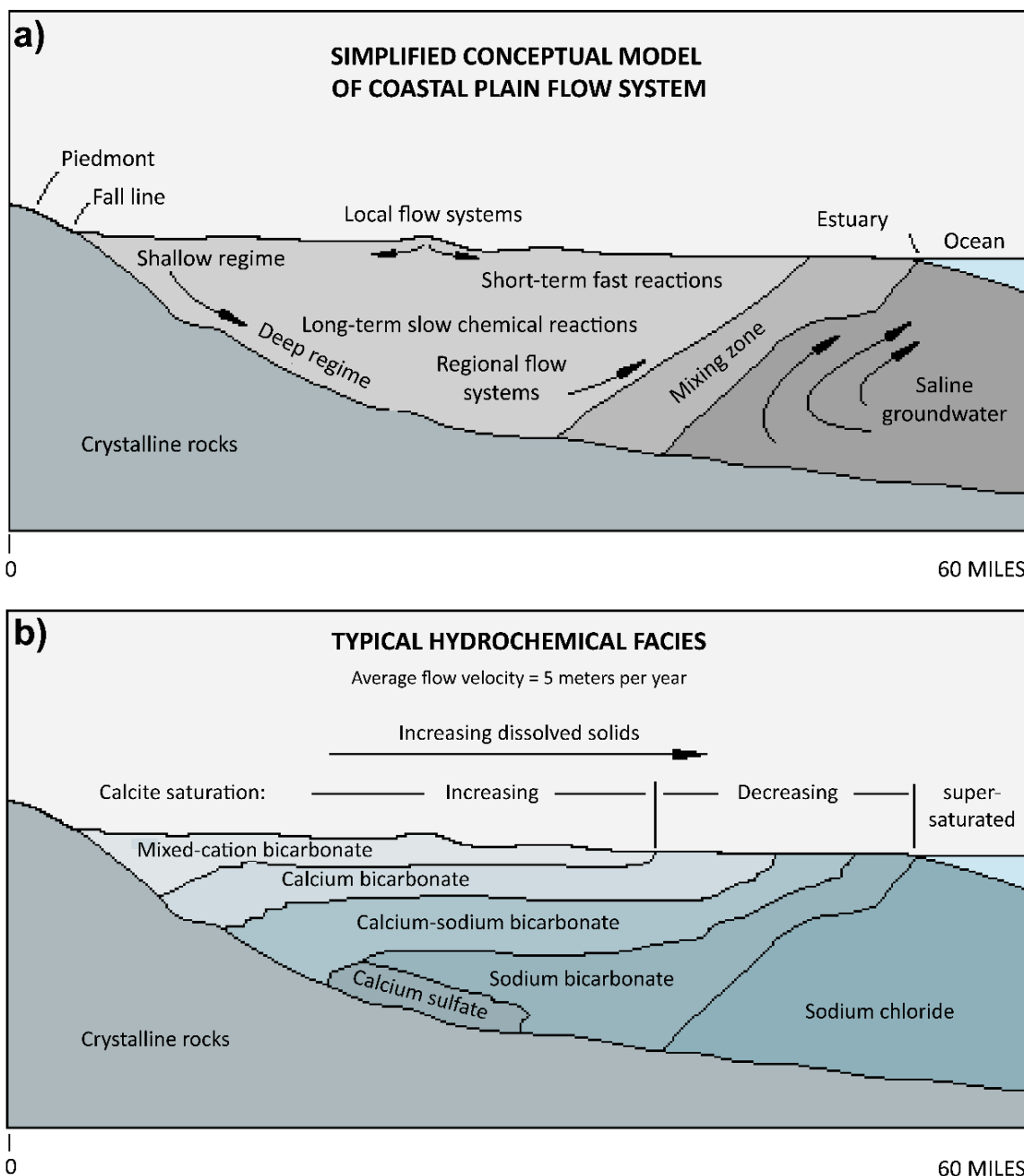


Figure 120 - Hydrogeology of the USA Coastal Plain. a) Simplified conceptual model of the regional groundwater flow system. b) Typical water types encountered in the aquifer illustrating the solute evolution of groundwater along the flow paths shown in (a). 60 miles is approximately 96.5 kilometers (reproduced from Back et al., 1993).

The US Coastal Plain is formed by a wedge of sediments ranging in age from Cretaceous to recent and consists primarily of sand, silt, and clay with minor amounts of gravel overlying the pre-Cretaceous age bedrock. The sediments are divided into deposits predominantly of continental origin and deposits predominantly of marine origin. A fourfold subdivision of these two significant units is made based on the percentage of clay within each sequence. The units are further differentiated as to the presence of greensand (glauconitic sand) or calcareous material. The percentage of clay and the presence or

absence of greensand and calcareous sediments are believed to be the dominant controls on the ion exchange and, thus, on the chemistry of the water (Back, 1966).

In the shallow recharge environment, water encounters elevated carbon dioxide, resulting in localized, short-term, rapid dissolution of minerals. These processes and reactions commonly produce calcium bicarbonate hydrogeochemical facies. In the Atlantic Coastal Plain, this calcium bicarbonate groundwater moves down the hydrologic gradient to the discharge area in the ocean. The calcium in the solution exchanges with the sodium on the marine clays and evolves from calcium bicarbonate with low concentrations of dissolved solids to sodium bicarbonate with greater concentrations of dissolved solids. The increase in dissolved solids is a result of the exchange of calcium for sodium, causing the water to be thermodynamically undersaturated by the mineral calcite, thus causing additional solution of calcite and adding bicarbonate ions and calcium ions, which increases the dissolved solids.

Sodium bicarbonate minerals are very soluble; thus, the concentration of both sodium and bicarbonate will increase and are not removed by mineral precipitation. Ultimately, this water—now sodium bicarbonate water—mixes with seawater to form a sodium, chloride-type water with a large concentration of dissolved solids (Figure 120).

5.4 Aquifer Solutes Dominated by Elevated pH: *Blue Pools* of the Sultanate of Oman

Many spring-fed small pools in a 500 km belt of ophiolite rocks in the northern portion of the Sultanate of Oman exhibit elevated pH approaching 11 (Fig 121). Solutes are dominated by sodium, carbonate, and chloride with relatively low total solutes of a few hundred mg/L (Table 13).

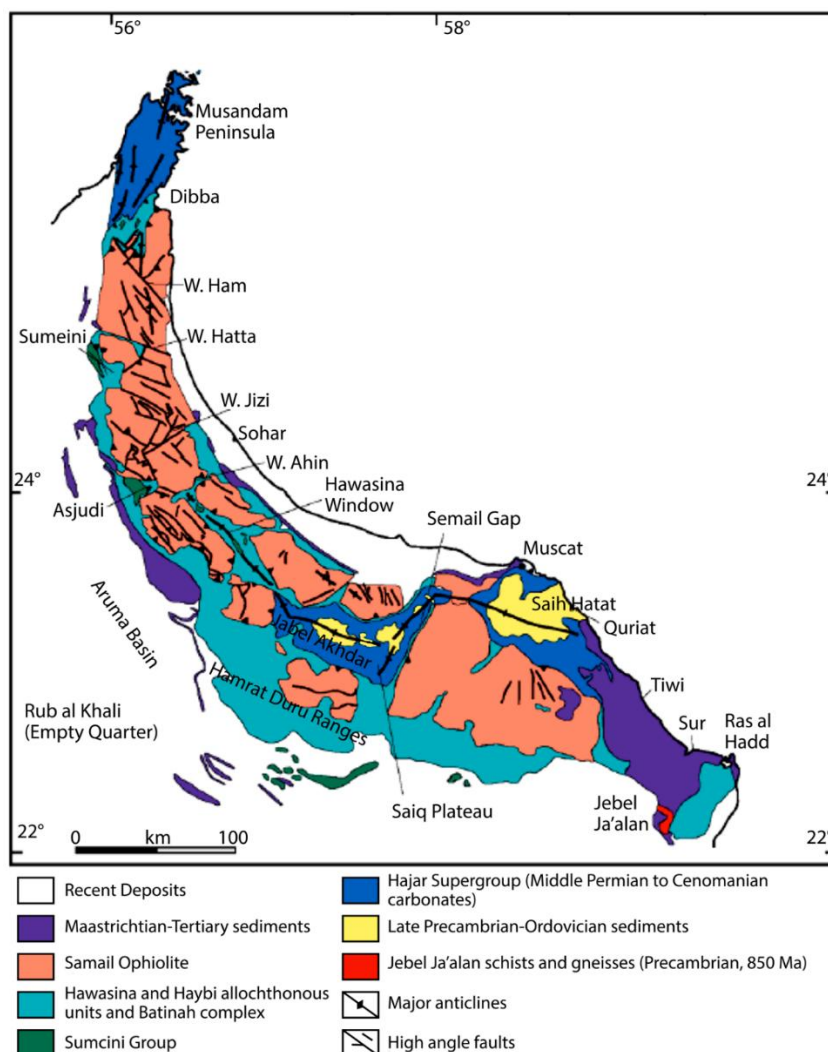


Figure 121 - Geologic map of Northern Oman showing the Semail Ophiolite outcrop (brownish-orange) area where Blue Pools form (reproduced from El-Hussain et al., 2018).

The elevated pH, abundant calcite, and bubbling methane and hydrogen are of interest in these features (Table 13). These are called *Blue Pools* because of their color. Water absorbs the red part of the light spectrum, leaving colors in the blue part of the light spectrum to be seen by the human eye. In this setting the effect is enhanced by the shallow clear water overlying the white calcium carbonate-covered bottom (Fig 122). Isotopes of water collected by the author indicate the water is local rainfall.

Table 13 - Chemical analysis of Wadi Madbah Blue Pool in the Sultanate of Oman. Analyses in mg/L for major and minor elements and µg/L for trace elements.

Name	Date	Zone	UTM E	UTM N	Ca	Mg	Na	K	Sr	HCO ₃ ⁻	Cl	SO ₄	F	Br	N	SiO ₂	pH	Sp. Cond.	TDS	Temp °C		
Wadi Madbah	25/4/91	40	410	2	4.0	24	76	4.5	0.04	145	130	40	0.1	0.1	0.97	6.8	10.15	600	373	27.50		
			362	664																		
				290																		
Chemical analyses of trace elements, in µg/L																						
					Ba	Be	B	Cd	Cr	Co	Cu	Fe	Pb	Li	Mn	Mo	Ni	Ag	V	Zn		
					2	0.5	60	1	5	3	10	8	20	14	1	10	10	1	6	88		

Sp. Cond.: Special Conditions; TDS: Total Dissolved Solids; Temp.: Temperature



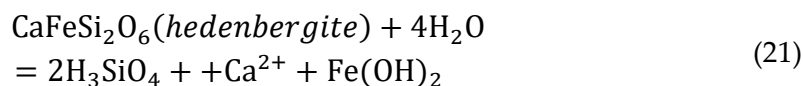
Figure 122 - Photographs of elevated pH (> 10) spring-fed Blue Pools of the Sultanate of Oman. The pools are blue because water absorbs the red part of the light spectrum, leaving colors in the blue part of the light spectrum that is enhanced by the clear water and white calcium-carbonate-covered bottom (photos by W. W. Wood).

This area of Oman (Figure 121) is one of the few areas on Earth where plate tectonics have transported material from the lower mantle that is tens of kilometers deep up to the surface through a geological process known as *obduction*. That is, the colliding oceanic plate is forced onto the continent's surface rather than being subducted below the continent which is the general case. The mineral composition of the uplifted material is one of forsterite (Mg_2SiO_4) and hedenbergite ($\text{CaFeSi}_2\text{O}_6$) that are thermodynamically unstable in this new lower temperature and pressure environment.

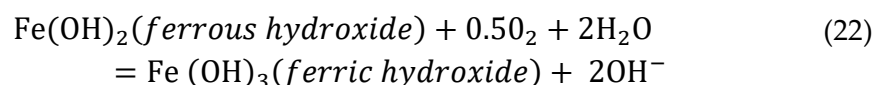
There are several steps in the development of the solute chemistry of the Blue Pools. The first step is hydrolysis weathering of forsterite that forms one molecule of dissolved silica (H_3SiO_4), two molecules of magnesium (Mg) ions, and four molecules of hydroxyl (OH^-) ions, as shown in Equation (20). The OH^- ions elevate the pH and the silica species is H_3SiO_4 (Fig. 46)



The second step is the aqueous weathering of one mole of hedenbergite ($\text{CaFeSi}_2\text{O}_6$) and four moles water, which produces two silica molecules (H_3SiO_4), one-mole calcium (Ca^{2+}), and one mole of ferrous hydroxide ($\text{Fe}(\text{OH})_2$), as shown in Equation (21).



In the presence of oxygen, the ferrous hydroxide precipitates to ferric hydroxide ($\text{Fe}(\text{OH})_3$) and two hydroxyl (OH^-) ions further increasing the pH of the water as shown in Equation (22).



The third component is the precipitation of calcite (CaCO_3). Whereas the Ca^{2+} ion originates from the weathering of hedenbergite, the carbonate (CO_3^{2-}) comes directly from the atmospheric interaction with the elevated pH of the water. The carbonate ion (CO_3^{2-}) is the dominant carbonate species at pH 11 (Figure 46) rather than the bicarbonate ion (HCO_3^-). As the water, with its elevated pH, discharges into the spring and reaches the water surface in contact with the atmosphere, the calcium ion reacts with carbonate ion (CO_3^{2-}), as shown in Equation (23) and precipitates a thin film of calcite (CaCO_3) on the surface (Figure 123).

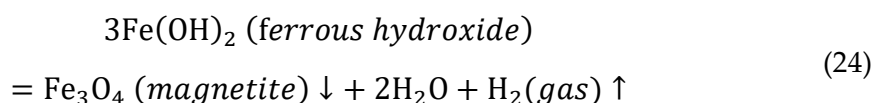




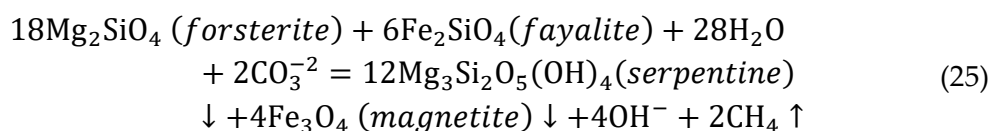
Figure 123 - Thin “rafts” of calcite floating on the surface of a Blue Pool (photo by W. W. Wood).

The calcite forms at the air-water surface and floats as thin rafts (Figure 123) until a gust of wind disturbs the surface, and the calcite falls to the bottom of the pool, resulting in a white blanket of calcite on the bottom.

Hydrogen (H_2) and methane (CH_4) gases are observed to be bubbling out of these springs. Hydrogen is released from a reducing environment by precipitation of magnetite from ferrous hydroxide generated by the dissolution of fayalite (iron-rich olivine) or iron-rich pyroxene present in the ophiolites, as shown in Equation (24).



Methane (CH_4) gas is also observed to be bubbling out of the springs, generated by reduction of carbon dioxide (CO_2) by the reaction of serpentine and magnetite under the condition shown in Equation (25).

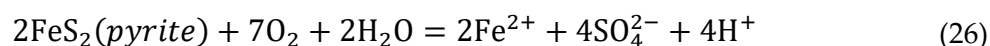


5.5 Aquifer Solutes Dominated by Low pH

Low pH or acid groundwater, like high pH water, is somewhat unusual in natural freshwater aquifer systems; the global mean value of over 11,000 groundwater samples is 7.2 pH with a median of 6.57 (Wood et al., 2022). In general, there are two general causes of

geogenic acidic groundwater. The first is generated by the oxidation of pyrite in geologically young terrains, usually with elevated dissolved solutes, and the second is generated by carbonic acid in older, highly weathered terrains with low concentrations of dissolved solutes.

Geologically young, volcanically active areas of the world typically exhibit acidic water and include hot springs, mud pots, fumaroles, and geysers. The solutes associated with these features are typically a calcium chloride or sodium chloride type with a pH of 3 to 4 in which dissolved solids are usually less than 1,000 mg/L. Typically, geothermal water's low pH results from weathering of the mineral pyrite (FeS_2) by oxygen. This reaction of seven moles of O_2 with two moles of pyrite (FeS_2) produces two moles of ferrous iron (Fe^{2+}), four moles of sulfate (SO_4^{2-}), and four moles of hydrogen ions (H^+). It is the generation of the H^+ ions that causes the low pH as shown by Equation (26).



On exposure to the atmosphere oxygen (O_2) in springs and rivers, the ferrous (Fe^{2+}) ions are precipitated as ferric hydroxide ($\text{Fe}(\text{OH})_3$; Figure 124), further decreasing the pH by the addition of more hydrogen (H^+) ions as illustrated in the two-step process shown by Equations (27) and (28).

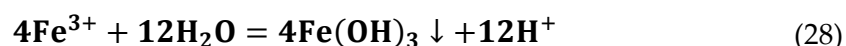
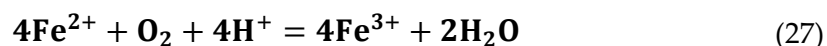


Figure 124 - Photograph of an acidic thermal spring in Yellowstone National Park, USA, illustrating precipitation of yellow ferric hydroxide ($\text{Fe}(\text{OH})_3$) on exposure to atmospheric oxygen (photo by Jim Peaco, National Park Service).

The classic problem of acid mine drainage where pyrite is oxidized is an example of this process (Figure 125).



Figure 125 - Acid mine drainage showing the precipitation of yellow ferric hydroxide, known colloquially as “yellow boy” (photo by USGS).

The solutes associated with these features are typically either calcium or sodium chloride types with a pH of 3 or 4, in which dissolved solids are usually less than 1,000 mg/L (Rowe et al., 1973; Stauffer et al., 1980). This decrease in pH frequently results in elevated concentrations of many rare-earth elements (REEs). However, the solute chemistry of the individual systems is strongly dependent upon the lithology. Owing to the dominant carbon species H_2CO_3 , the pH is less than 5 (Figure 46), HCO_3^- is not a major component.

In a classic geochemical study of the geothermal system in Carnmenellis granite in the Cornwall mining district of the southwestern UK, Edmonds and others (1985) and Smedley (1991) illustrated the solute source in an older Devonian—but still warm ($\approx 50\text{ }^\circ\text{C}$)—system that generates acid groundwater and mobilizes trace elements and REEs (Figure 126).



Figure 126 - Map of the UK showing the location of Carnmenellis granite in the Cornwall mining district in southwestern UK.

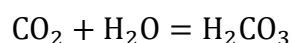
The rocks of this area consist of a muscovite–biotite granite containing alkali feldspar, plagioclase, and quartz with accessory minerals of tourmaline, apatite, epidote, chlorite, zircon, and monazite (Smedley, 1991). Groundwaters from the granite are typical of Na (and K) or Na-Ca type. Chloride dominates anionic concentrations in waters from this granite. The pH of water circulating through the Carnmenellis granite ranges from 4.3 to 7.2 with a median of 5.7 as shown in Table 14 (Smedley, 1991). Their major element chemistry is mainly controlled by water–rock interaction processes with some atmospheric input. A significant mass of Na and Cl ions are likely the result of precipitation derived from the nearby ocean and some from fluid inclusions.

Table 14 - Chemical analyses of groundwater from the Cammenellis granite in mg/L (reproduced from Smedley, 1991).

Temperature °C	14.0	13.0	12.0	12.0	16.4
pH	6.13	5.08	6.07	5.85	5.61
SEC (µS/cm)	152	207	66	360	260
Na	20.2	14.4	15.4	20.7	20.4
K	5.7	2.3	2.3	10.3	6.5
Ca	21.3	5.9	8.3	19.8	15.4
Mg	5.1	4.1	2.0	4.3	3.2
HCO₃	5.1	4.5	8.8	21.4	9.1
Cl	35	25	24	38	34
SO₄	18.7	13.4	11.5	21.9	22.2
NO₃-N	13.8	4.8	2.6	7.2	6.8
Si	2.9	3.9	2.7	1.9	3.1
Al	0.45	< 0.10	0.34	0.29	0.28
P	< 0.1	< 0.1	0.3	< 0.1	< 0.1
Sr	0.148	0.040	0.050	0.127	0.083
Ba	0.020	0.005	0.011	0.012	0.017
Li	0.011	< .004	0.010	< 0.004	< 0.004
B	0.04	< 0.02	0.03	0.012	0.02
Fe_{total}	0.15	< 0.01	0.02	< 0.01	0.02
Mn	0.059	0.026	0.013	0.004	0.014
Cu	0.01	< 0.01	0.01	< 0.01	0.02
Zn	0.03	0.03	0.05	0.01	0.02

Acidifying the groundwater typically mobilizes metals such as copper (Cu), mercury (Hg), arsenic (As), uranium (U), and many REEs such as neodymium (Nd), lanthanum (La), cerium (Ce), praseodymium (Pr), gadolinium (Gd), terbium (Tb), europium (Eu), and others. Waste rock from mining ore can become an environmental problem as the pyrite is oxidized.

Perhaps the most common cause of acidic groundwater in older and well-weathered terrains is carbonic acid (H₂CO₃) resulting from the reactions in the vadose zone of CO₂ and H₂O that produces one free hydrogen ion Equation (29).



If the aquifer is already highly weathered, the water will remain acidic with low dissolved solutes, typically with local atmospheric precipitation as the significant source of

solutes. The Precambrian terrain of many continents is highly weathered; low pH groundwaters are expected from the carbonic acid reactions. The water in these systems is usually local meteoric and frequently has elevated tritium activity, indicating atmospheric input since 1954—not magmatic or fossil water.

5.6 Aquifer Solutes Impacted by Ultrafiltration: Saginaw Formation, Michigan, USA

Most documented field examples of ultrafiltration are from deep geologic basins (Berry, 1959, 1960, 1969; Bredehoeft et al., 1963, 1966; Hanshaw & Coplen, 1973;). Only a few cases propose ultrafiltration in freshwater aquifer systems (Long & Larson, 1983; Wood, 1976). Neuzil and Person (2017) thoroughly summarize what is currently known about the process.

Wood (1976) identified ultrafiltration in a potable water system in the upper Grand River Basin of the central part of the southern peninsula of Michigan, USA (Figure 127), which is shown schematically in Figure 128.

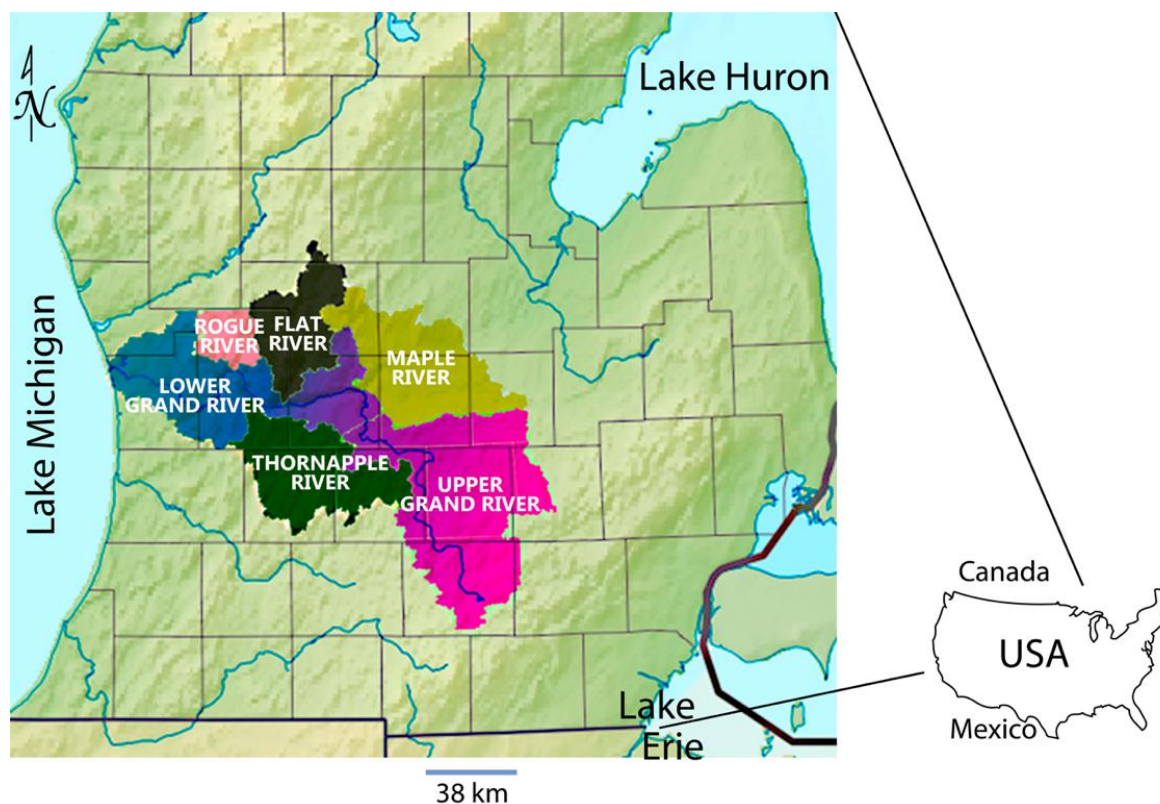


Figure 127 - Several drainage basins compose the Grand River Basin, Michigan, USA, where ultrafiltration in groundwater has been identified as a significant mechanism in controlling solutes.

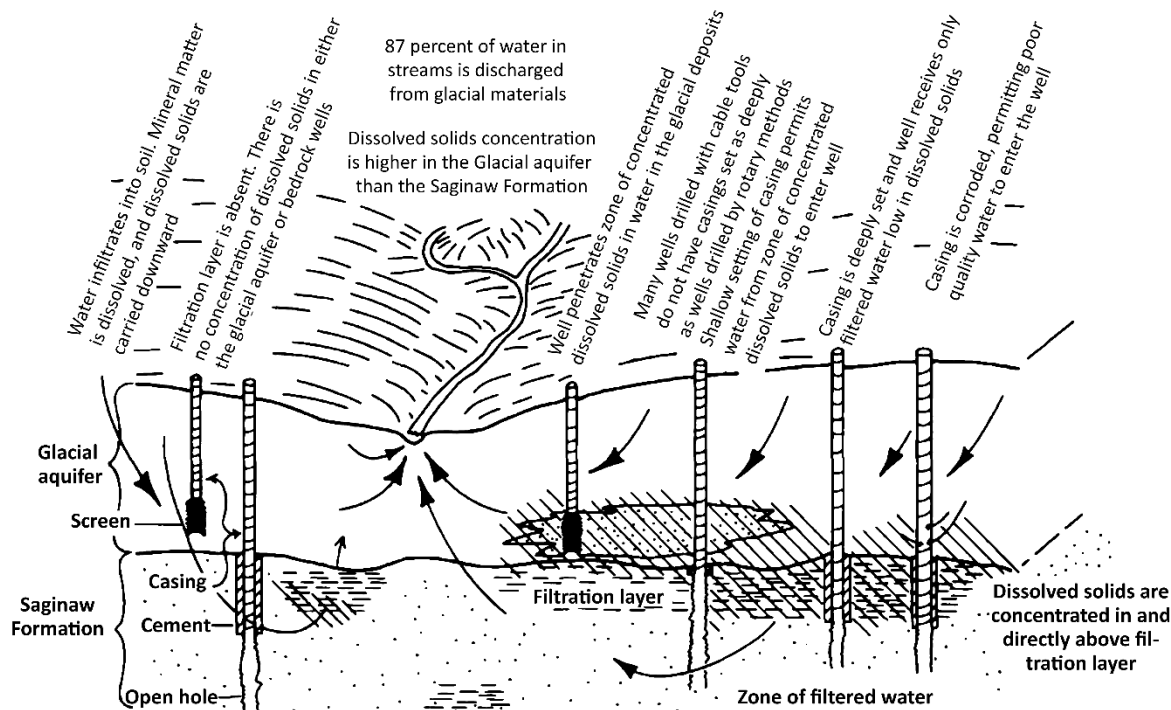


Figure 128 - Schematic illustration of ultrafiltration processes ongoing in the Glacial aquifer and Saginaw Formation in central Michigan, USA (reproduced from Wood, 1976).

The aquifer is described in Section 5.2 as a system receiving solutes from rock–water weathering, the atmosphere, and upwelling brines. While this is true, the solute distribution is controlled to some degree by ultrafiltration. Pleistocene-age glacial deposits unconformably overlie and are hydraulically connected with the Pennsylvania-age Saginaw Formation.

The Saginaw is a continental/marine sandstone, shale, and limestone containing minor coal deposits (Vanlier et al., 1973). It is hypothesized that shale beds in the Saginaw Formation act as membrane filters, restricting solutes from passing through the membrane and concentrating on the up-gradient side of the membrane. In contrast, the uncharged water molecule moves through the shale, where it dilutes solutes in the down-gradient sandstone member of the aquifer. The hydraulic head provides the energy necessary to filter the water. The following four observations of this system are relevant.

1. There is considerable variation in the concentration of several geochemical parameters over a very short horizontal distance. For example, sulfate changed two orders of magnitude from 2 to 200 mg/L in wells completed at the same depth but 100 m apart laterally.
2. There is no correlation between solute concentration and the depth of wells.
3. Drillers reported wells in the overlying glacial material yielded water of greater dissolved solids than water in the Saginaw Formation.
4. The baseflow of streams contains a higher concentration of dissolved solids than water from wells in the Saginaw Formation.

These observations, illustrated in Figure 128, can be explained by utilizing the concept of ultrafiltration. Nearly all the water and most of the solutes in the Saginaw Formation are believed to originate in the overlying glacial material.

With respect to the first observation (i.e., 1 in the list above), it was proposed that the well was sampled on the upper side (high TDS) and the other on the lower side (low TDS) of a shale membrane. In regard to the second observation, it was not the depth of the well that was critical but its position relative to the filtering membrane. For the third observation, it was proposed that glacial material was on the upper side of most membranes, owing to its stratigraphic position, and thus recharge was through the glacial material into the Saginaw with some of the solutes remaining in the glacial material. Finally, in response to the fourth observation, it was proposed that the shallow glacial flow system with a higher-hydraulic conductivity has a much greater water flux than the lower-hydraulic conductivity and deeper Saginaw Formation, thus contributing more water and solutes to the baseflow.

Owing to the similarity of this system to many others in the glaciated northern hemisphere, it was hypothesized that these phenomena might be widespread. However, the impact in dilute systems is subtle and difficult to define without extensive field data.

5.7 Solutes Dominated by Loss of Gas to the Atmosphere: Nitrogen and Bromine from the Coastal Sabkha of Abu Dhabi, UAE

In addition to the phase change from liquid to solid with mineral precipitation, several elements change phase: from liquid to gas, including the bromide ion to (BrO), dissolved organic carbon to methane (CH₄), nitrate (NO₃⁻) to (N₂) sulfate (SO₄²⁻) to hydrogen sulfide (H₂S), radium-226 to radon-222, and potassium (K⁴⁰) to argon (Ar⁴⁰).

Mass balance analysis of the Abu Dhabi, United Arab Emirates (UAE) sabkha solutes suggests the dominant nitrogen source is atmospheric precipitation. The nitrogen mass ratio—the mass of solute observed in sabkha relative to that of input brines—is an order of magnitude larger (68) relative to other ions with a mass ratio of approximately 6.8 (Figure 129). The most likely source is from local atmospheric precipitation on the sabkha.

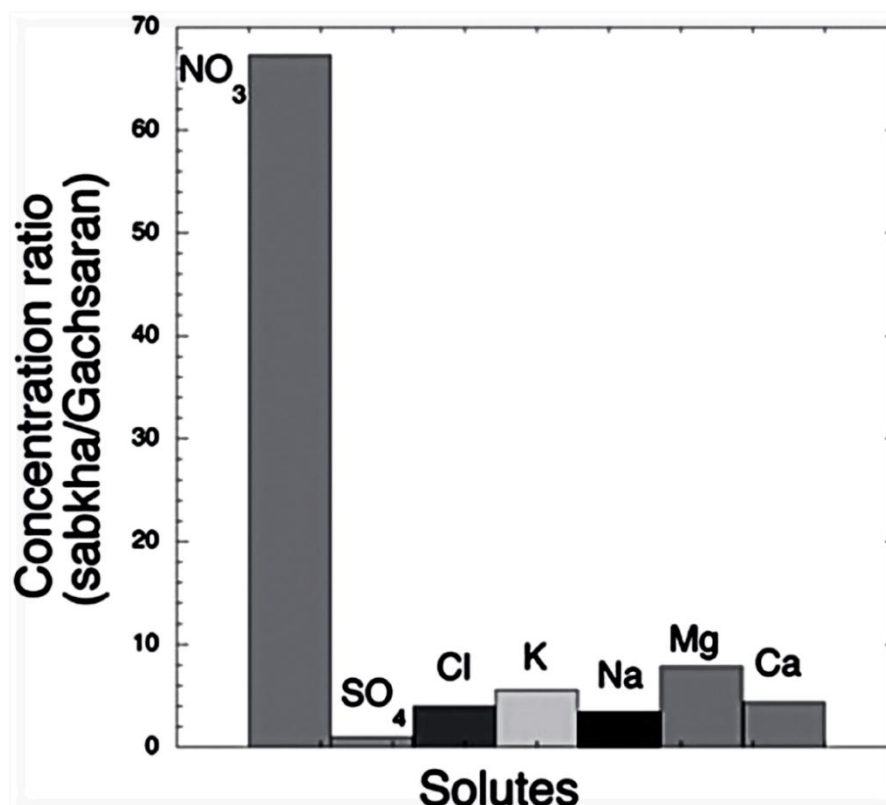


Figure 129 - Concentration ratio is the concentration observed in the sabkha divided by the concentration water in the underlying Gachsaran brine that flows into the sabkha. The ratio suggests that nitrogen is from a different source than the other solutes that are derived from ascending brines of the underlying Gachsaran aquifer (reproduced from Wood et al., 2002).

The nitrogen isotopes are, however, significantly heavier than the atmosphere—an apparent paradox. This paradox is resolved when it is recognized that density-driven convection within the sabkha aquifer transports oxidized nitrate (NO_3^-) from the local precipitation into a reducing environment at the base of the sabkha aquifer, where some of the nitrate is reduced to an isotopically light N_2 gas. This N_2 gas then escapes to the atmosphere, leaving the remaining nitrogen isotopically heavier, thus changing the isotopic ratio of the remaining nitrogen (Wood & Böhlke, 2017). This reduction process is repeated each time density-driven free convection occurs and gradually converts the nitrogen to an isotopically heavier form while losing a significant mass of isotopically light N_2 gas into the atmosphere (Figure 130).

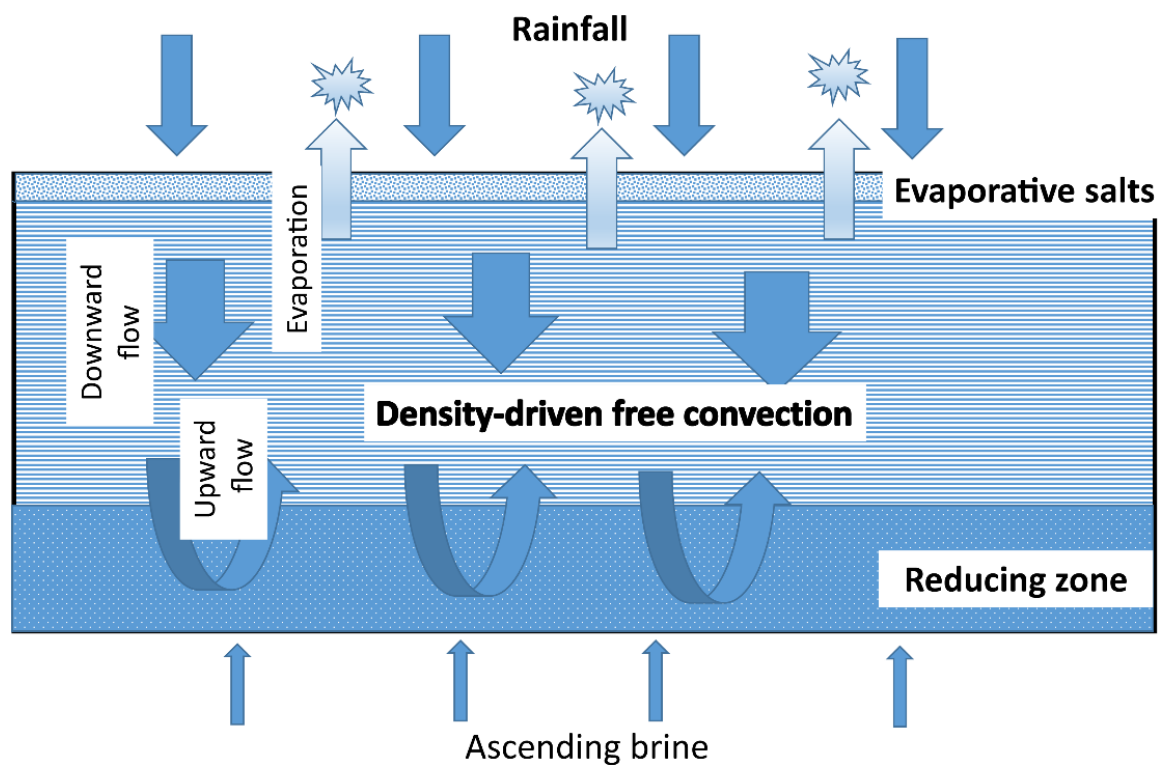


Figure 130 - Schematic depiction of a density-driven free-convection model that brings NO_3^- from the surface to a depth that has reducing conditions. This environment results in a reduction of NO_3^- to N_2 . The isotopically lighter N_2 gas is lost to the atmosphere and the nitrogen remaining in the sabkha is isotopically heavier (reproduced from Wood & Böhlke, 2017).

Differential optical absorption spectroscopy (DOAS) measurements showed that bromide is lost as gas from the surface of the Dead Sea in the Middle East (Hebestreit et al., 1999; Matveev et al., 2001), the Great Salt Lake in North America (Stutz et al., 2002), and Salar de Uyuni in Bolivia (Honninger et al., 2004). Mass balance analysis of salt flats from the coastal sabkha of Abu Dhabi, UAE, was used by Wood and Sanford (2007) to illustrate the loss of bromide mass. The mass balance analysis suggested an annual flux loss of 85 kg/km^2 from the sabkha, which is supported by laboratory studies that demonstrated the conversion of solute to gas (Wood & Sanford, 2007).

Only a small mass of bromide can fit into the halite lattice in substitution for chloride (Braitsch, 1971); thus, losses from this process are likely small. Furthermore, there is little halite on or in the system; much of what forms on the surface is dissolved and reenters the aquifer with occasional recharge. There is no vegetation to which bromide can be incorporated. Mass ratio (*MR*) values for bromide of 2.8 were observed in the sabkha relative to that of 6.8 for conservative magnesium in this system, which is consistent with a significant bromide mass loss. Input values and average solutes in the sabkha are given in Table 15.

Table 15 - Mean solute data of input brine to the sabkha and observed sabkha concentration (reproduced from Wood & Sanford, 2007).

Source Aquifer	Identification	UTM East	UTM North	UTM Zone	Depth meters BLS	Date Sampled	Mg, mg/L	K, mg/L	Cl, mg/L	Br, mg/L	Cl/Br	Number of Samples
Tertiary brine	GWP-287A	600,328	2,647,191	39	121	Jan-98	2,600	1,300	69,500	130	535	1
Tertiary brine	GWP-288A	687,801	2,666,649	39	89	Jan-98	950	300	19,700	11	1,790	1
Tertiary brine	GWP-289	777,587	2,655,712	39	119	Jan-98	675	120	10,300	5	2,060	1
Tertiary brine	GWP-290A	210,989	2,655,365	40	88	Feb-98	950	450	25,000	15	1,667	1
Tertiary brine	GWP-291A	205,481	2,670,574	40	142	Feb-98	1,350	950	55,100	20	2,755	1
Tertiary brine	GWP-292	236,909	2,671,579	40	119	Feb-98	2,400	1,500	87,300	6	14,550	1
Tertiary brine	GWP-306A	208,465	2,668,318	40	129	Mar-99	1,250	1,100	62,500	12	5,208	1
Tertiary brine (mean)					7		1,454	817	47,057	28	4,081	
Sabkha brine (mean)					2	97-99	10,003	4,239	176,346	78	7,248	172

5.8 Radon-222: Solutes Dominated by Diffusion

Large populations in rural North and South America, southern Africa, western Australia, and northern Europe are served by groundwater from fractured silicic igneous and high-grade metamorphic rocks. Wells completed in such rocks commonly produce water from a single fracture or network of fractures. The water frequently exhibits a wide range of radon (Rn-222) activity within the same area and general lithology (Hall et al., 1987). Interestingly, the activity of Rn-222 in water is frequently significantly greater than can be reasonably accounted for by the amount or distribution of uranium-238 in the rock matrix. The short half-life of 3.8 days for Rn-222 means that it must be generated close to wells where it is measured, yet insufficient uranium is present to generate the equilibrium mass of radium-226. Thus, there must be some method of concentrating radium Ra-226 in the fractures.

Wood and others (2004) proposed a diffusion-based model. In this model, radium-226 ions generated from the decay of uranium-238 diffuse from the rock matrix to fracture surfaces, where weathering products (largely iron oxide) sorb the radium-226 ions. As a result of the relatively long half-life of radium-226—1,601 years—significant activity can accumulate on fracture surfaces. The proximity of this sorbed radium-226 to the active groundwater flow system allows its decay progeny radon-222—with a short 3.8-day half-life—to enter directly into the water, providing the observed elevated activity.

Laboratory analyses of the rock matrix's primary porosity, diffusion coefficients, radon emanation, and ion exchange at fracture surfaces are consistent with the requirements of a diffusion/ion exchange model (Wood et al., 2004). Also consistent, were the results of a dipole-magnesium brine injection/withdrawal stress test experiment that was conducted between bedrock boreholes in the high-grade metamorphic and granite rocks at the Hubbard Brook Experimental Forest, New Hampshire, USA. This test chemically stressed hundreds of square meters of surface area under ambient conditions—rather than the few square centimeters available from a core under laboratory conditions—and was considered a comprehensive evaluation of the ion exchange/sorption capacity of the system. That is, it was to test the model that radium-226 had diffused to the fractures where it was sorbed to the weathering products. It was hypothesized—if the model was correct—that if a large concentration of cations were introduced, the radium-226 would be exchanged from the sorbed positions on the iron oxides/weathering products to the water.

The dipole brine injection/withdrawal experiment was designed to use a step increase of elevated concentrations of magnesium chloride solution in four discrete intervals. Approximately 1,150 L of formation water from well FSE-14 (shown in Figure 131) was used in each of the four tanks to make solutions of $\approx 32,400$, $\approx 62,150$, $\approx 95,650$, and $\approx 137,100$ mg/L magnesium chloride hexahydrate $\text{MgCl}_2 \cdot 6 \text{H}_2\text{O}$. It was known from ion-exchange literature that divalent magnesium would be an effective exchanger and

likely would remove most exchangeable cations. The experimental design for the injection/withdrawal (i.e., dipole) test consisted of injecting brine in well FSE-8 and extracting it from well FSE-14, which was 13.9 m from FSE-8 (Figure 131).

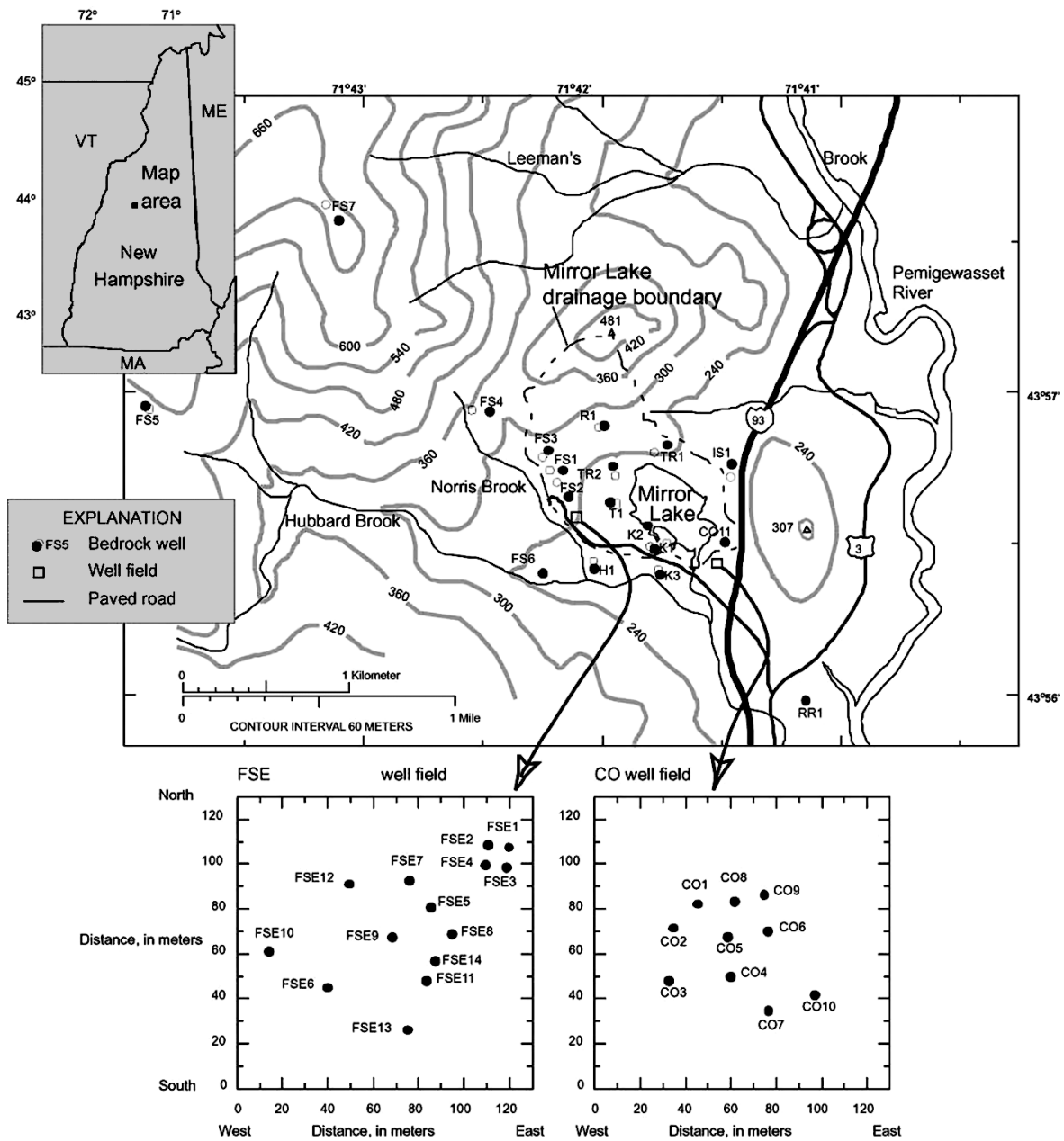


Figure 131 - Index map showing topography and location of wells in the Mirror Lake, Hubbard Brook Experimental Forest, NH, USA. Arrows indicate enlargement of observational well fields (reproduced from Wood et al., 2004).

The two wells are at approximately the same elevation. The bedrock surface was 14.3 m below the land surface in FSE-8 and 24.5 m below the land surface in FSE-14. Water pumped from well FSE-14 at an average of 3.4 L/min had the solute concentrations that are illustrated in Figure 132 and Figure 133. Figure 133 shows that large amounts of radium-226 were removed by ion exchange which is consistent with the proposed diffusion mode.

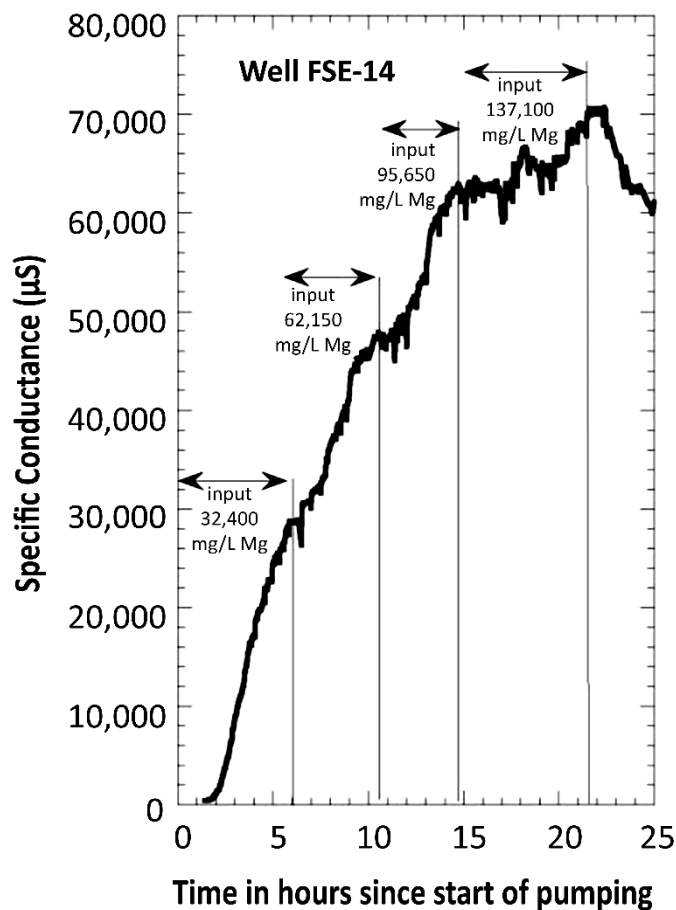


Figure 132 - Graph of specific conductance showing the arrival of different injection concentrations with time at the withdrawal well FSE-14 (reproduced from Wood et al., 2004).

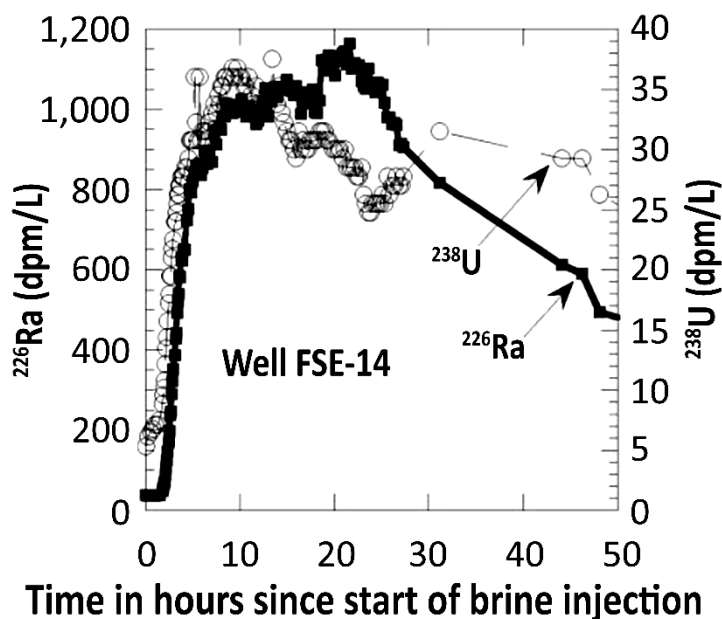


Figure 133 - Graph showing impact of magnesium ion exchanger on uranium-238 and radium-226 activity of water from the withdrawal well (FSE-14) as a function of the time since brine injection started. Whereas both uranium-238 and radium 226 are present as cations in exchange positions they are present in different activities and binding energies thus they respond to the magnesium exchanger in different ways (reproduced from Wood et al., 2004).

The diffusion coefficient estimated from the test data is of sufficient magnitude to allow geologically rapid diffusion of radium to the fracture faces (Wood et al., 2004). The presence of ubiquitous Liesegang rings adjacent to the rock fractures is consistent with diffusion in the system and provides a model for the accumulation of diffusion-controlled sorption sites.

This model is proposed to explain how it is possible to achieve high activities of radon-222 with only modest amounts of uranium-238 present in the matrix. The activity of radium-226 on the surface of a fracture—and, thus, radon-222 in the adjacent water-filled fracture—is a function of, among other factors:

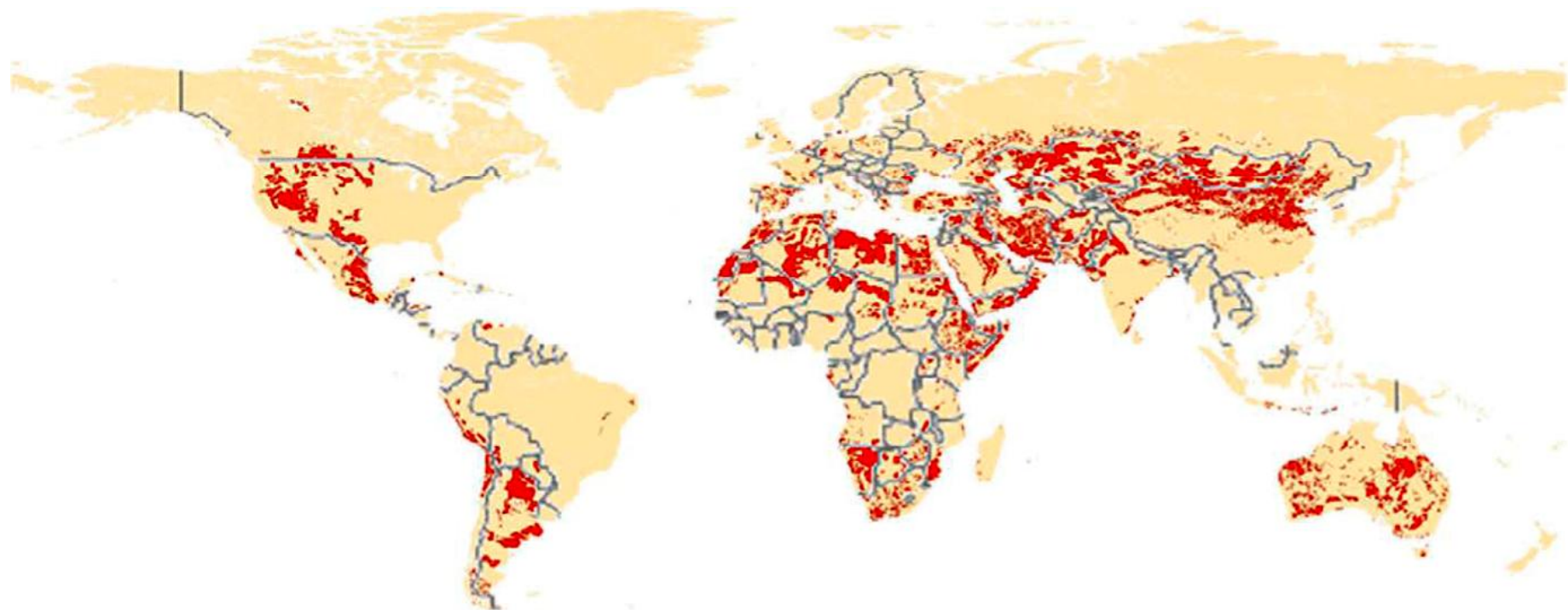
1. the nature and amount of the weathering products on the fracture,
2. the concentration and distribution of uranium-238 in the rock relative to the fracture,
3. porosity,
4. tortuosity, and
5. time since fracture formation.

The diffusion/ion exchange-model may apply to all fractured rock containing uranium, including carbonate and clastic rocks, in addition to crystalline silicic igneous and metamorphic rocks.

5.9 Systems Dominated by Soil Salinization

Salinization of land is a natural process, and many closed basins such as the Caspian Sea in Eurasia, the Great Salt Lake in North America, Lake Eyre in Australia, Lake Titicaca in South America, and Lake Chad in Africa exhibit salt deposits but they are also generated by human activity. We now understand that the decline of major civilizations of Sumeria, Greece, Rome, Central America, and others may in large part have been due to the destruction of their soil resources (Montgomery, 2012) and, thus, their ability to produce food. The 25 cm soil zone—the “skin of the Earth”—is the difference between life and death.

Salinization of soils is currently a major factor in the global destruction of agricultural soils and consequent loss of food production (Figure 134). It has been estimated that globally, 20 percent of total cultivated and 33 percent of irrigated agricultural lands are afflicted by high salinity (Shrivastava & Kumar, 2015); at least 3 hectares of arable land is currently degrading every minute which is $\approx 1,500,000$ ha/year (Food and Agriculture Organization (FAO) of the United Nations, 2021; Figure 134). However, most salinization is local or regional (Figure 135); an excellent regional analysis is given by Les Henry in *The Soil Salinity Story*, which deals with the salinization of the Canadian Prairie (Henry, 2023).



World map of saline soils

Legend

- Saline soils equal or above 4 dS/m
- Soils below 4 dS/m
- Country borders

0 5,000 10,000 kilometers

Figure 134 - Global land affected by salinization, much of which has been caused by rising groundwater primarily due to conversion of natural vegetation to agricultural crops and irrigation in excess of plant demand (reproduced from Food and Agriculture Organization (FAO) of the United Nations, 2021).



Figure 135 - Agricultural field undergoing salinization where the white area is salt (reproduced from Food and Agriculture Organization (FAO) of the United Nations, 2021).

Saline soils that contain excessive amounts of soluble salts, usually sodium, reduce the ability of plants to take up water from the soil by osmosis, thus inhibiting their development. Globally, an enormous area of agricultural land has been affected by salinization, most of which is caused by groundwater tables rising to the land surface due to agricultural development and irrigation followed by evaporation of water that concentrates the solutes. Salinization is most common in arid and semi-arid areas of the world where potential evaporation exceeds precipitation. In a normal groundwater environment, the water table and capillary fringe are below the land surface, and little, if any, evaporation occurs (Figure 136).

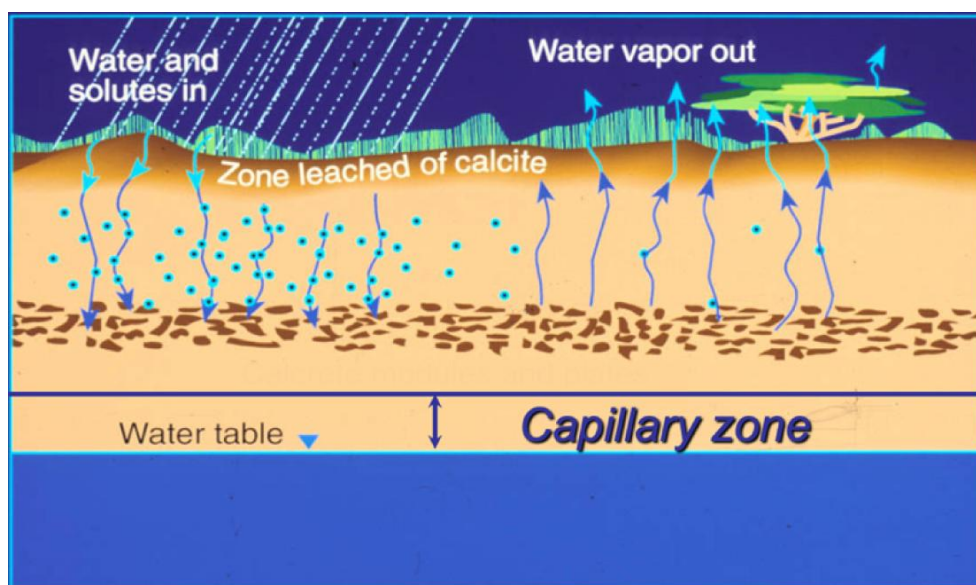


Figure 136 - Normal groundwater condition with the top of the capillary zone well below the land surface; thus, little or no evaporation occurs from the groundwater, and no salinization occurs.

If the water table rises to where the capillary fringe intersects the land surface (Figure 137), evaporation occurs, and solutes are concentrated, creating a saline environment. The capillary fringe is a zone about a meter thick above the water table in fine sand but can be several meters thick in clay-rich deposits that are fully saturated and where water saturation is maintained by capillary processes.

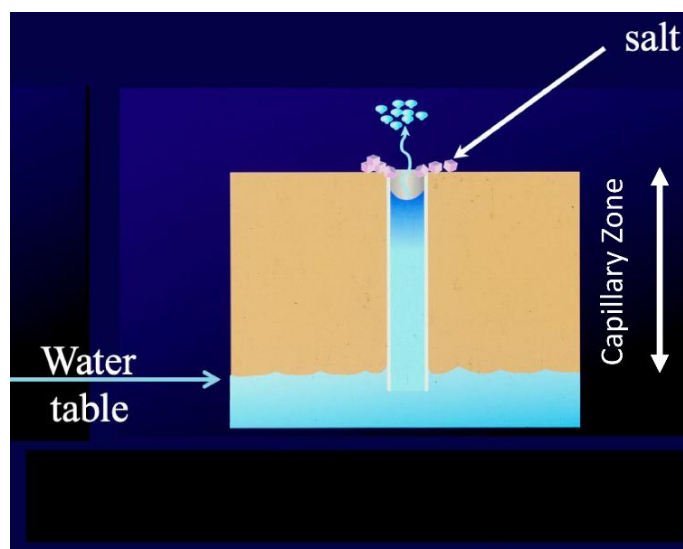


Figure 137 - In an arid or semi-arid environment the capillary fringe may intersect the land surface where evaporation removes the water but not the solutes. This figure illustrates the flow of water and solutes in a single capillary tube of the many thousands of capillaries in a square meter of the ground surface. This evaporative process concentrates the solutes, causing salinization and the formation of halite and other saline minerals on the surface.

Two major human activities cause the water table to rise and bring the capillary zone to the surface where evaporation can occur. The first, which is not immediately obvious, is the removal of native vegetation and substitution of crops. Many of these crops have a lower annual water demand or demand at different times than that of the native vegetation, which permits greater recharge than geogenic conditions. The second condition occurs when imported irrigation water is applied at a greater rate than plants use the water; the excess is then recharged to the groundwater, thus raising the water table where the capillary zone intersects the surface.

5.10 Evaluating Pristine Condition

It is sometimes necessary to determine the background concentration of a solute to ascertain its pristine geogenic concentration. Whether it is pristine, or not, has practical importance because where there is evidence of even one anthropogenic constituent present (such as detectable tritium or PFAS), then it is reasonable to expect that others may be present. However, it is not as apparent for solutes commonly present in groundwater, such as nitrogen, chloride, sulfate, or other elements that occur naturally in groundwater. Determining if water is pristine is more difficult than one might think owing to the normal

variability of geogenic solute concentrations in groundwater (Figure 9) and the several possible sources of solutes (e.g., water–rock weathering, relic, or transported in from outside sources (Figure 3). Generally, one does not have a historical sample collected before the anthropogenic impact; thus, it is necessary to use other approaches to evaluate the impact.

One approach is to use the rainfall solute input at the recharge zone to calculate a minimum value for the solute. If, for example, the chloride value in the sample is significantly greater than calculated by rainfall concentrated by evapotranspiration (described for the Grand River field example in Section 5.2), the additionally observed concentration may be from relic solutes, solutes from underlying brine, or anthropogenic contamination such as road deicing. One then needs to consider using another approach, either hydrogeologic (which considers head distribution) and/or hydraulic conductivity (which can eliminate a source) or chemical approaches such as ionic ratios, trace elements, isotopes, and so on (to eliminate one or another source). One always needs to remember that the water source may be significantly different from the solute source; that is, 5 percent of the water flux may transport 95 percent of the solutes.

Another approach in attempting to recognize the background is to look at the concentration distribution of the element and see if one can estimate the background. For example, the background concentration of nitrogen was of interest for a study of the impact of anthropogenic nitrogen on groundwater (Section 6.4.2). In this case, the probability distribution was plotted (Figure 138a) to evaluate the concentration distribution. This suggested that over 50 percent of samples were less than 0.5 mg/L NO_3^- as N; thus, the geogenic values are likely less than 0.5 mg/L, but it was not definitive. Next, the number of samples in different concentration ranges was plotted as a histogram (Figure 138b). In this case, the bins with < 0.25 mg/L NO_3^- as N appear to be the most numerous and likely the geogenic background concentration. Note this approach is not definitive but is a start at defining the pristine value.

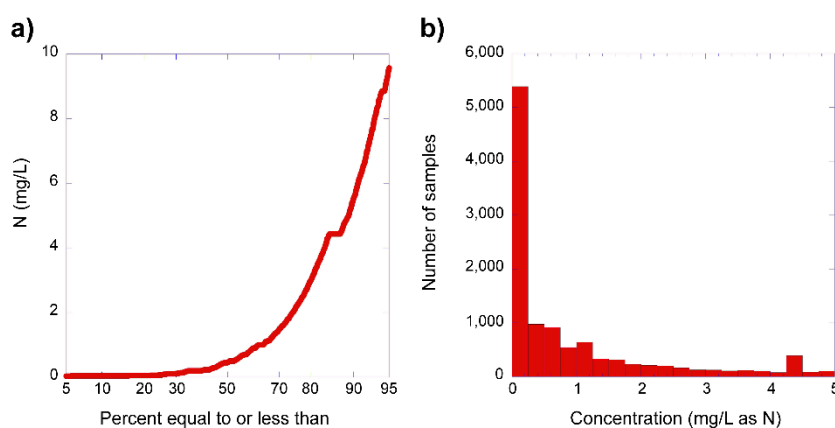


Figure 138 - a) Probability distribution of mg/L NO_3^- as N in the global aquifer database of 11,643 analyses (Wood et al., 2022); b) histogram of the same data that show the dominance of bin < 0.25 mg/L.

5.11 Section Wrap-up

The field examples presented in this section illustrate some of the hydrogeochemical processes identified in other parts of this monograph. This presentation is not extensive nor all-inclusive. There are thousands of examples of aquifer systems described in the literature that illustrate these processes; however, the author is familiar with the ones presented in this book.

[Exercise 4](#)  examines the basic approach necessary to identify various hydrogeochemical processes in a field environment.

6 Solute Mass Balance: Simple Mass Flux Modeling

The thrust of this monograph is a conceptual approach to understanding hydrogeochemistry within a groundwater flow framework. This approach is supported by utilizing a *back-of-the-envelope* mass balance calculation that can aid in defining solute sources and sinks using flow rates and solute concentrations.

Two fundamentally different modeling approaches are used to evaluate the origin of groundwater solutes. The first is a process-based approach that quantitatively evaluates all the relevant individual chemical processes impacting the solute concentration and composition as well as flow conditions and allows accurate prediction into the future with different flow and solute stresses. The limitation of this approach is that it requires a large amount of information that is typically unavailable or has considerable uncertainty in the parametrization of the many components.

The second modeling approach is that of mass-balance, which quantitatively evaluates the mass of individual solutes entering and leaving the aquifer. The limitation of the mass-balance approach is that it provides no direct analysis of the process by which the solutes were generated or removed; thus, it is of little value in predicting future changes if the system is stressed by changes in flow or solute concentration.

When using models, it is always wise to heed the words of statistician George Box, who in 1976 reportedly stated, "*All models are wrong. But some are useful.*"

As stated previously in this monograph, the solutes in an aquifer are the result of:

- solutes remaining from the time of deposition, the so-called relic, fossil, legacy, or connate solutes;
- solutes introduced from the surface (precipitation, rivers, lakes) and from adjacent, underlying, or overlying formations; and
- solutes generated from weathering and radioactive decay of the aquifer's mineral/rock framework.

If a simple calculation can show the likelihood that most solutes come from one of these three sources, then this is a significant start in explaining the hydrogeochemistry of the system.

As a first approximation, the mass balance approach is easy to apply, clarifies assumptions, and allows assumed values to be easily tested. Solute mass flux (mass/time/area) is determined by multiplying the groundwater flux (liters/year/meter square) entering the aquifer multiplied by solute concentration (mass/volume) (milligrams/liter). This value is then subtracted from the mass flux leaving the aquifer which is calculated by multiplying the groundwater flux leaving the aquifer by the discharge solute concentration. This steady state assumption commonly utilizes a representative control volume (RCV) to illustrate the mass changes. Setting up an RCV

early in planning an investigation can aid significantly in identifying where additional solutes and water flux data may be needed.

6.1 Representative Control Volume (RCV) Mass Flux Model

For most mass balance modeling of an aquifer system, an RCV approach is commonly used rather than an evaluation of the entire aquifer. In using the RCV as a first approximation, it is generally assumed that both chemical reactions and flow are in a *steady state* condition—not changing with time—and that the system is open; that is, solutes and water enter and leave the RCV.

Solute flux is defined as mass per unit time, per area; thus, one typically selects the dimensions of the RCV such that it is one meter wide, the thickness of the aquifer deep, and the length of the aquifer along the flow direction. With this configuration, no input or output occurs from the sides of the RCV, only from the ends, top, and bottom (Figure 139).

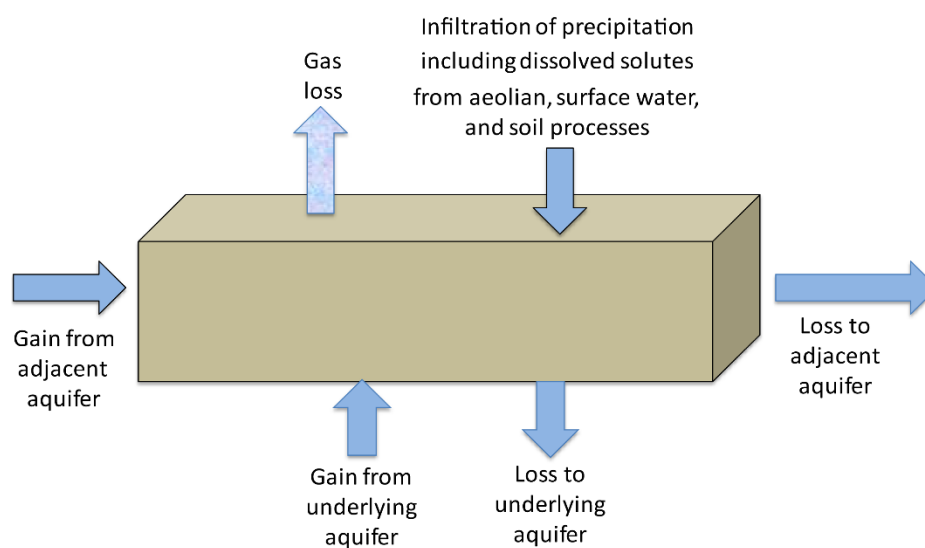


Figure 139 - Potential entrances and exits—sources and sinks—of solutes and water in a representative control volume (RCV) of an aquifer.

Quantitative modeling of mass balance for an RCV is analogous to a checkbook accounting system: keeping track of the amount deposited, the amount spent, and the amount remaining in the account. Furthering the analogy, any interest or service charges applied to the checking account can be considered equivalent to adding or removing solutes by weathering, iron exchange, radioactive decay, and so on, and the opening deposit in the checking account represents the equivalent of the relic solute component(s).

To use the RCV concept, one needs to estimate the relevant water fluxes entering and exiting the RCV and the concentration of solutes in the water. Multiplying the water flux by the concentration of that water, one obtains the solute–mass flux for each portal in the RCV. Summing the solute flux from all entries and subtracting the sum of solute flux exiting the RCV determines the mass loss or gain in the RCV.

Based on experience, one can then speculate about the possible geochemical processes controlling the solute concentrations and ratios. If thermodynamic processes (rock–water interactions) are occurring or relic solutes are present, they will generally be reflected in the mass gain or loss of various solutes. For example, if the output mass shows a mass of chloride and sodium greater than input sources, one might investigate the possibility of relic sodium and chloride in the system; if sulfate and calcium output are greater than input, perhaps gypsum or anhydrite are dissolving; if sulfate is greater, pH lower, and oxygen is lower in output then perhaps pyrite is dissolving; if calcium is less and bicarbonate and sodium are greater, then perhaps ion exchange is occurring; if radon gas is greater than input, perhaps it is being generated by the decay of radium within an RCV.

The lack of change between input and output does not necessarily mean there are no changes in individual ions, it just means there are no mass balance changes; the mass balance approach does not identify a specific chemical process. Individual atoms may be removed or added to the solution by different processes, but the gross difference may remain the same. If the solid framework is entirely non-reactive and there are no legacy solutes, the input solute flux will be the same as the output solute flux.

Groundwater flux and solute concentration are not symmetrical in their relation for most aquifer systems. The water flux into or out of the framework is mainly independent of solute concentrations. For example, 5 percent of the water entering the RCV may transport 90 percent of the solutes. Also, the solute fluxes into some aquifers from external sources may be far more important in controlling concentrations and ionic ratios than the chemical reaction of the water with the mineralogical framework.

Table 16 summarizes the processes one typically considers in evaluating the hydrogeochemical mass balance of an RCV. [Exercise 5](#) provides an opportunity to practice calculating an RCV.

Table 16 - Summary of common sources and removal of solutes in an RCV.

Source of solutes	Loss of solutes
External: precipitation recharge; inflow from adjacent, underlying, overlying water bodies or geologic formations; aeolian influx of particulate material onto the surface; overland run-on; gas removal from the atmosphere	External: outflow to adjacent, underlying, overlying water bodies, or geologic formations; aeolian outflux of particulate material from the surface; overland runoff; gas lost to the atmosphere
Internal: mineral solution; ion exchange; desorption; diffusion from low permeability matrix; radioactive decay; relic, fossil, legacy, or connate solutes	Internal: mineral precipitation; ion exchange; sorption; diffusion into low permeability matrix; radioactive decay

6.2 Pore Volumes

In evaluating the mass flux through an RCV, it is generally of value to estimate the number of pore volumes of water discharged through an aquifer system to understand the concentration and composition of aquifer solutes. A pore volume is the volume of pore

space within the RCV. The number of aquifer pore volumes discharged can help constrain the mechanisms controlling an aquifer's solute composition and concentration and is frequently useful with the mass balance approach described above.

Consider an RCV along the full flow length of an aquifer. The total number of pore volumes discharged from the end of an RCV flow system since the aquifer became active is equal to the total groundwater recharged, divided by the total pore volume of the RCV as shown in Equation (30)

$$\begin{aligned} & \text{Total number of pore volumes discharged from the RCV} \\ & = \left\{ \frac{\text{Total volume of groundwater recharged since formation of aquifer}}{\text{Total pore volume of the RCV}} \right\} \quad (30) \end{aligned}$$

In most aquifer systems, the climate is usually the controller of the number of pore volumes discharged; thus, an aquifer in a semi-arid or arid environment is much less likely to have discharged a significant number of pore volumes than an aquifer of similar type, age, and hydraulic properties, and topography in a humid environment.

6.3 Mass Flux Modeling in the Sabkha of Abu Dhabi, UAE

A field study in the coastal sabkha of the Emirate of Abu Dhabi was selected to illustrate the RCV process (Figure 140). These solutes are approximately ten times the concentration of the adjacent seawater (Table 1), and owing to their proximity to the Arabian Gulf, the solutes were initially hypothesized to originate from seawater flooding recharging the sabkha and subsequent concentration by evaporation. Sanford and Wood (2001) and Wood and others (2002) demonstrated using an RCV that the solutes most likely originated from underlying brine-bearing formations, not the ocean. Kraemer and others (2014) confirmed this by using radium concentration and other geochemical techniques of separating the chemical fingerprint of deep brines from seawater in this system. The mass balance model suggests that solutes increase with time and are circulated within the system by density-driven convection initiated by major rainfall events (Van Dam et al., 2009, 2014).



Figure 140 - Coastal sabkha northwest of the city of Abu Dhabi, UAE, on the Arabian Gulf, showing polygons of halite (salt) forming on the surface. Polygons are approximately 1 meter in diameter (photo by W. W. Wood, April 1991).

The Abu Dhabi Formation (Figure 141) is a sabkha exposed as a strip approximately 300 km long by 10 km wide along the coast of the Arabian Gulf in the United Arab Emirates. The wedge-shape, formed of carbonate and quartz from reworked dunes, is of Holocene age and thickens toward the coast with an average thickness of approximately 10 m at the coast. The hydraulic conductivity is approximately 1 m/d, and the hydraulic gradient is extremely low at $1/5,000$ (0.0002). These sediments are superimposed over an incised geologic basement consisting of 6,000 to 8,000 m of a Paleozoic–Pleistocene-age sedimentary sequence, of largely carbonates and evaporites, containing brines. The upper few hundred meters of the Paleozoic–Pleistocene-age sedimentary sequence has a vertical hydraulic conductivity of 1×10^{-4} m/d and a vertical gradient of 0.1 m/m (Wood et al., 2002).

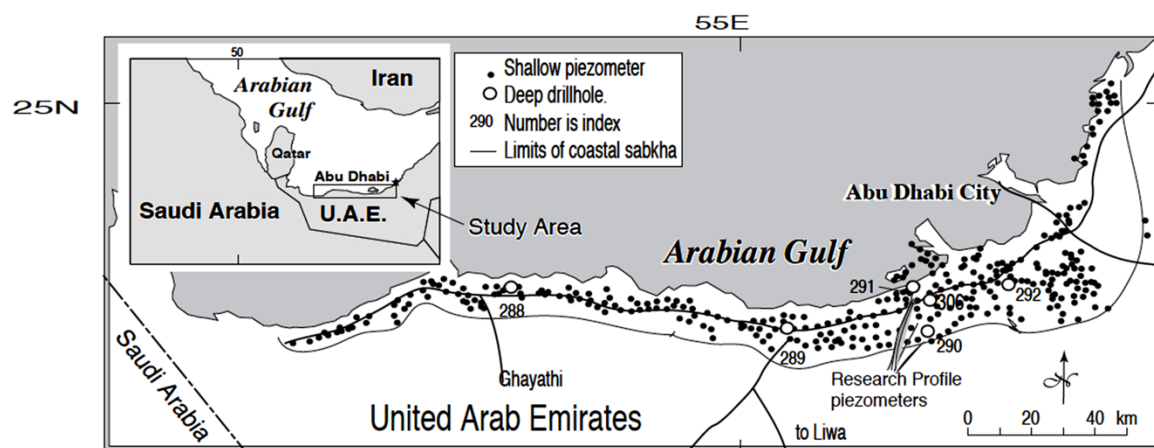


Figure 141 - Map showing approximate location of the coastal sabkha Abu Dhabi Formation with deep wells (numbered) and piezometers (dots) (reproduced from Wood et al., 2002).

The system is hydrologically open with a small annual solute discharge flux to the gulf with intermittent recharge events to sabkha occurring every 15 to 20 years. There is no mineral solution in the mineralogical framework as the critical solutes are thermodynamically supersaturated with respect to calcite CaCO_3 , dolomite $\text{CaMg}(\text{CO}_3)_2$, gypsum $\text{CaSO}_4 \cdot 2\text{H}_2\text{O}$, and anhydrite CaSO_4 . Thus, the solutes must originate from atmospheric precipitation, aeolian deposition, horizontal groundwater flux, or upward flow of underlying brine or the adjacent gulf. It is assumed that all pores were initially filled with relic sea water as the aquifer was formed from reworking dune material in a marine environment in the late Pleistocene.

Water flux is given by Darcy's law, which states that under steady-state conditions, the amount of flow from a specific area—the flux q —is equal to the hydraulic conductivity K multiplied by the rate of change of the head (h) with distance (l) along the flow path, as shown in Equation (31).

$$q = -K \frac{dh}{dl} \quad (31)$$

where (parameter dimensions are dark green font with mass as M , length as L , time as T):

- q = water flux (LT^{-1})
- K = hydraulic conductivity (LT^{-1})
- $\frac{dh}{dl}$ = hydraulic gradient (dimensionless)—change in hydraulic head with distance. The negative sign indicates the flow is from higher to lower hydraulic potential.

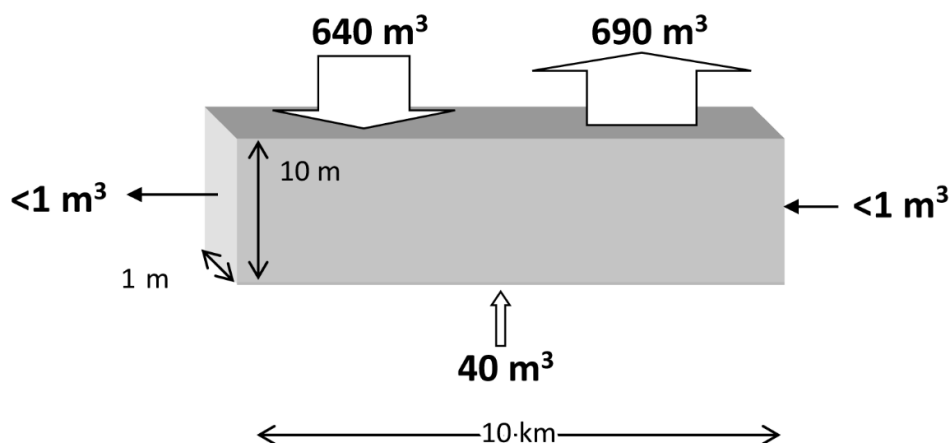
Upward vertical flux q from the underlying formations was determined to be approximately 4 mm/y/m^2 into the RCV; horizontal flow into the RCV is less than $1 \text{ m}^3/\text{y}$ (Table 17; Figure 142a).

Table 17 - Summary of water flux into and out of control volume (1 m)(10 m)(10,000 m).

Water source	Hydraulic Conductivity (m/d)	Gradient dh/dl (m/m)	Water Flux m ³ /y
Horizontal GW flow in	1	0.0002	0.73 ~ 1
Horizontal GW flow out	1	0.0002	0.73 ~ 1
Vertical GW flow in	1 x 10 ⁻⁴	0.1	36.5 ~ 40
Evaporation	—		690
Precipitation	—		640

GW = groundwater

a) Water



b) Solutes

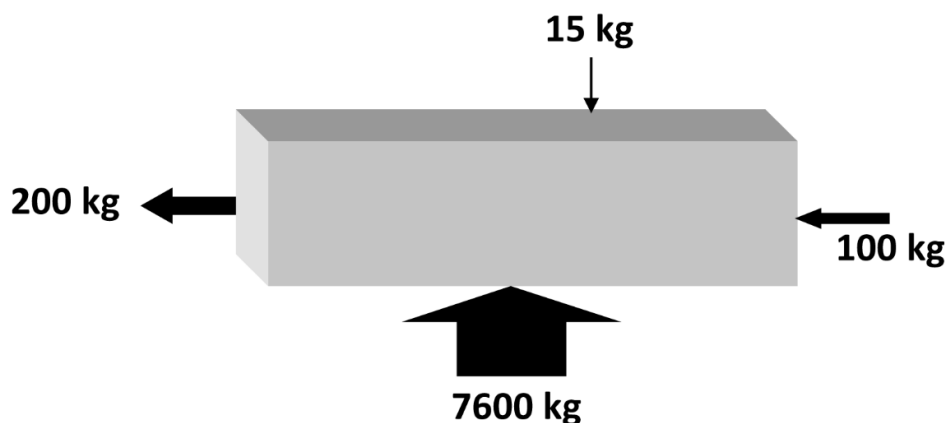


Figure 142 - a) Diagram illustrating annual water flux in a control volume that is 1 m wide by 10 m deep by 10 km long, representative of the coastal Sabkha aquifer; and b) annual solute flux from the same RCV (modified from Wood et al., 2002).

Evaporation measurements from the sabkha surface were made using a humidity chamber and a technique described by Stannard (1988). Evaporative flux—there is no vegetation, thus no transpiration—at a site with 70 mm/y/m² rainfall, evaporation was found to be 0.24 mm/d/m² or 68 mm/y/m² averaged over four seasons. A second site where rainfall is 50 mm/y, evaporation was found to average 0.14 mm/d/m² or 51 mm/y/m² averaged over four seasons (Sanford & Wood, 2001). That is, the system is in equilibrium

with recharge and evaporation within the error of the experiment; so it is unlikely that ocean water is a significant source of water and thus solutes (Table 17; Figure 142a).

Putting these annual water fluxes together into an RCV 1 m wide, 10 m deep, and 10 km long results in the following values (Table 17; Figure 142a):

- less than 1 m³/y of groundwater enters and exits by lateral flow;
- about 40 m³/y enters by upward vertical leakage;
- 640 m³/y enters by rainfall recharge; and
- 690 m³/y is lost to evaporation.

Little or no significant storm surge flooding and consequent recharge was observed.

Average concentrations of solutes in g/L were obtained from each water source and multiplied by the water flux to obtain a mass flux into and out of the control volume (Table 18; Figure 142b).

Table 18 - Summary of mass flux into and out of control volume (1 m)(10 m)(10,000 m).

Solute source	Water Flux m ³ /y	Concentration	Mass flux kg/y
Horizontal GW flow in	1	100 g/L = 100 kg/m ³	100
Horizontal GW flow out	1	300 g/L = 300 kg/m ³	300
Vertical GW flow in	40	190 g/L = 190 kg/m ³	7,600
Rainfall	640	0.023 g/L = 0.023 kg/m ³	15

GW = groundwater

In this RCV model, most of the solutes are derived from ascending continental brines, while most of the water is provided by local rainfall. There was no evidence of significant sea water entering the sabkha by surface flooding, nor is there any indication of it in the solute balance. This conclusion was upheld by Kraemer and others (2014), who showed by elevated radium and other analyses that solutes in sabkha are geochemically consistent with deep basin brines and not ocean water of the gulf. Occasional recharge events selectively dissolve soluble surface minerals, and this high-concentration solution—denser than the groundwater in the sabkha—sinks into and mixes with the aquifer water (Van Dam et al., 2009, 2014; Figure 143).

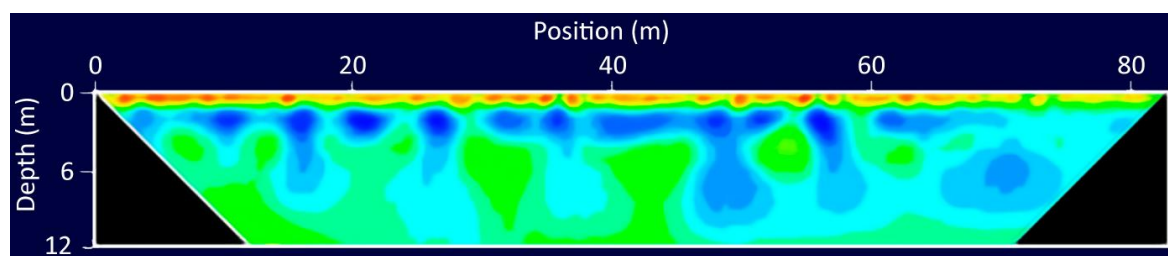


Figure 143 - Profile of dissolved solutes in the Abu Dhabi sabkha, UAE, where evaporite minerals on the surface are dissolved after a major precipitation event roughly once every 20 years, creating a dense brine that is recharged to the groundwater sinking to the bottom of the aquifer, forcing circulation, and mixing with ascending brines. Red indicates highest salinity and green lowest with blues intermediate. The labels a and a' indicate a NE to SW profile (reproduced from Van Dam et al., 2009).

The original seawater solute ratios and concentrations are modified by adding ascending brines, resulting in increasing concentration over time.

6.4 Global Mass Flux Modeling of Carbon, Nitrogen, and Total Solutes

In this section, the mass balance approach is utilized in evaluating the global mass flux of solutes from groundwater (Wood et al., 2023a, 2023b and Wood et al., 2024). These mass flux values provide some insight and understanding of the large-scale impacts of groundwater on the environment. The mass flux, associated with the transport of solutes by groundwater, is a significant geologic process on the same order of magnitude as mass transported by riverine or aeolian processes, but because it is unseen, it is commonly ignored.

The following three examples—carbon, nitrogen, and total solutes—of global groundwater illustrate the power of simple mass flux modeling in understanding groundwater's geogenic impact. For this monograph, the modeled global geospatial concentration of Wood and others (2022; Table 1) is used. These values are converted to solute mass flux using the baseflow values shown in Figure 144. Closed basins constitute 19 percent of the continental area (Lehner, 2014) and adds 819 km³/y of groundwater discharge. The direct ocean discharge of groundwater ranges from approximately 0.6 percent (Luijendijk et al., 2020) of total integrated riverine continental discharge to 7 percent (Taniguchi et al., 2007). A direct ocean of about 4% with a discharge flux of 610 km³/y was estimated. This component is not well constrained, but because it is small, it has a negligible effect on the estimates. The basins divided into endorheic (topographically closed) and exorheic (topographically open). The exorheic basins were further divided into four climates: cold–dry, cold–wet, warm–dry, and warm–wet. The cutoff between cold and warm is a mean annual temperature of 15 °C and the division of dry and wet is a mean annual groundwater discharge flux of 10 cm/y (Figure 145). The distribution of basins by temperature and recharge is shown in Figure 145. Each geospatial pixel of a solute concentration was multiplied by the groundwater recharge flux of that pixel, thus providing a solute mass flux for each pixel. These pixel values were then summed to provide an average mass flux for each basin type. The solute mass fluxes are presented in Table 20.

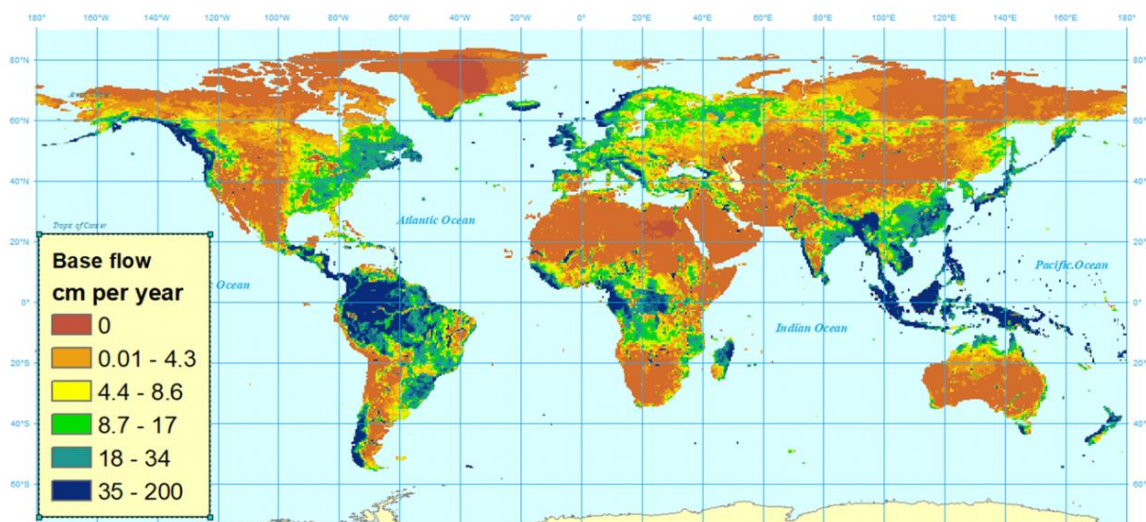


Figure 144 - Global maps of baseflow (representing recharge) used to calculate solute flux from groundwater. The base flow to streams was calculated from the WaterGAP simulation model averaged over the years 2001 to 2010 (reproduced from Schmied et al., 2021).

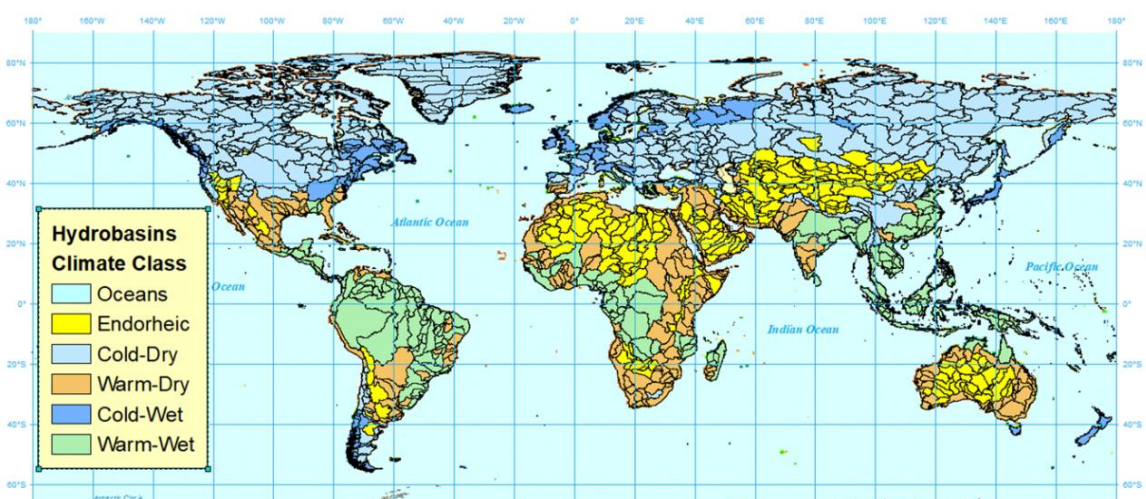


Figure 145 - Hydrologic basins of the world divided into endorheic and exorheic, with the exorheic basins divided into four climate types: cold-dry, warm-dry, cold-wet, and warm-wet. The values of warm-cold are based on a cutoff at 15 °C and wet-dry on a cutoff of 10 cm/y groundwater discharge (modified from Lehner, 2014).

Table 19 - Mean groundwater solute concentration estimates aggregated by climate zone (data modified from Wood et al., 2023 a, b; Schmied et al., 2021).

Basin type with exorheic divided by climate type	Endorheic		Exorheic			Direct to Ocean	Global average
			Cold Dry	Warm Dry	Cold Wet		
Area Million km ²	26.1	43.1	27.9	7.3	30.4		135
Percent of Global Area	19%	32%	21%	5%	23%		100%
GW Discharge km ³ /yr	819	1793	1444	1084	10101	610	15,241
Percent of Global GW Flux	5%	11%	9%	7%	64%	4%	100%
Soil-log PCO ₂ *	-2.62	-2.52	-2.10	2.29	-1.73	-1.95	-1.95
pH	7.02	7.01	6.85	6.79	6.42	6.55	6.55
T (degrees C)	17.6	5.1	22.1	6.6	26.2	21.5	21.5
Ca	50	64	49	55	43	47	47
Mg	25	23	19	20	14	17	17
Na	69	68	52	51	47	52	52
K	5.5	3.1	3.8	3.1	3.8	3.8	3.8
H ₄ SiO ₄ ⁰	72	72	51	58	38	44	44
HCO ₃	239	255	199	184	128	160	160
Cl	117	30	133	74	88	86	86
SO ₄	137	117	59	63	31	52	52
Nitrogen as N	1.5	0.8	1.1	0.7	1.1	1.1	1.1
Dissolved Solutes	716	633	567	509	394	463	463
Charge imbalance	-7.1%	1.8%	-6.9%	0.8%	0.8%	-0.5%	-0.5%

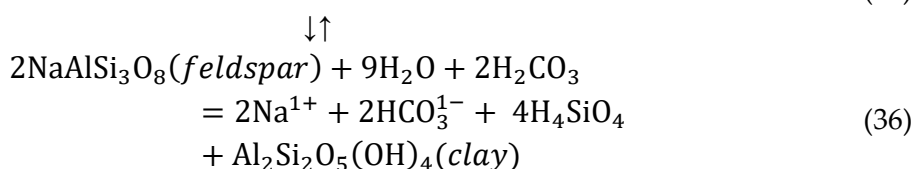
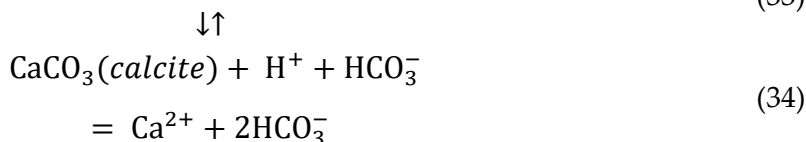
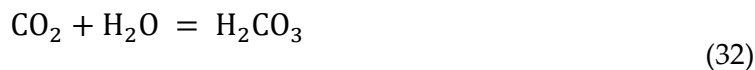
6.4.1 Carbon in Global Groundwater

Society currently has a great interest in carbon owing to its relation to global climate change; thus, a question of interest is: “How much carbon does groundwater contributed to the global carbon budget?”

Quantifying the global dissolved carbon mass flux discharging from the terrestrial aquifer element pool has been historically challenging. However, estimates have largely been along river reaches rather than directly from groundwater, and they have not fully captured the mass transport of carbon from aquifer systems to the riverine ecosystem owing to the degassing of carbon dioxide. This analysis is modified from Wood and others (2023 a, b), which provides significantly more detail of the process and slightly different calculations.

Water flows downward through the vadose zone between the land surface and the top of the capillary zone. The pores in this environment contain air, water vapor, and liquid water. Water passing through this zone dissolves a large mass of CO₂ gas. The CO₂ gas reacts with the water, creating carbonic acid that dissolves minerals Equations (32), (33),

(34), (35), and (36). In these equations, calcite (CaCO_3) is a surrogate for carbonates, and albite ($2\text{NaAlSi}_3\text{O}_8$) is a surrogate for silicates.



As the groundwater discharges to rivers, closed basins, or directly to the ocean, it re-equilibrates with the atmospheric CO_2 —which has orders of magnitude lower concentration of CO_2 —by degassing CO_2 to the atmosphere and precipitating the solid phase CaCO_3 (calcite) (Figure 146).

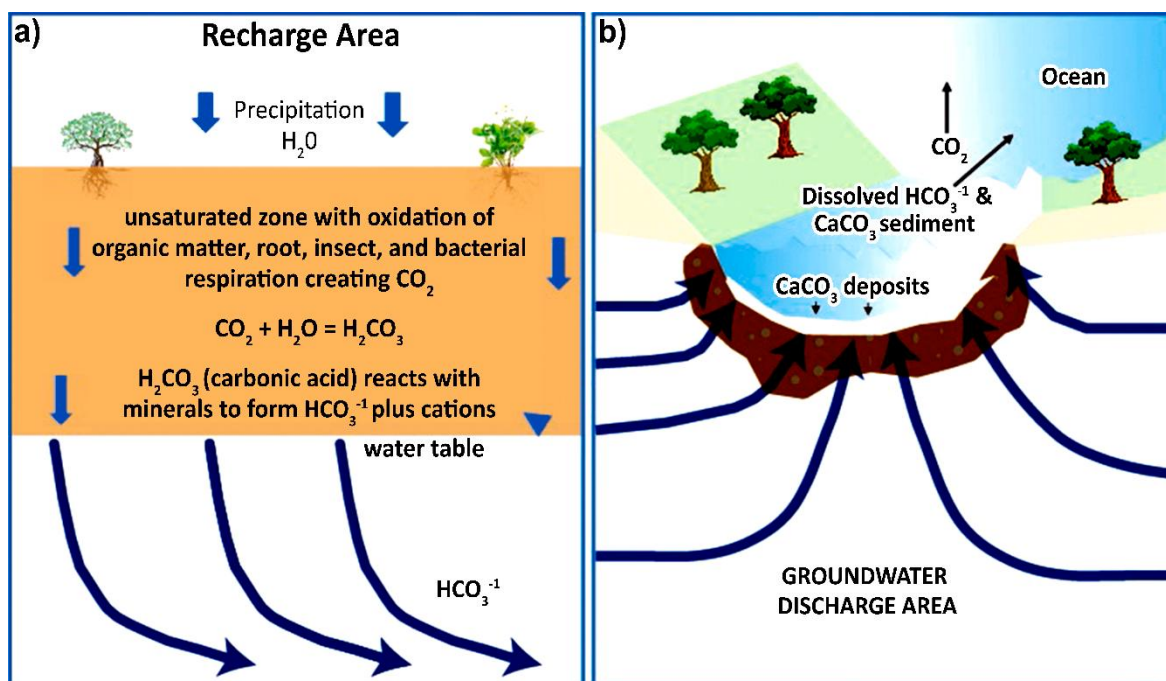


Figure 146 - Conceptual model for groundwater weathering and transport of DIC (dissolved inorganic carbon) to the riverine environment. a) In the vadose zone recharging groundwater encounters elevated partial pressure of carbon dioxide (CO_2), ten to a hundred times greater than the atmosphere, to form carbonic acid (H_2CO_3) that aggressively reacts with the aquifer’s mineral framework, creating bicarbonate (HCO_3^-) and cations. b) As groundwater enters the riverine environment which has lower partial pressure of CO_2 , it forces re-equilibrium of the carbonate system with degassing of CO_2 to the atmosphere and precipitation of solid calcite (CaCO_3) (from Wood et al., 2024).

The total carbon-mass flux discharge to the surface ecosystems from the groundwater element pool is approximately 0.88 to 0.97 PgC/y (1Pg is 1 Petagram, or 10^{15} g, or 1 Gigatonne) (Wood et al., 2024). Utilizing the code PHREEQC (Parkhurst & Appelo, 2013), the carbon can be separated into its individual species as it equilibrates with the atmosphere, thus, 0.53 PgC/y is discharged as bicarbonate (HCO_3^-) ion, 0.35 PgC/y as CO_2 gas, and 0.004 PgC/y as solid calcite (CaCO_3) (Table 20).

Table 20 - Carbon and silica flux from the global aquifer pool to the surface ecosystems in Pg/y (modified from Wood et al., 2024).

Parameter	Endorheic	Exorheic				Direct to ocean	Global flux (Pg/y)
		Cold dry	Warm dry	Cold wet	Warm wet		
HCO₃ flux as C	0.034	0.122	0.055	0.041	0.255	0.020	0.530
CO₂ gas flux as C	0.013	0.039	0.018	0.023	0.255	0.014	0.350
Calcite solid flux as C	0.004	0.000	0.002	0.000	0.000	0.002	0.004
Silica as Si flux	0.017	0.038	0.021	0.018	0.110	0.008	0.210
Si/C molar ratio	0.330	0.240	0.280	0.280	0.220	0.220	0.230

This analysis also underscores the amplification of CO_2 levels from the atmosphere to groundwater via vegetation (Beerling & Berner, 2005; Berner, 1998). Globally, more than 90 percent of the groundwater acidity that drives rock weathering comes from CO_2 generated in the root, fungal, insect, and microbial respiration—a fact frequently left out of most descriptions of CO_2 feedback that implicitly assumes weathering is by atmospheric concentration of CO_2 . In fact, nearly all silicate weathering occurs in the vadose zone environment of aquifer systems, not in the atmosphere (Wood et al., 2024).

The separation of organic carbon from inorganic carbon discharged is of some interest and can be determined by the relative global molar flux of silica and carbon. That is, in looking at the carbon budget it is desirable to know the mass of current active organic carbon and that that is from the inactive carbon mineral pool. (Table 20 shows a groundwater mass flux of 0.21 PgSi/y or 0.0073 Pmols Si/y (Petamoles of silica per year) and 0.88 PgC/y (the sum of the first three rows of Table 20) or 0.0733 PmolsC/y (Petamoles carbon per year). This observation suggests that 0.0073 PmolsC/y are generated in silicate weathering by carbonic acid (Equation 34) and half of the remaining carbon, or 0.0172 PmolsC/y, is generated from the weathering of inorganic carbonate minerals (Equation 33. Thus, the molar rock $\frac{\text{Si}}{\text{C}}$ weathering ratio is $(0.0073 \text{ Pmols Si/y} \div 0.0172 \text{ Pmols C/y})$ or 0.42.

We can further assess the carbon source as it is known that 0.0071 PmolsC/y are consumed in silicate weathering of 0.0071 PmolsSi/y. Of the remaining carbon (0.0653 Pmols C/y), half or 0.0327 Pmols C/y is inorganic derived from weathering of carbonate minerals. That is, approximately 55 percent of carbon discharged by groundwater is generated by recent organic carbon, and 45 percent is from legacy inorganic

mineral carbon. Other sources of carbon from weathering by sulfuric acid or dissolved organic carbon are small globally and neglected in this analysis.

6.4.2 Nitrogen in Global Groundwater

Global geogenic nitrogen concentration (approximately 0.22 mg/LN) has been controlled by natural biogeochemical cycles for billions of years of the Earth's history but has been significantly modified by anthropogenic activities associated with food production—both fertilizer and animal waste—human sewerage, and fossil-fuel combustion (Gruber & Galloway, 2008). Anthropogenic nitrogen in the Earth's terrestrial and aquatic ecosystems has affected human health, protein supply, the Earth's heat balance, and recreation. The formulation of public policy governing anthropogenic nitrogen requires a well-constrained mass-flux estimate from each of the global element pools (Rockström et al., 2009; Steffen et al., 2015). This alteration of the nitrogen cycle has dramatically modified the biogeochemical cycles in aquatic ecosystems and adversely impacted human health outcomes of methemoglobinemia in infants, colorectal cancer, thyroid disease, and neural tube defects (Galloway et al., 2004; Schullehner et al., 2018; Stayner et al., 2021; Ward et al., 2018).

The annual global mass flux of nitrogen from the global aquifer element pool to different hydro/climate ecosystems (Table 21), the storage mass, and the residence time of this nitrogen are addressed in this section; a map of modeled nitrogen (as N concentration) in the global freshwater aquifer pool is provided in Figure 147. A more detailed and complete evaluation of the nitrogen mass flux is given in Wood and others (2023).

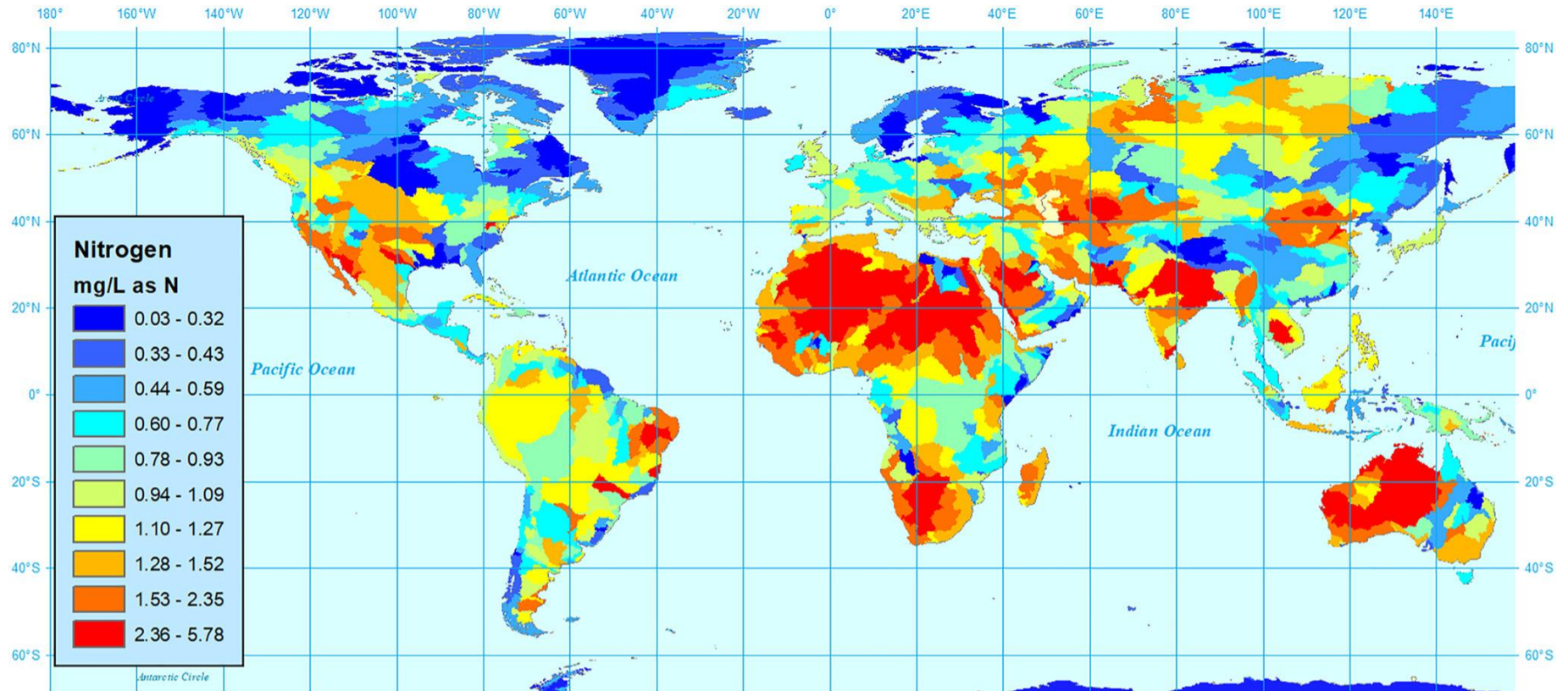


Figure 147 - Map of modeled nitrogen as N concentration in the global freshwater aquifer pool. Vertical scale degrees latitude, horizontal scale degrees longitude, and concentrations in mg/L are given by color (reproduced from Wood, Sanford, Cherry, & Wood, 2023).

Table 21 - Annual global aquifer mass flux of nitrogen for six groundwater discharge ecosystems, in Teragrams per year). The area of continents is calculated between 20°N and 20°S.

Environment	Direct to ocean	Endo-rheic	Exorheic				Global flux
			Cold dry	Warm dry	Cold wet	Warm wet	
Groundwater flux km ³ /y	610	820	1,080	1,793	1,440	10,100	15,850
Concentration mg/L	1.1	1.5	0.8	0.8	1.1	1.1	1.1
Mass flux Tg/y	0.67	1.2	0.82	1.4	1.6	11	17
% of global GW	4	5	7	11	9	64	100
% of mass flux	3	7	5	9	9	66	100
Area million km ²		26.1	7.3	43.1	27.9	30.4	135

Tg/y = Teragrams per year; GW = groundwater

Thus, the global groundwater mass flux discharge of nitrogen to the surface ecosystems is 17 TgN/y (Teragrams/year). In comparison, the surface water discharge of nitrogen from exorheic basins (integrated riverine system) during a similar time interval (2001 to 2010) is estimated to be between 40 TgN/y (Green et al., 2004) and 48 TgN/y (Boyer et al., 2006). With 17 TgN/y of that nitrogen flowing into the surface water system from groundwater discharge. The total mass of nitrogen discharged by surface water to the surface environment is somewhat greater than 40 to 48 TgN/y because the value of total nitrogen discharged by surface water needs to include both the additional 19 percent of the continents representing endorheic basins that contribute 1.2 TgN/y (Table 21) and the ≈4 percent of direct groundwater discharge that adds 0.67 TgN/y (Table 21), which sum to about 2 TgN/y. Thus, the total global nitrogen discharge from surface water ecosystems during this time interval is likely between 42 to 50 Tg N/y.

The mean nitrogen concentration in the global freshwater aquifer element pool is 1.1 mg/L as N, (Table 22), more than four times the estimated geogenic mean (0.22 mg/LN). This elevated concentration generates a mass flux of 17 Tg N/y (Teragrams of nitrogen, as N per year) to the surface ecosystems, thus it contributes 35 to 40 percent of the total nitrogen riverine mass flux. The nitrogen mass flux is expressed as the sum of six climate/hydrologic controlled ecosystems—direct ocean discharge (0.67 Tg N/y); endorheic basins (1.2 Tg N/yr); and the four types of exorheic basins—cold–wet (0.82 Tg N/y); cold–dry (1.4 Tg N/y); warm–dry (1.6 Tg N/y); and warm–wet (11 Tg N/y). An effective active freshwater aquifer volume of 1.3 million km³ was estimated from the change in recharge nitrogen concentration with time. The current global legacy nitrogen mass in the freshwater aquifer element pool is estimated to be 1.5 PgN to 4.7 PgN (Petagrams nitrogen as N) with a minimum mean residence time of approximately 140 years (Wood et al., 2023b).

In these analyses, it has been assumed that there is no reduction of nitrate and subsequent escape from the aquifer as nitrogen gas. On a global basis, this assumption is reasonable as the aquifer element pool has an average dissolved oxygen concentration of

1.8 mg/L (Wood et al., 2022), thus it is oxidizing and not conducive to a reduction of nitrogen solute to the gas phase. It is acknowledged, however, that there is certainly some loss to the atmosphere via reduction to a gas phase and subsequent outgassing to the atmosphere (Wood & Böhlke, 2017). Globally, this mass of nitrogen gas remains enigmatic and likely small. This illustrates one of the disadvantages of using the mass balance analysis versus the process-based analysis.

The use of steady-state analysis is justified by using a short time interval of 2001 to 2010—because the system is so large, the year-to-year changes are minimal. Using the average concentration—while not capturing the transient nature of the nitrogen recharge concentrations—provides realistic mass-flux limits and clarity of assumptions and allows assumed values to be inserted to test specific hypotheses quickly. This mass balance approach provides useful values and avoids the uncertainty of parametrization and phenomenological adjustments of many components in process-based numerical modeling in a highly heterogeneous natural system with extremely variable and poorly constrained inputs.

6.4.3 Groundwater Weathering of the Continents

Identifying and quantifying mass removed from the continents has been an Earth-science challenge since the conflict between the uniformitarianism of Hutton and Lyell and the catastrophism of Cuvier in the early nineteenth century. Charles Darwin (1859) used denudation rates to illustrate the Earth's great antiquity. The total global mass of rock that is removed from the continents in the form of bedload and suspended solids in rivers including anthropogenic impact is estimated to be 15 Pg/y (Petagrams per year; Milliman & Meade, 1983), and without anthropogenic input removal of rock from the continents has been estimated to be 12.6 Pg/y (McLennan, 1993). The total dissolved solids (TDS) removed from the continents by both groundwater baseflow and quick flow (rapid storm runoff) is estimated to be 3.9 PgTDS/y (Milliman, 2001), or ≈ 30 percent of the geogenic sediment transport.

The mass balance approach is used to reconsider the global estimate of dissolved solutes. The conceptual origin of these solutes is illustrated in Figure 148; the total solute flux, as well as the individual flux from the six different environments, is given in Table 22.

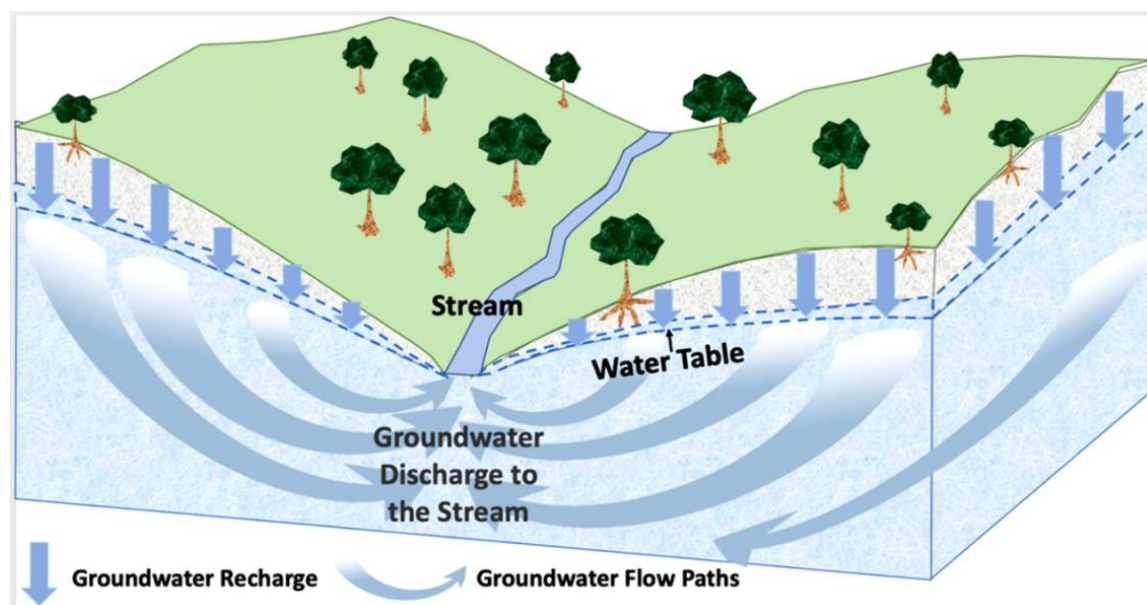


Figure 148 - A Conceptual three-dimensional regional flow of groundwater discharging to riverine systems that integrate the solute chemistry. Groundwater flow lines that meet at the stream have different lengths, each with a different residence time in the system (i.e., water age), solute concentration, and composition (modified from Poeter et al., 2020).

Table 22 - Fluxed-based concentrations modified from geospatial averages (Wood et al., 2022), area of basins (Lehner, 2014), water flux (Schmied et al., 2021), and mass flux of each major element in the aquifer element pool. TS (Total Solutes) is the sum of all solutes and differs from TDS (Total Dissolved Solids).

	Closed Basin	Cold Dry	Warm Dry	Cold Wet	Warm Wet	Direct Discharge	Global Total
Groundwater flux (km³/y)	820	1,795	1,445	1,085	10,100	610	15,850
Area (million km²)	26.1	43.1	27.9	7.3	30.4	–	135
Solute mass flux	Pg/y	Pg/y	Pg/y	Pg/y	Pg/y	Pg/y	Pg/y
Ca	0.041	0.115	0.071	0.060	0.434	0.029	0.745
Mg	0.020	0.041	0.027	0.022	0.141	0.010	0.269
Na	0.057	0.122	0.075	0.055	0.475	0.032	0.824
K	0.005	0.006	0.005	0.003	0.038	0.002	0.060
HCO₃	0.196	0.457	0.287	0.199	1.293	0.098	2.536
Cl	0.096	0.054	0.192	0.080	0.889	0.052	1.363
SO₄	0.112	0.210	0.085	0.068	0.313	0.032	0.824
Nitrogen as N	0.001	0.001	0.002	0.001	0.011	0.001	0.017
H₄SiO₄	0.058	0.130	0.075	0.061	0.380	0.027	0.732
Total Solutes	0.586	1.136	0.819	0.549	3.974	0.283	7.347

The global mass of solute discharged is 7.35 PgDS/y (Table 22) in contrast to the previous estimate of 3.9 PgTDS/y (Milliman, 2001). The mass of suspended sediments (SS) has been reported to range between 14.03 PgSS/y (Syvitski et al., 2005) and 12.6 PgSS/y (McLennan, 1993). Thus, the global mass solute discharge is between 52 and 58 percent of the suspended sediments. The 0.88 PgCaCO₃/y mass of calcite precipitated from the discharging groundwater needs to be subtracted from the total sediment transport—as this fraction (0.88 PgCaCO₃/y) was not generated by physical erosion but by precipitation from groundwater—thus, the percentage of solutes relative to suspended sediments is adjusted

and is between 56 to 63 percent. H_4SiO_4^0 was used in the mass flux model, which is the appropriate silica species for a pH less than 8 (Figure 46).

Some insight into the solute yield (mass/area) is acquired by evaluating the different climatic environments of groundwater solute discharge. The most significant solute flux per unit area (i.e., bottom row value of Table 22 divided by area given in the second row) is from the warm–wet environment, providing a yield of 0.13 Pg per million km^2 . The three environments with the lowest flux are the closed, cold–dry, and warm–dry basins with a yield of 0.02 to 0.03 Pg per million km^2 .

6.5 Section Wrap-up

These mass-flux models provide approximate limits on the solute discharge and are frequently an essential first step in more complex analyses of a system. In some cases, it may be sufficient just to know the total flux without details of the chemistry that is controlling the concentration in the element pool and to have insight and limits for more complex process-based calculations and solute transport models.

This type generalized thinking can be applied to problems large and small. A personal journey of this nature is presented in [Box 4](#)¹. It relates the story of how I set out to answer what seemed to be a simple question, albeit applied to the global scale but could just have well been a basin or site scale, and it took me on an unexpected journey.

7 Geochemical Evolution of Groundwater Solutes

When considering the chemical evolution of groundwater, both the groundwater flow and the chemical system are assumed to be in a steady or quasi-steady state—that is, not changing with time. However, on a local scale, the solutes change slowly with time and space. Thus, the chemical composition evolves along the flow paths within an aquifer.

Equilibrium concepts, however, play an essential role in the pursuit of understanding the chemical composition of groundwater at a point location because solute concentration changes very slowly at that point. This view of equilibrium can be thought of as disharmony, but it is a key part of the strategy for understanding the geochemical evolution of groundwater. Geologic time is too long to be relevant to society's current issues about groundwater quality. However, in some cases, what has happened over geologic time is essential to the explanation needed to address immediate societal problems. It is possible to gain insight into what has occurred over time by substituting solute changes with distance along the flow direction at present, with time, to visualize solute changes through geologic time. Along a flow path, one can see the aquifer zone where reactions have gone to completion, a zone where the solute changes are occurring, and a zone in which reactions have yet to occur.

This evolutionary view holds that as groundwater moves along its flow path and increases in age, the ions evolve in relative abundance and ratios corresponding to the three general hydrogeochemical zones (i.e., reactions that are complete, underway, or yet to occur). When space is substituted for time, it is implied that the hydrogeochemical processes and conditions, including aquifer composition and climate, are sufficiently uniform that we can extrapolate back in time. As science is about predicting the future, knowledge of how a system has evolved to its present condition can provide some confidence in predictions of how it will evolve in the future.

In contrast, nearly all groundwater flow systems achieve a steady state quickly after geological processes form the landscape. There are, however, climate cycles—like those associated with the glacial eras—that change the input of both water and solutes on scales less than the age of the water in some aquifers, particularly in arid regions.

To describe a system, one first attempts to construct a steady-state solute mass-balance model using the RCV (Representative Control Volume) concept described in Section 6. If justified by the data, a more sophisticated and constrained one-dimensional flow transport model of the system can be constructed. With additional data and carefully defined boundary and initial conditions, these models can be expanded to two- or three-dimensional transient conditions with process-based equations that represent an existing groundwater system within a mathematical construct.

The approach used in this monograph is a first approximation, also known as a back-of-the-envelope calculation, intended to get a sense of the processes and perhaps to

determine where critical data are missing; it is not a complete quantitative evaluation. In general, recharge from rainfall in freshwater aquifers enters the subsurface containing the solutes from rainfall. It then acquires additional solutes from the solution of minerals in the vadose zone mineralogic framework, and in some cases acquires solutes from legacy sources. The dissolution process continues until all soluble minerals and legacy solutes are removed, and their solutes are transported out of the system. The full extent of solution and transport occurs over thousands to hundreds of thousands of years. It is a function of mineral solubility, recharge flux, hydraulic conductivity, and hydraulic gradient of the aquifer that determines the number of pore volumes of water that need to be recharged to fully dissolve and transport solutes out of an aquifer.

In general, the hydrogeochemical evolution of solutes occurs as water moves from recharge to discharge. It is divided into three general hydrogeochemical zones (Figure 149):

1. the recharge zone,
2. the regional flow zone, and
3. the discharge zone,

where different hydrogeochemical processes dominate in each of the three zones.

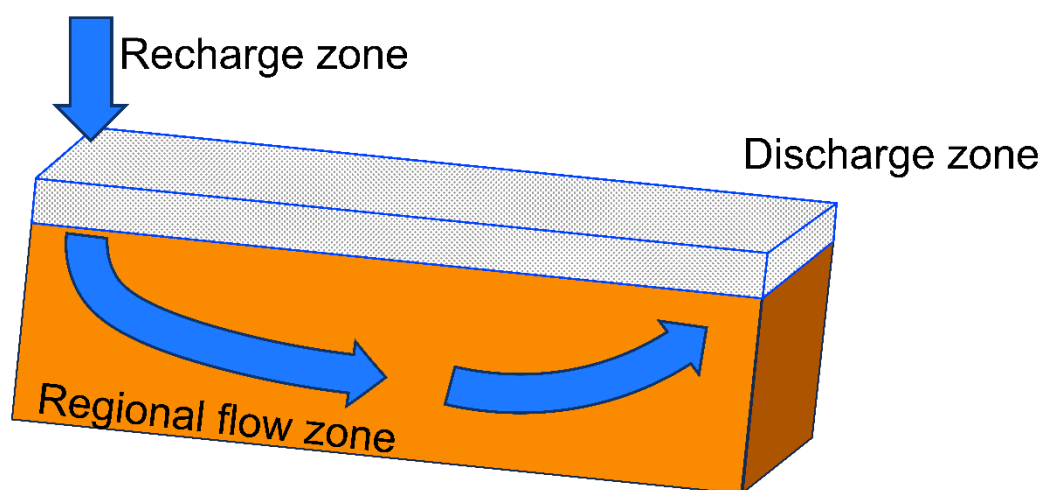


Figure 149 - A diagram illustrating the three generalized hydrogeochemical zones of solute evolution of groundwater: recharge, regional flow, and discharge zones.

As the water and solutes enter the soil zone, evaporation and plant transpiration remove water, thus concentrating the solutes from precipitation. In the soil zone, some nutrients—particularly nitrogen, phosphate, and potassium—are removed (Figure 150). As the water moves through the vadose zone (including the soil zone), it encounters elevated concentrations of carbon dioxide gas that are ten to a hundred times greater than in the atmosphere owing to the oxidation of organic material by root, insect, and bacterial respiration. The carbon dioxide dissolves in the water, forming carbonic acid and making the water acidic, which then dissolves minerals of the aquifer framework. Ecologists refer to this area as the *critical zone*. It is where there is an active biological community and where most of the mass of solutes enters the groundwater. This “critical” characterization,

however, misses many of the other vital reactions controlling or modifying the solute composition and ratios that occur throughout the flow path. This zone is much less chemically critical in a mature aquifer system that is dominated by a combination of solute sources along the flow path and relic solutes.

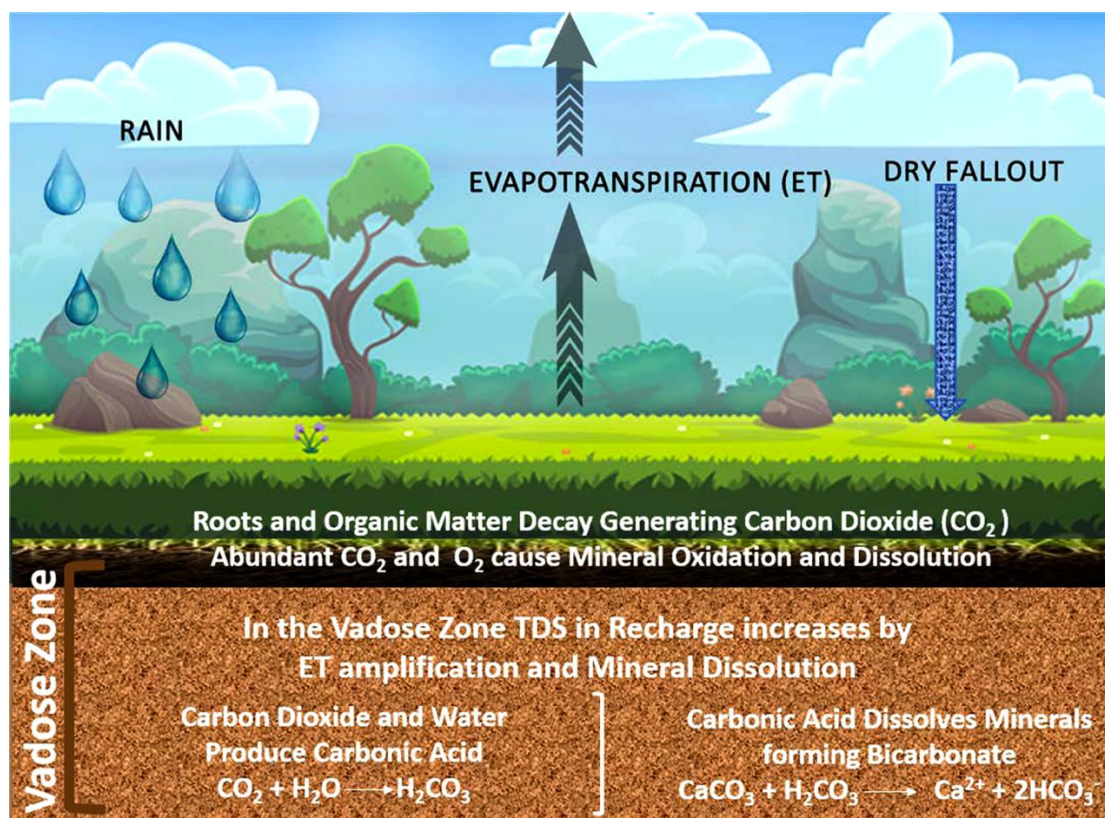


Figure 150 - The recharge zone is active geochemically because of the generation of carbonic acid that enhances mineral solution, resulting in the solution of minerals and generating bicarbonate and cations such as Ca²⁺. Typically, over 50 percent of total solutes are added from carbonic and sulfuric acid reactions occurring in the vadose zone during the recharge process (reproduced from Poeter et al., 2020).

Next, the solutes enter the second hydrogeochemical zone, the regional flow zone, and move along the flow path toward the discharge zone with, typically, modest increases in the ionic concentration and changes in ionic ratios. Additional solutes are generated by hydrolysis weathering, diffusion of relic solutes from aquitards, and advection from underlying and overlying formations. As there is typically little mineral dissolution, observation of solutes in this regional flow zone enhances the awareness of any ion exchange, sorption, radioactive decay, or ultrafiltration processes that are occurring in the system.

The third and final zone of the hydrogeochemical evolution occurs as groundwater approaches the discharge area. If groundwater discharges directly into a lake, stream, marsh, or ocean, then the groundwater loses carbon dioxide to the atmosphere, precipitates calcium carbonate, and elevates the pH, but little additional hydrogeochemical evolution will occur. If, however, it is discharged to a closed basin or a locale with a shallow water table—as in an arid or semi-arid areas where evaporation exceeds precipitation—solute

can concentrate thousands of times, and salinization of the groundwater may occur with calcium carbonate, dolomite, gypsum, anhydrite, halite, trona, and other minerals precipitating. In this environment, where evaporation exceeds precipitation, brines, saline lakes, and saline soils form.

One can see similar evolution by varying the rate of groundwater flow or by varying reaction rates. That is, a slow flow rate may produce the same solute distribution as a rapid reaction rate thus, the model is not unique (Figure 151).

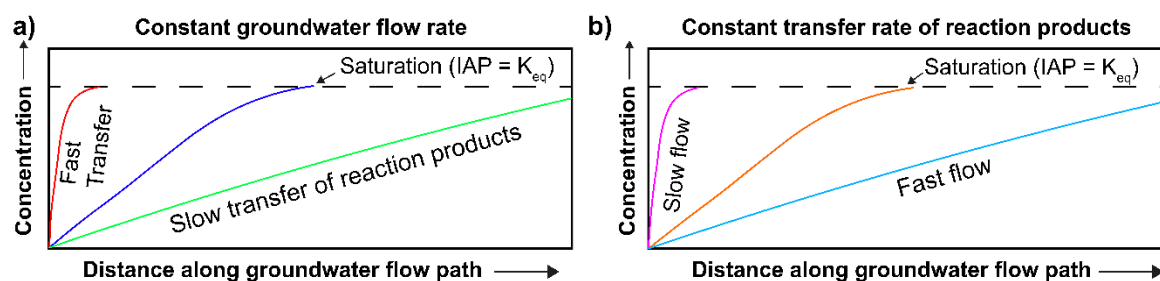
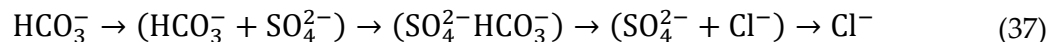


Figure 151 - Schematic diagram showing the calculated flushing of solutes from an aquifer by a) varying the reaction rate or b) varying the groundwater flow rate (modified from Freeze & Cherry, 1979).

The following discussion provides some simplified conceptual models for solute evolution (Palmer & Cherry, 1984), as shown by Equation (37), in which bicarbonate (HCO_3^-) is typically the first major ion that is found along the flow path, followed by sulfate (SO_4^{2-}), and finally by chloride (Cl^-).



This equation is somewhat misleading in that it represents a combination of mixing and chemical reactions. This relation was recognized by Chebotarev (1955) and Schoeller (1956) then utilized graphically by Back (1960, 1966) with the concept of *hydrogeochemical facies* in which a set of facies is defined by the combination of dominant cations or anions (Figure 152).

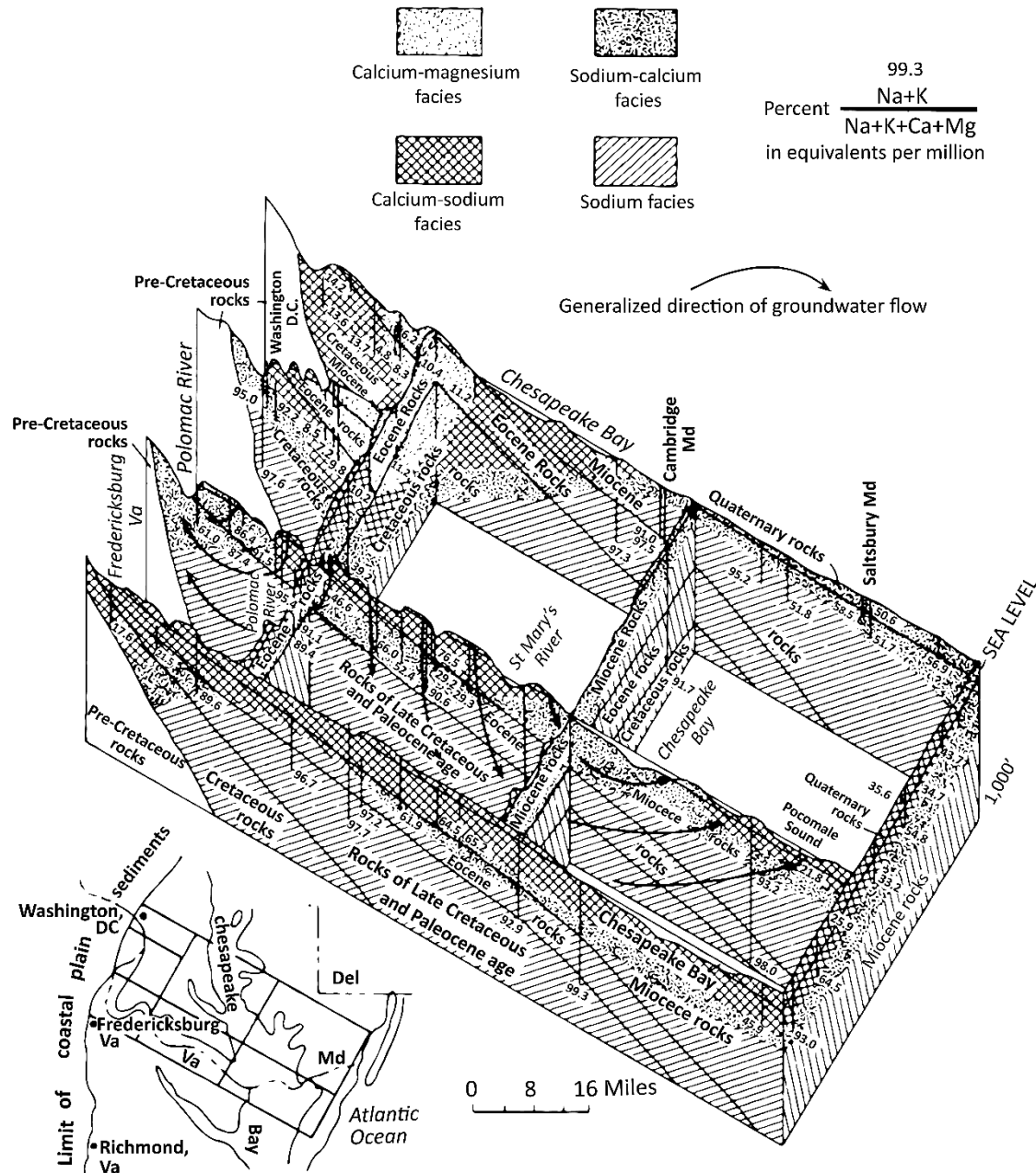


Figure 152 - Geochemical fence diagram illustrating different solute facies in the aquifer framework of the coastal plain area of the northeastern US as a function of flow (Md = state of Maryland, DC = District of Columbia, VA = state of Virginia, Del = state of Delaware; reproduced from Back, 1966).

Trilinear plots of solute ratios are frequently used (Section 4) in conjunction with these diagrams. These hydrogeochemical facies maps integrate the geochemical processes and the groundwater flow patterns. The geochemical evolution of the groundwater is then described in terms of moving from one hydrogeochemical facies into another.

7.1 Evolution of Sulfate from Dissolution of Gypsum

How much time is required for the geogenic solutes to evolve from a newly created landscape? First, we envision an RCV as 1 kilometer-long by 1 m wide by 1 m high with an effective porosity of 20 percent ($0.2 \text{ m}^3/\text{m}^3$). Next, we envision groundwater flow to be

driven by a recharge flux of 0.1 m per year ($0.1 \text{ m}^3/\text{m}^2/\text{y}$), thus $100 \text{ L}/\text{m}^2/\text{y}$ is entering the 1 m^2 inflow face of the RCV. If the groundwater moves like a piston (i.e., as plug flow) through the RCV, and the porosity is 100%, then 1 year of recharge would push groundwater out of the first 0.1 m^3 of the RCV. However, given the 20 percent porosity, the annual recharge contribution results in a plug of groundwater flow that displaces groundwater over a distance of $0.5 \text{ m}/\text{y}$ along the groundwater flow path, that is determined as $0.1 \frac{\text{m}^3}{\text{m}^2 \text{y}}$ divided by $0.2 \frac{\text{m}^3}{\text{m}^3} = 0.5 \frac{\text{m}}{\text{y}}$. Thus, the movement of one pore volume (pv) of groundwater the recharge location to the discharge location along the one-kilometer-long RCV requires 2,000 years ($1,000 \text{ m} / 0.5 \text{ m}/\text{y}$). Knowing that flushing of one pore volume takes 2,000 years, and knowing that the system is 11,000 years old, then 5.5 pv (pore volumes) have been discharged (i.e., $11,000 \text{ y} / 2,000 \text{ y}/\text{pv} = 5.5 \text{ pv}$) since the system formed. This system is typical of many non-indurated aquifers created by glaciers that left the landscape exposed to rainfall/recharge beginning at the end of Pleistocene time 11,000 years ago. A schematic of plug flow is shown in Figure 153.

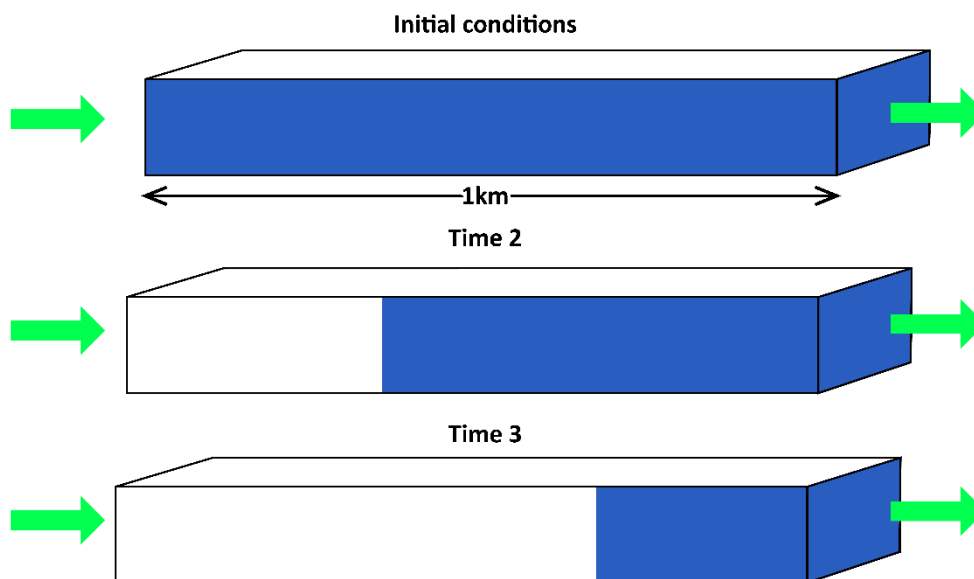
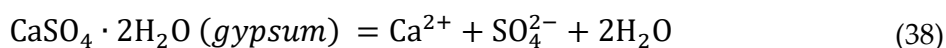


Figure 153 - Plug flow—i.e., no hydrodynamic dispersion—dissolution of gypsum associated with increasing pore volumes over time in the evolution of this system. The solid blue represents the initial condition with gypsum; the light blue represents the removal of gypsum.

If the system is at $25 \text{ }^\circ\text{C}$, has a typical aquifer bulk density of $1,600 \text{ kg}/\text{m}^3$, and contains gypsum ($\text{CaSO}_4 \cdot 2\text{H}_2\text{O}$) that is uniformly distributed in the amount of 1 percent by weight, then each cubic meter of the formation contains $16 \text{ kg}/\text{m}^3$ of gypsum (i.e., $(0.01) 1600 \text{ kg}/\text{m}^3$). In an aqueous medium, gypsum will dissolve by hydrolysis into calcium and sulfate ions, as shown by Equation (38).



Gypsum is a moderately soluble mineral with a solubility of approximately $2 \text{ g}/\text{L}$ (Table 6); thus, a water flux of $100 \text{ L}/\text{y}$ can remove $200 \text{ g}/\text{y}$. Given that there are 16 kg (i.e.,

16,000 g) of gypsum in each cubic meter of bulk material, it will take 80 volumes of recharge ($16,000 \text{ g/m}^3 / (200 \text{ g/y})$) to remove the gypsum from one cubic meter of geologic material. The control volume contains 1,000 cubic meters; thus, it would take 80,000 years to remove the gypsum from the control volume (Figure 153).

In Figure 153, solute dissolution along the flow path is illustrated as occurring by plug flow. In a more realistic system hydrodynamic dispersion would spread the zone of active solution of gypsum over a greater area, such that the removal would not create an abrupt change from completely dissolved to no gypsum dissolved, instead a smeared tail would follow the front (Figure 154).

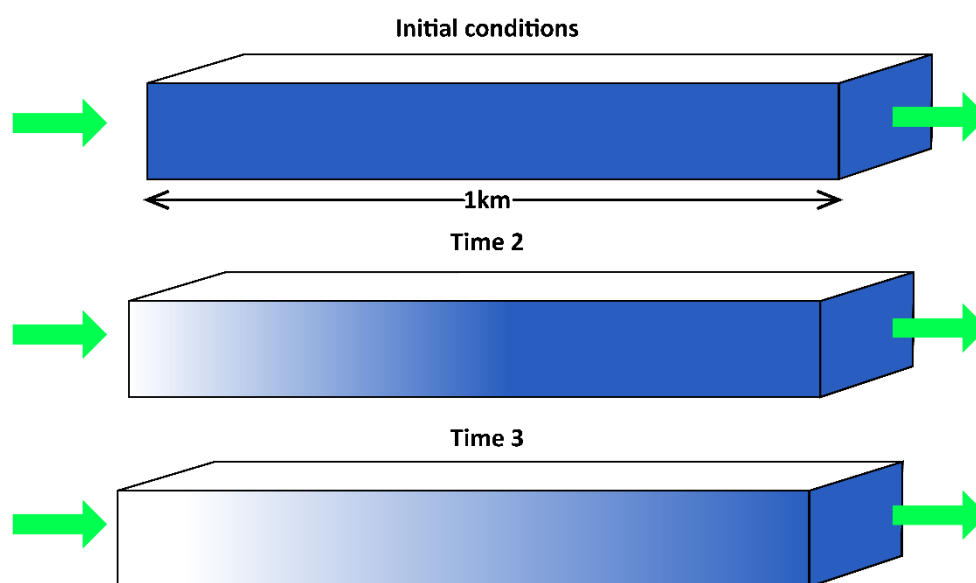


Figure 154 - The distribution of gypsum dissolution is smeared in field systems due to hydrodynamic dispersion. This figure is the equivalent of Figure 153 in a more realistic system where hydrodynamic dispersion occurs.

7.2 Cation Exchange

If the same RCV used in the gypsum model discussed in Section 7.1 with the same water flux of 100 L/y contains 1 percent marine clay by weight and the cation exchange sites are filled with Na^+ ions, Ca^{2+} and Mg^{2+} ions in the solution will be exchanged for Na^+ ions on the mineral surfaces as the water and solutes are transported along the flow path. The cation exchange capacity (CEC) is typically measured in moles of electric charge per mass of geologic material (cmoles/kg), thus a material with a cation-exchange capacity of 10 cmoles/kg could hold 10 moles of Na^+ per kilogram because it has an ionic charge of +1, but only 5 moles of Ca^{2+} because it has an ionic charge of +2.

Given the small clay concentration of 1 percent by weight (i.e., 16 kg for each cubic meter) then if the clay has a CEC of 6 cmoles/kg filled with Na^+ ions, each cubic meter of the RCV has 96 cmoles/m³ (i.e., $6 \times 16 = 96$) of exchange capacity. If it is assumed that the recharge water has a Ca^{2+} concentration of 50 mg/L, then, given that one mole is 40,078 mg of Ca^{2+} ions, the recharge water contains 1.25×10^{-3} moles/L Ca^{2+} (i.e., 50 mg/L divided by

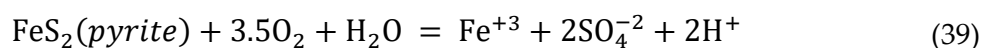
40,078x10⁻³ mg/L per mole. Given that the calcium ion has a +2 charge, thus there are 48 cmoles (i.e., 96 cmoles / 2 charges = 48) of exchange capacity available for divalent calcium in each cubic meter. Thus, satisfying the exchange capacity requires 38.5x10³ L of recharge (48cmoles/1.25x10⁻³ moles Ca²⁺). As the recharge rate is 100 L/y it requires 385 years = (38.4x10³ L)/(100 L/y) to exchange the Ca²⁺ in solution for Na⁺ on the clay for one cubic meter or 385,000 years for the exchange to take place throughout the entire RCV.

This model is a vast oversimplification as it has been assumed no other divalent ions are in the solution and the exchanged sodium ion will increase in concentration and it will compete with the calcium ions. Cation ion exchange is more complicated than just the exchange of ions, as it changes the calcium carbonate equilibrium. Removing Ca²⁺ from the solution by exchange creates a disequilibrium with the calcite system, causing additional calcite to dissolve, adding Ca²⁺ and HCO₃⁻ to the solution. The additional calcium is exchanged, dissolving more calcite, and further driving the development of a NaHCO₃ type of water, as shown in the fence diagram of Figure 152. This process also increases the pH as the hydrogen is consumed in dissolving the additional calcite. Sodium bicarbonate minerals are highly soluble and are not generally precipitated in this environment; thus, sodium and bicarbonate can continue to increase to a rather large concentration of thousands of milligrams per liter.

The chemistry and flow system have been simplified to illustrate the time involved in the evolution of solutes. For example, the system is sensitive to pH as the H⁺ ion is a cation; thus, the H⁺ ions compete with other cations at each site as the pH changes. If seawater intruded into an aquifer formed in a terrestrial environment with the exchange sites initially filled with Ca²⁺ ions, a different scenario would develop with Ca²⁺ ions pushed into solution where they precipitate in calcite. Many competing factors occur in ion exchange, and numeric modeling is necessary for more sophisticated analysis. However, this back-of-the-envelope model provides some insight into solute evolution with time.

7.3 Pyrite Oxidation

Sulfuric weathering accounts for approximately 2 percent of the solutes in a typical groundwater analysis (Wood et al., 2024), but is important in some groundwater systems containing pyrite. Considering the RCV discussed earlier with the same water flux and aquifer bulk density of 1,600 kg/m³ and containing 0.1 percent weight percent pyrite (FeS₂) (1.6 kg/m³) or 13.4 moles, the solubility is controlled by the mass of oxygen that can be transported through the system. This reaction is shown in Equation (39).



Equation (39) shows that 7 moles of oxygen are required to oxidize 1 mole of pyrite; thus, 93.8 moles of oxygen are needed to oxidize the 13.4 moles of pyrite in one cubic meter of the RCV (7 mO₂)(13.4 mFeS₂). As it takes 7 moles of oxygen for every mole of pyrite,

93,331 moles of oxygen are needed to oxidize the pyrite in a cubic meter of the control volume. With an average O_2 concentration of approximately 5 mg/L, O_2 (0.005 g/L)/(32 gO/m) or 0.000156 mO/L, there is limited dissolution of pyrite. For example, if 100 L/y are recharged, then 0.0156 mO/y are entering the system. Thus, it requires 859 years (13.4 m/0.0156 m/y) to remove pyrite in 1 cubic meter or 859,000 years to remove pyrite from the RCV.

7.4 Molecular Diffusion in Solute Evolution

Several aspects of diffusion are important in groundwater: one involves liquid to liquid (Figure 155), one is involved with solid to liquid, and one involves liquid to solid (Figure 156). The liquid-to-solid type of diffusion (Wood et al., 1990) occurs as the solute in the active pore spaces moves into blind pores, fractures in the rock matrix, crystal boundaries, and along mineral cleavage. For example, a solute such as a tritium (3H) ion induced by thermonuclear atmospheric testing in the mid-1950s can diffuse into the rock matrix, decreasing the concentration in the active pore spaces below what one would expect based on input activity and radioactive decay. Similarly, chlorofluorocarbons introduced to the atmosphere in the late 1930s can diffuse into the aquifer matrix, which reduces the concentration in water samples from the fractures. That is, a concentration gradient for these solutes exists between the solutes in the active flow system and the blind (e.g., dead end) pores, causing the tritium, chlorofluorocarbon, or other substances not ordinarily present to be transported by diffusion into the matrix, thus decreasing the concentration in the active pore space. Liesegang bands—zones of increased ferric hydroxide—are commonly found near fractures (Figure 156) and are formed by oxygen in the pore water diffusing into the rock matrix and reacting with ferrous iron to form ferric hydroxide.

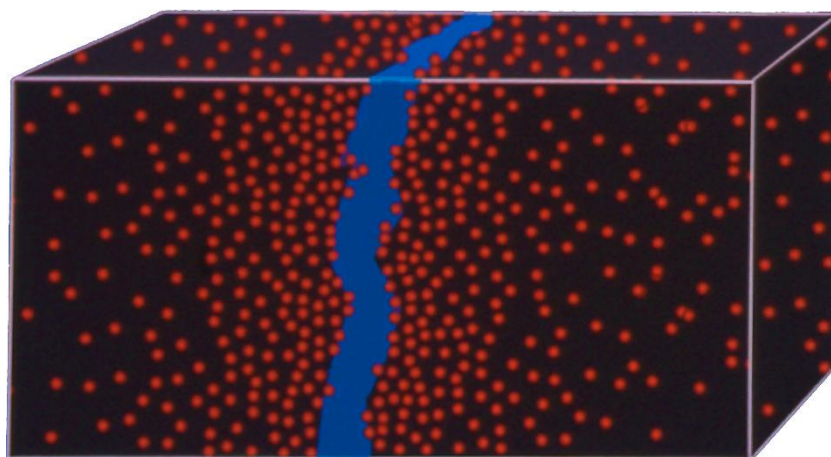


Figure 155 - An illustration of solute diffusion (orange dots) from a liquid in the fracture (blue) into the surrounding rock.

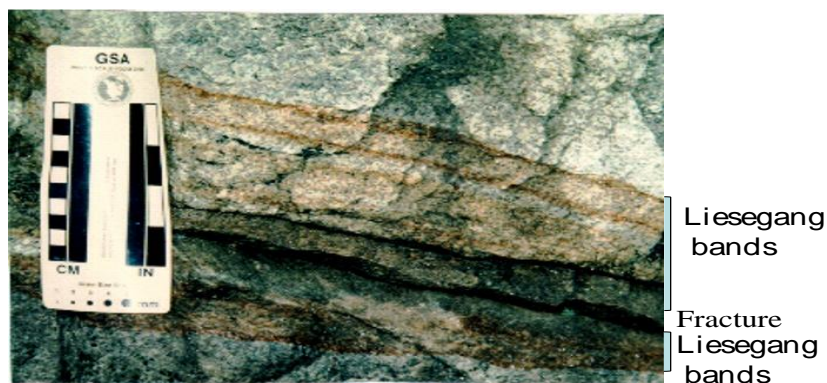


Figure 156 - Bands of orange ferric hydroxide $\text{Fe}(\text{OH})_3$ in a fractured granite providing a visual example of solute diffusion between liquid groundwater that supplies the oxygen and the solid rock matrix that provides the iron.

Solid-to-liquid diffusion occurs when a solute is generated in the solid that is not present in the surrounding pore water. For example, consider radium-226 which is generated in the uranium-238 decay series. As radium-226 ion is generated in the mineral framework, it migrates in response to the diffusion gradient towards the lower concentration in the pore water. Iron hydroxide in Liesegang bands will sorb radium-226 and radium-226 will decay to radon-222. Thus, these bands provide a source for the short-lived radon-222—with a half-life of 3.8 days—close to the active fracture that supplies water to a well and explain the commonly observed high concentration of radon-222 in groundwater with low to modest uranium concentration in the rock matrix (Wood et al., 2004).

An example of liquid-to-liquid diffusion is a conservative non-reacting solute such as chloride diffusing upward from a shale through an overlying sandstone aquifer into a glacial outwash aquifer (Figure 157). A steady concentration gradient exists across the sandstone (between the shale and the outwash) because the diffusing chloride is swept away by a high velocity of flow in the permeable, gravel glacial outwash that overlays the sandstone aquifer and maintains a constant 1 mg/L at the top of the sandstone (Figure 157). The top of the shale at the sandstone boundary always has a chloride concentration of 50,000 mg/L (i.e., 5×10^7 mg/m³) as maintained by the dissolution of halite in the shale.

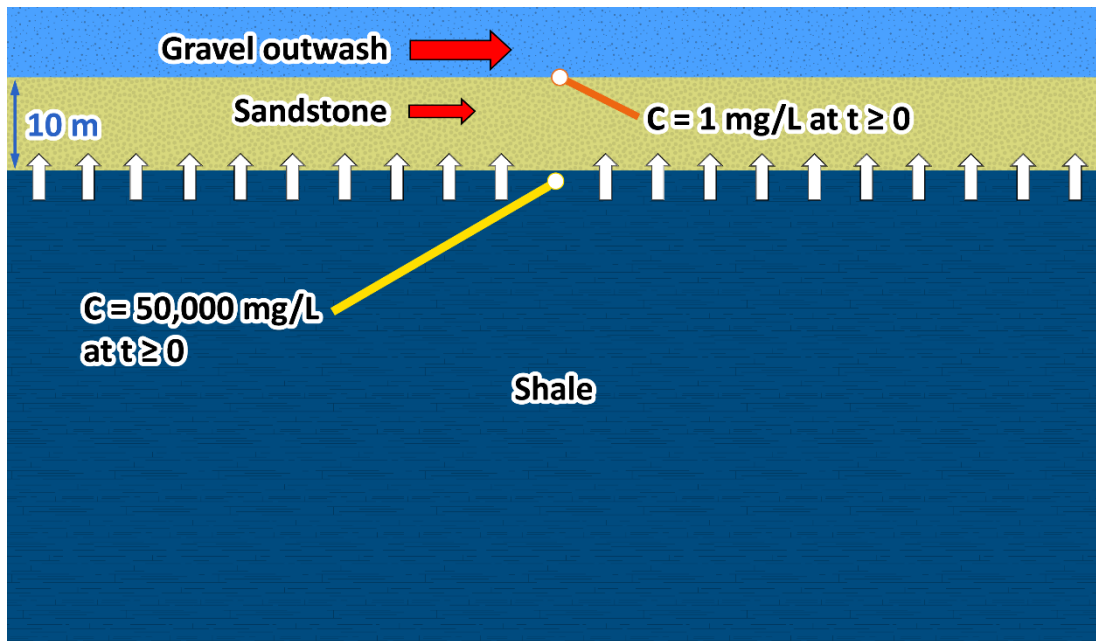


Figure 157 - A steady state, one-dimensional application of Fick's First Law of diffusion to a hydrogeologic system with a boundary condition of constant chloride concentration of 50,000 mg/L in the shale at the sandstone/shale interface and a constant concentration of 1 mg/L in the gravel at the sandstone/gravel interface because rapid lateral flow in the outwash flushes the Cl^- .

Flow in the sandstone is slow and diffusion continues all along the flow path thus the vertical distribution of chloride across the sandstone is controlled by vertical diffusion through the sandstone. With these boundary conditions and the assumption of steady state conditions, one can make a one-dimensional, steady-state calculation of the mass flux of chloride diffusing from the shale into the outwash using Fick's First Law of diffusion.

Fick's law states the mass flux (J) leaving the surface of the shale is a function of the diffusion coefficient (D) and concentration gradient—the change in concentration of a solute with distance ($\frac{dC}{dx}$) is expressed mathematically as Equation (40). The negative sign indicates solute movement is from higher to lower concentration.

$$J = -D^* \frac{dC}{dx} \quad (40)$$

where (parameter dimensions are dark green font with mass as M , length as L , time as T):

- J = mass flux ($\text{ML}^{-2}\text{T}^{-1}$)
- D^* = effective diffusion coefficient that accounts for the physical conditions of the media such as porosity and tortuosity (that is, the winding path a solute takes in moving through a porous medium) (L^2T^{-1})
- dC = change in concentration (ML^{-3}) where d is the mathematical notation for change over a small distance
- dx = change in distance x (L), where d is the mathematical notation for change over a small distance

To determine the steady-state diffusive flux for conditions shown in Figure 157, using a reasonable effective diffusion coefficient D^* of $1 \times 10^{-11} \text{ m}^2/\text{s}$ for the sandstone, first D^* is converted to years, knowing there are 31,536,000 seconds in a year, accordingly, D^* is $3.15 \times 10^{-4} \text{ m}^2/\text{y}$. The flux is then D^* multiplied by the concentration gradient. The concentration gradient across the sandstone varies linearly from 50,000 mg/L at its base to 1 mg/L its top, 10 m above the base ($5 \times 10^7 \text{ mg}/\text{m}^3$ to $1000 \text{ mg}/\text{m}^3$).

$$J = - \frac{3.15 \times 10^{-4} \text{ m}^2}{\text{yr}} \frac{\left(5 \times 10^7 \frac{\text{mg}}{\text{m}^3} - 1,000 \frac{\text{mg}}{\text{m}^3} \right)}{10 \text{ m}} = 1,577 \frac{\text{mg}}{\text{m}^2 \text{ yr}}$$

An equivalent amount of sodium is also added to maintain the electrical balance. However, Na is not conservative and may react and be removed from the solution by mineral precipitation, cation exchange, sorption, or other processes.

If the shale did not contain halite such that there was no opportunity to maintain the concentration in the shale, then a non-steady condition would occur and the chloride concentration would gradually decrease with distance into the shale from its boundary with the sandstone as chloride is lost by diffusion into the sandstone. This transient condition is expressed by Fick's Second Law, which evaluates the change in concentration (C) with both time $\left(\frac{\partial C}{\partial t}\right)$ and distance $\left(\frac{\partial^2 C}{\partial x^2}\right)$ as shown in Equation (41).

$$\frac{\partial C}{\partial t} = D \frac{\partial^2 C}{\partial x^2} \quad (41)$$

The Fick's Second Law is expressed using a partial differential equation as shown in Equation (41). It addresses the condition of a declining concentration of C over the time interval t at a distance x , and results in the intimidating-looking analytical expression given by Equation (42).

$$C = C_0 \operatorname{erfc} \left(\frac{x}{\sqrt{2D^*t}} \right) \quad (42)$$

where (parameter dimensions are dark green font with mass as M, length as L, time as T):

C	concentration at a specific x location at time t (M/L^3)
erfc	complementary error function
C_0	initial concentration at $x = 0$ and $t = 0$
D^*	effective diffusion coefficient defined by Fick's First Law shown by Equation (40) (L^2T^{-1})

The complementary error function (erfc) provides a numerical value resulting from the solution of an integral equation for the value within the parentheses (it is a function as a log or sine is a function). Values of the error function are given in Table 23.

This equation is often written as $C = C_0 \operatorname{erfc}(z)$, where z equals the numerical value of $\left(\frac{x}{\sqrt{2Dt}}\right)$. The numerical value for z is calculated, then the first digit of that value is found on the left edge of Table 23 and the hundredths place of the value is found across the top, then the *erfc* value is where that row and column intersects within the body of the table—values range between 0 and 1. When calculating the value for z , it is essential that the units of time and distance are consistent—mixing units such as seconds and years or cm and m will produce erroneous results.

Table 23 - Values of the complementary error function.
$$erfc(z) = \frac{2}{\sqrt{\pi}} \int_z^{\infty} e^{-t^2} dt$$

Hundredths Digit of z										
z	0	1	2	3	4	5	6	7	8	9
0.0	1.00000	0.98872	0.97744	0.96616	0.95489	0.94363	0.93238	0.92114	0.90992	0.89872
0.1	0.88754	0.87638	0.86524	0.85413	0.84305	0.83200	0.82099	0.81001	0.79906	0.78816
0.2	0.77730	0.76648	0.75570	0.74498	0.73430	0.72367	0.71310	0.70258	0.69212	0.68172
0.3	0.67137	0.66109	0.65087	0.64072	0.6306	0.62062	0.61067	0.60079	0.59099	0.58126
0.4	0.57161	0.56203	0.55253	0.54311	0.53377	0.52452	0.51534	0.50625	0.49725	0.48833
0.5	0.47950	0.47076	0.46210	0.45354	0.44506	0.43668	0.42838	0.42018	0.41208	0.40406
0.6	0.39614	0.38832	0.38059	0.37295	0.36541	0.35797	0.25062	0.34337	0.33622	0.32916
0.7	0.32220	0.31533	0.30857	0.30190	0.29532	0.28884	0.28246	0.27618	0.26999	0.26390
0.8	0.25790	0.25200	0.24619	0.24048	0.23486	0.22933	0.22390	0.21856	0.21331	0.20816
0.9	0.20309	0.19812	0.19323	0.18844	0.18373	0.17911	0.17458	0.17013	0.16577	0.16149
1.0	0.15730	0.15319	0.14916	0.14522	0.14135	0.13756	0.13386	0.13023	0.12667	0.12320
1.1	0.11979	0.11647	0.11321	0.11003	0.10692	0.10388	0.10090	0.09800	0.09516	0.09239
1.2	0.08969	0.08704	0.08447	0.08195	0.07949	0.07710	0.07476	0.07249	0.07027	0.06810
1.3	0.06599	0.06394	0.06193	0.05998	0.05809	0.05624	0.05444	0.05269	0.05098	0.04933
1.4	0.04771	0.04615	0.04462	0.04314	0.04170	0.04030	0.03895	0.03763	0.03635	0.03510
1.5	0.03389	0.03272	0.03159	0.03048	0.02941	0.02838	0.02737	0.02640	0.02545	0.02454
1.6	0.02365	0.02279	0.02196	0.02116	0.02038	0.01962	0.01890	0.01819	0.01751	0.01685
1.7	0.01621	0.01559	0.01500	0.01442	0.01387	0.01333	0.01281	0.01231	0.01183	0.01136
1.8	0.01091	0.01048	0.01006	0.00965	0.00926	0.00889	0.00853	0.00818	0.00784	0.00752
1.9	0.00721	0.00691	0.00662	0.00634	0.00608	0.00582	0.00557	0.00534	0.00511	0.00489
2.0	0.00468	0.00448	0.00428	0.00409	0.00391	0.00374	0.00358	0.00342	0.00327	0.00312
2.1	0.00298	0.00285	0.00272	0.00259	0.00247	0.00236	0.00225	0.00215	0.00205	0.00195
2.2	0.00186	0.00178	0.00169	0.00161	0.00154	0.00146	0.00139	0.00133	0.00126	0.00120
2.3	0.00114	0.00109	0.00103	0.00098	0.00094	0.00089	0.00085	0.00080	0.00076	0.00072
2.4	0.00069	0.00065	0.00062	0.00059	0.00056	0.00053	0.00050	0.00048	0.00045	0.00043
2.5	0.00041	0.00039	0.00037	0.00035	0.00033	0.00031	0.00029	0.00028	0.00026	0.00025
2.6	0.00024	0.00022	0.00021	0.00020	0.00019	0.00018	0.00017	0.00016	0.00015	0.00014
2.7	0.00013	0.00013	0.00012	0.00011	0.00011	0.00010	0.00009	0.00009	0.00008	0.00008
2.8	0.00008	0.00007	0.00007	0.00006	0.00006	0.00006	0.00005	0.00005	0.00005	0.00004
2.9	0.00004	0.00004	0.00004	0.00003	0.00003	0.00003	0.00003	0.00003	0.00003	0.00002
3.0	0.00002	0.00002	0.00002	0.00002	0.00002	0.00002	0.00002	0.00001	0.00001	0.00001
3.1	0.00001	0.00001	0.00001	0.00001	0.00001	0.00001	0.00001	0.00001	0.00001	0.00001
3.2	0.00001	0.00001	0.00001	0.00000	0.00000	0.00000	0.00000	0.00000	0.00000	0.00000

For example, assume that the value calculated for z is 1.22. You would go down the left side of the table to a value of 1.2, then you move horizontally to the fourth column (2) and find the erfc value of 0.08447. The erfc value is then multiplied by the initial concentration (C_0) to calculate the concentration C at the specified time t and distance x used in calculating z.

Returning to the hydrogeologic environment, there is no salt in the shale to maintain a constant chloride concentration, so the chloride concentration in the shale declines with time (Figure 159). The nonlinear variation of concentration with time described by Fick's second law (e.g., Equation (42)) is used with these boundary and initial conditions to determine the concentration as a function of time 1 cm below the top of the shale as shown in Figure 159.

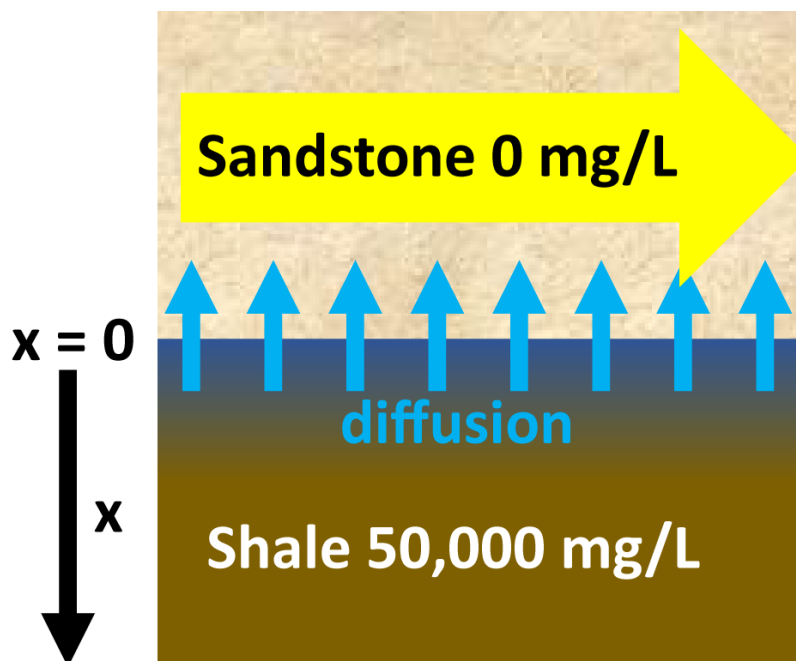


Figure 158 - The shale formation is envisioned as a semi-infinite material with an initial chloride concentration of 50,000 mg/L and lateral flow in the overlying sandstone maintains essentially zero concentration in the sandstone.

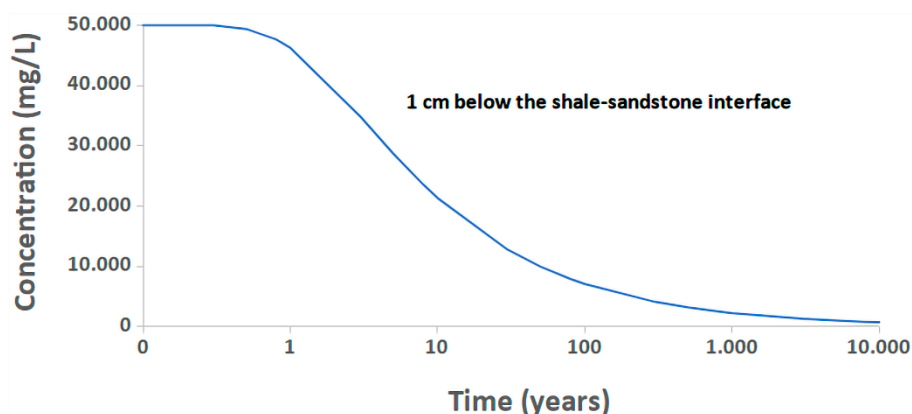


Figure 159 - Conceptual graph showing the nonlinear concentration decline described by Fick’s Second Law within the shale at a short distance (1 cm) from interface when dissolved solutes diffuse out of the shale into the sandstone and are swept away by flow in the sandstone, maintaining a zero concentration boundary conditions at the top of the shale.

One might ask how quickly will the concentration of chloride decline within the shale? Fick’s second law can be used to get a feel for the time frame of chloride diffusion from the shale by calculating the chloride concentration in the shale at different times and different depths, x , from the interface. Using Fick’s Second Law and a value of D^* that is an order of magnitude lower than the value in the sandstone ($3.15 \times 10^{-5} \text{ m}^2/\text{y}$) and an initial concentration of 50,000 mg/L throughout the shale, the decline in concentration with depth into the shale is displayed in Figure 160. From a hydrogeologic perspective, after 100,000 years, the chloride in the shale has been decrease to less than 1,000 mg/L at a distance of 1 meter into the shale, but at 5 and 10 meters it is still near 50,000 mg/L. This illustrates the long time-frame associated with diffusive processes.

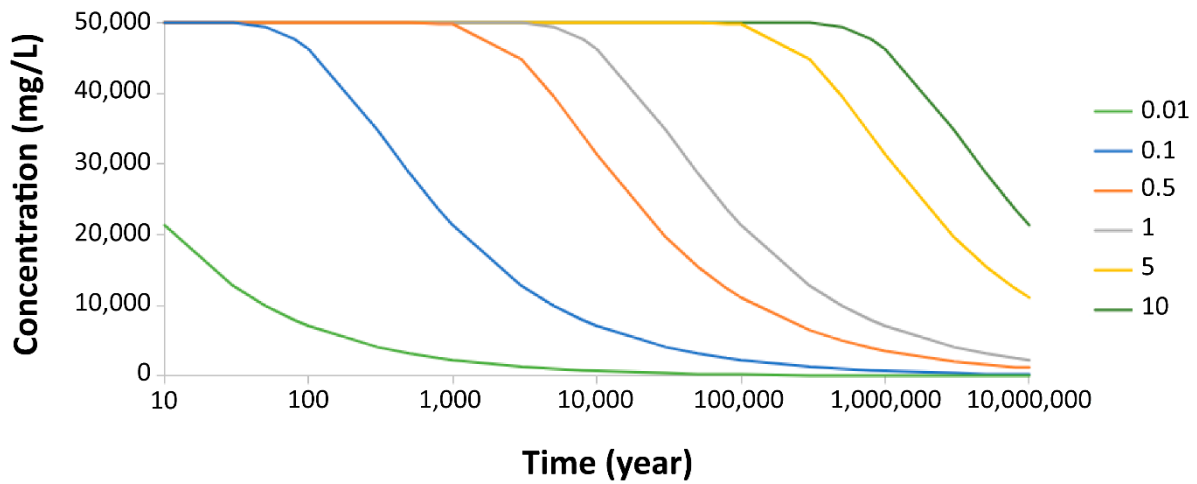


Figure 160 - Concentration with depth below the shale/sandstone contact of Figure 158 as chloride diffuses out of the shale into the sandstone and is swept away by lateral flow. In this case, x in Equation (42) represents the depth below the contact of the sandstone and shale.

7.5 Groundwater and Evolution of Karst Topography

A landscape with sinkholes, enlarged fractures, closed depressions, sinking streams, caves, and caverns resulting from chemical dissolution is known as a *karst* landscape, named after the Karst region in Slovenia and Italy, where the environment was first described. Unlike most aquifer evolutions, karst systems exhibit obvious topographic effects where occasional sinkholes swallow cars and houses. Various states of evolution can be observed, providing an excellent perspective on the karst evolutionary process.

Karst topography develops due to the chemical weathering of carbonate rocks by groundwater. Karst topography forms in soluble rocks, typically limestone, but to a lesser extent in dolomite (Figure 161 and Figure 162) and covers approximately 13 percent of the Earth’s land surface (Ford & Williams, 2007).

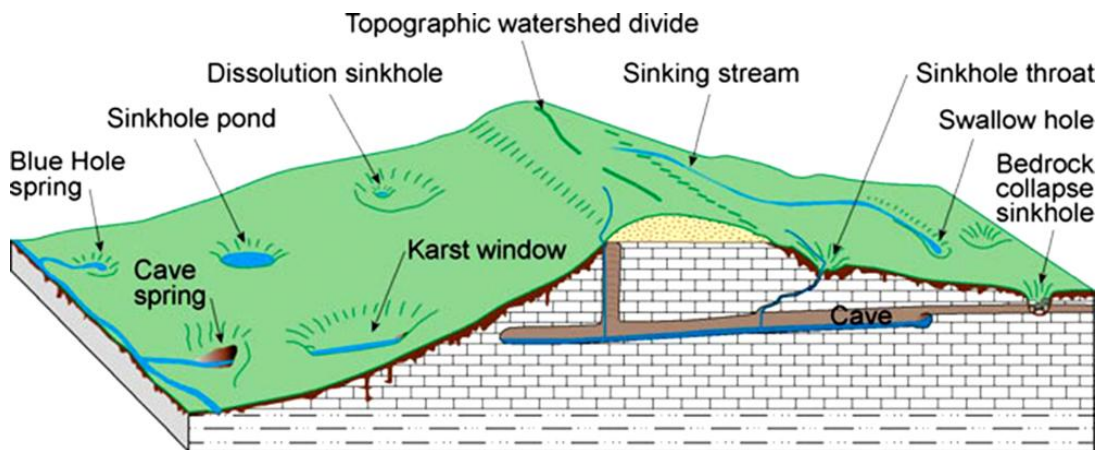


Figure 161 - Examples of karst features (Kentucky Geological Survey, no date provided)

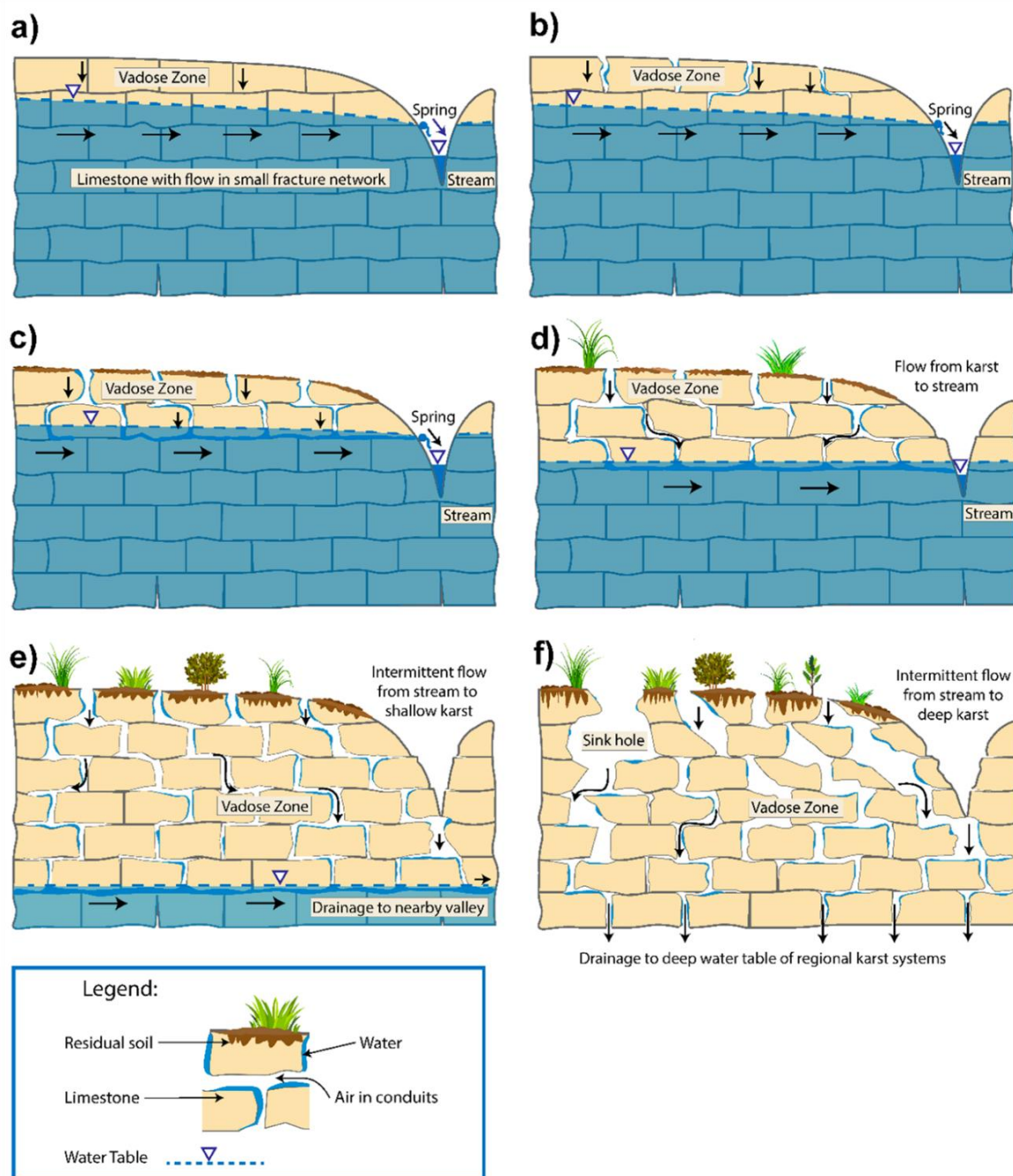


Figure 162 - The stages of karst aquifer evolution from a fractured flow system to a conduit flow system as a function of water table fluctuation: a) In the first stage, the limestone has small fractures that become enlarged by chemical weathering. b) In the second stage, some fractures have been enlarged but are insufficient to form a network of enhanced hydraulic conductivity, and, therefore, the rock does not yet have conduit flow. c) In the third stage, further dissolution has connected the enlarged fractures so that conduit flow begins. d) In the fourth stage, enlargement and interconnection have increased the hydraulic conductivity of the interconnected paths, and the water table declines. This lowering of the water table may be increased if it is accompanied by down cutting of streams in the area. e) In the fifth stage, a wetter period occurs, raising the water table and resulting in active conduit flow through the deep part of the vadose zone. f) In stage 6, the channel network drops below the local flow system with karst flow draining to a distant exit. The enlargement of karst channels is driven by chemically aggressive subsurface water, with its aggressivity continually renewed by the production and dispersion of CO₂ in the subsurface through the synergistic combination of hydrologic flow, downward erosion along surface stream channels and hydrogeochemical processes. (reproduced from Kuniandy et al., 2022). This physical explanation does not address the geochemical conditions necessary to dissolve the carbonates.

Typically, there is more than one episode of karst formation as climate and tectonic circumstances change over time, adding complexity to the development of a specific karst system. Comprehensive discussions of the processes of fracture enlargement and cave genesis based on hydrogeologic and geochemical concepts that involve complex interactions through time and space are given in Holland and others (1964), Thraikill (1968), Ford and Cullingford (1976), Ford and Williams (2007), Kuniansky and others (2022), and Stevanović and others (2024).

Consider initial conditions where groundwater originating as rainfall infiltrates through surficial soils and then flows through a network of fractures, joints, and bedding planes typical of carbonate rock. Although initially, the recharge water is thermodynamically undersaturated with respect to calcite (CaCO_3), it quickly attains equilibrium in the unsaturated zone and is incapable of additional solution. The most challenging problem in the origin of karst topography is to account for thermodynamically undersaturated water with respect to calcite or dolomite below the soil zone or upper part of the aquifer. Freeze and Cherry (1979) identified four general mechanisms that create thermodynamic undersaturation at depth:

1. decrease in groundwater temperature,
2. production of acid at depth,
3. floods in surface streams or rapid snowmelt causing exceptionally large rapid recharge of undersaturated water, and
4. mixing of dissimilar waters at fractures/joints.

It has proven challenging to generalize about the relative importance of these processes on a global scale.

In response to the suggestion of the production of acid at depth as a mechanism, Wood (1985) proposed that it resulted from groundwater transport of particulate and dissolved organic carbon deep in the aquifer system. It is relatively easy to transport particulate material in fractured carbonate. This transported carbon is oxidized to form CO_2 at depth and, thus, has the ability to provide an increasingly greater concentration of carbonic acid (H_2CO_3). The CO_2 establishes a CO_2 diffusion gradient in the vadose zone both to the surface and to the water table, following Fick's Laws of Diffusion. In general, as long as carbon is present in the vadose zone, CO_2 production occurs and, given the slow rate of CO_2 diffusion the concentration increases with depth, all other factors being equal. Thus, introducing even minute amounts of labile carbon transported deep in the unsaturated zone can result in CO_2 concentrations many tens of times greater than the atmosphere (Wood & Petraitis, 1984) and, importantly, increases with depth.

This is demonstrated by the model results shown in Figure 163. The model represents a permeable, homogeneous, unsaturated material of laterally infinite extent such that there is no lateral diffusion of gas. The upper surface is in contact with the atmosphere of constant and known CO_2 concentration with a steady recharge of water that carries

organic material to a depth L . Atmospheric oxygen diffuses into the vadose zone in response to a concentration gradient generated by the oxidation of the organic material. The resulting shape of the CO_2 profile was simulated for three different CO_2 flux conditions on the bottom of the simulated zone. Curve A represents the condition in which no CO_2 flux occurs through the bottom of the system. This condition might simulate a ground water in equilibrium with the CO_2 in the unsaturated zone at that depth, or a case in which the vadose zone is sealed at that depth (e.g., with caliche). Curve B represents a condition in which CO_2 is lost from the bottom of the system. This may simulate a case where CO_2 is lost to the ground water, or to the air in a cave that has an opening to the atmosphere. Curve C represents the condition in which CO_2 is added from the bottom. This might occur if CO_2 is degassing from groundwater; due to aerobic or anaerobic generation of CO_2 occurring in the groundwater, or CO_2 emission from the mantle or other deep-seated source.

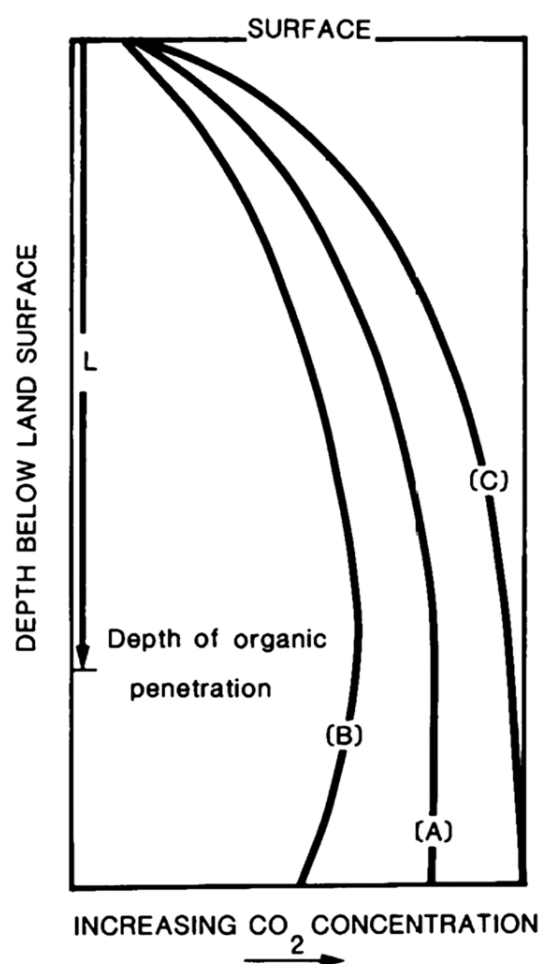


Figure 163 - Simulated, one-dimensional, steady-state profiles of CO_2 in a homogeneous vadose zone with constant input of labile organic carbon to the depth L . Curve A represents a sealed bottom with no CO_2 flux to the bottom. Curve B represents a case with CO_2 flux out of the bottom of the system and has the greatest amount of CO_2 lost to groundwater, while curve C receives input of CO_2 from the bottom of the system, thus has no CO_2 loss to the groundwater. The important observation is that, in all cases, CO_2 concentration increases downward to the depth of penetration of the organic material (reproduced from Wood, 1985).

The important observation is that, in all cases, CO_2 concentration increases downward to the depth of penetration of the organic material. Thus, recharging water encounters increasingly larger concentrations of CO_2 and becomes thermodynamically subsaturated and able to dissolve carbonate minerals at depth. Carbonate mineral precipitation can occur in the unsaturated zone under the condition postulated for curve B. In this case, recharging water that is in equilibrium with the CO_2 concentration and carbonate minerals at the depth L move downward into a part of the aquifer where the CO_2 concentration is less than that for which equilibrium has been established. Thus, the dissolved gases adjust to the new concentration and the water becomes thermodynamically supersaturated with respect to the carbonate minerals such that mineral precipitation can occur. The shape of the curves depend upon the amount and distribution of CO_2 production and empirical constants in the diffusion equation but are unimportant for this discussion. Owing to this CO_2 profile, water recharging through this environment encounters greater CO_2 concentration with depth; thus, it retains its undersaturated condition and ability to dissolve calcite.

If the water in the unsaturated zone is discharged into a previously formed cave or cavern, the CO_2 degases to the lower CO_2 pressure in the atmosphere of the cave or cavern, and calcite precipitates, forming speleothems: stalactites and stalagmites (Figure 164; Kowalczk & Froelich, 2010). Detailed dating of the layers in these features and analyses of isotopes of uranium, thorium, carbon, hydrogen, and oxygen have been used as records of climatic conditions over time (Burns et al., 1998).

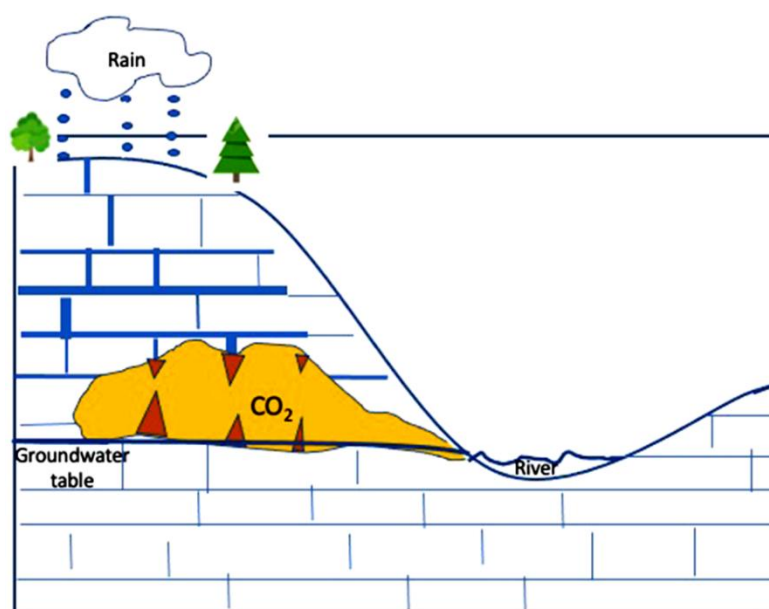


Figure 164 - Conceptual model for the formation of speleothems—stalactites and stalagmites (red triangles)—associated with groundwater degassing of CO_2 in caves and caverns and precipitating calcite.

With this brief background on the origin of karst, the question can be asked, “How rapid is the CO_2 chemical weathering and mass removal in karst systems?” To answer this,

we consider a karst groundwater flow system that discharges to a surface stream as illustrated in Figure 165.

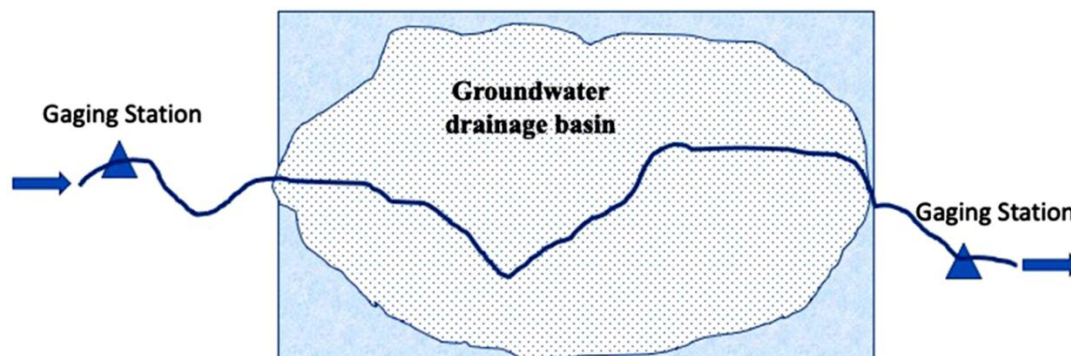


Figure 165 - Groundwater drainage basin in a karst area traversed by a “gaining” river (i.e., a river that groundwater flows into). Stream discharge and chemistry is measured at stations upstream and downstream of the karst area.

With this system of a gaining river traversing a karst system, the stream discharge and chemistry is known upstream and downstream of the area. Thus, the difference in mass flux over an interval of time—say, a year—between the measuring points gives an estimate of the mass removed by weathering. The median river discharge at the upstream gauging station is $3 \text{ m}^3/\text{s}$ with a calcium concentration of 30 mg/L . The discharge at the downstream gauging station is $4 \text{ m}^3/\text{s}$ with a 40 mg/L calcium concentration. For this analysis, it is assumed there is no surface runoff.

Converting calcium concentration in mg/L to kg/m^3 results in a concentration of 0.00003 and 0.00004 kg/m^3 of Ca, respectively, at the gauging stations. Recalling there are $31,536,000$ seconds in a year, the calculated mass flux of calcium at the upstream gauge is $2,838 \text{ kg/y}$ [i.e., $(31,536,000 \text{ s/y})(3 \text{ m}^3/\text{s})(0.00003 \text{ kg/m}^3)$] and the mass flux of calcium at the downstream gauge is $5,045 \text{ kg/y}$ [i.e., $(31,536,000 \text{ s/y})(4 \text{ m}^3/\text{s})(0.00004 \text{ kg/m}^3)$]. Thus, there is a net gain of $2,207 \text{ kg/y}$ of Ca resulting from groundwater discharge to the stream. That is, there was enough dissolution of calcite (CaCO_3) in the groundwater system to provide the additional $2,207 \text{ kg}$ of Ca during the year.

To calculate the volume of calcite dissolved, the molecular weight ratio of Ca to CaCO_3 is determined as 40.008 divided by 100.089 , which is 0.3997 , thus $5,523 \text{ kg CaCO}_3$ [i.e., $(2,207 \text{ kg Ca}/0.3997)$] dissolved to provide the observed increase of calcium in the stream water. The density of CaCO_3 is known to be 2.71 g/cm^3 ($2,710 \text{ kg/m}^3$); thus, the dissolution removed 2 m^3 [i.e., $(5,523 \text{ kg})/(2,710 \text{ kg/m}^3)$] of calcite from the drainage basin in that year. If the same conditions continued for a thousand years, $2,038 \text{ m}^3$ of CaCO_3 would be removed. To put this in perspective, this is equivalent to formation of an opening that is approximately $1,000 \text{ m}$ long by 1 m wide by 2 m high forming in a thousand years. This example illustrates the rapid evolution of karst landscapes.

7.6 On Evolution of Global Groundwater Solutes

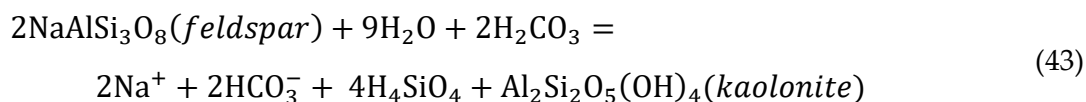
In addition to solute evolution along a flow path, the evolution of groundwater's mean global solute composition can be related to weathering using a process pioneered by Garrels and MacKenzie (1967). This approach yields a back-of-the-envelope intuitive feel for the geogenic reactions of a few minerals that control the major solute chemistry of groundwater. A more sophisticated approach would be to use the computer program NETPATH (Plummer et al., 1994) or a similar code. However, the assumptions one needs to make about the purity and presence of minerals in the system to provide input to more sophisticated models often does not justify their use.

The average global solute concentration of groundwater (Table 1) is converted to meq/L (Table 24). In this analysis, cations were slightly greater by 0.34 meq/L than anions; thus, the concentration values were adjusted to a perfect balance by distributing the 0.34 meq/L error proportionately to the value of meq/L for each anion. For example, the bicarbonate value of 3.51 meq/L is 72 percent of the total 4.88 meq/L of anions. Thus, 72 percent of the 0.34 meq/L error or 0.24 meq/L is added to the bicarbonate value resulting in an adjusted value of 3.75 meq/L. This approach was applied to all anions decreasing the difference between anions and cations to 0.01 meq/L (Table 24).

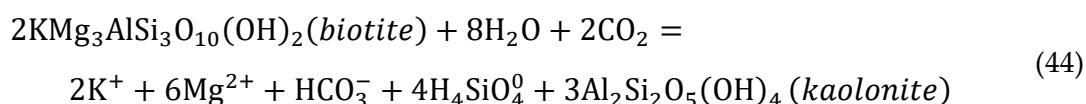
Table 24 - Concentration of median global groundwater in mg/L and meq/L, with values adjusted for charge balance.

	Conversion factor	Mean mg/L	Observed meq/L	Adjusted meq/L
Calcium	0.04990	42	2.10	
Magnesium	0.08229	13	1.07	
Sodium	0.04350	45	1.96	
Potassium	0.02558	3.5	0.09	
Bicarbonate	0.01639	214	3.51	3.75
Chloride	0.02821	24	0.68	0.73
Sulfate	0.02082	31	0.65	0.70
Nitrate NO₃	0.01613	2.7	0.04	0.05

Now we consider the likely source of the major ions in groundwater that are listed in Table 24. First, the chloride is assumed to be from precipitation. When 0.68 meq/L of chloride enters groundwater, it is likely associated with an equivalent 0.68 meq/L of sodium. The remaining 1.28 meq/L of sodium (1.96 meq/L in global groundwater, that is, 0.68 meq/L associated with the chloride from precipitation) and an equivalent amount of bicarbonate (1.28 meq/L) is derived from weathering of sodium feldspar to kaolinite by carbonic acid (H₂CO₃). In this reaction, equal amounts of sodium and bicarbonate are generated in the weathering products as shown on the right side of Equation ((44).



Next, we address the source of potassium. It is assumed that the weathering products of biotite (shown on the right side of Equation (44) account for all of the potassium (0.09 meq/L) in the global groundwater analysis. Equation 43 indicates that for every mole of potassium generated from the weathering of biotite, 3 moles of magnesium are generated, or in terms of equivalents (3×0.09 meq/L = 0.27 meq/L), and half a mole of bicarbonate is generated, or in terms of equivalents (0.045 meq/L).



The remaining 0.80 meq/L of magnesium (1.07 meq/L in global groundwater – 0.27 meq/L from weathering of biotite) occurs from the weathering of the mineral forsterite (Mg_2SiO_4), as shown by Equation (45).



We next assume that all the sulfate (0.70 meq/L in the global groundwater) is associated with an equivalent amount of calcium (0.70 meq/L) and they are generated by dissolving anhydrite (CaSO_4). Thus 1.40 meq/L of calcium still needs to be accounted for (2.10 meq/L in global groundwater – 0.70 meq/L from dissolution of anhydrite).

Dissolution of CaCO_3 accounts for the remaining 1.40 meq/L Ca and 2.80 meq/L bicarbonate as shown on the right side of Equation (46).



A summary of the calculated sources are given in Table 25. There is a small discrepancy between calculated and observed bicarbonate values (0.38 meq/L). The point of this exercise is to illustrate how a very few of the hundreds of minerals can influence the major solute chemistry of groundwater. This is not definitive as we could have used different common minerals like potassium/sodium feldspar and reduced the influence of biotite on the potassium concentration, or we could have addressed the source of magnesium by dissolving dolomite. The natural geochemical system is nuanced, however back-of-the-envelope modeling can be helpful in many instances to facilitate understanding of the origin of solutes in groundwater.

Table 25 - Summary of calculation of the major ions in the global average groundwater composition (in meq/L) assuming they are sourced from precipitation and weathering of five minerals.

Source	Ca	Mg	Na	K	HCO ₃	Cl	SO ₄
Precipitation			0.68			0.68	
Anhydrite	0.70						0.70
Feldspar			1.28		1.28		
Biotite		0.27		0.09	0.05		
Forsterite		0.80					
Calcite	1.40				2.80		
Calculated	2.10	1.07	1.96	0.09	4.13	0.68	0.70
Observed	2.10	1.07	1.96	0.09	3.75	0.68	0.70
Difference	0.00	0.00	0.00	0.00	0.38	0.00	0.00

7.7 Section Wrap-up

The examples described in Section 7 illustrate a few features common to the geochemical evolution of groundwater. Generally, one needs to consider the number of pore volumes that have passed through the point under examination since the aquifer became active. In these examples, the area nearest the recharge would have the gypsum, calcite, and pyrite removed; sodium exchange sites would have been filled with Ca, and the water might be suitable for drinking after a few hundred years of flow. However, solutes a few tens of meters farther along the flow path, likely exceed the concentrations suitable for human use.

Second, the approach proposed by Garrels and MacKenzie (1967) illustrated that it is possible to account for the composition of groundwater by the dissolution of a few common minerals. Fortunately, over 95 percent of the dissolved solutes are typically from only seven elements, thus significantly limiting the process. However, the solutes at any point along the flow path may have their hydrogeochemistry determined by the presence of a trace amount of reactive material and not by the bulk mineralogical composition. For example, a small weight percent of gypsum (such as 0.1%), pyrite (perhaps 0.01%), or clay possibly (1%) would likely go undetected in a typical analysis of mineral content—yet they would be important to consider in the evolution of solutes in groundwater. This illustrates a common feature of hydrogeochemistry: some solid phase components that govern the hydrogeochemistry are low or below detection in typical mineral analyses.

Third, insightful results can come from back-of-the-envelope modeling using simple conceptual models. These unassuming models provide a conceptual geologic estimate of the relative length of time required for different processes and reactions that control solute evolution. For example, karst topography can develop rapidly. For the example presented in this section, soluble gypsum is removed from the representative control volume in 80,000 years, removal of calcium by sodium-ion exchange takes 384,000 years, and oxidation and removal of pyrite requires many years. It is clear that a numerical solute transport code that incorporates all the processes is needed for a more sophisticated approach as these and other processes are going on simultaneously. The

simplified models, however, provide some insight. To quote the British statistician George Box, “all modes are wrong, but some are useful”.

8 Quantifying Physical Hydrologic Properties Using Geogenic Solutes

By conceptually combining physical flow with the chemistry of solutes, solute chemistry can be used to quantify some of the critical physical properties of an aquifer system, such as hydraulic conductivity, recharge flux, groundwater velocity, focused or diffuse recharge, hydrodynamic dispersion, and water age. The hydrogeochemical approach provides an independent evaluation of the physical parameter; in some cases, it provides a better integrated value in both time and space than can be obtained by physical measurements of the hydraulic parameters.

The methods of aquifer evaluation by hydrogeochemistry generally fall into the self-potential method or induced potential method. The self-potential method is used in response to a natural stress on gas, solutes, particulate material, isotopes, and/or temperature parameters in an aquifer or along a hydrologic gradient or flow path. This approach is relatively inexpensive and permits one to gain insight into processes that change the concentration or composition. In the induced potential method, a known concentration and volume of solutes or known thermal pulse are added to the aquifer and monitored as it moves through the aquifer. Many induced potential tracer tests (Cherry, 1983; LeBlanc et al., 1991) use conservative ions designed to measure flow paths, hydrodynamic dispersion, and the movement of trace constituents rather than chemical reactions.

In some induced potential methods, microcosms are used within the well to gain insight into reactions in the aquifer. For questions involving oxidation-reduction or pH, this approach may provide a valid approximation of reactions in the aquifer (Bengtsson & Annadotter, 1989). While chemical conditions can be easily controlled and a functional value can be obtained, this approach measures a small volume of the aquifer groundwater. As most aquifers display considerable spatial chemical heterogeneity, this approach has limited application to questions about larger-scale conditions.

The use of push-pull-induced potential methods has been proposed by Istok and others (1997) to extend the volume of influence by sampling a more prominent and presumably more representative portion of the aquifer. A reactive ion of known concentration is introduced into the well bore and either allowed to drift down the hydraulic gradient or is forced out into the surrounding aquifer with a "chaser" of untagged water. The well is then pumped, and the water is analyzed for differences between input solutes and recovered solutes.

These tests extend the sampled volume of the aquifer a few tens of centimeters beyond a well's radius but generally only evaluate an equilibrium environment. Some ions initially released from sites where they are attached to aquifer solids by the presence of an induced solute return to their sites when water is pumped back out of the aquifer. To

increase the aquifer volume sampled and avoid the restrictions of the push-pull method, an aquifer solute-induced potential method utilizing a two-well dipole stress test has been developed, as discussed in Section 7.8. In this approach, water with solutes of known composition, pH, and Eh are injected in one well, then withdrawn from a nearby well and analyzed.

The most appropriate approach to take depends on the project's goals and the resources available to accomplish the goals. The following examples utilize the self-potential approach.

8.1 Model of the Regional Recharge Flux: The Chloride Mass Balance (CMB)

In many aquifer systems, estimating the regional groundwater recharge flux is necessary as it provides a conservative estimate of sustainable aquifer development, which is often referred to as the safe yield of the aquifer. However, this approach may underestimate the potential yield of the aquifer (Bredehoeft, 2002). Estimating groundwater recharge with physical methods is often difficult as recharge events are typically heterogeneous in space and time. Thus, approaches that integrate large units of space and time, such as the chloride mass balance (CMB) method, have many advantages. A model of the mass of chloride entering and leaving a control volume is presented to illustrate the CMB method (Figure 166).

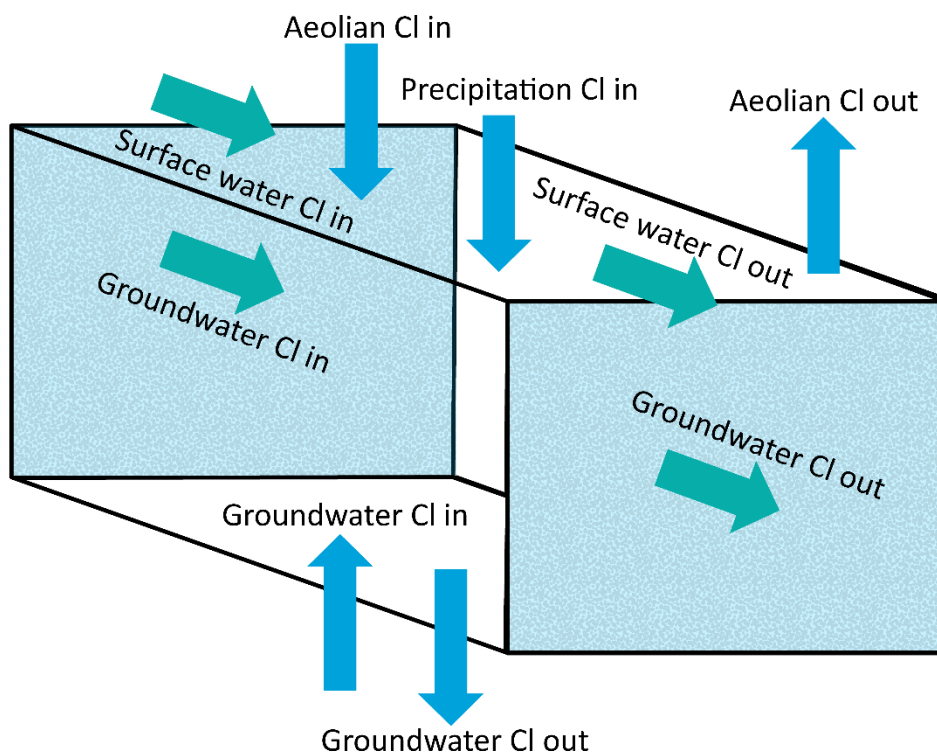


Figure 166 - Chloride (Cl) mass balance of a representative control volume with sides that are parallel to groundwater flow; thus, there is no flux of water or solutes into or out of the sides. Water and solutes move through the back, front, top and bottom of the volume.

Assume the precipitation flux can be determined, and the water and solutes are in a steady-state condition, then the regional-specific vertical recharge flux can be determined, given the following assumptions.

1. The chloride in the groundwater originates only from precipitation directly on the aquifer—no unmeasured chloride mass is recharged from overlying, underlying, or adjacent aquifers, nor is there unmeasured runoff.
2. The chloride is conservative in the system.
3. The atmospheric chloride flux—wet and dry—has not changed with time.
4. There is no recycling or concentration of chloride within the aquifer.

If these assumptions are valid, then the area-averaged specific vertical recharge flux (recharge per unit area per unit time) to the aquifer can be as expressed as a linear relationship shown in Equation (47).

$$Qv = \frac{(P)(Cl_{wap})}{Cl_{gw}} \quad (47)$$

where (parameter dimensions are dark green font with mass as **M**, length as **L**, time as **T**):

Qv = vertical ground-water recharge flux (LT^{-1})

P = average annual precipitation (LT^{-1})

Cl_{wap} = precipitation-weighted average chloride concentration (ML^{-3})

Cl_{gw} = average chloride concentration in the ground water (ML^{-3})

Cl_{wap} is calculated by Equation (48).

$$Cl_{wap} = \frac{\sum_{i=1}^n P_i Cl_{pi}}{\sum_{i=1}^n P_i} \quad (48)$$

where (parameter dimensions are dark green font with mass as **M**, length as **L**, time as **T**):

Cl_{pi} = chloride concentration in precipitation of the i th sample

P_i = precipitation flux of the i th sample

n = number of samples

One of the earliest field applications of the CMB method (but of questionable boundary assumptions) was made by Eriksson and Khunakasem (1969) based on earlier observations of atmospheric composition by Schoeller (1941) and Eriksson (1952). Manna and others (2016) presented an excellent recent study utilizing CMB. The CMB method was also applied to the large regional Southern High Plains aquifer of Texas and New Mexico, USA (Wood & Sanford, 1995b; Figure 167).

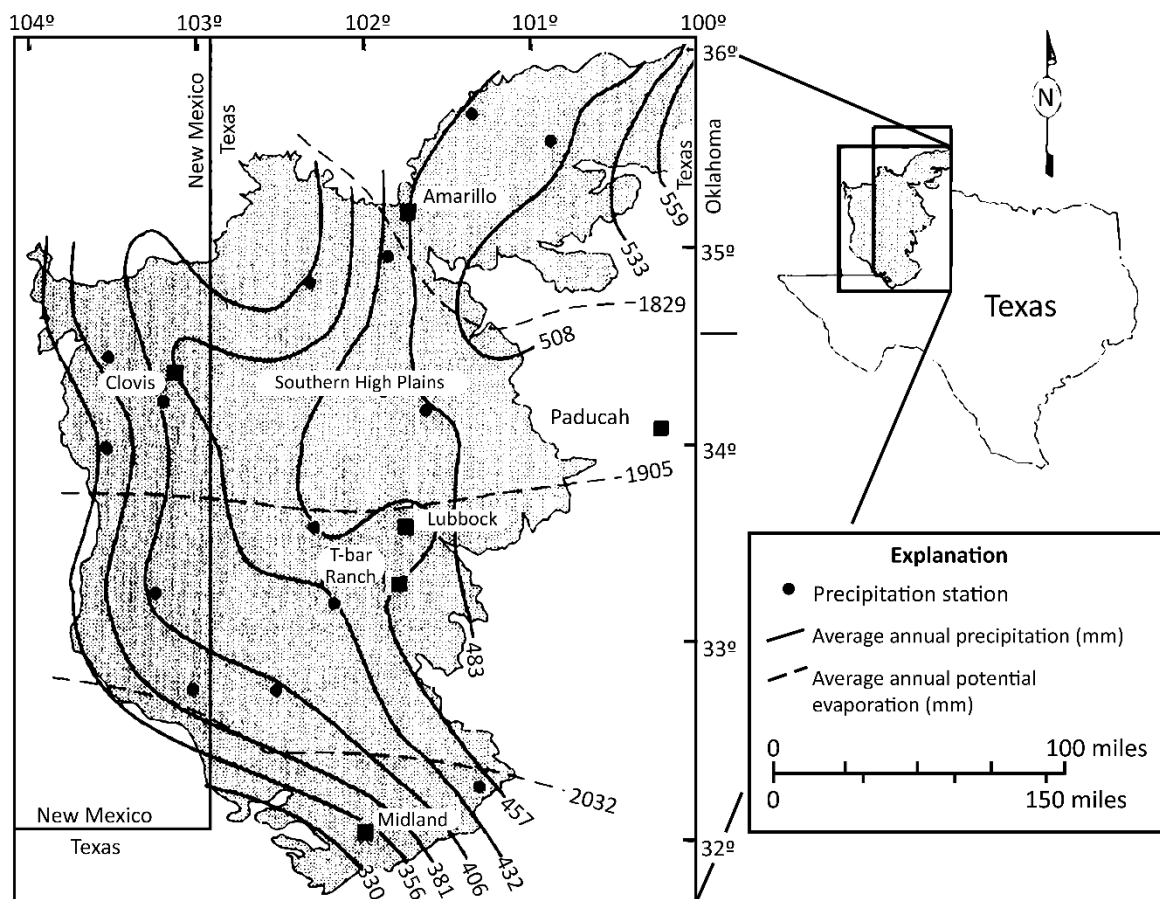


Figure 167 - Map of annual precipitation and pan evaporation on the Southern High Plains of Texas and New Mexico, USA (reproduced from Wood & Sanford, 1995b).

The Southern High Plains aquifer system has 98 percent internal drainage with little runoff loss or run on from overland flow. The hydraulic heads in the High Plains water table aquifer are downward; thus, there is no contribution of (Cl) via upward groundwater flow. Halite (NaCl) has not been extensively used for highway ice control; thus, the assumptions 1 through 4 presented at the beginning of this subsection are met.

The precipitation-weighted average chloride (Cl_{wap}) concentration for samples of wet and dry precipitation during the years 1984 to 1985 at Amarillo, Texas, was approximately 0.531 mg/L. The average chloride concentration in 3,071 widely spaced groundwater samples (Cl_{gw}) in the northern half of the Southern High Plains was approximately 25 mg/L.

Spatial and temporal precipitation (P) over the area was estimated to average 0.485 m/y; thus, using Equation (47), the predevelopment groundwater-specific vertical recharge flux (Qv) for the northern half of the Southern High Plains was estimated to be 0.010 m/y [i.e., $(0.485 \text{ m/y})(0.531 \text{ mg/L})/(25 \text{ mg/L})$]. Within the limits of error, this value is nearly identical to the 0.014 m/y estimate by Theis (1937) based on gradient and cross-sectional area, fluctuation of the water table with recharge events, and shape of the water table on the entire Southern High Plains. These recharge fluxes are between 2 to 3 percent

of annual precipitation, consistent with other recharge estimates in semi-arid environments.

Manna and others (2016) used a more complete wet and dry CMB data set to constrain their recharge estimate in a semi-arid California aquifer and found approximately 4 percent of the precipitation was recharged. Different topography, precipitation rates and temporal distribution, soil types, and other factors lead to this variability. However, groundwater recharge of 2 to 4 percent of the precipitation is a typical range for semi-arid areas. It may be helpful as a first approximation of recharge flux for similar areas that lack data, or as a broad constraint on estimates using other methods. The most likely sources of error are the chloride concentrations in dryfall owing to the generally limited spatial and temporal data collection. Precipitation flux in arid and semi-arid systems is also highly variable and can lead to a large range of estimates.

The calculated recharge flux is the maximum amount entering a system under the assumed boundary conditions and should not by itself be used to estimate the amount of water available for development as there may be unmeasured losses from the basin by underflow or transpiration. Developed basins may capture rejected recharge and thus have higher rates than virgin systems (Bredehoeft, 2002; Theis, 1940).

8.2 Estimates of Hydraulic Conductivity Using Chloride Mass Balance (CMB)

The recharge estimates by the CMB method can be evaluated by comparing hydraulic conductivity calculated by the proposed recharge flux with that determined by physical methods using well logs, pumping tests, and laboratory analyses of the sediments. To illustrate the approach, consider a control volume of the High Plains aquifer system 1 m wide, 100 m thick, and 160,000 m long that is parallel to flow from the northwest toward the southeast in the northern portion of the Southern High Plains of Texas and New Mexico, USA (Figure 168).

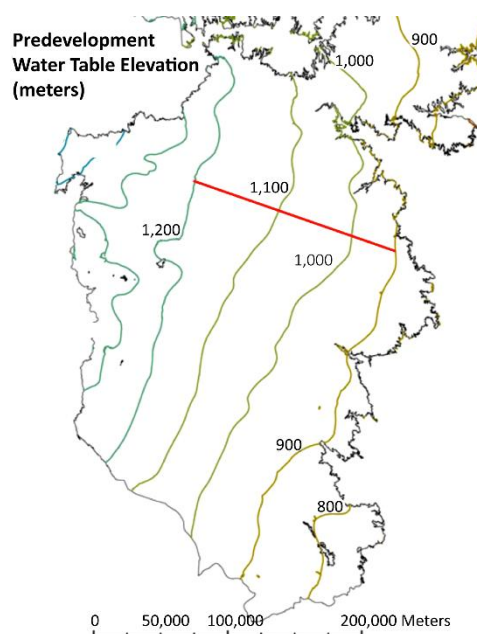


Figure 168 - Map of the predevelopment water table, in meters above sea level, of the Southern High Plains of Texas and New Mexico, USA (modified from Haacker et al., 2016). The hydraulic gradient is a fairly uniform ≈ 0.001875 to the east throughout the system, suggestive of reasonably uniform hydraulic conductivity as the regional thickness varies little. The red line is perpendicular to the gradient, i.e., parallel to flow and represents the area of the control volume presented in Figure 169. It starts at the groundwater divide in the west which is a hydraulic no-flow boundary and ends at the eastern escarpment which is the discharge boundary.

The assumptions require that the total discharge from the proximal end of the control volume equal the total input to the surface (Figure 169), that is, precipitation is the only water source. Hydrogeologists are frequently interested in the specific horizontal flux q_{hz} , thus, the total recharge area is multiplied by the recharge flux q_v (i.e., 0.01 m/y as determined in Section 8.1) to calculate the annual recharge volume, then divided by the total discharge area, as shown in Equation (49). The value of q_{hz} is then 16 m/y [(0.01 m/y)(1 m)(160,000 m)/((1 m)(100 m))]. Equation (50) shows the specific horizontal flux as expressed by Darcy's Law.

$$q_{hz} = \frac{q_v(\text{area of recharge})}{\text{area of discharge}} \quad (49)$$

$$q_{hz} = k_{hz} \frac{dh}{dl} \quad (50)$$

where (parameter dimensions are dark green font with mass as **M**, length as **L**, time as **T**):

q_{hz} = specific horizontal discharge flux (LT^{-1})

q_v = recharge flux (LT^{-1})

k_{hz} = horizontal hydraulic conductivity (LT^{-1})

$\frac{dh}{dl}$ = the horizontal hydraulic gradient (dimensionless)

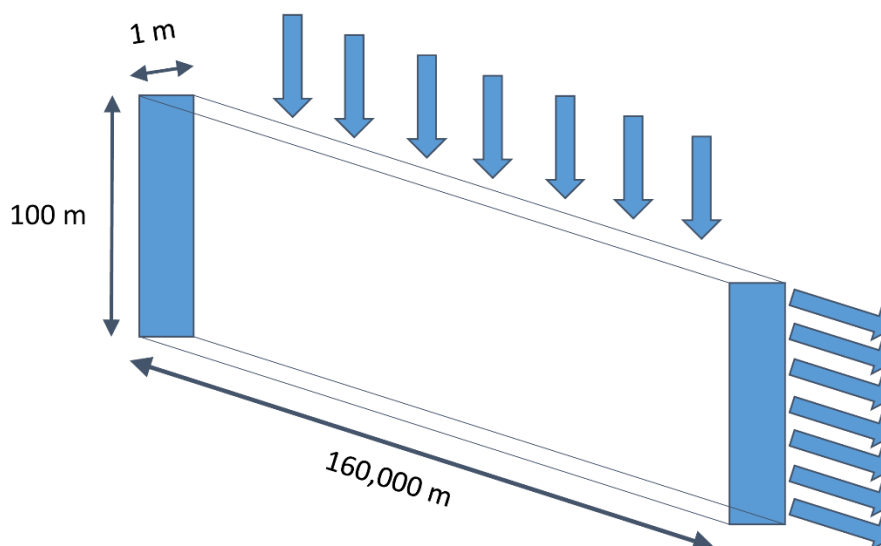


Figure 169 - Recharge details of the control volume of the Southern High Plains aquifer, as shown in Figure 168. The volume of water recharged between the distal end (groundwater divide) and proximal end (Eastern escarpment of the aquifer) must equal the volume of water discharged at the distal end.

Hydraulic conductivity (k_{hz}) can be calculated by rearranging Equation (50). Converting q_{hz} to days gives 0.045 m/day [i.e., (16 m/y)/(365 days/y)] and dividing by the average predevelopment hydraulic gradient of 0.001875 m/m (300 m decline in head over 160,000 m as shown in Figure 168) provides a regionally integrated value of hydraulic conductivity (k_{hz}) as 24 m/d.

Estimates of average hydraulic conductivity by site-specific physical methods—well logs, pumping tests, specific capacity tests, and so on—for this area are approximately 18 m/d (Cederstrand & Becker, 1998). Thus, the two independent methods yield nearly the same value.

The above analysis assumes a steady-state water and solute system that is open for both water and solutes, and is valid because it is consistent with the following assumptions:

- flow is parallel to the long dimension of a rectangular-shaped control volume (Figure 168 and Figure 169), thus no flow occurs in or out the sides;
- there is no flow in or out of the bottom or distal end (low permeability base and groundwater divide);
- chloride in the groundwater originates only from precipitation directly on the aquifer—no unmeasured chloride mass is recharged from overlying, underlying, or adjacent aquifers, nor is there unmeasured runoff or run on;
- chloride is conservative in the system; and
- there is no recycling or concentration of chloride within the aquifer.

Further, the analysis assumes that the configuration of the water-table contours in areas without streams is controlled by:

- slope of the bedrock base of the aquifer which is assumed to be the same as the surface;

- changes in the thickness and hydraulic conductivity of saturated materials which are assumed to be constant; and
- vertical recharge flux which is assumed to be spatially and temporally constant.

The assumption of a uniform thickness of 100 m is probably not realistic. Whereas the surface of the Southern High Plains is uniform, the bedrock surface is not. The hydraulic gradient, however, incorporates both thickness and hydraulic conductivity, thus is an integrating value. As the water table gradient is rather uniform, the small variations in bedrock elevation are ignored for this regional generalization. The distal end of the control volume is at a groundwater divide so there is no flow in that end.

Given that Darcy's Law is linear, a 10 or 15 percent variability in recharge flux or gradient would mean a 10 to 15 percent change in hydraulic conductivity, which is a relatively small value when compared to the range of field values that spans several orders of magnitude. As there is little room for error in measuring hydraulic gradient, one can utilize a range of recharge flux to estimate a possible range of hydraulic conductivity. For example, even if recharge were 50% higher or lower, that is 0.000041 m/d (0.015 m/y) or 0.0000137 m/d (0.005 m/y), the regional hydraulic conductivity would be 36 m/d or 12 m/d. Often in hydrogeologic work, knowing hydraulic conductivity to the correct order of magnitude is useful.

8.3 Runoff Flux to Topographic Features: Chloride Mass Balance (CMB)

It is generally recognized that groundwater recharge is not uniform throughout a basin and is controlled by topography, rainfall intensity and duration, soil type, land use, and land covers such as native forest, agriculture, subdivision, commercial, and other factors. In some instances, such as when working on water supply or waste disposal, it is of interest to know the amount of overland runoff to topographic features such as dried river valleys, closed ephemeral lakes, or other landscape features that may be a focus for groundwater recharge. CMB can be used if some of the restrictions imposed on Equation (49) can be relaxed—for example, if one can measure vertical recharge flux using a mass-independent time marker that moves with the velocity of the water (e.g., tritium (^3H), ^{85}Kr , ^{36}Cl , CFC) for an event that occurred at a known time. That is, the recharge estimate is independent of the solute mass in the runoff to the surface feature that is sampled. Therefore, chloride loading from runoff in the mass balance of Equation (47) can be used to estimate runoff to the feature. For a closed ephemeral lake floor within a drainage basin, this can be written as shown by Equation (51) (Wood & Sanford, 1995b). If the runoff (r) is zero, then the chloride loading from runoff is zero, and Equation (51) reduces to Equation (47).

$$q_{vuz} = \frac{(P)(Cl_{wap})}{Cl_{uz}} + r \left\{ \frac{A_b Cl_r}{A_f Cl_{uz}} \right\} \quad (51)$$

where (parameter dimensions are dark green font with mass as M, length as L, time as T):

- q_{vuz} = vertical recharge flux in the unsaturated zone (LT^{-1})
- P = average annual precipitation (LT^{-1})
- Cl_{wap} = precipitation-weighted average chloride concentration (ML^{-3})
- Cl_{uz} = average chloride concentration in the unsaturated zone (ML^{-3})
- r = overland runoff flux to the lake basin (LT^{-1})
- A_b = drainage area of the basin (L^2)
- Cl_r = average chloride concentration in the runoff (ML^{-3})
- A_f = area of the playa lake floor receiving the drainage (L^2)

To determine runoff to the playa lake, first Wood and Sanford (1995b) measured the activity of tritium below the floor of a playa lake basin and, after adjusting for decay, the depth of the tritium peak suggested a vertical recharge flux (q_{vuz}) of 0.077 m/y \pm 0.008 m/y. That is, the tritium peak is at approximately 6.6 meters depth after 30 years in a sedimentary medium with a porosity of 0.35 thus $\{(6.6 \text{ m} / 30 \text{ y}) (0.35) = 0.077 \text{ m/y}\}$. At this site, the average chloride value in the unsaturated zone beneath the lake floor was 34 mg/L. The wet and dry chloride in ten precipitation events at the rain gauge at this site averaged 2.81 mg/L—it was near a large, dry saline salt flat—and the long-term precipitation at this location is approximately 0.460 m/y. Then, Equation (51) is rearranged to solve for runoff flux, r , as shown here.

$$r = \frac{q_{vuz} - \left(\frac{(P)(Cl_{wap})}{Cl_{uz}} \right)}{\left\{ \frac{A_b Cl_r}{A_f Cl_{uz}} \right\}} = \frac{0.077 \frac{\text{m}}{\text{y}} - \left(\frac{(0.46 \frac{\text{m}}{\text{y}})(2.81 \frac{\text{mg}}{\text{L}})}{34 \frac{\text{mg}}{\text{L}}} \right)}{20 \frac{2.81 \frac{\text{mg}}{\text{L}}}{34 \frac{\text{mg}}{\text{L}}}} = 0.024 \frac{\text{m}}{\text{y}}$$

The value of 0.024 m/y is close to the mid-range of runoff values for ephemeral playa lake basins in the area that were based on physical measurements at several rainfall–runoff research basins (Brown et al., 1978). The error range of \pm 0.008 m/y for unsaturated Darcy flux of 0.077 m/y is based upon parameter variation. First, the tritium curve has been slightly broadened and reduced in magnitude from the input signal, probably owing to mechanical dispersion and diffusion. However, this does not cause a significant error in choosing the peak which is used to determine velocity. If the peak tritium signal were 29 years ago instead of the 30 years used in the model, the recharge flux would be

approximately 0.079 m/y. If the tritium peak is at 7.0 m instead of the selected 6.6 m, the recharge flux would be approximately 0.082 m/y. Whereas hydrodynamic dispersion may have contributed to the broadening of the tritium peak, it is assumed it would not significantly change the depth of the peak below the surface. Thus, none of the individual variations alter the calculated flux by more than 10 percent.

The following assumptions were made to estimate runoff flux to the playa lake:

- chloride concentration of the runoff, Cl_r is the same as that of the precipitation, Cl_p —a reasonable assumption in this environment;
- flux q , based on tritium evaluation, is 0.077 m/y; and
- ratio of measured area of the basin to that of the lake floor is 20 to 1.

Further, it is assumed that the water and solute system is in a steady-state and the system is open for water and solutes to enter and leave, and the following assumptions are met:

- chloride in the groundwater originates only from precipitation directly on the aquifer—no unmeasured chloride mass is recharged from overlying, underlying, or adjacent aquifers, nor is there unmeasured runoff;
- chloride is conservative in the system;
- atmospheric chloride-mass flux—both wet and dry—has not changed over time;
- there is no recycling or concentration of chloride within the aquifer;
- tritium in the groundwater originates only from precipitation directly on the surface of the aquifer;
- tritium is conservative in the system; and
- there is no recycling or vapor transport of tritium within the aquifer.

It is much more likely that there is a significant variation in flux between basins or within a given basin than in the parameters used to calculate the flux. In the above sample, 12 percent of the porosity is air-filled. However, the calculated value assumes complete water saturation—accordingly, it may include additional errors. Significant loss of tritium into blind pores is likely to occur in rocks of low porosity but is not considered significant in this high-porosity system. Thus, it is concluded that the combination of tritium and chloride methods in arid and semi-arid areas can give a time-integrated runoff value consistent with physical measurements. Owing to the limited possible range of q_{vuz} values, this method of calculating runoff may be significantly better constrained than values estimated from site-specific physical methods.

8.4 Relative Groundwater Recharge as a Function of Geomorphology, Soils, or Land Use/Cover

It might be desirable to know where in a basin area would be best for storage of waste or to designate and protect an area of preferred groundwater recharge. In some environments, neither the CMB nor the mass-independent methods may be available. However, using chloride in the unsaturated zone, it is possible to estimate relative—not

absolute—recharge rates between different topographies, soil conditions, and land covers such as forest, agriculture, subdivision, commercial, or others.

For example, suppose chloride in the unsaturated zone averages 10 mg/L at one site and 500 mg/L at another within the same basin. In that case, one is confident in suggesting that the groundwater recharge rate is approximately 50 times higher in the first site than in the second because the lower value indicates more flushing of chloride through the system. As shallow—less than 1 m—cores or soil borings and chloride analyses are inexpensive, and landscapes are quickly evaluated for relative groundwater recharge, they may be useful in estimating relative recharge rates for developing Best Management Practices (BMP) for land use.

Error in this method is relatively small, and is mainly caused by analytical variation. If the sampling density is sufficiently large, the standard deviation within a soil type or geomorphologic feature is slight. The assumptions require that:

- chloride in the vadose zone water originates only from direct precipitation;
- chloride is conservative in the system; and
- there is no recycling or concentration of chloride within the soil zone.

A potential limitation of this method is the widespread use of salt (NaCl) in the deicing of highways in snowy climates. However, careful selection of areas not impacted by drainage from highways may still provide useful results. Or if the goal is to estimate where salt deicing is impacting recharge, this technique would be applicable for all the recharge sites in a snowy climate.

8.5 Defining Macropore or Diffuse Recharge using Stable Water Isotopes

To understand recharge in an aquifer system and provide insight into management, it may be desirable to know if recharge from precipitation is slow over a diffuse large area or rapid and focused through a small area. Stable isotopes ($\delta^2\text{H}$ and $\delta^{18}\text{O}$) of groundwater can be used to separate focused macropores from diffuse recharge. That is, diffuse recharge experiences more evaporation before recharging than macropore recharge, thus impacting the water isotopes. For example, the concentration of conservative solutes in the High Plains Aquifer, Southern High Plains of Texas and New Mexico, USA, suggest that the average composition of most solutes in groundwater is approximately 40 to 45 times the concentration observed in precipitation. Thus, it might be expected the groundwater would exhibit a highly evaporated signature. However, the groundwater isotopes plot on the local meteoritic line suggesting little evaporation (Figure 170).

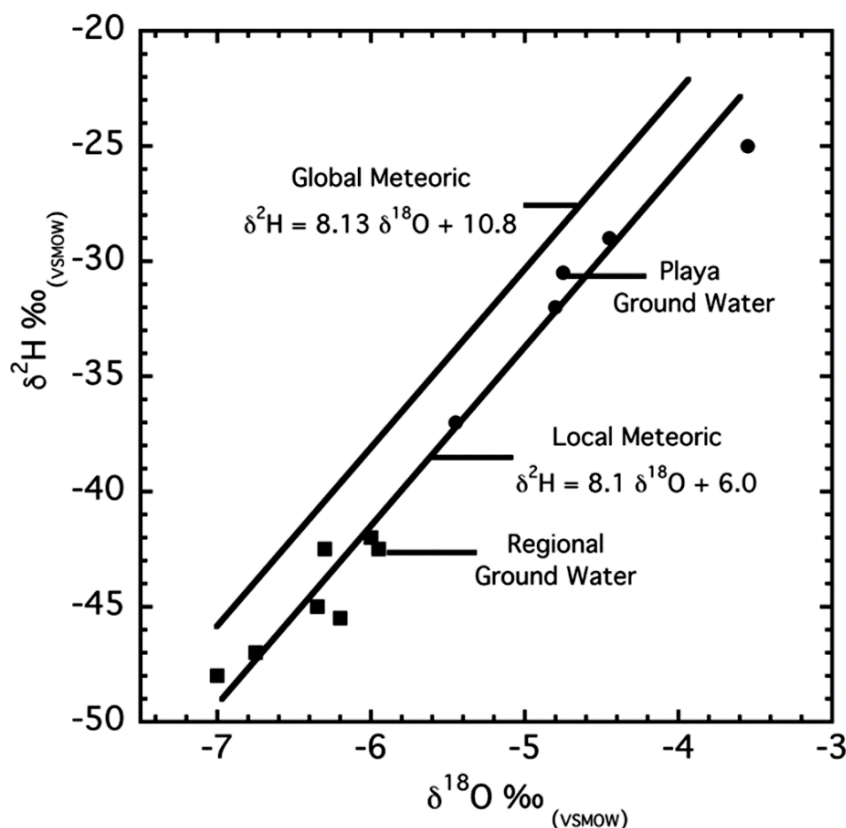


Figure 170 - Isotopes (in per mil) of global precipitation, local precipitation, groundwater below playa lake, and groundwater from the High Plains Aquifer, Southern High Plains of Texas and New Mexico, USA, suggest some evaporation before recharge at playa lakes but not 43 times as much as suggested by the high concentration of solutes in the groundwater (reproduced from Wood & Sanford, 1995b).

This apparent paradox can be resolved if it is assumed that most recharging water enters the aquifer relatively quickly through macropores in a focused area and, thus, is not subject to significant evaporation before recharge. The solutes in the precipitation that is not recharged are concentrated by evaporation near or at the surface and are readily mobilized and carried down to the groundwater by the next macropore recharge event. Thus, solutes in the aquifer are concentrated, but the water molecule does not reflect the same evaporation signature as the solutes. In this case, additional physical evidence supports the conclusion because significant piping is observed around playa lakes and these are the likely avenue of macropore recharge.

This example assumes a steady-state system that is closed and is useful if the following conditions are applicable:

- local meteoric precipitation line is known;
- recharge sources have not changed over time; and
- isotopic ratios of the groundwater is known.

Analytical uncertainty is likely to be small; however, estimating the parameter uncertainty is difficult, thus, in general the r^2 associated with the best-fit line to the data is

the only means of getting a feel for uncertainty. If the data fit the line closely one has greater confidence than if there is significant scatter around a line.

8.6 Water Source of Paleo Recharge Using Stable Water Isotopes

In reconstructing fossil aquifer systems, it is desirable to know the water sources as they may differ from current conditions. Stable isotopes of water ($\delta^2\text{H}$ and $\delta^{18}\text{O}$) may provide insight if they have had a different source in latitude, elevation, continental effects, humidity, and amount of precipitation (Clark & Fritz, 1997; Cook, 2020; Cook & Herzeg, 2000; Faure & Mensing, 2005; Fritz & Fontes, 1980). These different environmental conditions are typically reflected in both slope and intercept of the $\delta^2\text{H}$ and $\delta^{18}\text{O}$ graphs. The intercept of $\delta^{18}\text{O}$ is referred to as deuterium excess or “d” typically 9.47 on global data. Rewriting Equation (2) (Figure 23) to solve for the intercept as a function of $\delta^{18}\text{O}$ and the slope of the global meteoric water line provides Equation (52).

$$\text{“d”} = \delta^2\text{H}_{\text{VSMOW}} - 8.02 \delta^{18}\text{O}_{\text{VSMOW}} \quad (52)$$

Large negative values of “d” have been observed in rivers in the northern tier of states in the continental USA, where the moisture source is from evaporation from previous precipitation on lakes (Kendall & Coplen, 2001). Using this explanation of large negative values of “d”, two aquifers (Liwa and Gachsaran) on the eastern edge of the Rub Al Khali (Empty Quarter) near the border of UAE and Saudi Arabia, approximately 150 km northwest of the city of Abu Dhabi, UAE, are considered here.

The fossil water in these aquifers exhibit large values of negative “d”. The groundwater from the two aquifers has $\delta^{18}\text{O}$ slopes of 4.9 and 6.3, which is similar to the slope of 5.3 associated with current local precipitation, but they have large negative values of deuterium excess “d”: –15 and –28 relative to local current precipitation “d” of +7 (Figure 171; Wood, 2010). The similar slopes of the fossil water in the Liwa and Gachsaran aquifer and the current precipitation suggest these waters were derived from similar environmental conditions. The current rainfall is approximately 50 mm/y and is derived mainly from monsoons that occasionally originate in the Indian Ocean. However, the significant negative value of “d”, suggests a different water source or environment.

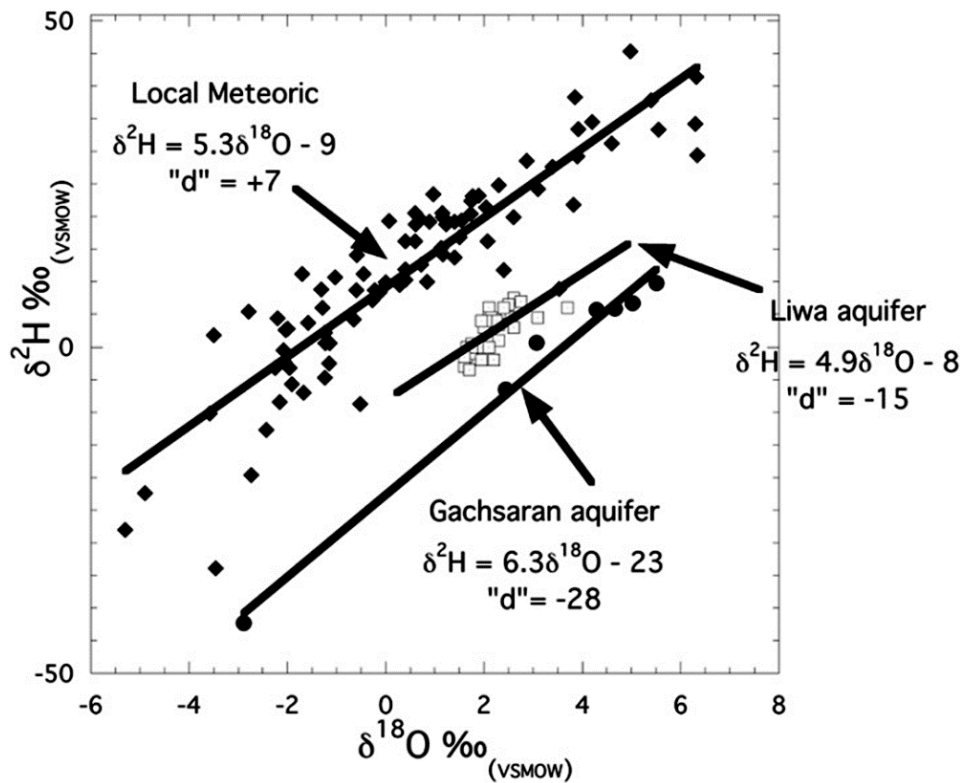


Figure 171 - Water isotopes from two aquifers showing significantly different values of “d”, deuterium excess, than current local meteoric water, suggesting the water is from different sources (reproduced from Wood, 2010).

The deuterium excess signature, in this case, is hypothesized to result from precipitation of evaporated continental runoff to the Red Sea catchment basin during the last wet period in the area from 5,000 to 9,000 BP. It is postulated that fresh low-density continental runoff water floated on the surface of the Red Sea, flowed onto the surface of the Indian Ocean, and was driven northeastward along the coast of modern Yemen and Oman under the influence of Indian monsoons, providing a moisture source that dominated precipitation during this time (Figure 172).

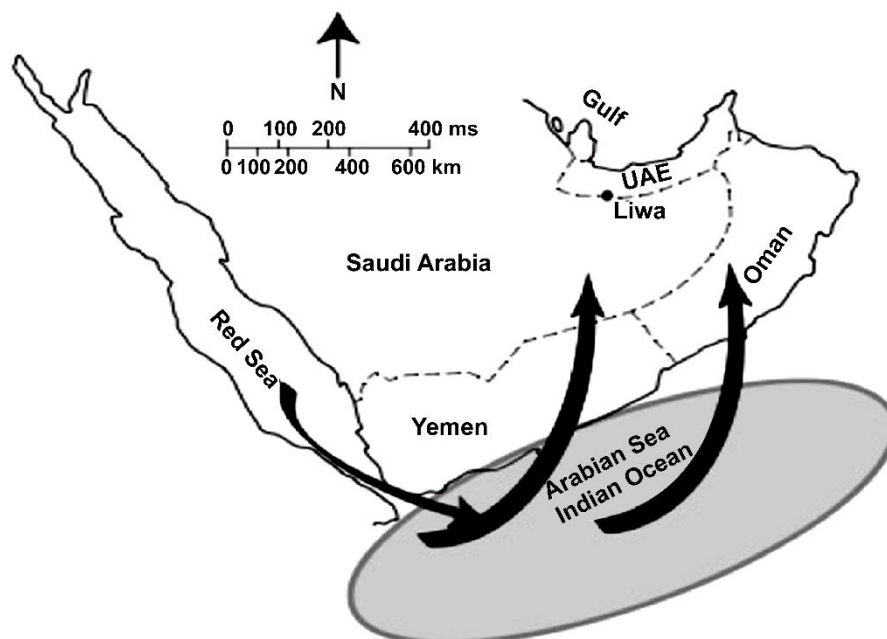


Figure 172 - Map showing the proposed source of continental water floating on the surface out of the Red Sea onto the Arabian Sea and the Indian Ocean, where it evaporated and provided a source of monsoon precipitation to the Liwa area (reproduced from Wood, 2010).

The amount of freshwater discharging from the Red Sea to the Arabian Sea during the period of enhanced precipitation would have been significantly greater than at present and would have been dominated by the isotopic signature of surface runoff to the Red Sea. Thus, the surface-water discharge to, and stable isotopes in, the Red Sea would be linked to precipitation in the Liwa and Gachsaran catchment area.

8.7 Dating Groundwater with Carbon-14

Dating groundwater—that is, determining the time since the water last contacted the atmosphere—can provide physically independent estimates of recharge rates, dates of recharge events, estimates of rainfall, and groundwater velocity. The caveat, however, is that the dating of groundwater systems is sensitive to initial recharge conditions and heterogeneity of the flow paths. That is, if nearly all the water in the aquifer has been recharged over a relatively short time interval of a few hundred years associated with local climate change, then dating can be successful as nearly all the water will be of the same age regardless of flow paths.

It is also possible to date aquifer systems with homogeneous flow paths that are approximately the same length—that is, with systems with small hydrodynamic dispersion. Conversely, if flow paths are of variable lengths with there is large hydrodynamic dispersion, then dating can give an inaccurate recharge age at the sampling point because of the mixing of the different flow paths.

Groundwater dating methods and approaches are commonly divided into “young” (post-1950s) and “old” (pre-1950s; Clark & Fritz, 1997; Cook & Herczeg, 2000; International Atomic Energy Agency, 2013). This age partition corresponds to worldwide atmospheric

contamination of identifiable soluble gases, including tritium, carbon-14, krypton-85, chlorofluorocarbon (CFC), and others introduced to the atmosphere by anthropogenic activity since the 1950s. Dating of younger groundwater typically uses “event dating” – that is, does the aquifer contain a substance whose time of introduction is known, such as tritium ^3H from above ground nuclear explosions in the 1950s – whereas dating older groundwater normally utilizes radioactive decay relative to a known input and assuming a closed system after recharge. Ions commonly used for dating older groundwater are carbon-14, chlorine-36, and krypton-81. Others have been used but less commonly.

Accurate absolute dating of groundwater exhibiting two- and three-dimensional flow is exceptionally challenging owing to two inherent constraints:

1. the act of sampling generally integrates many flow paths of different lengths thus, different ages; and
2. diffusion of the solute or gas into blind pores and the aquifer skeletal framework, dilutes its concentration.

Additional limitations result from the non-conservative behavior of the ion in question, lack of a well-defined input function, and analytical requirements or the large sample size required. Despite these restrictions, groundwater dating has proven successful in many cases (Clark & Fritz, 1997; Cook & Herczeg, 2000; International Atomic Energy Agency, 2013).

For radioactive substances, the age t since the last contact with the atmosphere is given by Equation (53).

$$t = \frac{-T_{1/2}}{\ln(2)} \ln\left(\frac{N}{N_0}\right) \quad (53)$$

where (parameter dimensions are dark green font with mass as **M**, length as **L**, time as **T**):

$-T_{1/2}$ = half-life of radioactive element (**T**)

$\ln(2)$ = (0.693) (**dimensionless**)

N = current number of parent atoms (**dimensionless**)

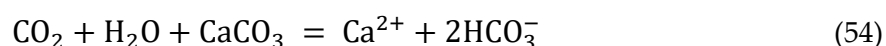
N_0 = original number of parent atoms (**dimensionless**)

Many laboratories report the ratio (N/N_0) portion of the equation as a decimal value. For example, in ^{14}C dating, percent modern carbon (PMC) is generally given as a decimal less than one (i.e., 0.67). A ratio greater than 1.00 indicates an atmospheric contribution from anthropogenic thermonuclear testing and suggests a recent—post 1950s—recharge.

Carbon-14 is perhaps the most common method for dating old groundwater and is based on radiocarbon being generated in the atmosphere at a known rate. The radiocarbon generated becomes part of the atmospheric carbon dioxide and is incorporated in plants

and the atmosphere of the unsaturated zone. As the groundwater is removed from contact with the atmosphere in the unsaturated zone, the system becomes closed to new input from the atmosphere, and carbon-14 decays at a known rate with a half-life of 5,730 years. Thus, a measure of the activity of carbon-14 provides an estimate of the age since water last was in contact with the atmosphere.

In addition to the inherent limitations outlined above, carbon used in radiocarbon or ^{14}C dating is not conservative and commonly reacts with the skeletal framework of the aquifer. For example, current atmospheric carbon dioxide and water react with “old” (> 50,000 years) calcite to form a calcium ion and two bicarbonate ions, as shown in Equation (54).



In this case, one-half of the bicarbonate ions would be from dead carbon, resulting in a 50 percent dilution of PMC. In some cases, old organic carbon deposited in the unsaturated zone may be oxidized, creating an old-input carbon dioxide. The impact of the addition of dead carbon is evaluated by using the relative values of $\delta^{13}\text{C}$ in the sample, the unsaturated zone gas, and the skeletal framework to determine the relative contributions of carbon to the liquid sample (Clark & Fritz, 1997; Cook & Herczeg, 2000). Various models have been proposed to adjust the age for a variety of assumptions and boundary conditions (Cook & Herczeg, 2000; Parkhurst & Appelo, 2013). For use in dating young groundwater, an additional adjustment arises from the burning of fossil fuels in large quantities in the twentieth century that added dead carbon, and the above-ground nuclear tests in the 1950s and early 1960s that added carbon-14. Furthermore, the production of atmospheric carbon-14 has not been constant over time, as assumed in the analyses; thus, dates must generally be calibrated or adjusted for this factor (Reimer et al., 2009).

Some care is required in evaluating carbon-14 laboratory data because different laboratories use different assumptions when correcting and reporting the data. As most analytically determined carbon-14 dates are on wood or charcoal used for archeological purposes, many analytical laboratories assume that a $\delta^{13}\text{C}$ correction for carbon is -25‰ which is typical for wood, rather than using the geologically oriented common marine value of 0‰ or typical groundwater value of -4‰ or -7‰ . Further, to allow comparison of older sites, many archeologists continue to use the older “Libby” half-life (5,568 years) rather than the more accurate half-life (5,730 years). Thus, when age is reported, it is necessary to determine: which half-life was used; whether the age was calibrated; and any other assumptions or adjustments that were made. Owing to the possibility of younger carbon-14 from thermonuclear testing, it is usually advisable to analyze water for the presence of ^3H or other younger contamination that may invalidate carbon-14 dates. Even with these restrictions and caveats, carbon-14 has been an important groundwater dating tool (Clark & Fritz, 1997; Cook & Herczeg, 2000; International Atomic Energy Agency, 2013)

In the following example, carbon-14 was used to determine the average age of groundwater in the Liwa area of the Ar Rub Alkali (Empty Quarter) desert in the UAE (Wood & Imes, 2003). The Liwa water-table aquifer is located approximately 150 km southwest of the city of Abu Dhabi. Evaluation of current rainfall suggests that the aquifer is not currently receiving measurable recharge. Thus, the question is asked, “What is the age of the water in the aquifer?”

From studies in the area, it has been established that rainfall in the region was significantly greater during 33,000 to 19,000 BP and 9,000 to 5,000 BP (Clark & Fontes, 1990; Stokes et al., 2003). Thus, the question is, does the water's age reflect either of these periods? As carbon-14 dating potential falls within these intervals, it was selected to address the question. Four ages corrected for dead bicarbonate dilution ranged from 6,800 to 4,220 BP and averaged 5,200 BP, consistent with recharge during the youngest period of greater rainfall in the area (9,000 to 5,000 BP).

Assumptions for analysis of this system are

- carbon-14 in the groundwater originates only from recharge directly on the aquifer;
- the percent of modern carbon is only controlled by bicarbonate reaction;
- there is no recycling or concentration of carbon-14 within the aquifer;
- soil gas at the time of recharge was $-12.9\text{‰}_{\text{VPDB}}$, the same as currently observed;
- marine calcite in the sediments was $0.0\text{‰}_{\text{VPDB}}$; and
- there is no organic carbon in the system.

The ages were not calibrated as it was felt that the observed ages addressed the question asked; calibration would not have significantly impacted values in this age range, and calibrated ages would imply greater accuracy than is justified by the uncertainty of several components.

8.8 Estimate of Recharge Flux and Rainfall from a Paleo-Groundwater Surface: Liwa, UAE

It is sometimes desirable to have both estimates of paleo recharge flux and the associated paleo rainfall flux for climate modeling. In arid and semi-arid areas, the aeolian process is frequently in dynamic equilibrium with the top of the groundwater capillary zone. Thus, coastal areas and interdunal environments are characterized by evaporative aquifer discharge from the capillary surface where precipitation of gypsum, anhydrite, and calcite occurs. This cemented material forms an erosion-resistant deposit. If the water tables decline, erosion selectively leaves remnants of the former surface protruding above the current land surface.

The carbon in calcite (CaCO_3) was in equilibrium with atmospheric carbon dioxide at the deposition time; thus, it is possible to carbon-date the formation of the deposit if it is less than 50,000 years of age and obtain an elevation of the water table at that time. In many instances, the quartz sand in these surfaces can also be dated by optically stimulated

luminescence (OSL) methods. One can reconstruct the groundwater surface at a specific time by measuring the elevation of these dated features. Then, a numerical groundwater model used to vary the recharge flux to obtain the best fit to the observed shape and elevation of the paleo-water table.

The Liwa area of the Rub Al Khali desert, southwestern UAE (Figure 173), approximately 150 km southwest of the city of Abu Dhabi, exhibits a large regional water-table aquifer approximately 100 km by 100 km. This aquifer is up to 150 m thick and is formed of dunes composed of nearly uniform-sized grains, but is not currently receiving recharge—rainfall in the area appears to be less than 0.05 m/y. Based on paleoclimate in nearby Oman, this area is known to have had two periods of increased precipitation during approximately 33,000 to 19,000 BP and 9,000 to 5,000 BP (Clark & Fontes, 1990; Stokes et al., 2003).

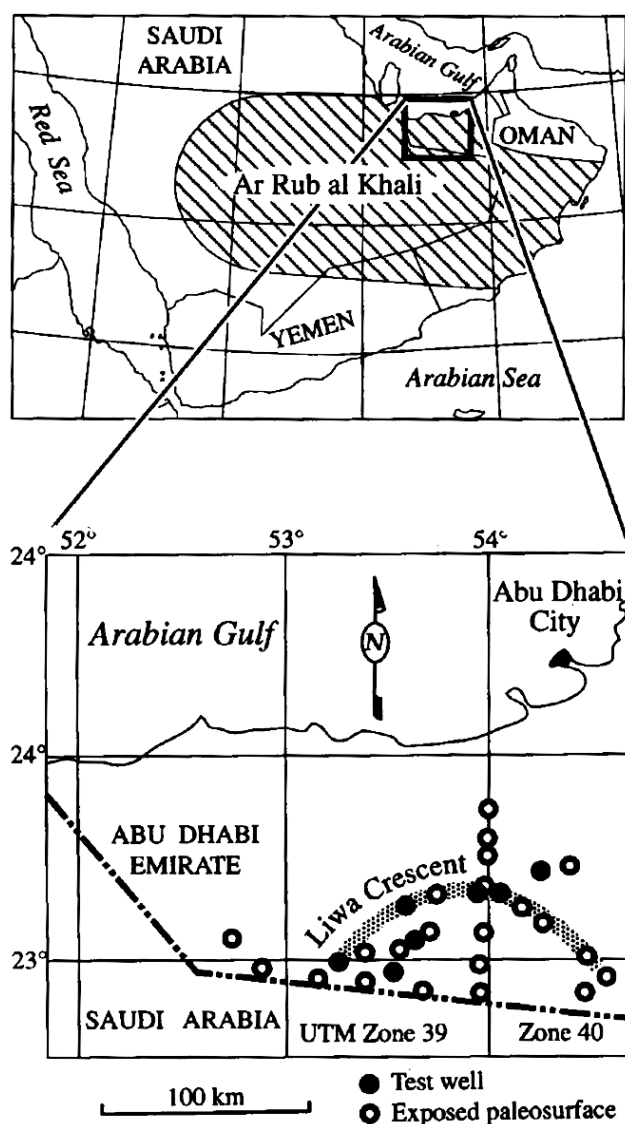


Figure 173 - Map showing locations of Zeugen (short, flat-topped, mesa-shaped features formed by resisting aeolian erosion of cemented calcite/sulfate deposits as indicated by open o's in the Liwa area of the UAE (reproduced from Wood & Imes, 1995).

As current hyper-arid conditions developed, the former cemented calcite/sulfate interdunal capillary surface resisted aeolian erosion and is represented by numerous isolated flat-topped mesa-shaped features (i.e., Zeugen) as indicated in Figure 173. The following questions arise, “Which of these periods formed the observed paleosurface? What were the recharge and precipitation fluxes at that time?” The average date was determined to be approximately 28,000 years BP, suggesting that the earlier wet period was the most dominant. The contoured elevation of these dated features represents a smooth former regional water table.

The hydraulic conductivity of the aeolian dune sand is exceptionally uniform and, based on numerous pumping tests, has a narrow range of between 1 to 5 m/d. A numerical groundwater model demonstrated that a recharge flux of approximately 1.4 mm/y yielded the best steady-state match of groundwater elevations for this 28,000-year-old paleo-water table (Wood & Imes, 1995). If it can be assumed that topography, sandy surfaces, and current general rainfall patterns and intensity of 28,000 years ago were like today, then recharge suggests rainfall of approximately 200 ± 50 mm/y—approximately three to five times greater than present (Wood & Imes, 1995).

As with any proxy for paleo-climate conditions, it is difficult to quantify uncertainty, and the estimates of recharge might range from 100 to 300 mm/y. Carbon-14 model dates can be adjusted for dead carbon using carbon-13 (Clarke & Fritz, 1997; Kalin in Cook & Hertzog, 2000). The carbon-14 dates were not calibrated in this case because we were interested in dates separated by tens of thousands of years, thus a slight adjustment would not be significant.

8.9 Estimate of Active Global Groundwater Volume

An estimate of the global volume of groundwater is important for understanding of global groundwater residence times for anthropogenic solutes that have been added to the groundwater reservoir. It is known that the annual global groundwater discharge is approximately $16,000 \text{ km}^3/\text{yr}$, but a well-constrained estimate of the total volume of the young active groundwater reservoir is lacking. Gleeson and others (2016) using tritium analyses and lithologic data estimated the volume of active groundwater (defined as water less than 100 years old) to be 0.63 million km^3 but this is not well constrained. One can estimate the volume of young groundwater by evaluating the mass of the geogenic and anthropogenic nitrogen. That is, in a steady state condition the mass of geogenic nitrogen plus the mass of anthropogenic nitrogen minus the mass of pre-anthropogenic nitrogen that has been displaced must equal the total mass of nitrogen that has been accumulating for 100 years. If the concentration of this total 100-year mass is known then we can estimate the volume of the aquifer as indicated in Equation (55).

$$\begin{aligned} & \text{Volume of Young (less than 100 yrs old) Groundwater} & (55) \\ = & \frac{\text{mass geogenic N} + \text{mass anthropogenic N} - \text{mass displaced geogenic N}}{\text{concentration of N in the aquifer}} \end{aligned}$$

By making seven assumptions, the global aquifer volume can be calculated.

1. Young active groundwater is less than 100 years old.
2. There is no change in aquifer volume over the past 100 years.
3. Annual global groundwater recharge/discharge has been a constant at 15.9×10^{15} L/yr over the past 100 years.
4. The sampling distribution shown in Figure 138 (in which 40 percent of the samples analyzed are geogenic, and 60 percent are anthropogenic) indicates the decimal volume of global aquifers that are geogenic (0.4) and anthropogenic (0.6).
5. The average geogenic N concentration of recharge water has been 0.22 mg/L.
6. The average anthropogenic N concentration of recharge water has been 1.4 mg/L.
7. The current observed N concentration in the global aquifer volume is 1.1 mg/L.

Aquifer Volume =

$$\frac{\left(\begin{array}{l} 0.22 \frac{\text{mg}}{\text{L}} (0.4) 15.9 \times 10^{15} \frac{\text{L}}{\text{yr}} 100 \text{yr} + \\ 1.4 \frac{\text{mg}}{\text{L}} (0.6) 15.9 \times 10^{15} \frac{\text{L}}{\text{yr}} 100 \text{yr} - \\ 0.22 \frac{\text{mg}}{\text{L}} (1.0) 15.9 \times 10^{15} \frac{\text{L}}{\text{yr}} 100 \text{yr} \end{array} \right)}{1.1 \frac{\text{mg}}{\text{L}}} = 1.02 \times 10^{18} \text{L}$$

Assumptions 1, 3, 5, and 7 are taken directly from data, thus are reasonable. The constant volume (assumption 2) is generally correct (although recently there has been dewatering of some major aquifer systems, the dewatered volume is a small portion of the global aquifer volume). Assumption 4 is reasonable given the observed distribution in data from a large number of samples reflecting a broad range of environments. The value of 1.4 mg/L for recharge concentration in the last 100 years (assumption 6) is a reasonable approximation as it must be greater than 0.42 and less than 2 mg/L (Wood et al., 2023a). Given the uncertainty associated with the input parameters, this estimate is not well constrained but is within the error calculated by Gleeson and others (2016) and thus is consistent with their estimate. The aquifer volume is calculated to be approximately 1 million km^3 . This estimate is somewhat larger than Gleeson and others (2016) of 0.63 million km^3 . The above analysis is an improvement on the analysis given by Wood and others (2023a).

9 Wrap-up

The coverage of hydrogeochemistry in this introductory, discovery monograph is different in several ways from previous publications on the topic: That is, this book looks at the following types of solutes:

- solutes that originate outside the aquifer and are transported into the aquifer by advection and diffusion;
- solutes that are residual since formation—relic, fossil, legacy, or connate; and
- solutes generated within the aquifer by reaction of water with the mineral framework of the aquifer, i.e., rock–water interactions and radioactive decay.

This monograph is unique in three ways.

1. It emphasizes conceptual and intuitive concepts and reactions—not guidance on rigorous hydrogeochemical calculations. However, elementary mathematics like those used in balancing a checking account, provide a mathematical model for some of the chemical processes.
2. It provides background for understanding the chemistry needed to develop a conceptual, back-of-the-envelope, first-approximation model of hydrogeochemistry in an aquifer. Performing this simple modeling early in a study illustrates where additional data are needed which is important because data collection is typically one of the most expensive parts of any study. Ideally, one would collect the correct number of samples to address the problem, not one more or one less.
3. Finally, it illustrates how hydrogeochemistry differs from physical hydrogeology and elucidates the questions common to each discipline. Hydrogeochemistry pertains to what has happened in the distant past to explain present observations and how the solutes evolved to their present state over geologic time when the chemical constituents were reacting along the flow paths. In some cases, the aim is to use hydrogeochemistry to understand the groundwater flow system or how the landscape has evolved. In physical hydrogeology, the key parameters (such as water level) have no memory. Assessment of physical hydrogeology, requires far fewer parameters and equations than hydrogeochemistry, for which a multitude of equations and parameters are applied.

In hydrogeochemistry, the concept of chemical equilibrium is commonly the basis for the analysis or description of the chemical state of water. It can be important to assess the degree of disequilibrium concerning each mineral component of the geologic medium to understand how solute chemistry has evolved to its current composition. Much of the computational effort in hydrogeochemistry is directed at computing the solute chemistry that would occur under a variety of assumed chemical equilibria between the water and

various minerals. A simple model can illustrate where more data are necessary for a better understanding and can be evaluated by using more sophisticated numerical modeling. Many systems are numerically modeled to carry the interpretive endeavor to its most advanced stage.

The change in both the solutes and the mineral aquifer framework along the length of the flow paths, and the geologic time required for the stages of solute evolution can be estimated by using back-of-the-envelope models framed by introductory chemistry. This was undertaken to address the substantial solute mass in aquifers that is referred to as relic, fossil, legacy, or connate—that is, solutes left from past geologic environments when the geologic strata formed in an ocean, brine, or another environment. Depending on the age of the flow system (i.e., when it became an active aquifer), this legacy solute source often comes from low permeability zones that have resisted flushing and may have a significant impact on the hydrogeochemistry of an aquifer. In short, we go beyond chemical reactions to include elements of flow—advection, molecular diffusion, and ion filtering—occurring within the groundwater flow system. An essential part of explaining groundwater's chemical composition is solute accounting—that is, mass balance—of these soluble constituents.

In summary, this monograph presents an approach to infer how and when the solution evolved to its present composition (i.e., its solute concentrations and ionic ratio) rather than predicting chemical composition in the future. Projecting into the past from the present is common to historical sciences like geoscience and astronomy; it is intellectually analogous to future predictions and is a worthy pursuit.

10 Exercises

Exercise 1 - Intrinsic and environmental controls

Identify and briefly describe the intrinsic and environmental controls on the thermodynamics controlling mineral equilibrium.

[Solution to Exercise 1](#) ↓

[Return to where text linked to Exercise 1](#) ↑

Exercise 2 - Concentration of trace elements

Of the approximately 80 elements identified in groundwater, about 15 have deleterious effect on humans if consumed. What are the factors that determine the concentration of trace elements.

[Solution to Exercise 2](#) ↓

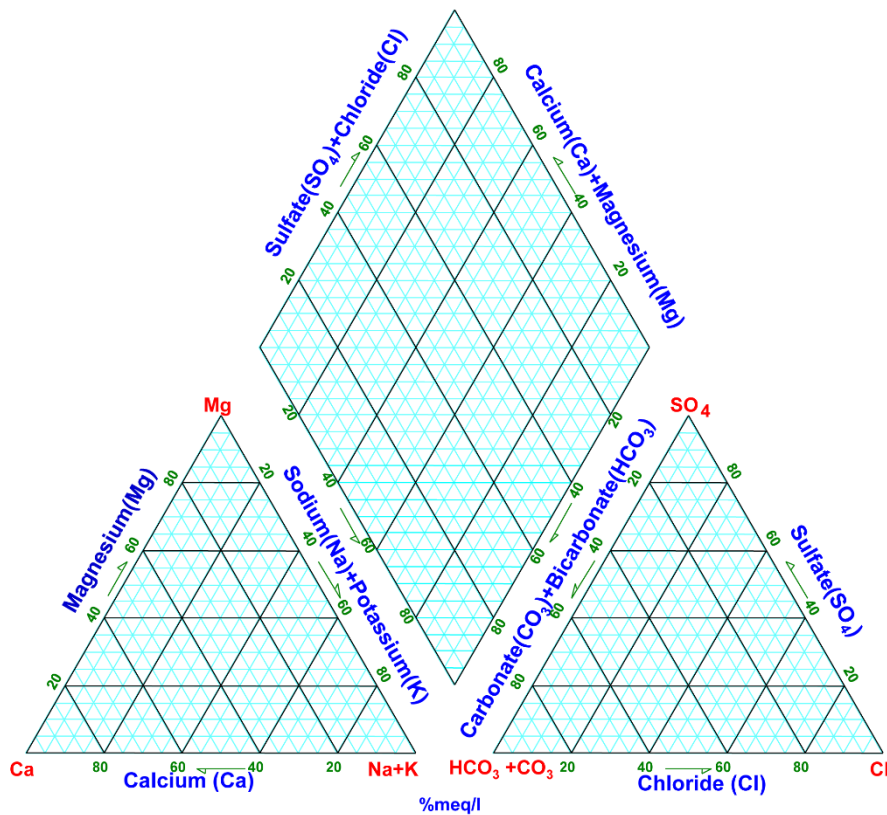
[Return to where text linked to Exercise 2](#) ↑

Exercise 3 - Graphical presentations

Articulate the reasoning and concept behind different graphical presentations of hydrogeochemical data.

ion	meq/L	percent
Ca	6.54	53.5
Mg	3.62	29.7
Na+K	2.05	16.8
CO₃⁻²+HCO₃⁻	3.28	25.6
SO₄	8.97	70.2
Cl	0.54	4.2

Determine the water type for the sample data from the Wild Rose sampling site in the Panamint Mountains west of Death Valley, California, USA. The data are shown in the following table. Blank trilinear diagram paper is included for your convenience.



[Solution to Exercise 3](#) ↓

[Return to where text linked to Exercise 3](#) ↑

Exercise 4 - Identifying hydrogeochemical processes in the field

Describe the basic approach necessary to identify various hydrogeochemical processes in a field environment.

[Solution to Exercise 4](#) ↓

[Return to where text linked to Exercise 4](#) ↑

Exercise 5 - Sources of solutes in groundwater and RCV

Solutes in groundwater are from four fundamental sources. Identify these sources and sinks and illustrate them in a representative control volume.

[Solution to Exercise 5](#) ↓

[Return to where text linked to Exercise 5](#) ↑

11 References

- Alley, W. M., Reilly, T. E., & Franke, O. L. (1999). *Sustainability of ground-water resources* (Vol. 1186). US Geological Survey.
- Appelo, C. A. J., & Postma, D. (2005). *Geochemistry, groundwater and pollution*. CRC Press. <https://doi.org/10.1201/9781439833544>.
- Ayotte, J. D., Gronberg, J. M., & Apodaca, L. E. (2011). *Trace elements and radon in groundwater across the United States, 1992–2003* (Vol. 2011). US Geological Survey. <http://pubs.usgs.gov/sir/2011/5059>.
- Back, W. (1960). Origin of hydrochemical facies of ground water in the Atlantic Coastal Plain. In *Geochemical cycles: 21st International Geology Congress Proceedings, part 1, Copenhagen* (pp. 87–95).
- Back, W. (1966). *Ground-water flow patterns in northern part of Atlantic Coastal Plain* (Professional Paper 498A). US Geological Survey.
- Back, W., Baedecker, M. J., & Wood, W. W. (1993). Scales in chemical hydrogeology: A historical perspective. In W. M. Alley (Ed.), *Regional ground-water quality* (pp. 111–128). John Wiley & Sons.
- Beerling, D. J., & Berner, R. A. (2005). Feedbacks and the coevolution of plants and atmospheric CO₂. *Proceedings of the National Academy of Sciences*, 102(5), 1302–1305. <https://doi.org/10.1073/pnas.0408724102>.
- Bengtsson, G., & Annadotter, H. (1989). Nitrate reduction in a groundwater microcosm determined by 15N gas chromatography-mass spectrometry. *Applied and Environmental Microbiology*, 55(11), 2861–2870. <https://doi.org/10.1128/aem.55.11.2861-2870.1989>.
- Berner, E. K., & Berner, R. A. (2012). *Global environment: Water, air, and geochemical cycles*. Princeton University Press. <https://doi.org/10.1515/9781400842766>.
- Berner, R. A. (1998). The carbon cycle and carbon dioxide over Phanerozoic time: The role of land plants. *Philosophical Transactions of the Royal Society of London. Series B: Biological Sciences*, 353(1365), 75–82. <https://doi.org/10.1098/rstb.1998.0192>.
- Berry, F. A. F. (1959). *Hydrodynamics and geochemistry of the Jurassic and Cretaceous systems in the San Juan Basin, northwestern New Mexico and southwestern Colorado*. (Publication No. 5903682) [Doctoral dissertation, Stanford University]. ProQuest Dissertations and Theses Global.
- Berry, F. A. (1960). Geologic field evidence suggesting membrane properties of shales. *AAPG Bulletin*, 44(6), 953–954.

- Berry, F. A. (1969). Relative factors influencing membrane filtration effects in geologic environments. *Chemical Geology*, 4(1–2), 295–301. [https://doi.org/10.1016/0009-2541\(69\)90051-5](https://doi.org/10.1016/0009-2541(69)90051-5).
- Box, G. E. P. (1976). Science and statistics. *Journal of the American Statistical Association*, 71(356), 791–799. <http://doi:10.1080/01621459.1976.10480949>.
- Boyer, E. W., Howarth, R. W., Galloway, J. N., Dentener, F. J., Green, P. A., & Vörösmarty, C. J. (2006). Riverine nitrogen export from the continents to the coasts. *Global Biogeochemistry Cycles*, 20, GB1S91. <http://doi.org/10.1029/2005GB002537>.
- Braitsch, O. (1971). *Salt deposits: Their origin and composition* (Vol. 4). Springer Science & Business Media.
- Bredehoeft, J. D. (2002). The water budget myth revisited: Why hydrogeologists model. *Groundwater*, 40(4), 340–345. <https://doi.org/10.1111/j.1745-6584.2002.tb02511.x>.
- Bredehoeft, J. D., Blyth, C. R., White, W. A., & Maxey, G. B. (1963). Possible mechanism for concentration of brines in subsurface formations. *AAPG Bulletin*, 47(2), 257–269. <https://doi.org/10.1306/BC743983-16BE-11D7-8645000102C1865D>.
- Bricker, O. P. (1967). Cations and silica in natural waters: Control by silicate minerals. *International Association of the Science of Hydrology*, 78, 110–119.
- Brown, R. F., Signor, D. C. & Wood, W. W. (1978). *Artificial ground-water recharge as a water-management technique on the Southern High Plains of Texas and New Mexico* (Report 220). Texas Department of Water Resources.
- Burns, S. J., Matter, A., Norbert F., Mangini, A. (1998) Speleothem--based paleoclimate record from northern Oman. *Geology*, 26(6), 499–502. [https://doi.org/10.1130/0091-7613\(1998\)026<0499:SBPRFN>2.3.CO;2](https://doi.org/10.1130/0091-7613(1998)026<0499:SBPRFN>2.3.CO;2)
- Cederstrand, J. R., & Becker, M. F. (1998). *Digital map of hydraulic conductivity for the High Plains Aquifer in parts of Colorado, Kansas, Nebraska, New Mexico, Oklahoma, South Dakota, Texas, and Wyoming* (No. 98-548). US Geological Survey. <https://doi.org/10.3133/ofr98548>.
- Chamberlin, T. C. (1890/1965). The method of multiple working hypotheses. *Science*, 148(3671), 754–759. <http://www.jstor.org/stable/1716334>.
- Chebotarev, I. I. (1955). Metamorphism of natural waters in the crust of weathering-3. *Geochimica et Cosmochimica Acta*, 8(4), 198–212. [https://doi.org/10.1016/0016-7037\(55\)90053-3](https://doi.org/10.1016/0016-7037(55)90053-3).
- Cherry, J. A. (Ed.). (1983). Migration of contaminants in groundwater at a landfill: A case study. *Journal of Hydrology*, 63(1–2), 1–197. <https://www.sciencedirect.com/journal/journal-of-hydrology/vol/63/issue/1>.
- Clark, I. (2015). *Groundwater geochemistry and isotopes*. CRC Press. <https://doi.org/10.1201/b18347>.

- Clark, I. D., & Fontes, J. C. (1990). Paleoclimatic reconstruction in northern Oman based on carbonates from hyperalkaline groundwaters. *Quaternary Research*, 33(3), 320–336. [https://doi.org/10.1016/0033-5894\(90\)90059-T](https://doi.org/10.1016/0033-5894(90)90059-T).
- Clark, I. D., & Fritz, P. (1997). *Environmental isotopes in hydrogeology* (1st ed.). CRC Press. <https://doi.org/10.1201/9781482242911>.
- Cleveland, W. S. (1985). *The elements of graphing data*. Wadsworth. <https://doi.org/10.1109/TVCG.2022.3158093>.
- Cook, P. G. (2020). *Introduction to isotopes and environmental tracers as indicators of groundwater flow*. The Groundwater Project. <https://gw-project.org/books/introduction-to-isotopes-and-environmental-tracers-as-indicators-of-groundwater-flow/>.
- Cook, P. G., & Herczeg, A. L. (2000). *Environmental tracers in subsurface hydrology*. Kluwer Academic.
- Cooper, H. H. (1964). *A hypothesis concerning the dynamic balance of fresh water and salt water in a coastal aquifer* (Water Supply Paper 1613-C). US Geological Survey.
- Dai, A., & Trenberth, K. E. (2002). Estimates of freshwater discharge from continents: Latitudinal and seasonal variations. *Journal of Hydrometeorology*, 3(6), 660–687. [https://doi.org/10.1175/1525-7541\(2002\)003<0660:EOFDFC>2.0.CO;2](https://doi.org/10.1175/1525-7541(2002)003<0660:EOFDFC>2.0.CO;2).
- Darwin, C. (1859). *On the origin of species* (1st ed.). Murray.
- DeSimone, L. A., Hamilton, P. A., & Gilliom, R. J. (2009). *Quality of water from domestic wells in principal aquifers of the United States, 1991–2004: Overview of major findings* (Circular 1332). US Geological Survey.
- DeSimone, L. A., McMahon, P. B., & Rosen, M. R. (2014). *The quality of our nation's waters: Water quality in principal aquifers of the United States, 1991–2010* (Circular 1360). United States Geological Survey. <https://doi.org/10.3133/cir1360>.
- Diamond, R. E. (2022). *Stable isotope hydrology*. The Groundwater Project. <https://doi.org/10.21083/978-1-77470-043-3>.
- Downing, J. A., & Striegl, R. G. (2018). Size, age, renewal, and discharge of groundwater carbon. *Inland Waters*, 8(1), 122–127. <https://doi.org/10.1080/20442041.2017.1412918>.
- Drever, J. (1997). *The geochemistry of natural waters: Surface and groundwater environments*. Pearson College Division, 436 p.
- Drever, J. I., & Vance, G. F. (1994). Role of soil organic acids in mineral weathering processes. In E. D. Pittman & M. D. Lewan (Eds.), *Organic acids in geological processes* (pp. 138–161). Springer. https://doi.org/10.1007/978-3-642-78356-2_6.
- Edmunds, W. M., & Smedley, P. L. (2013). Fluoride in natural waters. In O. Selinus, B. Alloway, J. A. Centeno, R. B. Finkelman, R. Fuge, U. Lindh, P. Smedley (Eds.), *Essentials of medical geology* (Revised ed.) (pp. 311–336). Springer.

- Edmunds, W. M., Kay, R. L. F., & McCartney, R. A. (1985). Origin of saline groundwaters in the Carnmenellis granite (Cornwall, England): Natural processes and reaction during hot dry rock reservoir circulation. *Chemical Geology*, 49(1-3), 287–301. [https://doi.org/10.1016/0009-2541\(85\)90162-7](https://doi.org/10.1016/0009-2541(85)90162-7).
- El-Hussain, I., Saad, M. G., Deif, A., Mohamed, A. E. M., & Ezzelarab, M. (2018). Seismic liquefaction potential in Muscat, Sultanate of Oman. *Journal of Earth Science & Climate Change*, 9(2), 451. <http://doi.org/10.4172/2157-7617.1000451>.
- Erik, E. (1952). Composition of atmospheric precipitation II. Sulfur chloride, iodine compounds. *Tellus*, 4, 280–303.
- Eriksson, E., & Khunakasem, V. (1969). Chloride concentration in groundwater, recharge rate and rate of deposition of chloride in the Israel coastal plain. *Journal of Hydrology*, 7(2), 178–197. [https://doi.org/10.1016/0022-1694\(69\)90055-9](https://doi.org/10.1016/0022-1694(69)90055-9).
- Food and Agriculture Organization (FAO) of the United Nations. (2021). *Global map of salt-affected soils*. UN.
- Faure, G., & Mensing T. M. (2005). *Isotopes: Principles and applications* (3rd ed.). Wiley.
- Ford, T. D. & Cullingford, C. H. D. (Eds). (1978). The science of speleology. *Earth Surface Processes*, 3(3), 327–328.
- Ford, T. D., & Williams, P. (2007). *Karst hydrogeology and geomorphology*. Wiley.
- Freeze, R. A., & Cherry, J. A. (1979) *Groundwater*. Prentice-Hall Inc. <https://gw-project.org/books/groundwater/>.
- Fritz, P., & Fontes, J. C. (1980). *Handbook of environmental isotope geochemistry* (Vol. 1). Elsevier.
- Galloway, J. N., Dentener, F. J., Capone, D. G., Boyer, E. W., Howarth, R. W., Seitzinger, S. P., Asner, G. P., Cleveland, C., Green, P. A., Holland, E. A., Karl, D. M., Michaels, A. F., Porter, J. H., Townsend, A. R., & Vöosmarty, C. J. (2004). Nitrogen cycles: Past, present, and future. *Biogeochemistry*, 70, 153–226. <https://doi.org/10.1007/s10533-004-0370-0>.
- Garrels, R. M. & MacKenzie, F. T. (1967). Origin of the chemical compositions of some springs and lakes. In W. Stumm (Ed.), *Equilibrium concepts in natural water systems* (pp. 222–242). Advances in Chemistry Series Vol. 67, American Chemical Society. <https://doi.org/10.1021/ba-1967-0067.ch010>.
- Gleeson, T., Befus, K. M., Jasechko, S., Luijendijk, E., & Cardenas, M. B. (2016). The global volume and distribution of modern groundwater. *Nature Geoscience*, 9(2), 161–167. <https://doi.org/10.1038/ngeo2590>.
- Goss, D. W., Smith, S. J., Stewart, B. A., & Jones, O. R. (1973). Fate of suspended sediment during basin recharge. *Water Resources Research*, 9(3), 668–675. <https://doi.org/10.1029/WR009i003p00668>.

- Grapher Helper (n.d.). *Durov and Durov class plots*. Retrieved 2023, from http://grapherhelp.goldensoftware.com/Graphs/Durov_plots.htm.
- Green, P. A., Vörösmarty, C. J., Meybeck, M., Galloway, J. N., Peterson, B. J., & Boyer, E. W. (2004). Pre-industrial and contemporary fluxes of nitrogen through rivers: A global assessment based on typology. *Biogeochemistry*, 68, 71–105. <https://doi.org/10.1023/B:BIOG.0000025742.82155.92>.
- Gruber, N. & Galloway, J. N. (2008). An earth-system perspective of the global nitrogen cycle. *Nature*, 451(7176), 293–296. <https://doi.org/10.1038/nature06592>.
- Haacker, E. M., Kendall, A. D., & Hyndman, D. W. (2016). Water level declines in the High Plains Aquifer: Predevelopment to resource senescence. *Groundwater*, 54(2), 231–242. <https://doi.org/10.1111/gwat.12350>.
- Hall, F. R., Boudette, E. L., & Olszewski, W. J., Jr. (1987). Geologic controls and radon occurrence in New England. In B. Graves (Ed.), *Radon, radium and other radioactivity in ground water*. Lewis Publishers.
- Hammer, U. T. (1986). *Saline lake ecosystems of the world*. Springer.
- Hanshaw, B. B., & Coplen, T. B. (1973). Ultrafiltration by a compacted clay membrane—II. Sodium ion exclusion at various ionic strengths. *Geochimica et Cosmochimica Acta*, 37(10), 2311–2327. [https://doi.org/10.1016/0016-7037\(73\)90106-3](https://doi.org/10.1016/0016-7037(73)90106-3).
- Hardie, L. A., & Eugster, H. P. (1970). The evolution of closed-basin brines. *Mineralogical Society of America Special Paper 3*, 253–273.
- Hebestreit, K., Stutz, J., Rosen, D., Matveiv, V., Peleg, M., Luria, M., & Platt, U. (1999). DOAS measurements of tropospheric bromine oxide in mid-latitudes. *Science*, 283(5398), 55–57. <https://doi.org/10.1126/science.283.5398.55>.
- Hem, J. D. (1985). *Study and interpretation of the chemical characteristics of natural water* (Water-Supply Paper 2254). US Geological Survey.
- Hendry, M. J., Cherry, J. A., & Wallick, E. I. (1986). Origin and distribution of sulfate in a fractured till in southern Alberta, Canada. *Water Resources Research*, 22(1), 45–61. <https://doi.org/10.1029/WR022i001p00045>.
- Henry, L. (2023, April 13). The soil salinity story. *Grainews*. <https://www.grainews.ca/columns/les-henry-the-soil-salinity-story/>.
- Herczeg, A. L., Dogramaci, S. S., & Leaney, F. W. J. (2001). Origin of dissolved salts in a large, semi-arid groundwater system: Murray Basin, Australia. *Marine and Freshwater Research* 52(1), 41–52. <https://doi.org/10.1071/MF00040>.
- High Plains Underground Water District. (1984). *The High Plains aquifer report* [Unpublished manuscript]. High Plains Underground Water District.
- Holland, H. D., Kirsipu, T. V., Huebner, J. S., & Oxburgh U. M. (1964). On some aspects of the chemical evolution of cave waters. *Journal of Geology*, 72(1).

<https://doi.org/10.1086/626964>.

- Holtschlag, D. J., Lukkonen, C. L., & Nichols, J. R. (1996) *Simulation of ground-water flow in the Saginaw Aquifer, Clinton, Eaton, and Ingham Counties, Michigan* (Water-Supply Paper 2480). US Geological Survey.
- Hönninger, G., Bobrowski, N., Palenque E. R., Torrez, R. & Platt, U. (2004). Reactive bromine and sulfur emissions at Salar de Uyuni, Bolivia. *Geophysical Research Letters*, 31(4), L04101. <https://doi.org/10.1029/2003GL018818>.
- Imes, J. L., & Wood, W. W. (2007). Solute and isotope constraint of groundwater recharge simulation in an arid environment, Abu Dhabi Emirate, United Arab Emirates. *Hydrogeology Journal*, 15, 1307–1315. <https://doi.org/10.1007/s10040-007-0177-x>.
- International Atomic Energy Agency (IAEA). (2013). *Isotope methods for dating old groundwater*. IAE.
- Istok, J. D., Humphery, M. D., Schroth, M. H., Hyman, M. R., & O'Reilly, K. T. (1997). Single-well, “push-pull” test for in situ determination of microbial metabolite activities. *Groundwater*, 35(4), 619–631. <https://doi.org/10.1111/j.1745-6584.1997.tb00127.x>.
- Jiang, X.-W., & Cherry, J. (2024). *History and hydraulics of flowing wells*. The Groundwater Project. <https://doi.org/10.21083/CPET1503>.
- Jurgens, B. C., McMahan, P. B., Chapelle, F. H., & Eberts, S. M. (2009). *An Excel workbook for identifying redox processes in ground water* (Open-File Report 2009-1004). US Geological Survey.
- Kloprogge, J. T., & Hartman, H. (2022), Clays and the origin of life: The experiments. *Life*, 12(2), 259. <https://doi.org/10.3390/life12020259>.
- Kendall, C., & Coplen T. B. (2001). Distribution of oxygen-18 and deuterium in river waters across the United States. *Hydrological Processes*, 15(7), 1363–1393. <https://doi.org/10.1002/hyp.217>.
- Kentucky Geological Survey (KGS) (n.d.). *Karst is a landscape*. KGS. <https://www.uky.edu/KGS/karst/>.
- Kessler, T. J., & Harvey, C. F. (2001). The global flux of carbon dioxide into groundwater. *Geophysical Research Letters*, 28(2), 279–282. <https://doi.org/10.1029/2000GL011505>.
- Kowalczyk, A. J., & Froelich, P. N. (2010). Cave air ventilation and CO₂ outgassing by radon-222 modeling: How fast do caves breathe? *Earth and Planetary Sciences Letters*, 289(1–2), 209–219. <https://doi.org/10.1016/j.epsl.2009.11.010>.
- Kraemer, T. F., Wood, W. W., & Sanford, W. E. (2014). Distinguishing seawater from geologic brine in saline coastal groundwater using radium-226; An example from the sabkhat of the UAE. *Chemical Geology*, 371, 1–8. <https://doi.org/10.1016/j.chemgeo.2014.01.018>.

- Kuniansky, E. I., Taylor, C. J., Williams, J. H. & Paillet, F. (2022.) *Introduction to karst aquifers*. The Groundwater Project. <https://doi.org/10.21083/978-1-77470-040-2>.
- Langmuir, D. (1996). *Aqueous environmental geochemistry*. Prentice Hall.
- Lasaga, A. C. (1984). Chemical kinetics of water–rock interaction. *Journal of Geophysical Research: Solid Earth*, 89(B6), 4009–4025. <https://doi.org/10.1029/JB089iB06p04009>.
- Lasaga, A. C., Soler, J. M., Ganor, J., Burch, T. E., & Nagy, K. L. (1994). Chemical weathering rate laws and global biogeochemical cycles. *Geochimica et Cosmochimica Acta*, 58(10), 2361–2386. [https://doi.org/10.1016/0016-7037\(94\)90016-7](https://doi.org/10.1016/0016-7037(94)90016-7).
- LeBlanc, D. R., Garabedian, S. P., Hess, K. M., Gelhar, L. W., Quadri, R. D., Stollenwerk, K. G., & Wood, W. W. (1991). Large-scale natural-gradient tracer test in sand and gravel, Cape Cod, Massachusetts: 1. Experimental design and observed tracer movement. *Water Resources Research*, 27(5), 895–910. <https://doi.org/10.1029/91WR00241>.
- Lee, S., Irvine, D. J., Duvert, C., Rau, G. C., & Cartwright, I. (2024). A high-resolution map of diffuse groundwater recharge rates for Australia. *Hydrology and Earth Systems Science*, 28, 1771–1790. <https://doi.org/10.5194/hess-28-1771-2024>.
- Lehner, B. (2014). *HydroBASINS: Global watershed boundaries and sub-basin delineations derived from HydroSHEDS data at 15 second resolution – Technical documentation version 1.c*. [Data set]. HydroSheds. <https://hydrosheds.org/page/hydrobasins>.
- Lindsey, B. D., Belitz, K., Cravotta C. A., III, Toccalino, P. L., & Dubrovsky, N. N. (2021). Lithium in groundwater used for drinking-water supply in the United States. *Science of the Total Environment*, 767, 1–15. <https://doi.org/10.1016/j.scitotenv.2020.144691>.
- Long, D. T., & Larson, G. J. (1983). *Field evidence for shale membrane filtration of groundwater, south-central Michigan* (PB83-190488, Completion Report). National Technical Information Service.
- Luijendijk, E., Gleeson, T., & Moosdorf, N. (2020). Fresh groundwater discharge is insignificant for the world’s oceans but important for coastal ecosystems. *Nature Communication*, 11(1), 1260. <https://doi.org/10.1038/s41467-020-15064-8>.
- Mahler, B., Personné, J., Lods, G., & Drogue, C. (2000). Transport of free and particulate-associated bacteria in karst. *Journal of Hydrology*, 238(3–4), 179–193. [https://doi.org/10.1016/S0022-1694\(00\)00324-3](https://doi.org/10.1016/S0022-1694(00)00324-3).
- Manna, F., Cherry, J. A., McWhorter, D. B., & Parker, B. L. (2016). Groundwater recharge assessment in an upland sandstone aquifer of southern California. *Journal of Hydrology*, 541(Part B), 787–799. <https://doi.org/10.1016/j.jhydrol.2016.07.039>.
- Manna, F., Walton, K. M., Cherry, J. A., & Parker, B. L. (2019). Five-century record of climate and groundwater recharge variability in southern California. *Scientific Reports*, 9, 18215. <https://doi.org/10.1038/s41598-019-54560-w>.

- Matthess, G. (1982). *The properties of water*. John Wiley.
- Matveev, V., Peleg, M., Rosen, D., Tov-Alper, D. S., Hebestreit, K., Stutz, J., Platt, U., Blake, D., & Luria, M. (2001). Bromine oxide–ozone interaction over the Dead Sea. *Journal of Geophysical Research: Atmospheres*, 106(D10), 10375–10378.
<https://doi.org/10.1029/2000JD900611> ↗.
- McLennan, S. M. (1993). Weathering and global denudation. *The Journal of Geology*, 101(2), 295–303. <https://www.jstor.org/stable/30081153> ↗.
- McMahon, P. B., Belitz, K., Reddy, J. E., & Johnson, T. D. (2019). Elevated manganese concentrations in United States groundwater, role of land surface–soil–aquifer connections. *Environmental Science & Technology*, 53(1), 29–38.
<https://doi.org/10.1021/acs.est.8b04055> ↗.
- McMahon, P. B., Brown C. J., Johnson, T. D., Belitz, K., & Lindsey, B. D. (2020). Fluoride occurrence in United States groundwater. *Science of The Total Environment*, 732, 139217. <https://doi.org/10.1016/j.scitotenv.2020.139217> ↗.
- Meybeck, M. (2003). Global occurrence of major elements in rivers. In H. D. Holland & K. K. Turekian (Eds.), *Treatise on geochemistry* (pp. 207–223). Elsevier Science.
<https://doi.org/10.1016/B0-08-043751-6/05164-1> ↗.
- Milliman, J. D. (2001). River inputs. In J. H. Steele, S. A. Thorpe, & K. K. Turekian (Eds.), *Encyclopedia of ocean science, ocean currents* (pp. 2419–2427). Academic Press.
- Milliman, J. D. & Meade, R. H. (1983). World-wide delivery of river sediment to the oceans. *Journal of Geology* 91(1), 1–21.
<https://www.journals.uchicago.edu/doi/abs/10.1086/628741> ↗.
- Montgomery, D. R. (2012). *Dirt: The erosion of civilizations*. University of California Press.
- Musgrove, M. L. (2021). The occurrence and distribution of strontium in U.S. groundwater. *Applied Geochemistry*, 126, 104867.
<https://doi.org/10.1016/j.apgeochem.2020.104867> ↗.
- National Atmospheric Deposition Program (NADP). (2019). *National Trend Network, Mercury Deposition Network, Atmospheric Integrated Research Monitoring Network, Atmospheric Mercury Network (wet and dry), and Ammonia Monitoring Network* [Data set]. NADP. <https://nadp.slh.wisc.edu> ↗.
- National Atmospheric Deposition Program (NADP). (2020). *Total deposition maps* [Data set]. NADP. <https://nadp2.slh.wisc.edu/data/annualmaps.aspx> ↗.
- Neuzil, C. E., & Person, M. (2017). Reexamining ultrafiltration and solute transport in groundwater. *Water Resources Research*, 52(6), 4922–4941.
<https://doi.org/10.1002/2017WR020492> ↗.

- Osterkamp, W. R., & Wood, W. W., 1987, Playa-lake basins on the southern high plains of Texas and New Mexico: Part I. Hydrologic, geomorphic and geologic evidence for their development. *Geological Society of America Bulletin*, 99(2), 215–223.
[https://doi.org/10.1130/0016-7606\(1987\)99<215:PBOTSH>2.0.CO;2](https://doi.org/10.1130/0016-7606(1987)99<215:PBOTSH>2.0.CO;2).
- Palmer, C. D., & Cherry, J. A. (1984). Geochemical evolution of groundwater in sequences of sedimentary rocks. *Journal of Hydrology* 75(1–4), 27–65.
[https://doi.org/10.1016/0022-1694\(84\)90045-3](https://doi.org/10.1016/0022-1694(84)90045-3).
- Parkhurst, D. L., & Appelo, C. A. J. (2013). Description of input and examples for PHREEQC version 3—A computer program for speciation, batch-reaction, one-dimensional transport, and inverse geochemical calculations. *US Geological Survey Techniques and Methods*, 6(A43), 497. <https://pubs.usgs.gov/tm/06/a43/>.
- Pummer, L. N., Prestemon, E. C., & Parkhurst, D. L. (1994). *An interactive code (NETPATH) for modeling net geochemical reactions along a flow path* (Water-Resources Investigations Report 94–4169). US Geological Survey.
- Plummer, L. N., Bexfield, L. M., Anderholm, S. K., Sanford, W. E., & Busenberg, E. (2004). Hydrochemical tracers in the middle Rio Grande Basin, USA: 1. Conceptualization of groundwater flow. *Hydrogeology Journal*, 12, 359–388.
<https://doi.org/10.1007/s10040-004-0324-6>.
- Podgorski, J. & Berg, M. (2020). Global threat of arsenic in groundwater. *Science* 368(6493), 845–850. <https://doi.org/10.1126/science.aba1510>.
- Poeter, E., Fan, Y., Cherry, J., Wood, W., & Mackay, D. (2020). *Groundwater in our water cycle*. The Groundwater Project. <https://doi.org/10.21083/978-1-7770541-1-3>.
- Ravenscroft, P. & Lytton, L (2022). *Seeing the invisible: A strategic report on groundwater quality*. World Bank Group.
- Reimer, P. J., Baillie, M. G. L., Bard, E., Bayliss, A., Beck, J. W., Blackwell, P. G., Bronk Ramsey, C., Buck, C. E., Burr, G. S., Edwards, R. L., Friedrich, M., Grootes, P. M., Guilderson, T. P., Hajdas, I., Heaton, T. J., Hogg, A. G., Hughen, K. A., Kaiser, K. F., Kromer, B., McCormac, F.G., Manning, S.W., Reimer, R.W., Richards, D.A., Southon, J.R., Talamo, S., Turney, C.S.M., van der Plicht, J., and Weyhenmeyer, C. E. (2009). IntCal09 and Marine09 radiocarbon age calibration curves, 0–50,000 years cal BP. *Radiocarbon*, 51(4), 1111–1150.
<https://doi.org/10.1017/S0033822200034202>.
- Rockström, J., Steffen, W., Noone, K., Persson, Å., Chapin III, F. S., Lambin, E. F., Lenton, T. M., Scheffer, M., Folke, C., Schellnhuber, H. J., Nykvist, B., de Witt, C. A., Hughes, T., van der Leeuw, S., Rodhe, H., Sörlin, S., Snyder, P. K., Costanza, R., Svedin, U.,...Foley, J. A. (2009). A safe operating space for humanity. *Nature*, 461, 472–475.
<https://doi.org/10.1038/461472a>.

- Rowe, J. J., Fournier, R. O., & Morey, G. W. (1973). *Chemical analysis of thermal waters in Yellowstone National Park, Wyoming, 1960–65* (No. 1303-1305). US Geological Survey.
- Sanford, W. E., & Wood, W. W. (1991). Brine evolution and mineral deposition in hydrologically open evaporite basins. *American Journal of Science*, 291(7), 687–710.
- Sanford, W. E., & Wood, W. W. (2001). Hydrology of the coastal sabkhas of Abu Dhabi, United Arab Emirates. *Hydrogeology Journal*, 9(4), 358–366.
<https://doi.org/10.1007/s100400100137>.
- Sanford, W. E., Doughten, M. W., Coplen, T. B., Hunt, A. G., & Bullen, T. D. (2013). Evidence for high salinity of Early Cretaceous Sea water from the Chesapeake Bay crater. *Nature*, 503, 252–256. <https://doi.org/10.1038/nature12714>.
- Schmied, M. H., Cáceres, D., Eisner, S., Flörke, M., Herbert, C., Niemann, C., Peiris, T. A., Popat, E., Portmann, F. T., Reinecke, R., Schumacher, M., Shadkam, S., Telteu, C.-E., Trautmann, T., & Döll, P. (2021). The global water resources and use model WaterGAP v2. 2d: Model description and evaluation. *Geoscientific Model Development*, 14(2), 1037–1079. <https://doi.org/10.5194/gmd-14-1037-2021>.
- Scholler, H. (1956). *Geochimie des eaux souterraines: Application aux eaux de gisement de pétrole* [Groundwater geochemistry: Application to oil field waters]. Paris.
- Schullehner, J., Hansen, B., Thygesen, M., Pedersen, C. B., & Sigsgaard, T. (2018). Nitrate in drinking water and colorectal cancer risk: A nationwide population-based cohort study. *International Journal of Cancer* 143 (1), 73–79.
<https://doi.org/10.1002/ijc.31306>.
- Shand, P., Edmunds, W. M., Lawrence, A. R., Smedley, P., & Burke, S. (2007). *The natural (baseline) quality of groundwater in England and Wales* (Research Report RR/07/06 and Technical Report NC/99/74/24). British Geological Survey.
<https://nora.nerc.ac.uk/id/eprint/3578/1/RR07006.pdf>.
- Shiklomanov, I. (1993). World freshwater resources. In P. H. Gleick (Ed.), *Water in crisis: A guide to the world's freshwater resources*. Oxford University Press.
- Shrivastava, P., & Kumar, R. (2015). Soil salinity: A serious environmental issue and plant growth promoting bacteria as one of the tools for its alleviation. *Saudi Journal of Biological Sciences*, 22(2), 123–131. <https://doi.org/10.1016%2Fj.sjbs.2014.12.001>.
- Smedley, P. L. (1991). The geochemistry of rare earth elements in groundwater from the Carnmenellis area, southwest England. *Geochimica et Cosmochimica Acta*, 55(10), 2167–2779. [https://doi.org/10.1016/0016-7037\(91\)90443-9](https://doi.org/10.1016/0016-7037(91)90443-9).
- Smedley, P., & Kinniburgh, D. (2002). A review of the source, behaviour and distribution of arsenic in natural waters. *Applied Geochemistry*, 17(5), 517–568.
[https://doi.org/10.1016/S0883-2927\(02\)00018-5](https://doi.org/10.1016/S0883-2927(02)00018-5)

- Smedley, P. L., & Kinniburgh, D. G. (2017). Molybdenum in natural waters: A review of occurrence, distributions and controls. *Applied Geochemistry* 84, 387–43.
<https://doi.org/10.1016/j.apgeochem.2017.05.008>.
- Stannard, D. I. (1988). *Use of a hemispherical chamber for measurement of evapotranspiration* (Open-File Report 88-452). US Geological Survey.
- Stauffer, R. E., Jenne, E. A., & Ball, J. W. (1980). *Chemical studies of selected trace elements in hot-spring drainage of Yellowstone National Park* (Professional Paper 1044-F). US Geological Survey.
- Stayner, L. T., Schullehner, J., Semark, B. D., Jensen, A. S., Trabjerg, B. B., Pedersen, M., Olsen, J., Hansen, B., Ward, M. H., Jones, R. R., Coffman, V. R., Pedersen, C. B., & Sigsgaard, T. (2021). Exposure to nitrate from drinking water and the risk of childhood cancer in Denmark. *Environment International*, 155(106613).
<https://doi.org/10.1016/j.envint.2021.106613>.
- Steffen, W., Richardson, K., Rockström, J., Cornell, S. E., Fetzer, I., Bennett, E. B., Biggs, R., Carpenter, S. R., de Vries, W., de Wit, C. A., Folke, C., Gerten, D., Heinke, J., Mace, G. M., Perrson, L. M., Ramanathan, V., Reyers, B., & Sorlin, S. (2015). Planetary boundaries: Guiding human development on a changing planet. *Science*, 347(6223).
<https://doi.org/10.1126/science.1259855>.
- Stevanović, Z., Gunn, J., Goldscheider, N., & Ravbar, N. (2024). *Karst: Environment and management of aquifers*. The Groundwater Project.
<https://doi.org/10.62592/AWCU2984>.
- Stokes, S., Bray, H., Goudie, A., & Wood, W. W. (2003). Later Quaternary paleorecharge events in the Arabian Peninsula. *Developments in Water Science*, 50, 371–378.
[https://doi.org/10.1016/S0167-5648\(03\)80032-1](https://doi.org/10.1016/S0167-5648(03)80032-1).
- Stutz, J., Ackermann, R., Fast, J. D., & Barrie, L. (2002). Atmospheric reactive chlorine and bromine at the Great Salt Lake, Utah. *Geophysical Research Letters*, 29(10)
<https://doi.org/10.1029/2002GL014812>.
- Suchet, P. A., & Probst, J. L. (1995). A global model for present-day atmospheric/soil CO₂ consumption by chemical erosion of continental rocks (GEM-CO₂). *Tellus B* 47(1–2), 273–280. <https://doi.org/10.1034/j.1600-0889.47.issue1.23.x>.
- Sun, R. J., Weeks, J. B., & Grubb, H. F. (1997). *Bibliography of regional aquifer-systems analysis program of the US Geological Survey 1978–96* (Water Resource Investigations Report 97-4074). US Geological Survey.
- Sweeney, R. E., Liu, K. K., & Kaplan, I. R., & Robinson, B. W. (Eds.). (1978). *Oceanic nitrogen isotopes and their uses in determining the source of sedimentary nitrogen*. New Zealand: DSIR Science Information Division, 220, 9–26.

- Syvitski, J. P. M., Vorosmarty, C. J., Kettner, A. J., & Green, P. A. (2005). Impact of humans on the flux of terrestrial sediment to the global coastal ocean. *Science*, 308(5720), 376–380. <https://doi.org/10.1126/science.1109454>[http](#)[↗].
- Szabo, Z., Stackelberg, P. E., & Cravotta, C. A., III. (2020). Occurrence and geochemistry of lead-210 and polonium-210 radionuclides in public-drinking-water supplies from principal aquifers of the United States. *Environmental Science & Technology*, 54(12), 7236–7249. <https://doi.org/10.1021/acs.est.0c00192>[↗].
- Taniguchi, M., Ishitoblt, T., Burnett, W. C., & Shmada, J. (2007, July). Comprehensive evaluation of the groundwater seawater interface and submarine groundwater. In *Proceedings of Symposium HS1001 at IUGG, Perugia*. IAHS Publ.
- Theis, C. V. (1937). Amount of ground-water recharge in the southern high plains. *Eos, Transaction American Geophysical Union* 18(2), 564–568. <https://doi.org/10.1029/TR018i002p00564>[↗].
- Theis, C. V. (1940). The source of water derived from wells: Essential factors controlling the response of an aquifer to development. *Civil Engineering*, 10(5), 277–280.
- Thraikill, J. (1968). Chemical and hydrologic factors in the excavation of limestone caves. *GSA Bulletin*, 79(1) 19–46. [https://doi.org/10.1130/0016-7606\(1968\)79\[19:CAHFIT\]2.0.CO;2](https://doi.org/10.1130/0016-7606(1968)79[19:CAHFIT]2.0.CO;2)[↗].
- Tufte, E. R. (1997). *Visual explanations: Images and quantities, evidence and narrative*. Graphic Press.
- Turkey, J. W. (1977). *Exploratory data analysis* (Vol. 2). Addison-Wesley.
- US Geological Survey. (n.d.). *Aquifers and groundwater*. US Geological Survey. https://www.usgs.gov/special-topic/water-science-school/science/aquifers-and-groundwater?qt-science_center_objects=0#qt-science_center_objects[↗].
- US Geological Survey. (n.d.). *National water-quality assessment (NAWQA)*. US Geological Survey. <https://www.usgs.gov/mission-areas/water-resources/science/national-water-quality-assessment-nawqa>[↗].
- US Environmental Protection Agency (EPA). (n.d.) *Drinking water regulations and contaminants*. US EPA. <https://www.epa.gov/sdwa/drinking-water-regulations-and-contaminants>[↗].
- UNICEF. (2018). *Arsenic primer: Guidance on the investigation and mitigation of arsenic contamination*. New York.
- Van Dam, R. L., Eustice, B. P., Hyndman, D. W., Wood, W. W., & Simmons, C. T. (2014). Electrical imaging and fluid modeling of convective fingering in a shallow water-table aquifer. *Water Resources Research*, 50(2), 954–968. <https://doi.org/10.1002/2013WR013673>[↗].

- Van Dam, R. L., Simmons, C. T., Hyndman, D. W., & Wood, W. W. (2009). Natural free convection in porous media: First field documentation in groundwater. *Geophysical Research Letter*, 36(11). <https://doi.org/10.1029/2008GL036906>.
- Vanlier, K. E., Wood, W. W., & Brunett, J. O. (1973). *Water supply, development and management alternatives for Clinton, Eaton, and Ingham Counties, Michigan* (Water-Supply Paper 1969). US Geological Survey. <https://pubs.usgs.gov/wsp/1969/report.pdf>.
- Vengosh, A., Coyte, R. M., Podgorski, J., & Johnson, T. M. (2022). A critical review on the occurrence and distribution of the uranium- and thorium-decay nuclides and their effect on the quality of groundwater. *Science of The Total Environment*, 808, 151914. <https://doi.org/10.1016/j.scitotenv.2021.151914>.
- Vitug, V. (2019). *Demystifying radiation*. Yale National Initiative. https://teachers.yale.edu/curriculum/viewer/initiative_19.04.09_u.
- Ward, M. H., Jones, R. R., Brender, J. D., De Kok, T. M., Weyer, P. J., Nolan, B. T., Villanueva, C. M., & Van Breda, S. G. (2018). Drinking water nitrate and human health: An updated review. *International Journal of Environmental Research and Public Health*, 15(7), 1557. <https://doi.org/10.3390/ijerph15071557>.
- Wilson, T. P., & Long, D. T. (1993). Geochemistry and isotope chemistry of Michigan Basin brines: Devonian formations. *Applied Geochemistry*, 8(1), 81–100. [https://doi.org/10.1016/0883-2927\(93\)90058-O](https://doi.org/10.1016/0883-2927(93)90058-O).
- Winter T. C., Harvey, J. W., Franke, O. L., & Alley, W. M. (1998). Ground water and surface water: A single resource (Circular 1139). US Geological Survey. <https://doi.org/10.3133/cir1139>.
- Wood, W. W. (1976). A hypothesis of ion filtration in a potable water aquifer system. *Groundwater*, 14(4), 233–244. <https://doi.org/10.1111/j.1745-6584.1976.tb03108.x>.
- Wood, W. W., & Petraitis, M. J. (1984). Origin and distribution of carbon dioxide in the unsaturated zone of the southern high plains of Texas. *Water Resources Research*, 20(9), 1193–1208. <https://doi.org/10.1029/WR020i009p01193>.
- Wood, W. W. (1985). Origin of caves and other solution openings in the unsaturated (vadose) zone of carbonate rocks, a model for CO₂ generation. *Geology*, 13(11), 822–824. [https://doi.org/10.1130/0091-7613\(1985\)13<822:OOCAOS>2.0.CO;2](https://doi.org/10.1130/0091-7613(1985)13<822:OOCAOS>2.0.CO;2).
- Wood, W. W. (2010) Source of paleo-groundwater in the Emirate of Abu Dhabi, United Arab Emirates: Evidence from unusual oxygen and deuterium isotope data. *Hydrogeology Journal*, 19, 155–161. <https://doi.org/10.1007/s10040-010-0626-9>.
- Wood, W. W. (2019). Geogenic groundwater solutes: The myth. *Hydrogeology Journal*, 27, 2729–2738. <https://doi.org/10.1007/s10040-019-02057-1>.

- Wood, W. W. (2021). *A conceptual overview of surface and near-surface brines and evaporite minerals*. The Groundwater Project. <https://books.gw-project.org/a-conceptual-overview-of-surface-and-near-surface-brines-and-evaporite-minerals/>.
- Wood, W. W., & Osterkamp, W. R. (1987). Playa-lake basins on the southern high plains of Texas and New Mexico, Part II. Hydrological model and mass-balance arguments for their development. *Geological Society of America Bulletin*, 99(2), 224–230. [https://doi.org/10.1130/0016-7606\(1987\)99<224:PBOTSH>2.0.CO;2](https://doi.org/10.1130/0016-7606(1987)99<224:PBOTSH>2.0.CO;2).
- Wood, W. W., Kraemer, T. F., & Hearn, P. P., Jr. (1990). Intergranular diffusion: An important mechanism influencing solute transport in clastic aquifers? *Science*, 247(4950), 1569–1572. <https://doi.org/10.1126/science.247.4950.1569>.
- Wood, W. W., & Sanford, W. E. (1990). Ground-water control of evaporite deposition. *Economic Geology*, 85(6), 1226–1235. <https://doi.org/10.2113/gsecongeo.85.6.1226>.
- Wood, W. W., & Imes, J. L. (1995). How wet is wet? Constraints on late Quaternary climate in southern Arabian Peninsula. *Journal of Hydrology*, 164(1–4), 263–268. [https://doi.org/10.1016/0022-1694\(94\)02551-L](https://doi.org/10.1016/0022-1694(94)02551-L).
- Wood, W. W., & Sanford, W. E. (1995a). Eolian transport, saline lake basins, and groundwater solutes. *Water Resources Research*, 31(12), 3121–3129. <https://doi.org/10.1029/95WR02572>.
- Wood, W. W., & Sanford, W. E. (1995b). Chemical and isotopic methods for quantifying ground-water recharge in a regional, semi-arid environment. *Groundwater*, 33(3), 458–468. <https://doi.org/10.1111/j.1745-6584.1995.tb00302.x>.
- Wood, W. W., Sanford, W. E., & Al Habschi, A. R. S. (2002). Source of solutes to the coastal sabkha of Abu Dhabi. *Geological Society of America Bulletin*, 114(3), 259–268. [https://doi.org/10.1130/0016-7606\(2002\)114<0259:SOSTTC>2.0.CO;2](https://doi.org/10.1130/0016-7606(2002)114<0259:SOSTTC>2.0.CO;2).
- Wood, W. W., & Imes, J. L. (2003). Dating of Holocene ground-water recharge in western part of Abu Dhabi (United Arab Emirates): Constraints on global climate-change models. *Developments in Water Science*, 50, 379–385. [https://doi.org/10.1016/S0167-5648\(03\)80033-3](https://doi.org/10.1016/S0167-5648(03)80033-3).
- Wood, W. W., Kraemer, T. F., & Shapiro, A. (2004). Radon (^{222}Rn) in ground water of fractured rocks: A diffusion/ion exchange model. *Groundwater* 42(4), 552–567. <https://doi.org/10.1111/j.1745-6584.2004.tb02624.x>.
- Wood, W. W., & Sanford, W. E. (2007). Atmospheric bromine flux from the coastal Abu Dhabi sabkhat: A ground-water mass-balance investigation. *Geophysical Research Letters*, 34(14), L14405. <https://doi.org/10.1029/2007GL029922>.
- Wood, W. W., & Bohlke, J. K. (2017). Density-driven free-convection model for isotopically fractionated geogenic nitrate in sabkha brine. *Groundwater*, 55(2), 199–207. <https://doi.org/10.1111/gwat.12463>.

- Wood, W. W., Smedley, P. L., Lindsey, B. D., Wood, W. T., Kirchheim, R. E., & Cherry, J. A. (2022). Global groundwater solute composition and concentrations. *Groundwater*, 60(6), 1–7. <https://doi.org/10.1111/gwat.13205>.
- Wood, W. W., Sanford, W. E., Cherry, J. A., Hyndman, D. W., & Wood, W. T. (2023a). Global nitrogen concentration in the active freshwater aquifer element pool. *Global Biogeochemical Cycles*, 37(10). <http://doi.org/10.1029/2023GB007878>.
- Wood, W. W., Sanford, W. E., Cherry, J. A., & Wood, W. T. (2023b). “Wrecking the rocks”: Continental weathering by groundwater. *Geology* 51(12), 1122–1126. <https://doi.org/10.1130/G51571.1>.
- Wood, W. W., Sanford, W. E., Cherry, J. A., & Wood, W. T. (2024). Global groundwater carbon mass flux and the myth of atmospheric weathering. *Groundwater*, online <https://doi.org/10.1111/gwat.13457>.
- World Health Organization. (n.d.). *Drinking water quality guidelines*. WHO. <https://www.who.int/teams/environment-climate-change-and-health/water-sanitation-and-health/water-safety-and-quality/drinking-water-quality-guidelines>.

12Boxes

Box 1 – Atomic Structure

Each element has a tiny nucleus of protons and neutrons surrounded by different shells of electrons given the nomenclature ($n=1$, $n=2$, $n=3$, and so on). Within each shell, there are a specific number of electrons, each with specific energy and paths, so they don't collide. These paths, or *orbitals*, are classified with the letters s, p, d, and f. The s orbital has a maximum of 2 electrons, the p orbital has a maximum of 6 electrons, the d orbital has a maximum of 10 electrons, and the f orbital has a maximum of 14 electrons. A chart—showing the order of filling of the shells (the Aufbau filling principle)—is given in Figure Box 1, from which the nomenclature for the element's electron configuration can be described. Aufbau comes from the German word *Aufbauen*, which means *building up*.

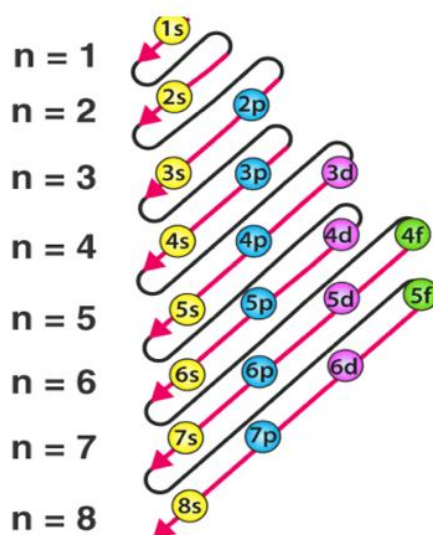


Figure Box 1-1 - Chart showing the Aufbau filling principle of orbital electrons nomenclature where “n” is the shell and 1s, 2s, 2p, and so on are the electron orbitals.

The nomenclature of electron convention dictates that the first digit indicates the shell ($n=1$, $n=2$, $n=3$, and so on), the second digit indicates the orbital energy level (s, p, d, or f), and the third digit is the number of electrons in that orbital (expressed as a superscript). Thus, the first shell ($n=1$) contains a maximum of two electrons in the 1s orbital ($1s^2$); the second shell has a maximum of 2 electrons in the 2s orbital and six electrons in the 2p orbitals ($2s^2 2p^6$); the third shell contains a maximum of two 3s orbital electrons, 6 electrons in the 3p orbital, 10 electrons in the 3d orbitals ($3s^2 3p^6 3d^{10}$) and can contain 18 electrons; the fourth shell can contain 32 electrons: $4s^2 4p^6 4d^{10} 4f^{14}$. The remaining shells contain a maximum of 32 electrons. There can never be more than 32 electrons in any shell.

The most chemically stable, unreactive electron configurations occur when the valence shell of any element is complete and contains the maximum number of electrons. All noble gases—He, Ne, Ar, Kr, Xe, Rn—have a full valence shell and are extremely stable and unreactive. For example, neon (Ne) has an atomic number of 10 (10 protons), and from the chart (Figure Box 1-1), the first two electrons go in the first shell (1s) orbital, the next 2 electrons go in the second shell (2s) orbital, and the remaining six electrons will go in the 2p orbital of the second shell. Thus, the Ne, electron configuration will have a total of 10 electrons and, accordingly, a complete outer shell of $(1s^2 2s^2 2p^6)$.

Suppose the electron shell has more electrons than the stable valence shell, such as sodium with 11 protons ($1s^2 2s^2 2p^6 3s^1$), then the ion has a 1+ charge—that is, Na^+ needs to lose an electron to obtain a stable electron shell configuration. Similarly, if an element like fluoride with 9 protons ($1s^2 2s^2 2p^5$) has one less electron than the stable valence shell, then the ion has a -1 charge, that is F^- needs to gain an electron to attain a stable configuration. The combination of the two can form a molecule of NaF in a stable electron configuration.

[Return to where text linked to Box 1](#) ↗

Box 2 – Applying activity calculations to the average groundwater composition

Information about the major ions in the average groundwater (Table Box 2-1) can be used to calculate the ionic strength and activity of the ions. This information is important for determining saturation index.

Required equations:

Ionic strength: $I = \frac{1}{2} \sum m_i z_i^2$ (that is, $\frac{1}{2}$ the sum of the molality (m) of each ion multiplied by the square of its ionic charge (z) for all ions present in solution)

Debye-Hückel: $\log \gamma = \frac{-Az^2\sqrt{I}}{1+\lambda B\sqrt{I}}$ (determines activity relationships, where activity, a , is the product of molality and γ , $a = m\gamma$) A and B are constants given below, z is ionic charge, λ is ionic size, I is ionic strength

Required information:

A = 0.5042 and B = 0.3273×10^8 at 1 Bar and 20 °C

Table Box 2-1 - Ionic strength and activity of ions for average groundwater.

Ion	Atomic mass (g/mol)	Ionic-size (λ is 10^{-8} m) (angstroms)	Concentration (mg/L)	Charge (z)
HCO ₃ ⁻	61.0168	4	214	-1
Ca ²⁺	40.078	6	42	2
Cl ⁻	35.453	3	24	-1
K ⁺	39.0983	3	3.5	1
Mg ²⁺	24.305	8	13	2
Na ⁺	22.99	4	45	1
SO ₄ ²⁻	96.06	4.5	31	-2

Step 1: Convert concentration from mg/L to mol/L

Using HCO₃ as an example:

$$\frac{214 \text{ mg}}{1 \text{ L}} \frac{1 \text{ g}}{1,000 \text{ mg}} \frac{1 \text{ mol}}{61.02 \text{ g}} = 0.0035 \frac{\text{mol}}{\text{L}}$$

Convert the concentrations from mg/L to mol/L for all the ions, resulting in the values presented in Table Box 2-2.

Table Box 2-2 - Ionic strength and activity of ions for average groundwater (concentrations in mol/L).

Ion	Atomic mass (g/mol)	Ionic-size (1Å is 10 ⁻⁸ m) (angstroms)	Concentration (mol/L)	Charge (z)
HCO ₃ ⁻	61.0168	4	3.507×10 ⁻³	-1
Ca ²⁺	40.078	6	1.048×10 ⁻³	2
Cl ⁻	35.453	3	6.770×10 ⁻⁴	-1
K ⁺	39.0983	3	8.951×10 ⁻⁵	1
Mg ²⁺	24.305	8	5.348×10 ⁻⁴	2
Na ⁺	22.99	4	1.957×10 ⁻³	1
SO ₄ ²⁻	96.06	4.5	3.227×10 ⁻⁴	-2

Step 2: Calculate the ionic strength of the water

$$\text{Using } I = \frac{1}{2} \sum m_i z_i^2,$$

$$I = 0.5[(\text{HCO}_3^-)(-1)^2 + (\text{Ca}^{2+})(2)^2 + (\text{Cl}^-)(-1)^2 + (\text{K}^+)(1)^2 + (\text{Mg}^{2+})(2)^2 + (\text{Na}^+)(1)^2 + (\text{SO}_4^{2-})(-2)^2]$$

$$I = 0.5[(3.507 \times 10^{-3})(-1)^2 + (1.048 \times 10^{-3})(2)^2 + (6.770 \times 10^{-4})(-1)^2 + (8.951 \times 10^{-5})(1)^2 + (5.348 \times 10^{-4})(2)^2 + (1.957 \times 10^{-3})(1)^2 + (3.227 \times 10^{-4})(-2)^2]$$

$$I = 6.926 \times 10^{-3} \text{ mol/L}$$

Step 3: Use the ionic strength to calculate the activity coefficients:

$$\text{For HCO}_3^-, \text{ using } \log \gamma = \frac{-Az^2\sqrt{I}}{1 + \alpha B\sqrt{I}}$$

$$\log \gamma = \frac{-(0.5042)(-1)^2\sqrt{6.926 \times 10^{-3}}}{1 + (4 \times 10^{-8})(0.3273 \times 10^8)\sqrt{6.926 \times 10^{-3}}}$$

$$\log \gamma = -0.03784$$

$$\gamma = 10^{-0.03784}$$

$$\gamma = 0.9166$$

Calculate the activity coefficients for all ions, resulting in the values presented in Table Box 2-3.

Table Box 2-3 - Activity coefficients.

Ion	γ	Concentration (mol/L)
HCO ₃ ⁻	0.9166	3.507x10 ⁻³
Ca ²⁺	0.7174	1.048x10 ⁻³
Cl ⁻	0.9146	6.770x10 ⁻⁴
K ⁺	0.9146	8.951x10 ⁻⁵
Mg ²⁺	0.7281	5.348x10 ⁻⁴
Na ⁺	0.9166	1.957x10 ⁻³
SO ₄ ²⁻	0.7087	3.227x10 ⁻⁴

Step 4: Calculate the activity of all ions in solution

Using $a = m\gamma$ for HCO₃⁻

$$a = (3.507 \times 10^{-3})(0.9166)$$

$$a = 3.215 \times 10^{-3} \frac{\text{mol}}{\text{L}}$$

Calculate the activity of all ions resulting in the values presented in Table Box 2-4.

Table Box 2-4 - Activity of all ions.

Ion	γ (dimensionless)	Concentration (m; mol/L)	Activity (a; mol/L)
HCO ₃ ⁻	0.9166	3.507x10 ⁻³	3.215x10 ⁻³
Ca ²⁺	0.7174	1.048x10 ⁻³	7.517x10 ⁻⁴
Cl ⁻	0.9146	6.770x10 ⁻⁴	6.192x10 ⁻⁴
K ⁺	0.9146	8.951x10 ⁻⁵	8.187x10 ⁻⁵
Mg ²⁺	0.7281	5.348x10 ⁻⁴	3.894x10 ⁻⁴
Na ⁺	0.9166	1.957x10 ⁻³	1.793x10 ⁻³
SO ₄ ²⁻	0.7087	3.227x10 ⁻⁴	2.287x10 ⁻⁴

For a water with an ionic strength of 0.007 are the activity coefficients what you would expect based on Figure Box 2-1? That is, does the trend of the calculated activity coefficients match the trend shown in Figure Box 2-1?

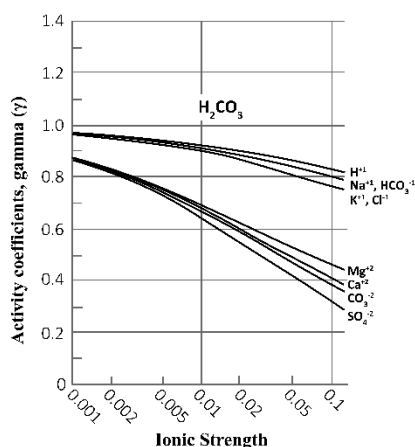


Figure Box 2-1 - Duplicate of Figure 50 for convenience.

[Return to where text linked to Box 2](#)

Box 3 – Instructions for Running PHREEQC on a Mac Laptop (Intel and Apple M Silicon chip)

This is a two-step procedure the first time you attempt to run MacPHREEQC. Sections highlighted in yellow and blue draw attention to critical issues in downloading and using the software.

Step 1 Installing MacPHREEQC and determining if it runs correctly

Discard all old PHREEQC folders or files containing anything but instructions or examples.

Download the “MacPHREEQC.dmg” file by clicking on

[https://visions-of-quality.com > macphreeqc](https://visions-of-quality.com/macphreeqc)

and accepting concerns about internet files.

The downloaded file the “phreeqc-3.5.0-1400.dmg” and the following file will appear on the desktop.



Figure Box 3-1 - Download file for installing PHREEQC.

Double clicking will open that .dmg file and a new file will appear on the desktop.

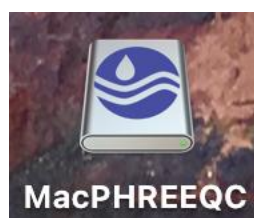


Figure Box 3-2 - Desktop file for installing PHREEQC.

Open that file and another new file will appear on the desktop

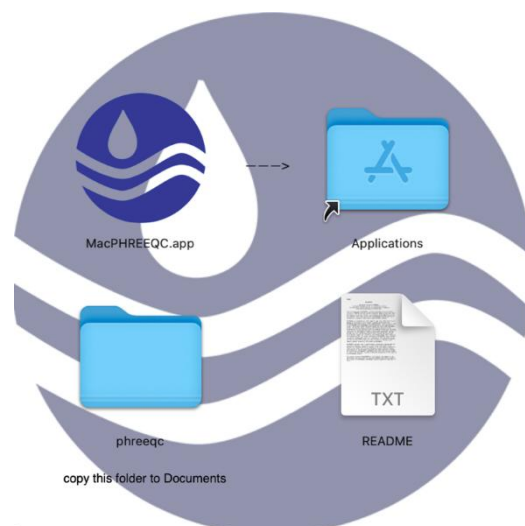


Figure Box 3-3 - New desktop folder for PHREEQC.

Open the main Application folder on the computer and slide the “Applications” as shown above into the Applications folder on your computer. Next, open the main Documents Folder on your computer and slide the “phreeqc folder” into the Documents Folder.

You are now ready to run MacPHREEQC.

In the MacPHREEQC folder click on the MacPHREEQC app.

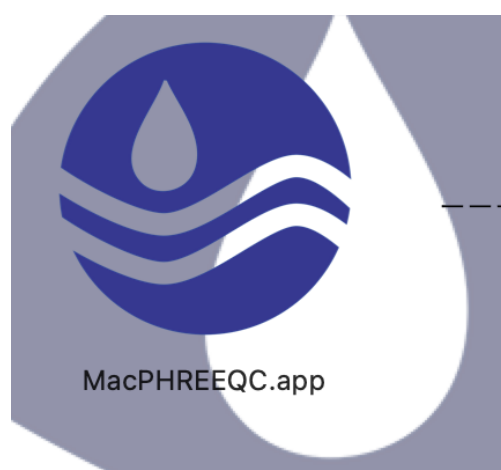


Figure Box 3-4 - Application for running PHREEQC.

After clicking on the app, the following window will appear with some extraneous files depending on what else is in your Documents folder.

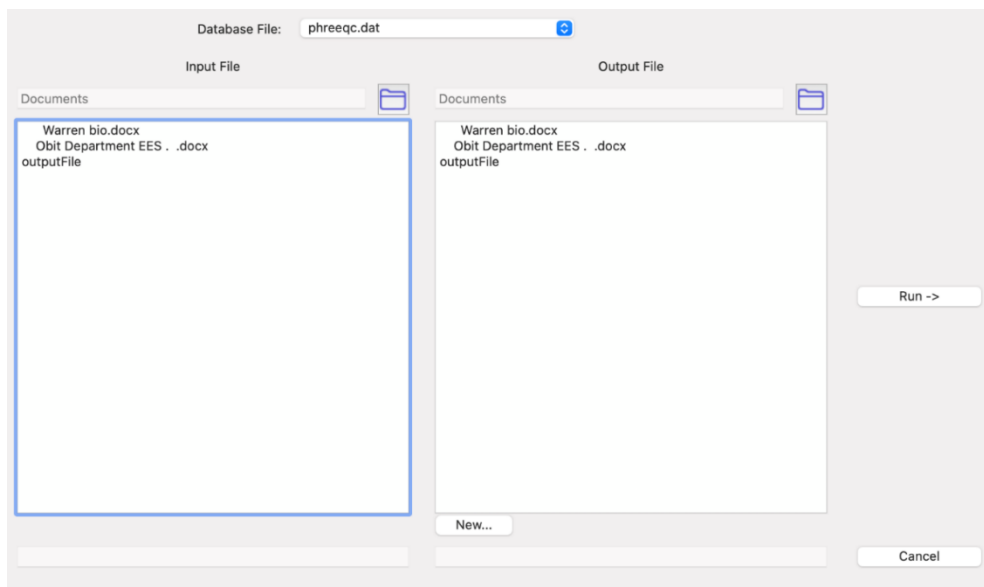


Figure Box 3-5 - PHREEQC window after clicking the application.

It is always best to check if the program is running as expected, so select an example from the example folder; this is a two-step process.

Click on the diagram of a file folder  on the upper right portion of the “Input” side of the window, and the following will be presented.

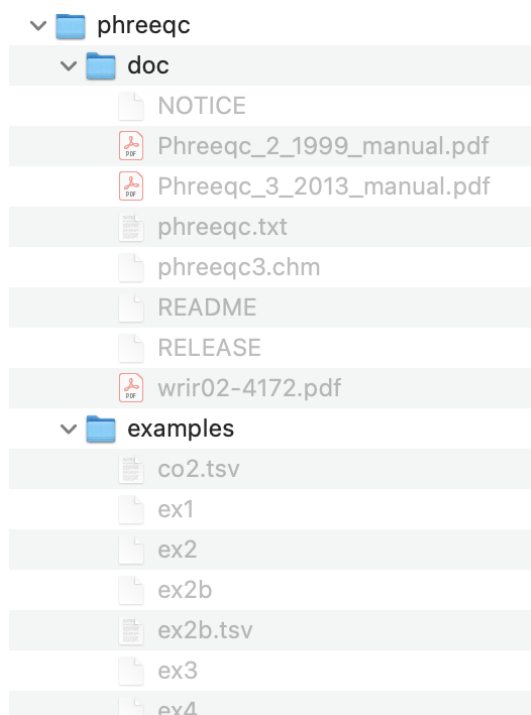


Figure Box 3-6 - Files in the PHREEQC file folder.

Highlight “examples” and press “open” at the bottom of the screen to see the active examples.

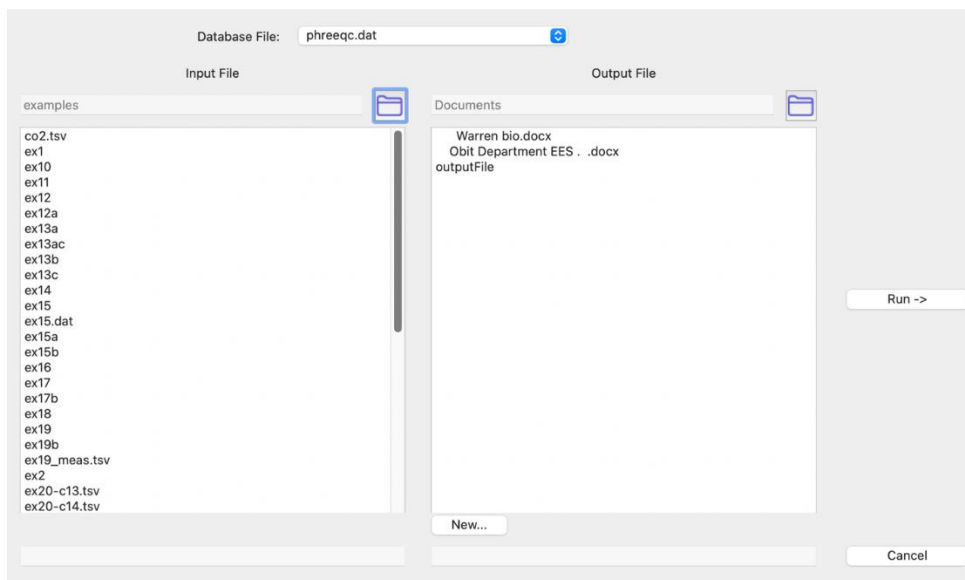


Figure Box 3-7 - Active examples after installing PHREEQC.

Highlight one of the examples. Next, go to “Database files” located in the center uppermost part of the window, and select the database you want to use. We have checked “phreeqc.dat”.

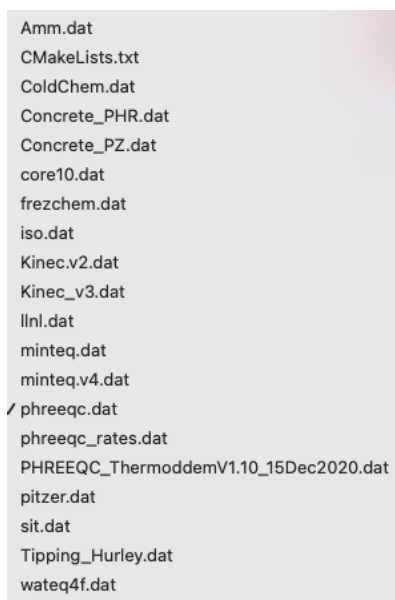


Figure Box 3-8 - Available databases after installing PHREEQC.

Next press “New” at the bottom of the right “Output” side of the screen this will offer the opportunity to name and select a location of the output file. After assigning a name and location, press the “Run” button (center on the right side of the window)

and the program will execute. Check to see if it ran as expected by comparing the output generated on your computer to the output published in the USGS manual.

Step 2 Creating an input file for a Mac

Creating an input file is a challenge for a Mac user as there is no GUI (Graphical Users Interface) program like “Windows 32-bit: [Notepad ++ interface](#), Appelo's Notepad ++ interface to PHREEQC version 3” for Windows users.

You will need to enter the program in a **text editor** as MS Word has many hidden characters that will confuse the PHREEQC application. I use the free BBEditor as my Text editor.

In many cases, you will want speciation of the solutes and their equilibrium with the minerals. Thus, the following example is perhaps the simplest use of PHREEQC. The input is free format so the column position for entering data is not critical.

Open a text editor and clear it of any text. On the upper leftmost margin type TITLE in caps and a description of the input file (**don't type < or > symbols and don't forget a period at the end**), that is:

```
<TITLE Speciation and equilibrium of mean global groundwater.>
```

Next press return and type in SOLUTION 1 in caps and a description (**and don't forget periods at the end**), that is:

```
SOLUTION 1 Global groundwater from Wood et al., 2022.
```

Next enter the units, pH, and Temp values on different lines

```
units  mg/L
pH      7.21
Temp    20.0
```

Element solutes like Ca, Mg, Na, K etc. are entered directly in mg/L

```
Ca      42
Mg      14
Na      45
K       3.5
Cl      23
```

However, molecules like HCO_3 , SO_4 , NO_3 , H_4SiO_4 , and so on are a little different. When you get to where you expect bicarbonate you see “alkalinity” not bicarbonate.

as SOLUTIONS does not recognize the term HCO_3 . However, typically your analytical data will be in the form of bicarbonate. You can convert it to alkalinity by multiplying bicarbonate values by 0.82, alternatively you can enter your analytical values of bicarbonate and add “as HCO_3 ” after the value. The `<as HCO3>` instructs the program to calculate alkalinity based on your analytical data of bicarbonate (don't type `< or >` symbols)

Alkalinity 214 as HCO_3^-

Next on the list of solutes is typically sulfate (SO_4^{2-}), but PHREEQC states the request as S(6). The program is requesting sulfur in the form of +6 valence. Thus, just use the concentration of sulfate SO_4^{2-} ; do not convert to elemental sulfur.

S(6) 31

Next on the list of solutes is typically NO_3 . The PHREEQC states the request as N(5) and this is a reminder that the program wants nitrogen in the +5 valence, thus NO_3^- , not as N. As the data are in terms of N, `< as N>` can be used.

N(5) 0.34 as N

Next is silica input. Again, this can be a bit tricky as analytical values of silica are commonly reported in many different forms (Si, H_4SiO_4 , SiO_2 , and so on) but PHREEQC is looking for silica as SiO_2 . Thus, you need to convert the form you have to SiO_2 or you could enter Si 17 and `< as Si >`.

Si 17 as Si

NOTE: Charge balance. Occasionally, you may wish to balance the ions in an analysis if the balance error is large, as it can impact many calculations. To balance, type a space after the solute value and then the word `<Charge>`. This choice will typically be Cl, Na, or occasionally SO_4 , or whatever ion you feel is the source of the error. This adds or subtracts the amount necessary to balance the analysis. This can only be typed on one solute—not a positive and a negative solute. In our example, the balance is positive, so chloride will be added.

Next, on the final line, type END

Thus, the completed file looks like the following.

TITLE Speciation and equilibrium of mean global groundwater.

SOLUTION 1 Mean global groundwater from Wood and others, 2022.

units	mg/L
pH	7.21
Temp	20.0
Ca	42
Mg	14
Na	45
K	3.5
Cl	23 Charge
Alkalinity	214 as HCO ₃
S(6)	31
N(5)	0.34 as N
Si	17 as Si

END

Save the file and in the Documents folder and press and follow the instructions as given above for running the test problem.

When the program runs, it opens, and it is important to “select all” and copy and paste results into an MS Word document if you want to modify the file for publication, however, you will lose the column format, so the output looks messy. A good file (i.e., one that maintains the column format) can be generated by using a text editor or Excel.

[Return to where text linked to Box 3 ↑](#)

Box 4 – An Unexpected Journey in Hydrogeochemical Thinking

Hydrogeology projects seldom go as planned. This exposé provides an example of the somewhat unexpected way that projects progress. While working on the book “Groundwater in Our Water Cycle” in 2019, John Cherry and I were asked by Eileen Poeter and Ying Reinfelder a simple direct question: “What is the global carbon flux related to groundwater?” I told John that I would address this as I thought the answer was simple, because we just needed to combine the value of global groundwater flux and global groundwater bicarbonate concentration to calculate a carbon mass flux. I knew of a global groundwater flux, and I thought that someone had likely compiled a global average bicarbonate concentration, but I could not find a compilation by undertaking a literature search.

As I could not find a satisfactory average global value for bicarbonate in the literature, I decided to build a global database and sent e-mail requests to about 170 water agencies throughout the world. The response was poor and varied from most ignoring my request to “We are willing to sell you analysis results for the equivalent of \$100US each” which was beyond my means. Some would not release data because they were concerned with the local repercussions of potential health concerns. Of the responses that I received, some countries said they did not have a national database, some sent databases that were poorly curated with many input errors and a lack of chemical balance, and others lumped surface water and groundwater analyses together which was not helpful for answering the question at hand. Thus, after two years of trying to form a global groundwater solute database, I was only able to get good regional data from Australia, Brazil, Chile, and the United States. While these data were interesting and covered all important hydrologic environments with about 25,000 samples and analysis of 250,000 solutes, I was concerned about estimating global values from such a poor geographic sampling distribution with nothing from Europe, Asia, or Africa. This is where the journey became more interesting!

Warren T. Wood (my son) had been using Geospatial Machine Learning (GML) in his studies of ocean bottom properties and gas hydrates for about ten to fifteen years and suggested that GML might provide a resolution of my sample distribution. That is, the available bicarbonate samples are poorly distributed over the Earth's land area but might be distributed far more evenly over the environmental space, e.g., minima, maxima, and standard deviations of temperature, precipitation, solar radiation, wind speed, and water vapor pressure, elevation, surficial geology, topography, and other factors. Thus, using his GML model and my solute database as a training environment, he created a modeled global concentration of bicarbonate and other major groundwater solutes (Wood et al., 2022).

The ultimate goal was to address the question of carbon flux, so I needed groundwater flux along with this bicarbonate concentration. And at this point, yet another turn made this more interesting. I intended to use the value of global groundwater recharge flux that I was familiar with (~16,000 km³/year), but while discussing it with Ward Sanford,

a good friend, former colleague, and coauthor at the USGS, he suggested that he could use Arc-GIS to determine a recharge rate for each of the concentration pixel. This would provide a much more detailed picture of mass flux by climate/hydrologic environment. Ward developed a recharge solute-mass flux for each solute in each of five separate climate/hydrologic environments -- wet-cold, wet-hot, dry-cold, dry-hot, and closed basins. We published the total global solute flux (Wood et al., 2023a) and total global groundwater nitrogen flux (Wood et al., 2023b). Finally, we addressed the question of total global groundwater carbon flux (Wood et al. 2024). Thus, the path to the answer to the initial question was much more convoluted and nuanced than one might have initially conceived.

[Return to where text linked to Box 4↑](#)

13 Exercise Solutions

Solution Exercise 1

1. A mineral's solubility is the intrinsic control on its dissolution. In general, it is the type of chemical bonding—how tightly the elements are held together in a mineral that determines its resistance to weathering. Covalent bonds of oxygen and silica in quartz are strong bonds and thus quartz is relatively insoluble in contrast to columbic bonding like that in halite, which is very soluble.
2. Temperature is one of the four fundamental environmental variables controlling mineral solubility. In most minerals, increasing temperature results in increasing solubility; however, several common minerals like calcite, dolomite, gypsum, and anhydrite have retrograde solubility; that is, they are less soluble with increasing temperature.
3. pH, which is a measure of the amount of hydrogen (H^+) and hydroxyl (OH^-) ions present in a solution, is another fundamental environmental variable controlling mineral solubility. Most minerals become more soluble with decreasing pH (becoming more acidic).
4. Eh (i.e., redox potential) is a measure of the potential to change the valence of an element (i.e., change the electrical charge) by adding or removing an electron, for example, Fe^{3+} and Fe^{2+} . This is another fundamental environmental variable that can have a major impact on mineral solubility
5. Thermodynamic activity (i.e., *effective concentration*) is a function of the concentration of all ions in solution, including their charge and size, ion pairs, complex ions, and oxyanions. Generally, solubility decreases with decreasing activity.

[Return to Exercise 1](#) ↑

[Return to where text linked to Exercise 1](#) ↑

Solution Exercise 2

Differences in concentration of trace elements generally reflect the source of the element in minerals of the aquifer as do several hydrologic conditions and geochemical processes, including ion competition, complexation, redox, pH, TDS, and temperature. For example, trace elements that commonly exist as cations, including cadmium (Cd), cobalt (Co), copper (Cu), lead (Pb), nickel (Ni), and zinc (Zn), are more likely to stay in solution at lower pH. Because of the greater concentration of positively charged hydrogen ions (H^+) competing for negative ($-$) sites on the aquifer mineral framework.

Conversely, trace elements such as arsenic (As), uranium (U), chromium (Cr), selenium (Se), and molybdenum (Mo) that form negative oxyanion complexes with oxygen ions are more likely to remain in solution as the pH increases because of competition from the negatively charged hydroxyl ion (OH^-) for positive sites on the aquifer mineral framework which reduces the places where negatively charged oxyanions can attach to the aquifer framework, thus more of them remain in solution.

[Return to Exercise 2](#) ↑

[Return to where text linked to Exercise 2](#) ↑

Solution Exercise 3

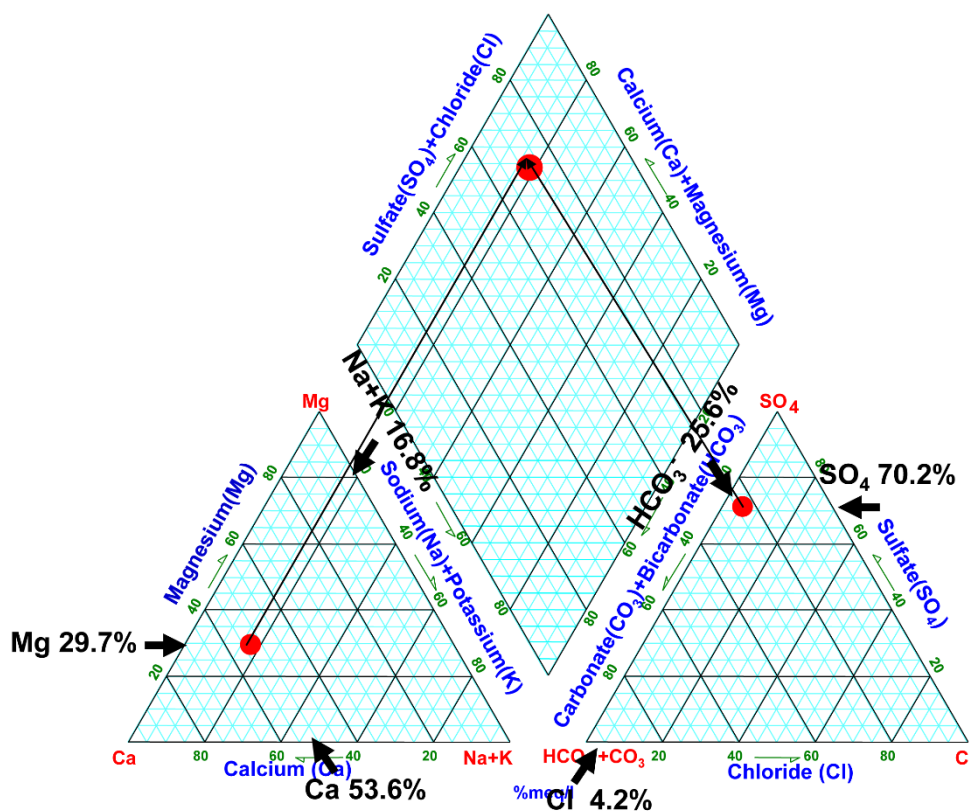
Individuals acquire and process information differently by listening, reading, writing, or visual presentations. To illustrate a concept, converting data tables to visual representation is frequently helpful; diagrams provide a quick visual summary of essential data or show a relationship.

In general, there are three fundamental types of illustrations typically used to display groundwater solute data, those that:

1. show variations in space or time (e.g., plan, cross-section, or fence diagrams of the aquifer at a specific location with time or in relation to flow paths) illustrating concentration or solute ratio changes laterally or vertically in an aquifer by use of contours or color heatmaps;
2. display ionic ratios and/or concentrations of individual analyses for a small number of analyses by use of bar graphs, pie diagrams, stick diagrams, among others to give a visual representation of the solute data; and
3. display the statistical distribution of many samples.

An approach for publications intended for popular consumption is to write the report around the graphs rather than just adding the graphs to the report.

The wild Rose water sample is a calcium-chloride type water.



[Return to Exercise 3](#) ↑

[Return to where text linked to Exercise 3](#) ↑

Solution Exercise 4

In general, first look to the source of the solutes, including those dissolved in precipitation, radioactive decay, transport into the aquifer from overlying, underlying or adjacent aquifers, weathering of the aquifer mineral framework, and aeolian or aerosol deposits. Then, look at the four environmental thermodynamic controls of temperature, pH, Eh, thermodynamic activity, and how they may be impacting the solutes. Finally, consider how major processes such as ion exchange and mineral precipitation might facilitate solute composition or concentration change.

[Return to Exercise 4](#) ↑

[Return to where text linked to Exercise 4](#) ↑

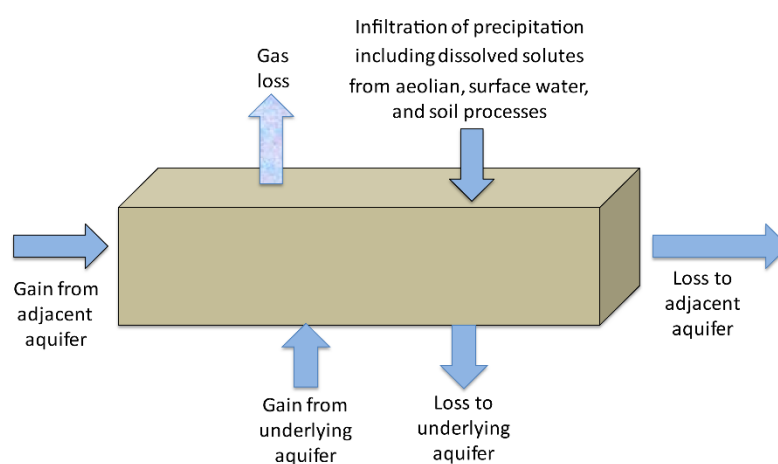
Solution Exercise 5

Solutes can enter the aquifer from the following sources, as illustrated in the associated figure:

1. dissolved in precipitation;
2. radioactive decay;
3. transport in from overlying, underlying, or adjacent aquifers; and
4. weathering of the aquifer mineral framework and aeolian or aerosol deposits.

Solutes can leave the aquifer as follows, as illustrated by the associated figure:

1. degassing;
2. mineral precipitation;
3. transport out to overlying, underlying, or adjacent aquifers; and
4. radioactive decay.



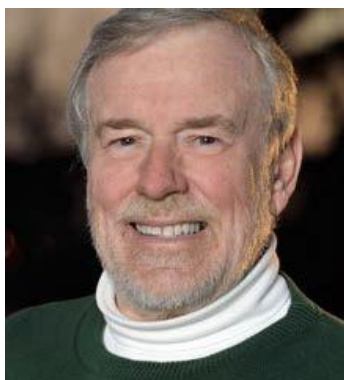
[Return to Exercise 5](#) ↑

[Return to where text linked to Exercise 5](#) ↑

14 Notations

A_b	=	drainage area of the basin (L^2)
AC	=	average anthropogenic concentration of recharging solute (ML^{-3})
A_f	=	area of the playa lake floor receiving the drainage (L^2)
AV	=	decimal percent of anthropogenic aquifer volume (dimensionless)
Cl_{wap}	=	precipitation-weighted average chloride concentration (ML^{-3})
Cl_{gw}	=	average chloride concentration in the ground water (ML^{-3})
Cl_r	=	average chloride concentration in the runoff (ML^{-3})
Cl_{uz}	=	average chloride concentration in the unsaturated zone (ML^{-3})
dh/dl	=	hydraulic gradient (LL^{-1})—change in hydraulic head with distance. The negative sign indicates the flow is from higher to lower hydraulic potential.
GC	=	average geogenic concentration of recharging solute (ML^{-3})
GV	=	decimal percent of geogenic aquifer volume (dimensionless)
K	=	hydraulic conductivity (LT^{-1})
k_{hz}	=	horizontal hydraulic conductivity (LT^{-1})
$\ln(2)$	=	Natural log of 2, 0.693 (dimensionless)
N	=	current number of parent atoms (dimensionless)
N_0	=	original number of parent atoms (dimensionless)
$Obs. C$	=	current observed global concentration (ML^{-3})
P	=	average annual precipitation (LT^{-1})
q	=	water flux ($L^3L^{-2}T^{-1}$)
q_{hz}	=	specific horizontal discharge flux (LT^{-1})
q_v	=	vertical ground-water recharge flux ($L^3L^{-2}T^{-1}$)
q_{vuz}	=	vertical recharge flux in the unsaturated zone ($L^3L^{-2}T^{-1}$)
r	=	overland runoff flux to the lake basin (LT^{-1})
TV	=	decimal percent of the total aquifer volume (dimensionless)
$T_{1/2}$	=	half-life of radioactive element (T)

15 About the Author



Warren W. Wood is currently a Visiting Professor of Hydrogeology in the Department of Earth and Environmental Sciences at Michigan State University and is formally Hannah Professor of Integrated Studies at Michigan State University; Christiansen Fellow, St. Catherine's College, Oxford University, UK; and Research Hydrologist, US Geological Survey. Warren has published more than 120 research articles on hydrogeology, largely of arid areas, and lectured at universities in Botswana, Canada, China, England, France, Germany, Israel, Japan, Jordan, North Ireland, Oman, Qatar, the Republic of South Africa, Kingdom of Saudi Arabia, Scotland, United Arab Emirates, and the USA. Warren received the Meritorious Service Award from the US Department of Interior, the M. King Hubbert Medal from the National Ground Water Association, the Distinguished Service Award from the Geological Society of America, and Elected Fellow of the Geological Society of America and was their Birdsall Lecturer. Warren served as Editor-in-Chief of the journal *Ground Water*. He testified before US Congress on nuclear waste disposal, briefed the US Secretary of Interior, US Chairman of the Nuclear Regulatory Commission, Administrator of the US EPA on the role of hydrogeology in nuclear waste disposal, and informed the Crown Prince of the Emirate of Abu Dhabi, UAE on sabkha mineral resources.

Please consider signing up to the GW-Project mailing list to stay informed about new book releases, events, and ways to participate in the GW-Project. When you sign up for our email list, it helps us build a global groundwater community. [Sign up](#)[↗].

